

**OPTIMIZATION OF RIB-TO-DECK WELDS FOR STEEL
ORTHOTROPIC BRIDGE DECKS**

Hao Yuan

Thesis submitted to the Faculty of the Virginia Polytechnic Institute and State University
in partial fulfillment of the requirements for the degree of

MASTER OF SCIENCE

in

CIVIL ENGINEERING

APPROVED:

William J. Wright, Chairperson

Finley A. Charney

Christopher D. Moen

November 4, 2011

Blacksburg, VA

Keywords: Steel orthotropic bridge deck, weld, fatigue, full-scale test, finite element
analysis, hot-spot stress, statistical analysis, MLR, ANCOVA

OPTIMIZATION OF RIB-TO-DECK WELDS FOR STEEL ORTHOTROPIC BRIDGE DECKS

Hao Yuan

ABSTRACT

Orthotropic steel deck has been widely used over the decades especially on long-span bridges due to its light weight and fast construction. However fatigue cracking problems on the welds have been observed in many countries. Rib-to-deck welds need special care since they are directly under wheel loads, which cause large local stress variations and stress reversals.

Currently the only requirement by AASHTO bridge code is that the rib-to-deck welds need to be fabricated as one-sided partial penetration welds with minimum penetration of 80% into the rib wall thickness. However considering the thin rib plate thickness, it is very difficult to achieve this penetration without a “melt-through” or “blow-through” defect. Large cost has been caused for the repair. However recent research has found that the fatigue performance of the rib-to-deck weld is not directly related to its penetration. Other factors contribute to the fatigue performance as well. Therefore, alternative requirements which are more cost-effective and rational are desired.

The objective of this research is to provide recommendations to the design and fabrication of rib-to-deck welds by investigating their fatigue performance with different weld dimensions, penetrations, and welding processes. Fatigue tests were performed to 95 full-scale single-rib deck segments in 8 specimen series fabricated with different welding processes and root gap openness. Specimens were tested under cyclic loads till failure. Three failure modes were observed on both weld toes and the weld root. Test results showed that the fatigue performance was more affected by other factors such as failure mode, R-ratio and root gap openness, rather than the weld penetration. The failure cycles were recorded for the following S-N curve analysis.

Finite element analysis was performed to determine the stress state on the fatigue

cracking locations. Special considerations were made for the application of hot-spot stress methodology, which post-processes the FEA results to calculate the stress values at cracking locations with the structural configuration taken into account. The hot-spot stress range values were derived and adjusted accounting for the fabrication and test error. Hot-spot S-N curves were established for each specimen series.

Statistical analyses were performed to study in depth the effect of weld dimensions and test scenarios. Multiple linear regression (MLR) was performed to investigate the effects of different weld dimensions; and multi-way analysis of covariance (Multi-way ANCOVA) for the effects of specimen series, failure mode, R-ratio and weld root gap. It was found that the weld toe size was more relevant to the fatigue performance, other than the weld penetration. The failure mode and R-ratio were very influential on the fatigue performance. Recommendations to the weld geometry were proposed based on the MLR model fitting. S-N data were re-categorized based on ANCOVA results and the lower-bound S-N curve was established. AASHTO C curve was recommended for the deck design.

ACKNOWLEDGEMENTS

This thesis took me a great amount of effort; however, more importantly it cannot be done without all the help that I received. Upon the completion of this thesis, I would like to extend my gratitude to everyone that devoted their time and attention for my favor.

First of all I would like to express my thanks to my advisor and Chairman of my committee, Dr. William J. Wright, who has guided me through this research from the beginning to the end. This research could never be possible without your vision, guidance and support. I also would like to thank you for giving me the opportunity to work on this challenging project, as well as your time and effort reviewing my thesis.

My gratitude also goes to Dr. Charney and Dr. Moen, who served as my committee members. I would like to thank Dr. Charney for sharing his knowledge and wisdom in his courses that I took, which were the ones that I enjoyed most throughout my graduate study. Your vast knowledge and righteous attitude toward science has been an inspiration and model to me. I also would like to thank Dr. Moen for serving in my committee and your continuous interest to my research.

I also would like to thank the people in the structures lab for their assistance. I would like to thank Dr. Roberts-Wollmann for organizing the lab; as well as Brett Farmer, Dennis Huffman and David Mokarem for assisting on various tasks. I would like to thank my fellow graduate students, Adrian Tola, Andrew Hardyniec, Fae Garstang, Garret Passarelli, Gokul Kamath, Jordan Jarrett, Leonardo Hasbun, Rakesh Naik, Yash Gajbhiye and many more, for their emotional support in both my research and life. It was you that made this place my home while I was half-the-planet away from my family.

As a cultural tradition, I would like to address the most important ones at last. I owe a huge debt of love to my parents that I could never repay them back. I feel the deepest gratitude for your unconditional and everlasting love, belief and support throughout my entire life. To be the single child, I feel regret that I have not done a great job of calling you frequently enough, nor visiting for over two years. But you are always the dearest in my heart and I could not feel luckier to be your son in this life.

Table of Contents

Chapter 1. Overview	1
1.1 Background	1
1.2 Objectives.....	3
1.3 Approach	5
Chapter 2. Literature Review	8
2.1 Fatigue Tests of Rib-to-Deck Welds on Steel Orthotropic Decks	8
2.1.1 Full-Scale Panel Tests.....	9
2.1.2 Single-Weld Tests.....	16
2.1.3 Full-Scale Single-Rib Tests	20
2.2 Fatigue Assessment Methodologies for Welded Joints.....	26
2.2.1 Hot-Spot Stress Methodology.....	32
2.2.2 Hot-spot Stress S-N Curves	40
2.2.3 Approaches Based on Fracture Mechanics	41
Chapter 3. Experimental Study	48
3.1 Preparation of Specimens.....	49
3.2 Test Matrix	55
3.3 Equipment	56
3.3.1 MTS Servo-hydraulic Test System.....	56
3.3.2 Customized Fixture.....	59
3.4 Test Setup and Procedure.....	60
3.4.1 Test Setup.....	60
3.4.2 Test Procedure	62
3.5 Post-Test Processing	66
3.5.1 Measurement of the Weld Profile.....	66

3.5.2	Measurement of the Effective Length (L_e)	70
3.5.3	Record of the Tack Weld Locations	71
3.6	Test Results and Discussion	73
Chapter 4.	Finite Element Modeling and Hot-Spot Stress Analysis	77
4.1	Recommended Procedures	79
4.1.1	DNV Recommendations	79
4.1.2	IIW Recommendations	84
4.2	2D Modeling	88
4.2.1	Construction of 2D Models.....	89
4.2.2	Element Type and Mesh Density	93
4.2.3	Modeling of the Weld Root Gap.....	107
4.2.4	Local Geometry Influence	115
4.2.5	Influence of the Bearing Plate Size.....	118
4.3	3D Modeling	122
4.4	Hot-Spot Stress Analysis.....	126
Chapter 5.	S-N Curve Study and Statistical Analysis.....	135
5.1	Multiple Linear Regression (MLR).....	138
5.1.1	Preliminary Simple Linear Regression	139
5.1.2	MLR for All Possible Models.....	141
5.1.3	Stepwise Model Fitting Analysis	142
5.1.4	Bivariate Regression Analysis for Relationships between Factors.....	144
5.1.5	Summary and Recommendations	151
5.2	Multi-way ANCOVA.....	156
Chapter 6.	Conclusions and Recommendations.....	160
6.1	Summary	160

6.2	Conclusions and Recommendations.....	161
6.3	Future Research.....	163
	References	165
	Appendix A Arrangement of Specimens on Full-Scale Deck Strips from TFHRC	173
	Appendix B Test Results from TFHRC	178
	Appendix C Test Results from VT	183
	Appendix D Weld Dimensions.....	186
	Appendix E Effective Length (L_e) Measurements.....	233
	Appendix F Locations of Tack Welds and Crack Initiation Points	235
	Appendix G Model Fitting Report – All Possible Factors	239
	Appendix H Simple Linear Regression Report – R=-1 under 36.67 ksi.....	253
	Appendix I Simple Linear Regression Report – R=-1 under 33.33 ksi.....	258
	Appendix J Simple Linear Regression Report – R=0 under 33.33 ksi	263
	Appendix K Simple Linear Regression Report – R=0 under 24.93 ksi, Specimens Failed at Weld Roots.....	268
	Appendix L Correlation between Factors – R=-1, Failed at WT@DECK	273
	Appendix M Correlation between Factors – R=0, Failed at WT@DECK.....	283
	Appendix N Model Fitting Report – Weld Dimensions for R=-1, WT@DECK.....	293
	Appendix O Model Fitting Report – Weld Dimensions for R=0, WT@DECK.....	300
	Appendix P Model Fitting Report – Weld Dimensions for R=-1, WT@RIB	309
	Appendix Q Model Fitting Report – Weld Dimensions for R=-1, WR.....	314
	Appendix R Model Fitting Report – All Significant Factors.....	319

List of Figures

Figure 1.1 Typical close-rib steel orthotropic deck panel.....	2
Figure 2.1 Typical strain gage layout on the diaphragm (Connor & Fisher, 2000).....	11
Figure 2.2 Finite element models for specimen 1 (left) and specimen 2-6 (right)	14
Figure 2.3 Test configurations (Maddox, 1974a)	17
Figure 2.4 Failure modes in series 1A (Maddox, 1974a)	18
Figure 2.5 Dimensions of specimens (Maddox, 1974b).....	20
Figure 2.6 Loading scenarios (Maddox, 1974b).....	22
Figure 2.7 Influence of R-ratio (Kolstein, 2007)	23
Figure 2.8 Influence of the spot-heating (Kolstein, 2007).....	24
Figure 2.9 Influence of root gap openness (Kolstein, 2007).....	25
Figure 2.10 Sheet-of-light measurement and measured weld surface (Fricke, 2007)	30
Figure 2.11 Fictitious rounding at weld toes and roots (Hobbacher, 2008)	30
Figure 2.12 Summary of the different fatigue assessment approaches (Fricke, 2003).....	31
Figure 2.13 Types of hot spots (DNV, 2008)	32
Figure 2.14 Linear surface extrapolation (0410) (Poutiainen, 2004).....	33
Figure 2.15 Location of reference points (Hobbacher, 2008).....	34
Figure 2.16 Structural stress calculation (Dong, 2001a).....	35
Figure 2.17 Dong’s method for plate/shell elements (Dong, 2001a).....	36
Figure 2.18 Definition of the modified through-thickness structural stress method (Poutiainen, 2006a).....	38
Figure 2.19 Multi-linear stress distribution for different plate thickness and weld size (Poutiainen, 2005).....	38
Figure 2.20 Relationship Between Crack Propagation Rate and Range of Stress Intensity Factor (Radaj, 1990)	45
Figure 3.1 Typical weld	50
Figure 3.2 Prepared specimens	50
Figure 3.3 Dimensions of specimens	51
Figure 3.4 Typical weld profile in each series	52
Figure 3.5 Over-beveled (OB) and under-beveled (UB) rib plate preparation.....	53

Figure 3.6 Typical over-beveled (OB) and under-beveled (UB) specimens after welding	54
Figure 3.7 Saw-cuts introduced at the weld roots on the OB (Left) and UB (Right) specimens	54
Figure 3.8 MTS servohydraulic test system at VT	57
Figure 3.9 Flextest 40 controller (series 494) and handset (model: 494.05)	58
Figure 3.10 Comparison of command and response signals at a 4 Hz test speed showing “over-driving” of the command signal	58
Figure 3.11 Customized fixture	60
Figure 3.12 Spherical bearing washers	60
Figure 3.13 Test setup.....	61
Figure 3.14 Moment and axial diagrams for the tests at VT	62
Figure 3.15 Test Setup at VT	63
Figure 3.16 Test Setup at TFHRC	63
Figure 3.17 Test procedure in the MPT	66
Figure 3.18 AutoCAD drawings of weld profiles.....	68
Figure 3.19 Denotation of weld locations.....	68
Figure 3.20 Measured dimensions	69
Figure 3.21 Definition of L_e	70
Figure 3.22 Setup for breaking specimens from fatigue cracks.....	72
Figure 3.23 Typical crack surface.....	73
Figure 3.24 Failure modes: WT@DECK, WT@RIB, and WR.....	74
Figure 4.1 Schematic of the hot-spot stress distribution (DNV CN-30.7).....	78
Figure 4.2 Stress extrapolation in 3D FE Models (DNV-RP-C203)	81
Figure 4.3 Interpolation of stress from the element integration points to the read-points (DNV-RP-C203).....	82
Figure 4.4 Hot-spot stress derivation for element sizes larger than $t \times t$ (DNV-RP-C203)	82
Figure 4.5 Principal stress components and potential fatigue crack orientations (DNV- RP-C203)	84
Figure 4.6 Weld toe type classifications (IIW-1823-07)	85
Figure 4.7 Global geometry of the 2D FE models.....	91

Figure 4.8 Local weld geometry in the 2D FE models	92
Figure 4.9 Mesh for models with Q4/Q8 elements.....	95
Figure 4.10 Mesh for the model with T6 Elements	96
Figure 4.11 Stress read-out lines in the 2D models	97
Figure 4.12 Normal stress on line 1 from different element types	97
Figure 4.13 Normal stress on line 2 from different element types	98
Figure 4.14 Normal stress on line 4 from different element types	99
Figure 4.15 Normal stress on line 5 from different element types	99
Figure 4.16 Normal stress on line 6 from different element types	101
Figure 4.17 Normal stress on line 7 from different element types	101
Figure 4.18 Normal stress on line 3 from different element types	102
Figure 4.19 Meshing schemes for each model.....	103
Figure 4.20 Normal stress on line 1 from different meshing schemes	104
Figure 4.21 Normal stress on line 2 from different meshing schemes	105
Figure 4.22 Normal stress on line 4 from different meshing schemes	105
Figure 4.23 Normal stress on line 5 from different meshing schemes	106
Figure 4.24 Normal stress on line 3 from different meshing schemes	107
Figure 4.25 Modeling of root gaps	109
Figure 4.26 Distributions of maximum principal stress near weld toes	110
Figure 4.27 Normal stress on line 1 from different root gap conditions.....	111
Figure 4.28 Normal stress on line 2 from different root gap conditions.....	111
Figure 4.29 Normal stress on line 4 from different root gap conditions.....	112
Figure 4.30 Normal stress on line 5 from different root gap conditions.....	112
Figure 4.31 Normal stress on line 3 from different root gap conditions.....	114
Figure 4.32 Distributions of maximum principal stress near weld roots	114
Figure 4.33 GM-83 model	115
Figure 4.34 Normal stress on line 1 from different local geometries	116
Figure 4.35 Normal stress on line 2 from different local geometries	116
Figure 4.36 Normal stress on line 4 from different local geometries	117
Figure 4.37 Normal stress on line 5 from different local geometries	117
Figure 4.38 Moment Diagrams for Different Bearing Plate Sizes (in-kips).....	118

Figure 4.39 Normal Stress on Line 1 from Different Bearing Plate Sizes	119
Figure 4.40 Normal stress on line 4 from different bearing plate sizes	119
Figure 4.41 Normal stress on line 2 from different bearing plate sizes	120
Figure 4.42 Normal stress on line 5 from different bearing plate sizes	120
Figure 4.43 Structural stresses according to ttwt method	121
Figure 4.44 Stress read-out lines in 3D models	122
Figure 4.45 Maximum principal stress distribution for BP = 5" (left) and BP = 3.75" (right)	123
Figure 4.46 Maximum principal stress distributions through deck plates (left) and rib plates (right) with 5" wide bearing plate (top) and 3.75" wide bearing plate (bottom) at weld toes	124
Figure 4.47 Normal stress on line 1 with 5" bearing plate	124
Figure 4.48 Normal stress on line 2 with 5" bearing plate	125
Figure 4.49 Normal stress on line 3 with 5" bearing plate	125
Figure 4.50 S-N curves for specimen series (R=-1)	133
Figure 4.51 S-N curves for specimen series (R=0).....	133
Figure 5.1 d_1 as a redundant factor to A_w	144
Figure 5.2 Factor d_1 as a suppressor to the weld penetration factor	146
Figure 5.3 Interactions among weld dimensions on predicting the fatigue life.....	151
Figure 5.4 Mean S-N curves for all specimens.....	158
Figure 5.5 Lower bound S-N curves for all specimens	158
Figure 5.6 Lower bound S-N curves in comparison with proposed curves.....	159

List of Tables

Table 2.1 Designation of specimens (Sim & Uang, 2007)	13
Table 2.2 Test results (Sim & Uang, 2007)	15
Table 2.3 Fatigue test results from Maddox (1974a).....	19
Table 2.4 Fatigue tests between 1974-2000 (Kolstein, 2007)	26
Table 2.5 Comparison of the three basic approaches to fatigue analysis	27
Table 2.6 Fatigue resistance against structural hot spot stress (IIW-1823-07).....	41
Table 3.1 Test specimen series.	55
Table 3.2 Test matrix	56
Table 3.3 Floor-standing load frame specifications (model: 370.50).....	57
Table 4.1 Thickness Correction Exponents (IIW-1823-07)	86
Table 4.2 Average weld dimensions throughout the specimen series	92
Table 4.3 Hot-Spot Stress Results	127
Table 5.1 Types of regression analysis	136
Table 5.2 Outcomes of a hypothesis test	137
Table 5.3 Summary of Model Fitting—All Potential Factors	138
Table 5.4 Summary of Simple Linear Regressions	140
Table 5.5 Models with high overall fit.....	142
Table 5.6 Stepwise model fitting analysis	143
Table 5.7 Combined effect of d_1 and A_w	145
Table 5.8 Combined effect of d_1 and weld penetration	146
Table 5.9 Redundancy within d_1 (1) and A_w (2).....	148
Table 5.10 Cooperative suppression between d_1 (1) and the weld penetration (2).....	148
Table 5.11 Minimum Dimensions for d_1 (in).....	154
Table 5.12 Summary of Model Fitting — Fatigue Test Scenarios	156
Table 5.13 Summary of Model Fitting — All Significant Factors	157
Table B.1 Test Results of GM-80 Series	178
Table B.2 Test Results of FIL Series	179
Table B.3 Test Results of SA-20 Series.....	180
Table B.4 Test Results of SA-40 Series.....	181

Table B.5 Test Results of SA-60 Series.....	182
Table C.1 Test Results of SA-80 Series.....	183
Table C.2 Test Results of OB Series	184
Table C.3 Test Results of UB Series	185
Table D.1 Weld Dimensions of GM-80 Series.....	186
Table D.2 Weld Dimensions of FIL Series.....	194
Table D.3 Weld Dimensions of SA-20 Series	198
Table D.4 Weld Dimensions of SA-40 Series	202
Table D.5 Weld Dimensions of SA-60 Series	206
Table D.6 Weld Dimensions of SA-80 Series	210
Table D.7 Weld Dimensions of OB Series	217
Table D.8 Weld Dimensions of UB Series	225
Table E.1 L_c Values	233
Table F.1 Location of Tack Welds and Crack Initiation Points	235

Chapter 1. Overview

1.1 Background

Many steel orthotropic bridge decks have been built over the last 60 years in Europe, United States, Japan, and many other countries. The origin of this bridge deck type dates back to the “orthotropic plate” patent issued in Germany in 1948 (Sedlacek, 1992). The major advantages of steel orthotropic decks include their light weight, rapid erection, and easy assembly. The original patent claimed that the steel consumption could be reduced by half. With these advantages, orthotropic bridge decks have been widely used on long-span highway bridges, movable bridges, cable-stayed bridges, and suspension bridges due to their light weight. They also have been used on other types of bridges where fast construction is desired, such as temporary bridges and bridges in high population density areas. Orthotropic steel decks are also a common solution for re-decking old bridges due to their easy assembly. Wolchuk (2001) gives a summary of the guidelines for using steel orthotropic decks in re-decking bridges.

A steel orthotropic deck typically consists of a steel deck plate with welded stiffeners or ribs parallel to each other in the longitudinal direction. Transverse cross beams are typically used to support the ribs and provide stiffness in the transverse direction. The transverse cross beams typically serve as floor beams transferring the deck loads to the main structure. These floor beams are often integrated with the deck structure where the top flanges of the floor beams are often formed by the deck plate itself. The stiffening ribs can be open shapes such as plates, inverted T-sections, angles, and channels or closed box-type ribs with different geometric shapes; trapezoidal closed ribs are the most common. Figure 1.1 gives an illustration of a typical trapezoidal close-rib steel orthotropic deck panel. The first orthotropic steel deck with closed ribs was constructed in Germany in 1954. Compared to open stiffeners, the closed ribs have many advantages. First, closed ribs can transfer the traffic load much more efficiently in the transverse direction. As a result, closed ribs can have wider spacing than open ribs. This results in fewer ribs and therefore lighter weight compared to open rib systems. Second, closed

ribs can provide much higher flexural and torsional rigidity in the longitudinal direction allowing longer spans to be achieved. In other words, fewer cross-beams are required, thereby reducing the deck self-weight and the number of welds associated with the cross-beams. Lastly, since single-sided welds are used to attach the closed ribs to the deck versus double-sided welds for open ribs, the number of rib-to-deck welds is reduced by half. However, the one-sided welds cause quality control and inspection issues which can be a disadvantage for closed ribs.

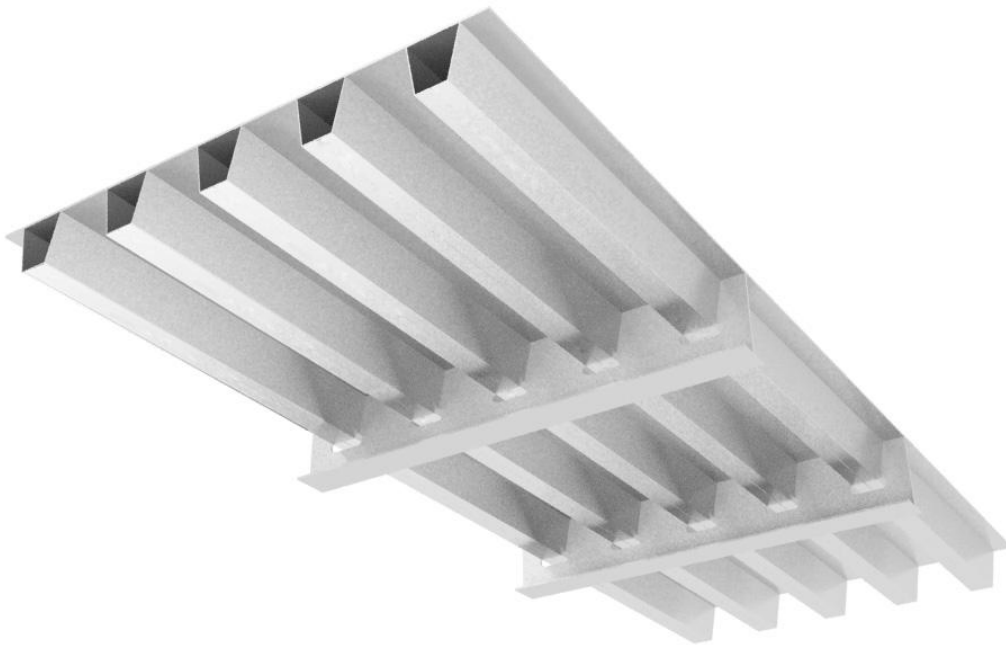


Figure 1.1 Typical close-rib steel orthotropic deck panel

To overcome the disadvantages of one-sided welding and prevent premature fatigue failure, more careful consideration is needed to design rib-to-deck welds. Many of the earlier vintage orthotropic decks with closed ribs experienced fatigue cracking problems. There was a lack of knowledge about fatigue and a lack of guidance in the structural design codes. The complex stress state present at the rib-to-deck welds makes fatigue design even more difficult. Many orthotropic decks before late 1970s were constructed

under this state of knowledge. The quest for lighter self-weight led to relatively thin deck plates in the structural design. However, many of the designs with thinner deck plates were vulnerable to high local stress effects from wheel loads. The contribution of the wheel-load effect was not fully considered in early deck designs and many bridges experienced fatigue cracking problems. Compared to main structural members, orthotropic steel decks tend to have a higher incidence of fatigue problems because of the local effects of wheel loads. Wheel loads cause large local stress variations, stress reversals, and an increased number of stress cycles that must be considered in fatigue design.

Steel orthotropic decks have been part of engineering practice and extensively studied in Europe for decades. Partially due to the use of relatively thin deck plates, premature fatigue cracking was observed in many European countries (Mehue, 1981, 1990, 1992; Burdekin, 1981; Leendertz, 2003). Steel orthotropic decks have also been widely constructed in the United States with mixed experiences relating to fatigue behavior. The situation has been steadily improving as more knowledge becomes available on how to improve fatigue resistance. Eurocode 3 and the AASHTO bridge design code currently have similar fatigue design philosophy and detailing requirements for rib-to-deck welds which employ the traditional nominal stress based design concept. Experience has led to an 80% minimum weld penetration requirement for one-sided welds to control fabrication 165 in service. Kolstein (2007) has recently studied rib-deck weld performance and has proposed revisions to Eurocode 3. Guidelines for fatigue design of rib-to-deck welds have also been proposed by Det Norske Veritas (DNV) and the International Institute of Welding (IIW). There are differences in welding processes, workmanship, material properties, detail classification, and plate thickness between US and European practice. Therefore, not all of the guidance developed for European practice can be directly used in the US.

1.2 Objectives

The present project involves experimental fatigue testing of orthotropic deck specimens performed at both the Federal Highway Administration's Turner-Fairbank Highway

Research Center and the Structures Laboratory at Virginia Tech. The goal is to provide recommendations on both design methods and fabrication detailing to provide adequate fatigue resistance of the rib-deck weld commonly utilized in the U.S. The effects of different weld geometric dimensions are studied to optimize the weld shape and size and fatigue data is collected to develop S-N curves for the design of rib-to-deck welds under different loading scenarios.

The first objective is to determine the effect of weld process and geometry on the fatigue resistance of the rib-deck weld. This is accomplished by fatigue testing a series of 95 specimens with different welding processes (GMAW and SAW), different levels of weld penetration (45.4% to 96.5%), under two different loading regimes. A statistical analysis of the data is used to determine the effect each variable has on fatigue resistance. The data can then be classified into fatigue resistance curves (S-N curves) for use in design. In other words, rib-to-deck welds with different welding process, workmanship and failure modes can be classified into appropriate fatigue design categories if nominal stress is calculated.

The second objective is to investigate methodologies for calculating stress ranges through finite element analysis that can be associated with the S-N curves. The “hot-spot” stress based method will be investigated to determine how it can be applied to the complex stress state present in the rib-deck weld. Currently both Eurocode 3 and AASHTO code still utilize the nominal stress range approach to generate S-N curves that include the effects of geometry and welding process. This approach requires full-scale testing where the detail geometry, residual stresses, and other effects are included in the resistance curves. Nominal stress is easy to understand and feasible to calculate manually, but it is accurate only when the structure has relatively simple geometry and loading conditions. The development of computer-aided stress analysis enables a better understanding of the local stress occurring at details. Finite element analysis can determine local stress values at weldments. The “hot-spot” method has been developed by research to compare the local stress to a fatigue master curve for design. Therefore, new master S-N curves need to be established or selected for comparison to finite-element-based hot-spot stress values. Standardized hot-spot methodologies have been proposed utilizing hot-spot S-N

curves and a standardized method of calculating the hot-spot stress. (DNV, 2008; Hobbacher, 2008).

Another objective of this research is to optimize the size and shape of rib-to-deck welds as the basis of the detailing requirements. Currently it is common practice in the United States to produce partial penetration rib-to-deck welds with a minimum penetration of 80% into the rib plate. For the upper bound, the welds cannot have “blow-through” or “melt-through” that creates defects inside the ribs. In reality, due to the thin rib plate thickness that is commonly used in steel orthotropic decks, 80% penetration without melt-through or blow-through is difficult to achieve. A more tolerant penetration requirement is needed to reduce the need for weld repairs and increase fabrication efficiency. However, any relaxation of the 80% penetration must not increase the potential for fatigue cracking.

1.3 Approach

Fatigue design of the rib-to-deck weld is more complicated compared to the AASHTO fatigue design procedures for most bridge members. The AASHTO methodology relies on calculating a far-field stress range that ignores any local stress concentration effects close to welded details. The stress ranges are caused by the overall truck loading event on the bridge. This contrasts with the rib-to-deck weld where local wheel load effects combine with the global truck event loads to create a complicated stress state. Because the rib-to-deck weld is typically a one-sided partial penetration weld, a crack-like defect exists at the root notch. Classical elastic stress analysis using solid mechanics encounters a singularity problem at the crack tip. The local stress effects and the crack tip singularity cannot be readily analyzed using the far-field stress range approach. Therefore, alternative approaches need to be established to analyze the fatigue resistance of the rib-to-deck weld. This section provides a brief overview of several alternative approaches that are currently available, with an emphasis on those chosen for study in this research.

Fatigue resistance is typically characterized into S-N curves where fatigue test data is plotted based on the stress range (S) and the number of cycles to failure (N) on a

logarithmic scale, the fatigue data can be characterized by a straight line relationship for metallic materials. If the live load stress range is known at the detail, this relatively simple straight line relationship can be used to predict the number of cycles needed to cause fatigue failure. In fatigue assessment, the stress range values are calculated and used to predict the fatigue life, while in fatigue design the required number of service load cycles is used to determine the allowable stress range. The S-N curve is determined experimentally by performing logarithmic linear regression on test data developed at different stress ranges. Different welded details will have different S-N curves; therefore the curves need to be developed individually for each detail type. When fatigue resistance of a new type of structural detail needs to be evaluated, new fatigue tests need to be conducted to establish the S-N curve. Alternative approaches have been developed where a locally calculated stress range is compared to a master S-N curve for the fatigue resistance of all weldments. Two alternative approaches, the notch stress approach and the hot-spot stress approach, are investigated in this study.

Fracture mechanics is an alternative approach to theoretically understand fatigue and fracture. The discipline of fracture mechanics was initially developed in the 1940's and has seen widespread application since. The fracture mechanics approach determines the fracture resistance as a material property (toughness) and compares this to the stress intensity determined by the flaw size and applied stress. Linear elastic fracture mechanics (LEFM) is usually applied to brittle fracture and fatigue crack growth problems while more advanced elastic-plastic fracture mechanics (EPFM) and limit load theories are required for ductile fracture problems. A brief introduction of fracture mechanics is made in Section 2.2.

The traditional S-N curve methodology is used in this study for two reasons: 1) the fracture-mechanics-based approaches based on predicting crack growth rates require assumptions of the flaw size. It is difficult to assess the microscopic flaw size in bridge welds since it depends on the welding procedure design and quality control; and 2) Fatigue assessment using the crack growth approach depends on numerical integration of a stress intensity factor equation that can only be approximated for the rib-to-deck weld.

To perform S-N curve analysis, both the stress range and the number of cycles to failure need to be obtained. The stress range can be calculated using the structural stress approach (“hot-spot” stress approach), which requires finite element modeling (FEM) of the welded structure. Because the local stress predicted by FEM is dependent on the element type and mesh density, the linear surface extrapolation (LSE) method is applied. While this still requires special considerations for element type and mesh density, the results are largely mesh insensitive. Welds can be included or excluded in the modeling methodology. The detailed hot-spot stress analysis methodology and implementation of the LSE method are introduced in Section 2.2.1 and Chapter 4.

The full-scale small specimen fatigue test specimen is used in this study to establish S-N curves for the rib-to-deck weld. These specimens were cut from full-scale weldments fabricated with different welding processes and procedures. The specimens are cyclically loaded in special fixtures that allow load reversal to be applied to the specimens. The number of cycles to failure was recorded and used to develop S-N curves using linear regression. The testing was performed both at the FHWA Turner-Fairbank Highway Research Center in McLean, Virginia and in the Thomas Murray Structures Laboratory at Virginia Tech. More information on the specimen preparation, test equipment, loading configuration, and testing procedure is presented in Chapter 3. Similar fatigue tests conducted by other researchers can be found in Section 2.1.

After obtaining results from both the fatigue tests and the finite element modeling, S-N curves were developed for each specimen group with a particular weld type and loading scheme. Different parameters were measured to characterize the different welds and weld groups, including the weld dimensions, R-ratio, failure mode, and root gap openness. Statistical tools were utilized to analyze the effect these parameters have on fatigue resistance. Two types of statistical analysis were performed. Multiple linear regression (MLR) was performed to determine the effect of various weld dimensions on the fatigue resistance. Multi-way analysis of covariance (ANCOVA) was also performed to study the effect of the failure mode, R-ratio, and root gap openness. Analyses and conclusions are discussed in Chapter 5.

Chapter 2. Literature Review

The first research related to the fatigue design of steel orthotropic decks was carried out in 1976 under the working group “Dynamic Loads on Bridges” founded by the European Coal and Steel Executive Committee F4 (Haibach, 1991). The purpose of this working group was to experimentally study the fatigue strength of the weld details in steel orthotropic decks and to provide guidelines for the analysis of traffic-induced stresses in orthotropic decks. Multiple research projects were performed by this working group between 1976 and 1994. First, the traffic-induced stress distribution in the decks was measured in a series of bridges. These measured stresses were recreated in experimental tests. This work became the foundation of the Eurocode 1, Part 3 “Traffic Loads on Bridges” (ENV 1991-3, 1995). Fatigue behavior of steel orthotropic decks under simulated loads was then studied to assess the fatigue performance of different details in the deck. S-N curves for these details were proposed based on the nominal stress range. Recommendations for detailing were also developed. This work ultimately led to the provisions in Eurocode 3 “Design of Steel Structures”, Part 1.9 “Fatigue” (EN 1993-1-9, 2005).

2.1 Fatigue Tests of Rib-to-Deck Welds on Steel Orthotropic Decks

There have been multiple research studies on the fatigue performance of rib-to-deck welds on steel orthotropic decks. Fatigue test data had been generated in different research projects to establish reliable S-N curves for different weld details on an orthotropic steel bridge. The fatigue tests can be roughly categorized into three levels. First, small scale tests have been performed to understand the fatigue behavior of welds, especially under bending loads. These test specimens usually only include the local structural details and do not include the overall deck system behavior. The specimens are subjected to idealized loading conditions and the resulting stress patterns that are not necessarily the same as those in actual decks in service.

Second, fatigue tests using specimens cut from full-scale rib-deck weldments have been performed to study the fatigue performance of rib-to-deck welds under more realistic

loading conditions. Individual small-scale test specimens are cut from a full-scale weldment consisting of a single rib attached to a strip of deck plate. Concentrated loads are applied to the specimens on either the top of the deck plate or the bottom of the rib plate. Various supporting configurations can be applied in order to simulate the stress fluctuations measured in actual decks. One major advantage of this test type is that it allows long weld lengths to be cumulatively sampled under identical loading conditions. This contrasts to full size test panels under a wheel load where only a very localized area under the wheel load is subjected to maximum stress conditions. Since the fatigue resistance of welded details is usually governed by the presence of “weak-link” defects, sampling longer weld lengths provides a more accurate measure of fatigue resistance. One disadvantage is that it is not possible to recreate all aspects of the local stress state in the test specimens. Despite these trade-offs, full-scale, small-specimen tests are relatively feasible to fabricate and test in large numbers to generate statistically significant data sets for comparison of different testing variables.

Third, large-scale tests using full-size orthotropic steel deck panels have also been performed by several researchers. Real or simulated traffic loads are applied on the deck panels to create stress distributions that closely match conditions measured in actual decks in service. These tests include the structural system effects of the decks and produce the most realistic stress field at the test details. However, they are very costly to perform and only small regions of the panels are subjected to the maximum wheel load effects. This type of test is most useful to investigate other details in the orthotropic deck system such as the rib-to-floor beam connections.

2.1.1 Full-Scale Panel Tests

Two suspension bridges in New York City, the Williamsburg Bridge and the Bronx-Whitestone Bridge, experienced rehabilitation during 1991-2008. The rehabilitation process involved the replacement of the original concrete-filled steel grid decks with lighter-weight steel orthotropic decks completed in 1998 and 2003, respectively. Prior to completion, experimental research including both field tests and full-scale laboratory tests was performed to validate the fatigue performance of the deck design. The tests led to modified final designs for the steel orthotropic decks to maximize fatigue resistance.

Field tests were conducted on both two bridges and laboratory tests were conducted in Lehigh University's Center for Advanced Technology for Large Structural Systems (ATLSS) Engineering Research Center (Connor & Fisher, 2000).

A series of field tests on the Williamsburg Bridge was performed first through 1997-1999, providing information of stress distribution under truck loads to provide recommendations to the AASHTO LRFD fatigue provisions. (Connor & Fisher, 2000). Stain gages were installed on the diaphragm and bulkhead plates where it was considered to be critical to fatigue failure (Figure 2.1). Both low speed crawl tests (5 mph) and high speed dynamics tests (24 mph and 43 mph) were carried out before and after the application of the wearing surface. A number of conclusions resulted from the field test: 1) The wearing surface had little effect on the stress range in the diaphragms and ribs but reduced the stress range in deck plate by 15%~25%; 2) deck response under both the crawl and dynamic tests were almost identical, therefore truck speed did not affect the peak measured stress range; 3) the stress cycle was dominated by in-plane stresses transverse to the ribs in the diaphragm; and 4) the magnitude of the measured stress ranges exceeded the values obtained from finite element modeling. These tests also showed that the number of stress cycles per truck passage exceeded the number predicted by the AASHTO LRFD fatigue design provisions.

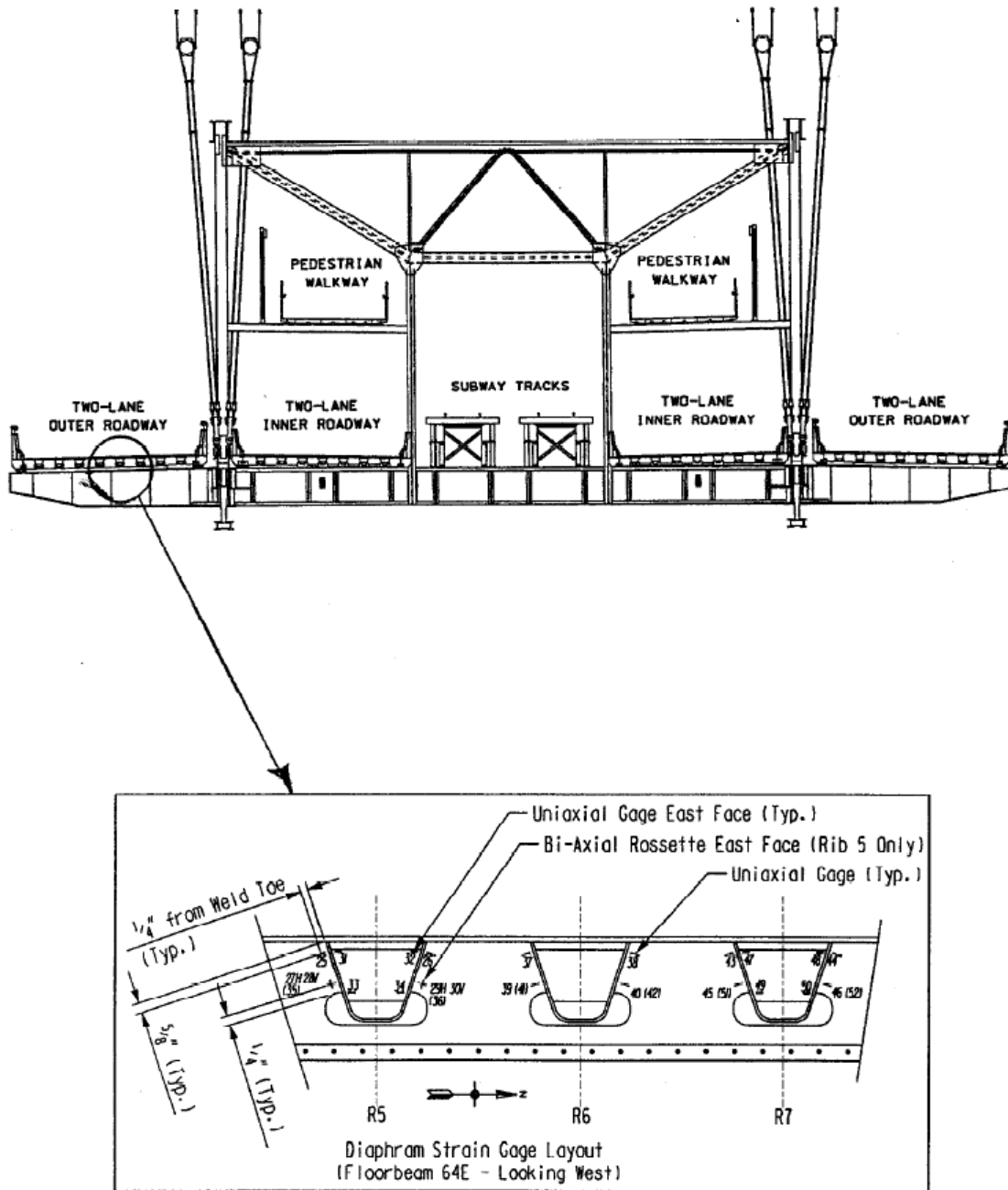


Figure 2.1 Typical strain gage layout on the diaphragm (Connor & Fisher, 2000)

Two laboratory tests with prototype deck panels, supporting fixtures, and loading conditions similar to the two bridges were carried out at ATLSS during 1995-1998 and 2001-2002, respectively. The first test aimed at recovering the behavior of the Williamsburg Bridge while the second test aimed at the Bronx-Whitestone Bridge (Tsakopoulos & Fisher, 2003, 2005). Strain gages were installed at multiple locations on

the two deck panels. The same strain gage locations in the field tests were included in the laboratory tests to allow direct comparison between the results from field tests and laboratory tests. The primary objective was to experimentally evaluate the fatigue performance of the proposed deck design with a primary focus on the rib-to-diaphragm joint design. A broader purpose was to determine the appropriate fatigue design categories for different welded details in the deck. Two rib-to-diaphragm joint design schemes were tested. One (“Option B”) followed the guidelines in the 1994 AASHTO LRFD Bridge Design Specification; an alternative (“Option A”) was proposed to provide higher fatigue resistance. In Option B the rib and diaphragm plates were connected together by back-to-back fillet welds terminated 6 mm away from the cutouts on diaphragm plates, while the welds in Option A consisted of 102-mm-long full-penetration groove welds starting from the cutout followed by back-to-back fillet welds for the remainder. The rib-to-deck weld was not of major concern in this study so it was only investigated in the second test. The fabrication of rib-to-deck welds also followed the guidelines in the AASHTO LRFD Bridge Design Specification, aiming at partial penetration welds with at least 80% penetration into the rib plate. The edges of rib plates were beveled prior the welding process.

The results from the first test showed nearly identical stress ranges with the field test on Williamsburg Bridge at the same strain gage locations under simulated loads, which is a good validation of the laboratory test setup. It was found that the fatigue resistance of the Option B welds was insufficient. The fatigue resistance was determined to be Category E compared to Category D that is predicted by the AASHTO specifications. On the other hand, the Option A welds exhibited satisfactory fatigue performance characterized as Category C. Regarding the rib-to-deck welds, the measured weld penetration varied between 71% and 91% for the 64 cross-sections examined in the first test. Seventy percent of them satisfied the 80% minimum penetration requirement. For the second test, the measured weld penetration varied between 61% and 96% for the 62 cross-sections examined. Four longitudinal fatigue cracks initiated from the weld root into the deck plate. The cracks were located directly under the wheel load patch used for loading in the laboratory. Since this was considered more severe than loading conditions present in actual bridge decks, the overall fatigue performance of the rib-to-deck welds was

considered to be adequate without further investigation.

Another full-scale steel orthotropic deck panel test by Sim & Uang (2007) was carried out to investigate the effect of fabrication procedures and weld melt-through. Six, 2-span, 10m×3m full-scale steel orthotropic deck panels were tested with different combinations of distortion control measures and weld penetrations. Three of the six test specimens were heat-straightened to remove welding distortion prior to testing. The other three were also pre-cambered. Three weld penetration profiles were studied as indicated in Table 2.1. . A primary purpose of the testing was to determine the effect that the melt-through has on fatigue resistance. Out-of-phase loads were applied at the center of each of the two spans up to 8 million cycles to simulate the load effect induced by a moving truck. Finite element models were built and analyzed prior the tests to determine strain gage locations. 3-D shell element models with six degrees of freedom per node were used. Figure 2.2 shows the geometry and loading pattern for the finite element models; this also serves as a good illustration of the test specimens.

Table 2.1 Designation of specimens (Sim & Uang, 2007)

	Without Pre-camber	With Pre-camber
80% penetration welds without melt-through	Specimen 1	Specimen 4
100% penetration welds with continuous melt-through	Specimen 2	Specimen 5
Alternating 80% and 100% penetration welds every meter	Specimen 3	Specimen 6

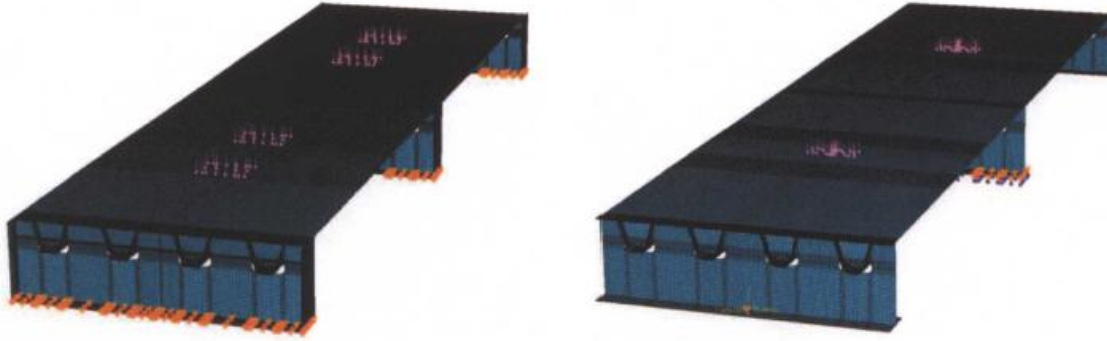
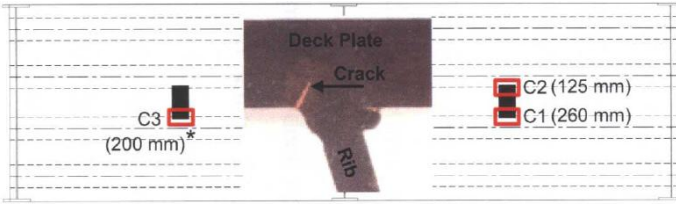
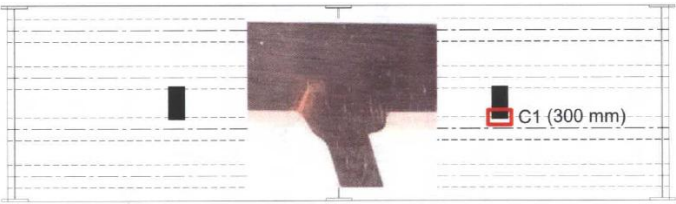
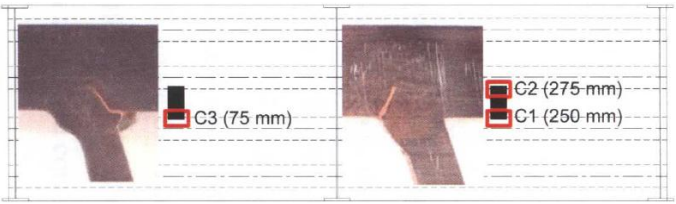


Figure 2.2 Finite element models for specimen 1 (left) and specimen 2-6 (right)

(Sim & Uang, 2007)

The test results showed that the melt-through had a negative effect on the fatigue performance, while the pre-cambering had a positive effect on the fatigue performance of rib-to-deck welds. Table 2.2 shows the test results from all specimens. Observing the failures, only one crack out of seven initiated from the weld root propagating into the deck plate. The six remaining fatigue cracks occurred at the weld toes on the rib plates. This result was somewhat unexpected; cracking was expected from the melt-through areas of the weld root. The only fatigue crack that initiated from the weld root was on Specimen 6; it was located at the transition point between the 80% and 100% penetration lengths of the weld. Considering a melt-through is more likely to take place accidentally rather than continuously in the actual deck fabrication; a transition point is likely to present when a melt-through occurs. Therefore it was suggested that melt-through should be prevented.

Table 2.2 Test results (Sim & Uang, 2007)

Welding Process	Without Pre-cambering	With Pre-cambering
Rib-to-deck welds with 80% penetration without melt-through	Specimen 1: no cracks	Specimen 4: no cracks
Rib-to-deck welds with 100% penetration with continuous melt-through	<p>Specimen 2: 3 cracks at C1, C2 and C3</p> 	Specimen 5: no cracks
Rib-to-deck welds with alternating 80% and 100% penetration every meter	<p>Specimen 3: 1 crack at C1</p> 	<p>Specimen 6: 3 cracks at C1, C2 and C3</p> 

* Length of the crack

Pre-cambered specimens did not experience any fatigue cracks at rib-to-deck welds except Specimen 6 which was considered to be insufficiently pre-cambered. It was therefore concluded that pre-cambering was beneficial to the fatigue performance of rib-to-deck welds. It is noted that several fatigue cracks occurred at the rib-to-bulkhead fillet welds on Specimen 1. Six large fatigue cracks developed at rib-to-bulkhead fillet welds on end supports, and it is believed they initiated earlier than one million cycles.

2.1.2 Single-Weld Tests

One advantage of full-scale deck panel tests is that many different details and possible failure modes can be tested simultaneously. However, this can also be a detriment for some purposes since the behavior of a specific weld or failure mode cannot be isolated and the number of data points for forming S-N curves is limited. A better way to study the behavior of a certain weld detail is to use full-scale, small-specimen tests with a single welded detail under idealized loading. Maddox (1974a) conducted a series of tests in this fashion.

Specimens with 11 mm deck plate and 6.35 mm rib plate thickness were welded together manually. Ten specimen series with 5 different configurations (Figure 2.3) were tested to investigate various parameters. The R-ratio of minimum stress/maximum stress was applied differently to each series to create different loading scenarios.

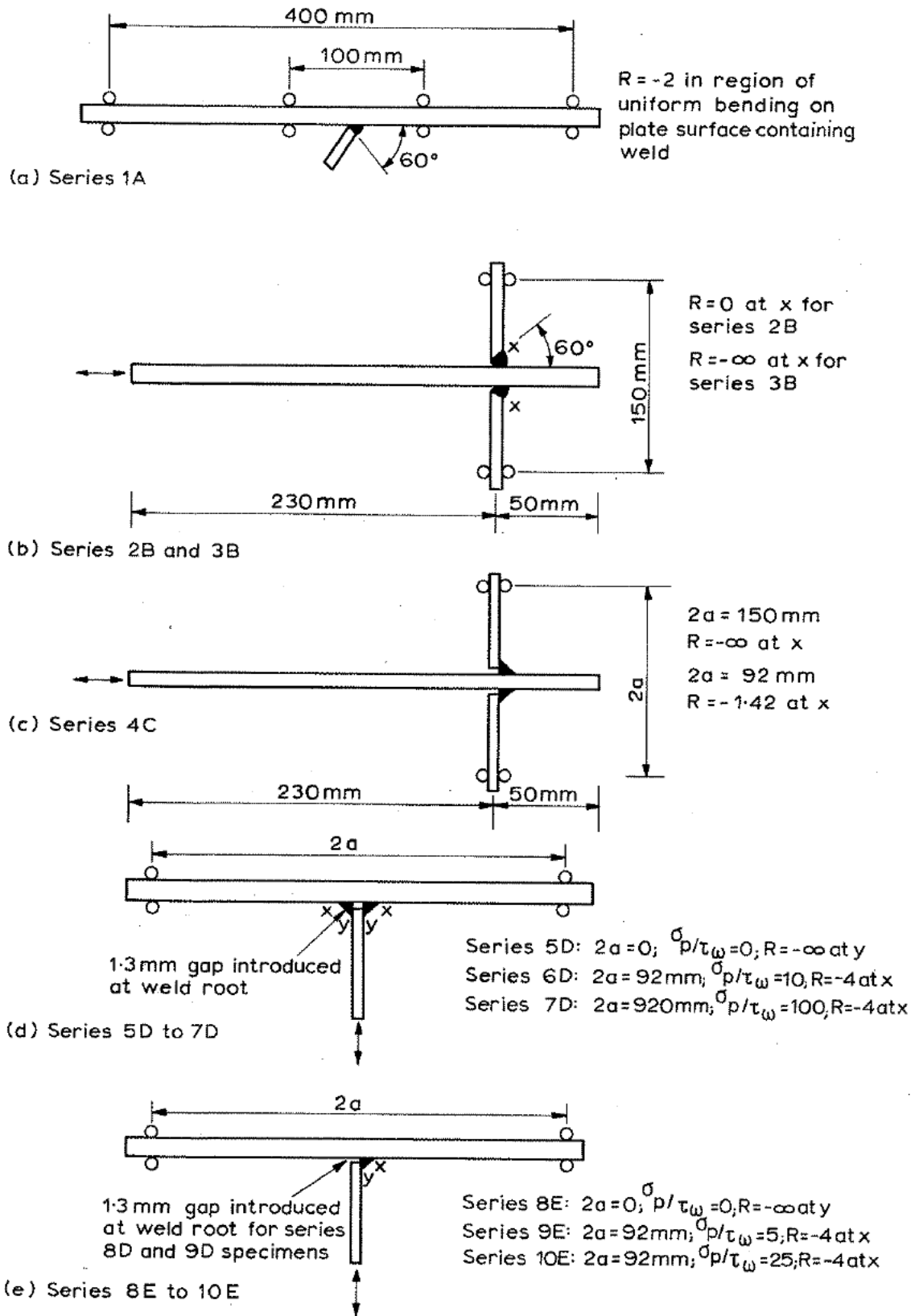


Figure 2.3 Test configurations (Maddox, 1974a)

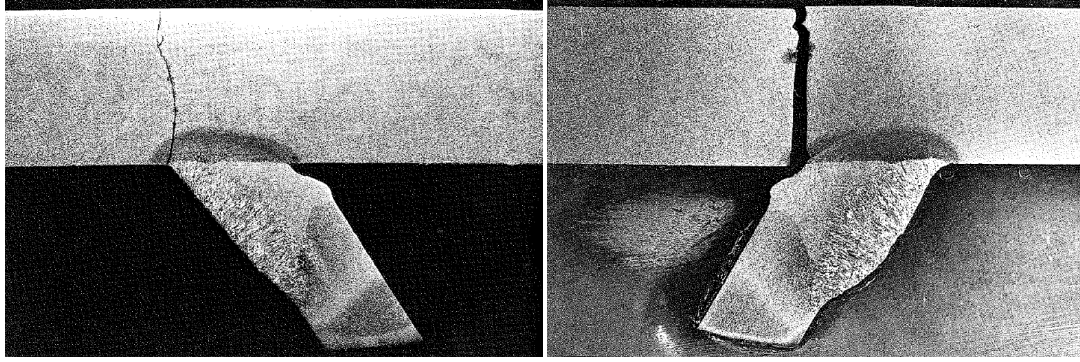


Figure 2.4 Failure modes in series 1A (Maddox, 1974a)

Test series 1 through 4 investigated the fatigue performance of rib-to-deck welds under bending stresses. Three different specimen types were loaded at four different R-ratios. Series 1A simulated the rib-to-deck weld under pure bending. This is the primary loading expected for the rib-to-deck weld in regions not directly affected by wheel loads. Partial penetration butt welds with a 60° edge bevel were used in this series. Series 2, 3 and 4 followed the same configuration but were loaded under different R-ratios. Series 2B and 3B used partial penetration butt welds with $R=0$ and $R=-\infty$, respectively, to generate fully tensile or compressive stress ranges at the weld toes on the stiffeners. This created an inverse stress range at the weld root. Series 4C was fabricated with fillet welds and was loaded similar to series 3B, except for a modification of the distance between the supports. As a result, series 1A exhibited two failure modes with fatigue cracks initiated from either weld toes or weld roots but the majority failed at weld roots (Figure 2.4). Both failure modes had similar fatigue resistance. Specimens in series 2B and 3B, as expected, all failed at either weld toes on the stiffeners or weld roots, respectively. Series 4C had the same failure mode with series 3B but with slightly less stress cycles (Table 2.3). It was concluded that generally R ratio had little influence on the fatigue life.

Table 2.3 Fatigue test results from Maddox (1974a)

Specimen Number	R-ratio	Stress Range, N/mm ²	Cycles to Failure	Failure Description
1A/1	R=-2 at weld toe	300	447,000	Crack propagation from weld toe Crack present at weld root
1A/2	R=-2 at weld toe	285	458,000	Crack propagation from weld root
1A/3	R=-2 at weld toe	253	523,500	Crack propagation from weld root
1A/4	R=-2 at weld toe	240	378,000	Crack propagation from weld root Crack present at weld toe
1A/5	R=-2 at weld toe	227	1,772,000	Crack propagation from weld root
1A/6	R=-2 at weld toe	193	1,943,000	Crack propagation from weld root
2B/1	R=0 at weld toe	304	250,000	Crack propagation from weld toe
2B/2	R=0 at weld toe	250	3,000,000 (unbroken)	Crack propagation from weld toe
2B/3	R=0 at weld toe	277	1,250,000	Crack propagation from weld toe
2B/4	R=0 at weld toe	270	2,000,000	Crack propagation from weld toe
2B/5	R=0 at weld toe	289	310,000	Crack propagation from weld toe
2B/6	R=0 at weld toe	279	582,500	Crack propagation from weld toe
3B/7	R=0 at weld root	139	3,400,000 (unbroken)	Crack propagation from weld root
3B/8	R=0 at weld root	160	945,500	Crack propagation from weld root
3B/9	R=0 at weld root	199	290,500	Crack propagation from weld root
4C/1	R=0 at weld root	314	74,000	Crack propagation from weld root
4C/2	R=0 at weld root	289	168,000	Crack propagation from weld root

Series 5 through 10 tested the rib-to-crossbeam welds under combined bending stress and shear stress. Different shear stress/bending stress ratios were applied as shown in Figure

2.3. The effect of root gap openness was also studied. The results showed the fatigue resistance of fillet welds was insensitive to shear stress; bending stress was the dominant cause of cracking. Also, the root gap openness had an obvious effect on the failure mode. For the specimens with single-sided welds (9E & 10E), fatigue cracks initiated and propagated through the weld throat if a root gap was present. The cracks initiated and propagated into the deck plate if a root gap was not present. All cracks initiated from weld root.

2.1.3 Full-Scale Single-Rib Tests

Maddox (1974b) carried out another experiment involving fatigue tests of single-rib steel orthotropic deck segments to investigate the fatigue performance of the rib-to-deck weld. Manual welds with a leg size of 6 mm were produced to connect the 6.35 mm thick rib plate and 11 mm thick deck plate. The dimensions of the specimens are shown in Figure 2.5. The specimens were tested under three different loading scenarios to study the effects of R-ratio and residual stresses, as shown in Figure 2.6.

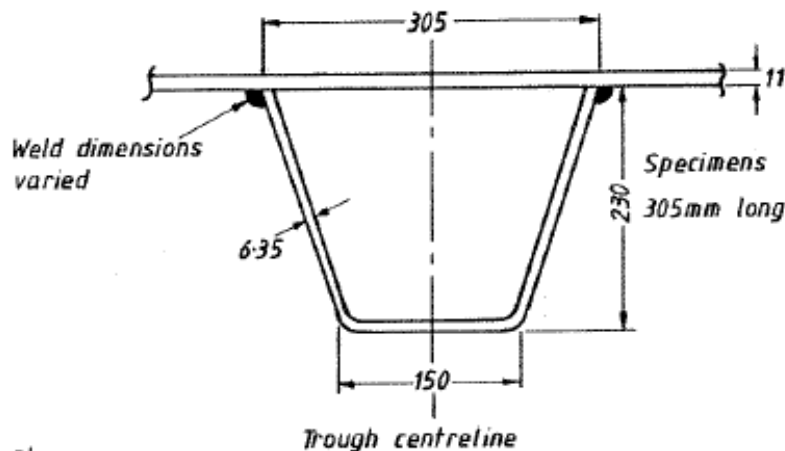
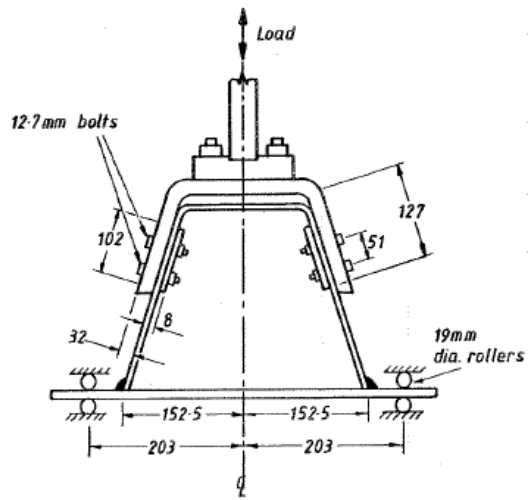


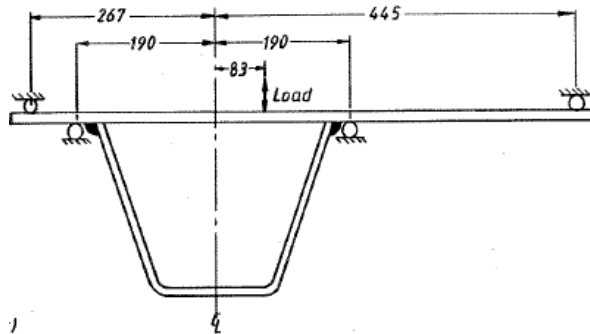
Figure 2.5 Dimensions of specimens (Maddox, 1974b)

Two specimen series (0/1/- & 0/2/-) were tested under the loading configuration shown in Figure 2.6 (a) with $R=-1$ and $R=0$, respectively. The purpose of these test series was to test the fatigue resistance of the weld toe on the deck plate. However, all specimens failed at the weld root with fatigue crack propagating through the weld throat. This was attributed to the bending stress induced by distortion of the rib plate.

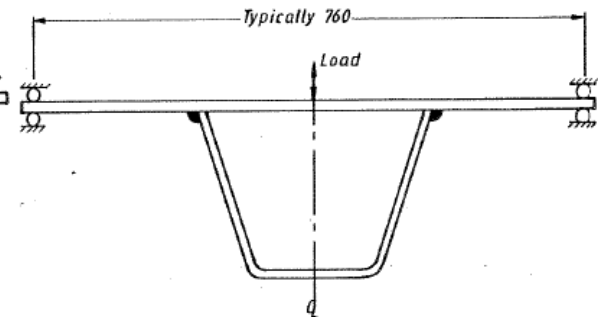
The loading configuration shown in Figure 2.6 (b) was used to create a realistic stress ratio at both the weld toe on the deck plate ($R=-8.75$) and the weld toe on the rib plate ($R=-1.42$). However, it was impossible to achieve the two target R ratios simultaneously, so two different testing series were required. Series A/1/- was tested at $R=-8.75$ for the deck plate resulting in an R-ratio ranging between -1.73 and -8.3 in the rib plate. Series A/2/- was tested at $R=-1.42$ for the rib plate resulting in an R-ratio ranging between -1.67 and -6.4 in the deck plate. There was no significant disparity between the results from the two test series. Again, all specimens failed through the weld throat from the weld root. The test data were plotted by Kolstein (2007) based on the stress range at the weld toe on the deck plate (Figure 2.7). The comparison between these two data sets revealed that the residual stress played an important role in the fatigue performance. The magnitude of the tensile residual stress was believed to be high enough to overwhelm the influence of R-ratio, thereby converting the compressive portions of the applied stress cycle into tension.



(a)



(b)



(c)

All units in mm

Figure 2.6 Loading scenarios (Maddox, 1974b)

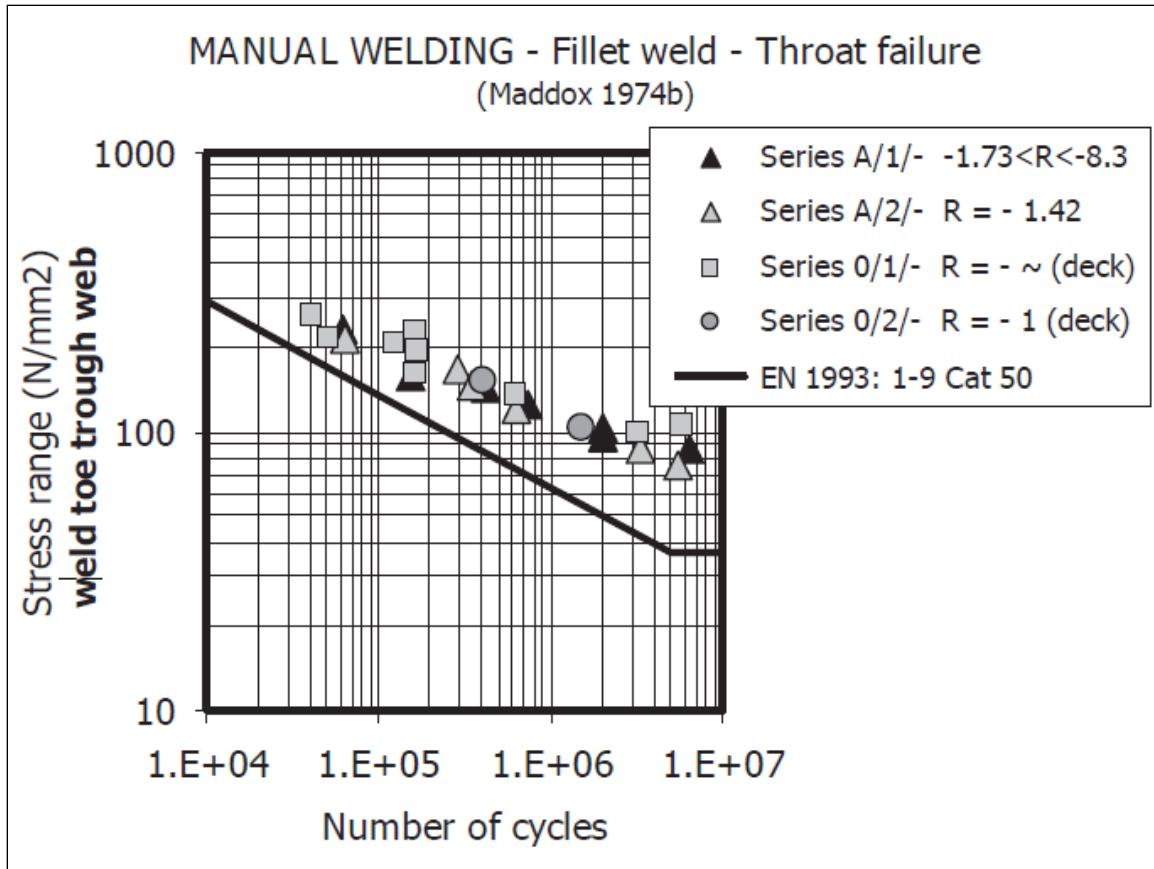


Figure 2.7 Influence of R-ratio (Kolstein, 2007)

Three additional specimen series (B/-, C/- and D/-) were tested to further study the effect of residual stresses under the same loading configuration and R-ratio used for Series A/2/-. Each series was spot-heated in a distinctive way to introduce different residual stress patterns. The results were compared with Series A/2/- but still little disparity was observed (Figure 2.8).

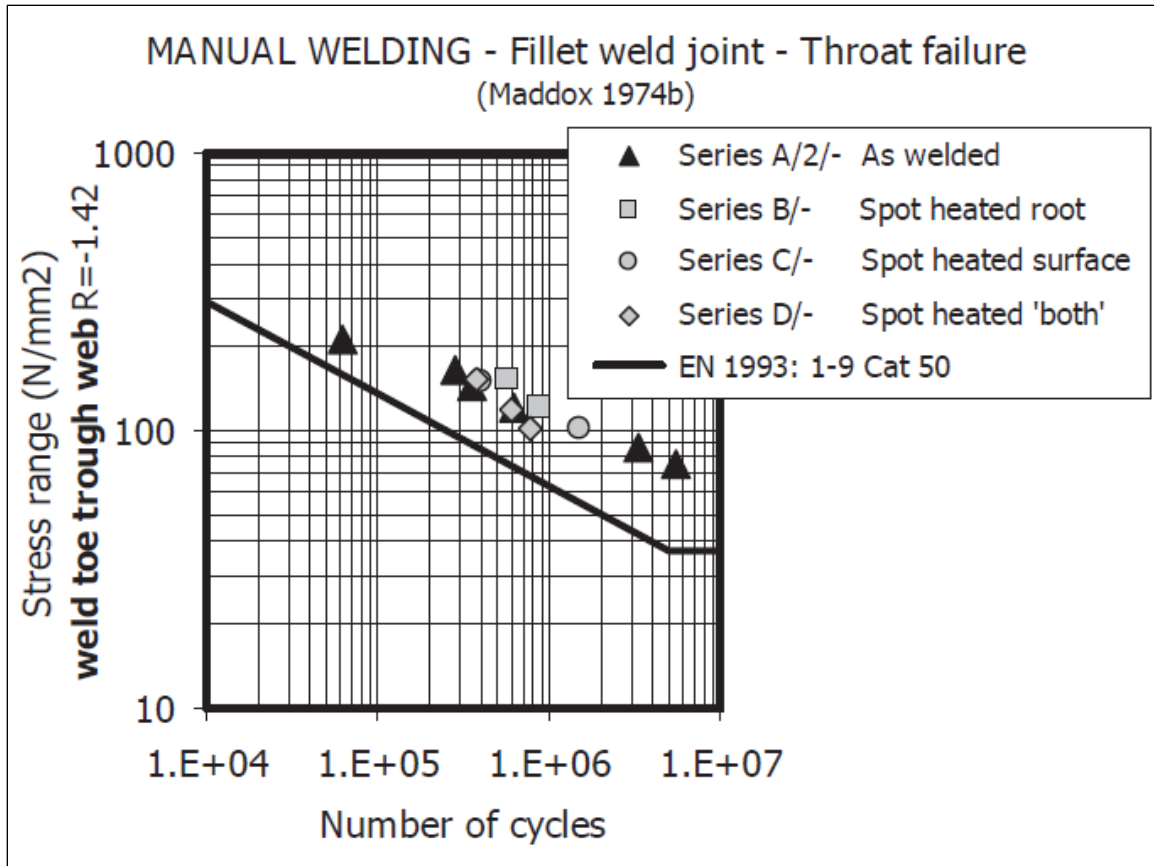


Figure 2.8 Influence of the spot-heating (Kolstein, 2007)

The third loading scenario shown in Figure 2.6 (c) applied a concentrated load at the center of the deck plate. Two specimen series (E/1/- & E/2/-) were tested under this loading scenario to study the effect of root gap openness on the fatigue performance of the weld root. By setting $R=-\infty$ at the weld root for series E/1/-, the stress cycle closed the root gap although residual stresses kept the stress cycle partially or fully in tension. For series E/2/-, the R-ratio was set to 0 to produce gap opening over the entire stress cycle. The test results showed that it was beneficial to have closing gap cycles since 4 out of 6 specimens in series E/1/- failed at weld toes on rib plates. The fatigue life of this series was also slightly longer than the average of series A/-/. The fatigue life of series E/2/- fell on the lower bound of the average (Figure 2.9).

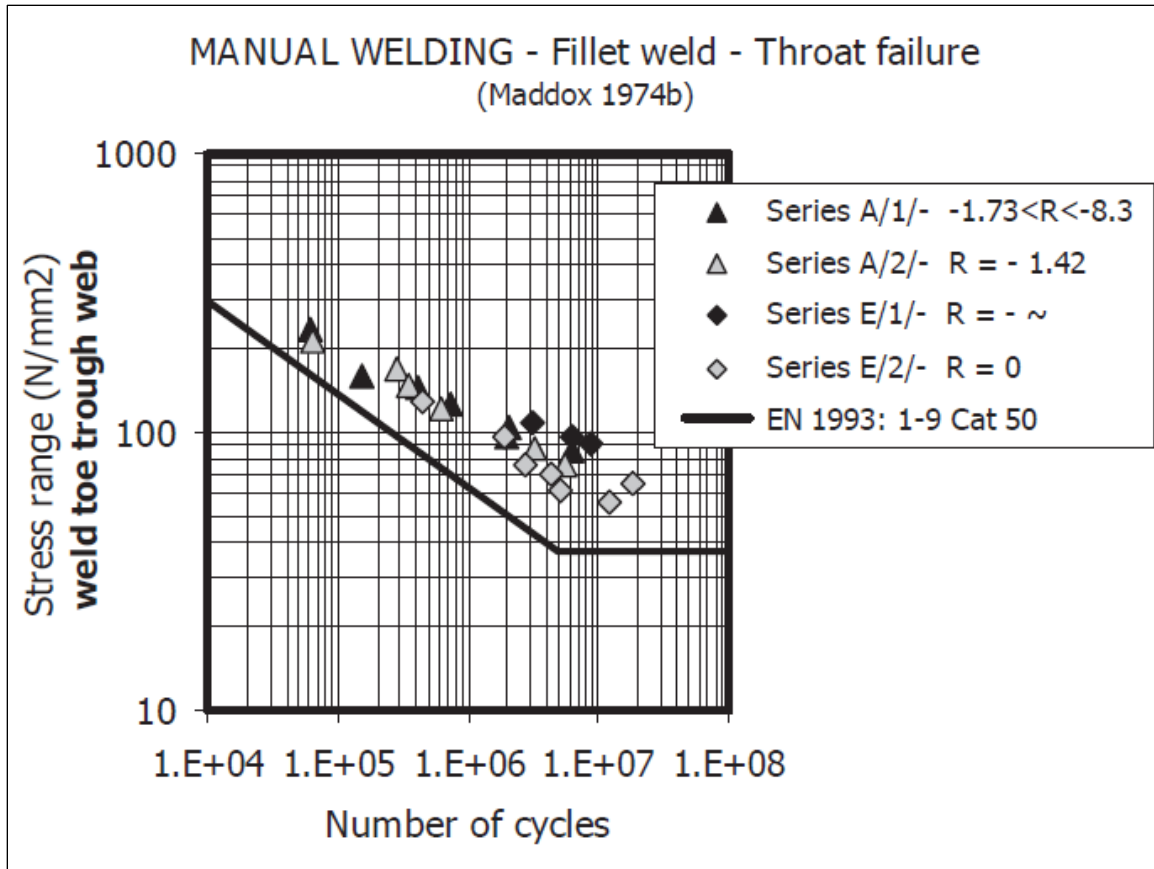


Figure 2.9 Influence of root gap openness (Kolstein, 2007)

Based on these test results, the bending stress across the weld throat was determined to be the appropriate stress range for plotting the S-N curve. An equation was proposed to calculate the bending stress in the weld throat:

$$\sigma_{\text{weld}} = \frac{T^2}{t^2} \left[\sigma_b - \left(3 + 4 \frac{t}{T} \cos \frac{\theta}{2} \right) \sigma_d \right] \quad (\text{Equation 2.1})$$

Where:

- σ_{weld} = stress in the weld throat
- σ_b = bending stress in the rib plate
- σ_d = normal stress in the rib plate
- T = rib plate thickness
- t = weld throat size

θ = angle between the rib plate and the deck plate

Using the proposed equation, an S-N curve for all data was established. Based on the resulting S-N curve, Maddox (1974b) suggested the rib-to-deck weld detail, including both weld toe and weld root, should be classified as Class F in the British Standard. Class F refers to an S-N curve with a stress range of 95 N/mm² at 2 million cycles, falling between the FAT-90 and FAT-100 curves established by International Institute of Welding (IIW).

Tests with a similar setup and specimen geometry were conducted by other researchers. Over the period between 1974-2000, 181 fatigue tests were performed in 7 research projects as listed in Table 2.4. A thorough description of them can be found in Kolstein (2007).

Table 2.4 Fatigue tests between 1974-2000 (Kolstein, 2007)

Fatigue Test & Time Conducted	Number of Specimens
Maddox (1974b)	30
Johnston (1978)	22
Maddox (1979)	53
Thonnard, Janss (1985, 1988)	36
Bruls (1990)	14
Bigonnet (1990)	20
Dijkstra, Kolstein (2000)	6
Total	181

2.2 Fatigue Assessment Methodologies for Welded Joints

The fatigue process can be roughly divided into three phases as will be discussed in the Section 2.2.3, but the first two, the crack initiation and crack propagation phases, consume most of the fatigue life. In welded details, the crack initiation stage is relatively

short since the welds are not refined enough to eliminate all crack-like flaws. The fatigue strength of weldments in these two phases depends on the local notch stress and the local stress intensity factor. Both of these parameters are affected by the local notch effect. The notch effect induced singularity at the weld toe and weld root cannot be predicted by classical linear solid mechanics. While the stress intensity factor can be used to characterize the singularity, approximations are required for the stress intensity factor solution and the applied stress field present in the rib-to-deck detail. Instead, the effective notch stress and alternative approaches are introduced into the S-N curve analysis. These include the nominal stress and structural/hot-spot stress approaches as listed in Table 2.5.

Table 2.5 Comparison of the three basic approaches to fatigue analysis

Type of Stress	Factors Considered	Associated S-N Curve	Implementation Method
Nominal Stress	Loading scenario and global/structural geometry, under simplified assumptions	A series of S-N curves for different detail categories	Hand calculation, classical structural analysis software (e.g. MASTAN2)
Structural/Hot-Spot Stress	Loading scenario and global/structural geometry	Single S-N curve for different details (only for weld toes)	Finite element modeling
Effective Notch Stress	Loading scenario, global geometry, and local geometry	Single S-N curve (AASHTO A curve) for all	Finite element modeling with special considerations

S-N curve analysis is by nature an empirical approach. Stress range values are directly related to the fatigue life defined by S-N curves established from fatigue test data. Most S-N curves in the worldwide codes are based on the nominal stress range (ENV, 2005;

AASHTO, 2007; DNV, 2008; Hobbacher, 2008). The concepts and guidelines are widely presented in the literature (Maddox, 1991 and Radaj, 1990, 1998). The nominal stress approach assumes the fatigue cracks occur in the base metal instead of through the welds. The calculated nominal stress range and cycles to failure are used to develop the S-N curves. The data scatter is handled by performing linear regression on the $\log(N)$ and $\log(S)$ data pairs. The slope of the regression line is typically assumed to be -3, although the individual data sets may differ slightly from this value. Assuming the slope of -3 for all data, the intercept becomes the single parameter that defines the S-N curve. The slope of -3 is also consistent with experimental observations of fatigue crack growth rates (see Section 2.2.3). As a result, different S-N curves need to be established to account for different details in terms of joint geometry, weld type, loading type, and manufacturing influences (Radaj, 1990). Different detail categories are established in similar fashion in all of the international codes for civil structures (ENV, 2005; AASHTO, 2007; DNV, 2008; Hobbacher, 2008). A brief overview of the nominal stress approach can be found in Fricke (2003).

The structural stress approach, also called the hot-spot stress approach or geometric stress approach, considers the non-homogeneous stress distribution in welded structures but excludes local notch effect. Assuming the notch effect has similar magnitude for all structural details, the structural stress approach combines S-N curves for different structural details into a single master S-N curve. This assumption generally works for evaluating weld toes as shown in Figure 2.13, but is not valid for analysis of the weld root. Therefore, the structural stress approach is currently limited to application on weld toes. In this thesis, hot-spot stress analysis is performed to establish hot-spot S-N curves specifically for different weld types and crack locations on rib-to-deck welds.

The structural stress can be obtained either by calculation or direct strain measurements. Many methodologies exist to calculate the structural stress mostly from finite element models. Three major methods, Linear Surface Extrapolation (LSE), Through Thickness at Weld Toe (TTWT), and Dong's method are discussed in Section 2.2.1. The LSE method was selected for analysis of the rib-to-deck welds in this study.

The fatigue resistance of a welded detail heavily depends on the notch effects occurring at the weld toe and weld root. The notch effect induces both severe stress concentrations and strength reductions. Since the maximum stress due to live load, dead load, and other loads is not allowed to exceed yield in structural design, it can be assumed that no plastic deformation occurs at the weld toe. Under these high-cycle fatigue conditions, the notch stress can be evaluated as completely elastic (Radaj, 1998). The elastic stress at the weld toe can be assessed with numerical methods such as the finite element method (FEM) or boundary element method (BEM).

Evaluation of the effective notch stress usually employs finite element models that have a fictitious rounding with a certain radius at the notch root. Fricke (2006) studied variations of the notch rounding approach for predicting the fatigue resistance of three structural details with both FEM and BEM. Fricke applied rounding with a 1-mm-radius as recommended by Radaj (1990). The effective notch stress was obtained from models of each structural detail. Both the weld toes and weld roots were modeled with different notch rounding (keyhole, oval), element type (quadratic, linear), and element size. Fricke recommended quadratic elements with a maximum size of 0.25 mm. The S-N data based on the effective notch stress had a lower bound corresponding to the FAT 225 curve proposed by the IIW. Fricke (2007) furthered this approach by constructing finite element models based on the detailed weld geometry measured with a high-precision laser-based sheet-of-light technique (Figure 2.10). The resulting S-N curve had lower fatigue resistance compared to the idealized rounded notch root curves, but the results were still close to the FAT 225 curve. The structural stress S-N curve was also calculated and it corresponds to FAT 90 curve recommended by the IIW. The data exhibited slightly larger scatter compared to the effective notch stress data for the different weld geometries. Pedersen (2010) re-analyzed a large number of fatigue test data from the literature following the same notch stress procedure. The results showed reasonable agreement with the FAT 225 curve but the FAT 200 curve was still recommended to provide a safety margin consistent with the conventional nominal stress approach. A summary of the guidelines for Pedersen's approach, together with other notch stress evaluation methods was made by Fricke (2008).

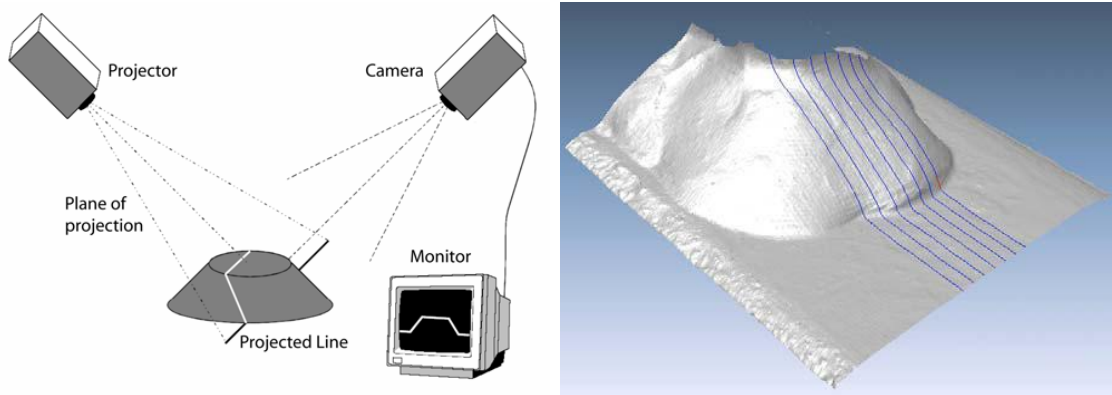


Figure 2.10 Sheet-of-light measurement and measured weld surface (Fricke, 2007)

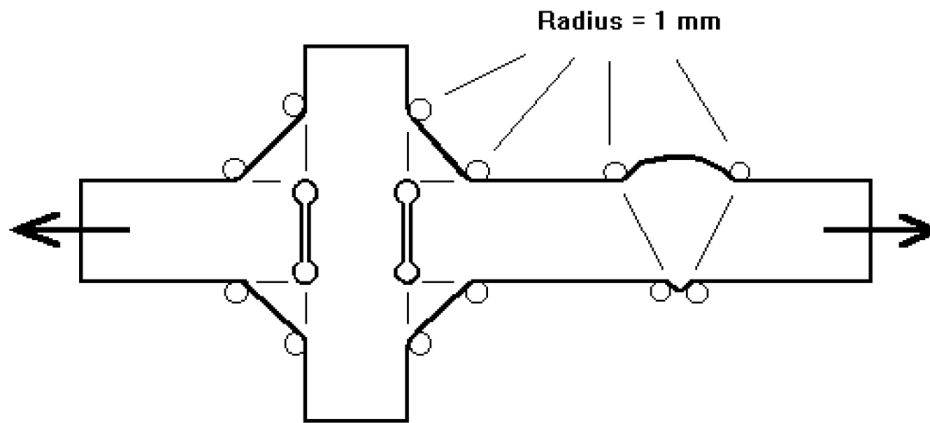


Figure 2.11 Fictitious rounding at weld toes and roots (Hobbacher, 2008)

Similar recommendations were also presented by the IIW (Hobbacher, 2008). Fictitious rounding with a 1 mm radius at both the weld toes and weld roots was proposed (Figure 2.11) with a 5 mm plate thickness limitation. For the determination of the effective notch stress by FEA, the linear element size should not exceed $1/6$ of the rounding radius ($1/4$ of the radius for quadratic elements). The derived effective notch stress values at weld toes should be at least 1.6 times of the structural hot-spot stress at the same location. Poutiainen (2006b) compared this effective notch stress approach with the two structural stress approaches proposed by Xiao (2004) and Poutiainen (2006a). It was observed that all three methods generated consistent results. It was also found that larger weld sizes have a positive influence on fatigue strength.

Fatigue life assessment can be also carried out using fracture mechanics approaches

based on fatigue crack propagation. Unlike the S-N curve equations which are based on regression from experimental data, stress intensity factors are calculated based on theoretical derivations from fracture mechanics. Mori (2009) applied this approach to study the fatigue strength of welded cruciform joints. The method showed high accuracy for predicting failure in specimens failing from the weld root under out-of-plane bending. As discussed in Section 2.2.3, the crack propagation approach requires establishment of the constant values in the equations, most importantly is the determination of an accurate initial crack size. Gurney (1991) used the crack growth rate approach to study the effect of local weld geometry on the fatigue strength of transverse fillet welded joints. He concluded that the predicted fatigue life is very sensitive to the assumed initial crack size. Since initial crack size data is not reliably known, fatigue crack growth rate methods remain a research tool and are not used for fatigue design purposes.

The nominal stress approach is considered to be a global approach since it is based on the global geometry and neglects the influence of local weld geometry on the stress distribution. The effective notch stress approach and the various fracture-mechanics-based approaches are considered to be local approaches since they require an assessment of the local notch effect. The structural stress approach acts as somewhat of a link between the two since it has features common to both (Radaj, 1998). A comparison of the above approaches is illustrated in Figure 2.12 and summarized in Fricke (2003). A comprehensive discussion of the local approaches can be found in Radaj (1998).

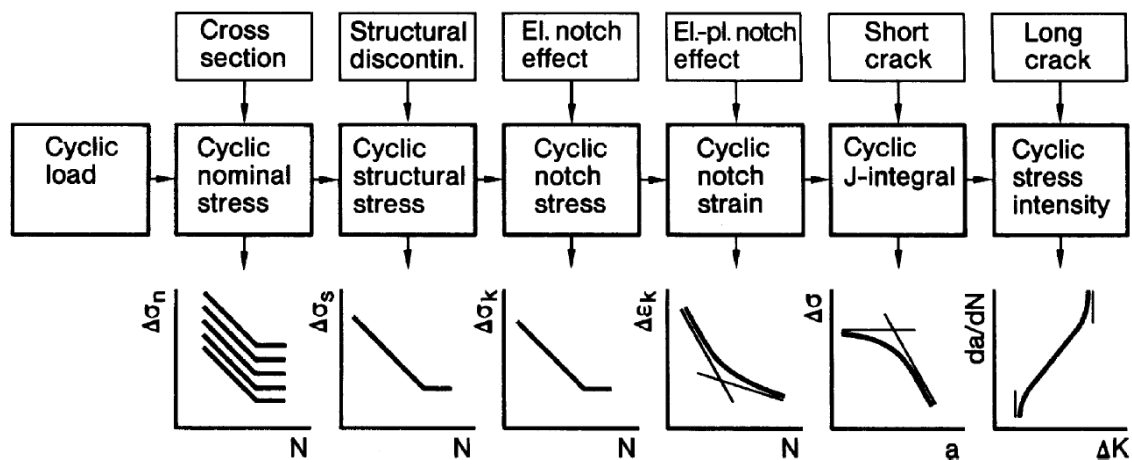


Figure 2.12 Summary of the different fatigue assessment approaches (Fricke, 2003)

2.2.1 Hot-Spot Stress Methodology

The original hot-spot stress method was proposed to solve the fatigue assessment problem for tubular joints in offshore structures (Dijkstra, 1980). Since the stress distribution is heavily influenced by the structural geometry of the tubular joints, such as tube diameter, tube thickness, and the joint angle, it is very hard to classify the joint into a single detail category. The nominal stress is also difficult to define. The method was later extended to plated structures. Three different hot-spot types were identified for weld toes in different orientations as shown in Figure 2.13.

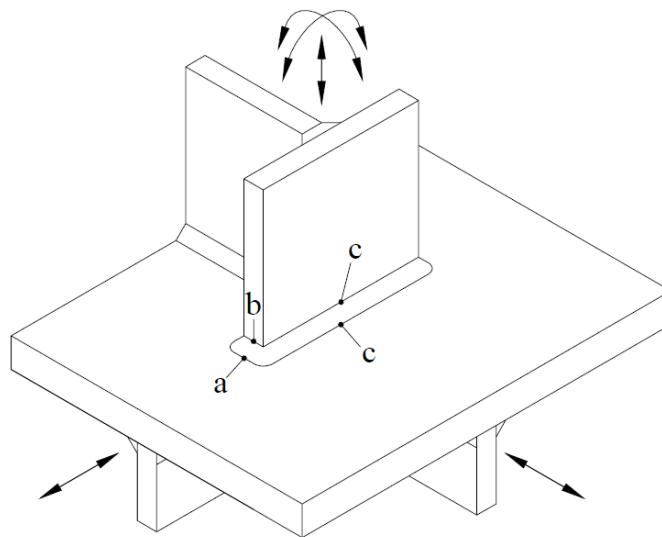


Figure 2.13 Types of hot spots (DNV, 2008)

The linear surface extrapolation (LSE) method calculates a weld toe stress based on the plate surface stress at a certain distance away from the weld toe. The stress values normal to the weld toe are determined at reference points or “read-out points”. The reference point stresses are then linearly extrapolated to the hot-spot at the weld toe. The reference points should be located far enough away from the weld toe to exclude the notch effect. The LSE procedure was first introduced by Niemi (1995a, 1995b, 2001) and Partanen (1996). Reference points located at $0.4t$ and $1.0t$ away from the weld toe (0410 extrapolation) were recommended, where t is the base plate thickness as shown in Figure 2.14. The calculated hot-spot stress values are compared to a master fatigue resistance S-N curve. A series of S-N curves were suggested for different structural

details that vary between FAT 90 to FAT 112 (Niemi, 2002).

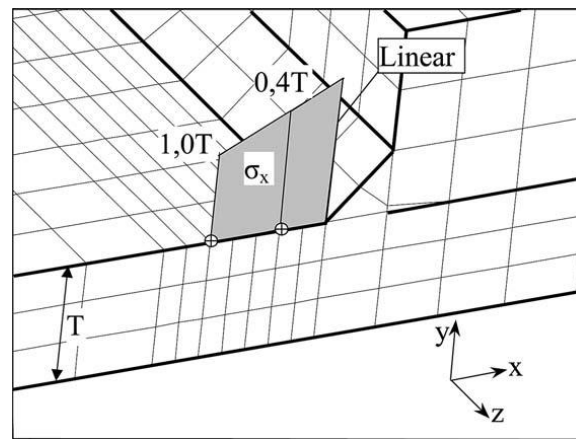


Figure 2.14 Linear surface extrapolation (0410) (Poutiainen, 2004)

A similar procedure was proposed by Fricke (2001a) with some additional considerations. Two alternative extrapolation techniques were investigated in addition to the 0410 technique. The 0515 technique uses reference points located $0.5t$ and $1.5t$ away from the weld toe. The single read-out point technique is based on a single reference point located $0.5t$ from the weld toe. The 0515 extrapolation showed high agreement with 0410 extrapolation for models with relatively fine mesh size but the 0410 extrapolation had greater scatter when coarser meshes were used. Therefore, 0515 extrapolation was recommended for coarser meshes while the 0410 extrapolation was only recommended for finer meshes. The single read-out point technique showed lower hot-spot stress values compared to the other two techniques. Therefore, the FAT 90 curve was recommended for use with the single read-out point technique while the FAT 100 curve was recommended for the other two extrapolation techniques. Fricke also showed that plate thickness was not the best parameter to determine the reference point locations for the type b weld toe shown in Figure 2.13. He concluded that the reference points should be placed at fixed distances of 5 mm and 15 mm away from the weld toe (Fricke, 2001b). These recommendations were adopted by the IIW (Hobbacher, 2008, 2009) as shown in Figure 2.15.

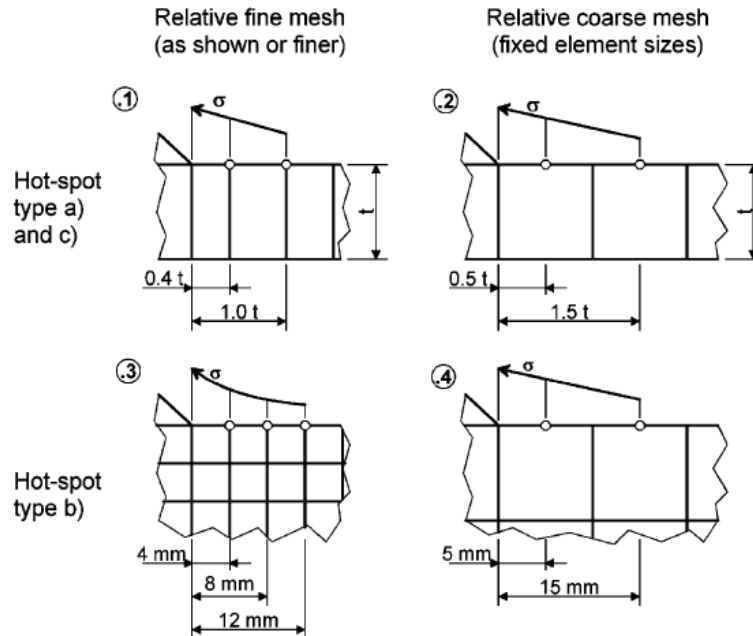


Figure 2.15 Location of reference points (Hobbacher, 2008)

Another hot-spot stress procedure is to linearize the through-thickness normal stress distribution at the weld toe (TTWT). Radaj (1990) states that the structural stress should be calculated as the summation of the membrane and bending stress, varying linearly through the thickness of the base plate. The hot-spot stress is taken as the maximum value occurring at the plate surface. The actual through-thickness stress distribution is non-linear due to the notch effect. Linearizing the distribution averages out the nonlinear peak stress thereby suppressing the notch effect (Radaj, 1998). According to Radaj, this is a better way to define the structural stress because the linear stress distributions can be calculated using Bernoulli-Euler beam theory or Kirchhoff plate theory without the need for finite element modeling. This structural stress definition was later adopted by ASME Boiler and Pressure Vessel Code (BPVC). It was noted that both the LSE and TTWT methods breakdown in the presence of heavy transverse shear stress because the shear stress also generates a notch effect at the hot-spot. The shear notch effect appears to be independent from the normal stress notch effect and is not considered by either the LSE or TTWT methods.

Dong (2001a) proposed an alternative structural stress determination method that

includes the transverse shear stress effects. Like the TTWT method, Dong's method assumes that the structural stress at the weld toe has a linear distribution based on the addition of membrane and bending stress. However, instead of calculating the stress distribution at the weld toe cross section, stresses are calculated on a section away from the weld toe. Based on the normal and shear stress distribution at the remote section, the hot-spot stress at the weld toe is calculated based on equilibrium. For the case where solid elements with monotonic through-thickness stress distribution are used, the structural stress at the weld toe can be expressed as the summation of membrane and bending stress calculated as follows:

$$\begin{aligned}\sigma_s &= \sigma_m + \sigma_b \\ \sigma_m &= \frac{1}{t} \int_0^t \sigma_x(y) \cdot dy \\ \sigma_m \frac{t^2}{2} + \sigma_b \frac{t^2}{6} &= \int_0^t \sigma_x(y) \cdot y \cdot dy + \delta \int_0^t \tau_{xy}(y) \cdot dy\end{aligned}\quad (\text{Equation 2.2})$$

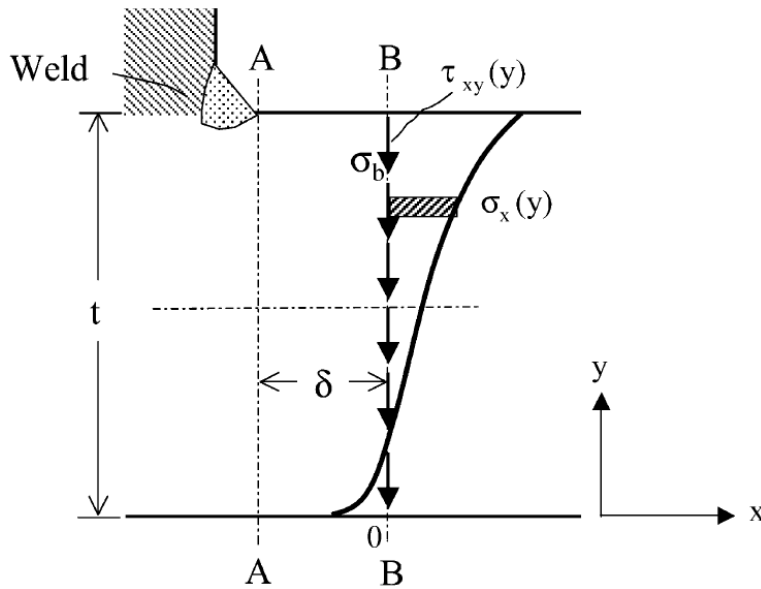


Figure 2.16 Structural stress calculation (Dong, 2001a)

Based on the stress distribution shown in Figure 2.16, the membrane and bending stress (σ_m and σ_b) were calculated from the last two equations then substituted into the first equation to get the structural stress. Further modifications are made to the equations to

account for finite crack depths and non-monotonic stress distributions. In cases plate/shell elements are used, Dong's method uses stress resultants (sectional forces and moments) or nodal forces to calculate the structural stress. If the sectional forces and moments are transferred into local coordinates and denoted as shown in Figure 2.17, the structural stress at section A-A can be calculated from the stress resultants at section B-B as:

$$\sigma_s = \sigma_m + \sigma_b = \frac{f_{x'}}{t} + \frac{6(m_{y'} + \delta \cdot f_{z'})}{t^2} \quad (\text{Equation 2.3})$$

In cases section B-B is not available in the FE model, the sectional forces and moments at section A-A can be alternatively calculated from the nodal forces using appropriate shape functions. Then the structural stress is calculated as below. Note that the transverse shear is taken into account by the nodal forces.

$$\sigma_s = \sigma_m + \sigma_b = \frac{f_{x'}}{t} + \frac{6m_{y'}}{t^2} \quad (\text{Equation 2.4})$$

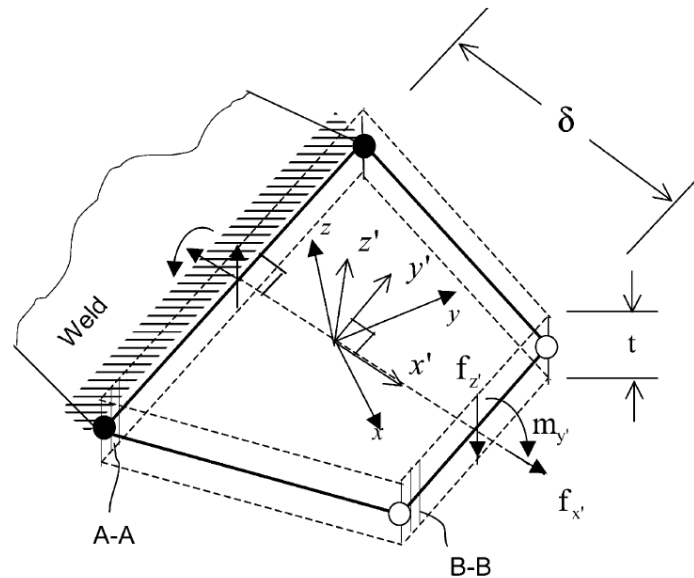


Figure 2.17 Dong's method for plate/shell elements (Dong, 2001a)

Dong's method claims to be mesh insensitive based on numerical evaluations on three different structural details. Guidelines and recommendations for application of this

method are documented in Dong (2001b). Dong (2004) later applied this approach to aluminum MIG and laser weldments. The calculated structural stress values correlated very well with the experimental fatigue life defined by the master S-N curve.

Kang (2007) applied Dong's method to study spot welds using the nodal forces and moments around the spot weld. The resulting structural stress showed a good correlation with existing fatigue data. Dong (2007) applied his method together with the LSE method and the TTWT method from the ASME code to analyze recent fatigue test data from pressure vessels and pipes. A master S-N curve was developed based on Dong's method.

Xiao and Yamada (Xiao, 2004; Yamada, 2004) developed another method for structural stress analysis accounting for the size and thickness effect observed in welded joints. It was observed that the effect of weld local geometry diminished faster in the thickness direction compared to the surface direction. The structural stress was calculated 1 mm below the plate surface at the weld toe, perpendicular to the direction of the anticipated crack path. The method was supported by crack propagation studies based on linear elastic fracture mechanics (LEFM). Application of this approach resulted in less scatter on the S-N plot compared to the other structural stress evaluation techniques, and a lower bound fit to the data corresponds to the FAT 100 curve.

Poutiainen (2005, 2006a) proposed another alternative approach to determine the structural stress considering both the nominal stress in the plate and the normal stress in the weld throat. The structural stress is evaluated on the plate surface at the weld toe based on the modified stress distribution shown in Figure 2.18. The structural stress was then taken as the nominal plate stress multiplied by a stress concentration factor ($\sigma_{nom}K_{sa}$). Equations to determine the stress concentration factor K_{sa} were presented as follows:

$$\begin{aligned}
 K_{sa} &= 1 + \frac{\sigma_{weld}}{\sigma_{nom}} \left(1 - \frac{l_w}{T} \right) & \left(l_w \leq \frac{T}{2} \right) \\
 K_{sa} &= 1 + \frac{\sigma_{weld}}{\sigma_{nom}} \frac{T}{4l_w} & \left(l_w \geq \frac{T}{2} \right)
 \end{aligned}
 \tag{Equation 2.5}$$

The definition of the terms in Equation 2.5 is illustrated in Figure 2.18. As shown above, the stress concentration factor depends on the weld stress that is affected by the weld size, plate thickness, and the loading scenario. These factors are inherently accounted for by the structural stress definition without further correction factors. Figure 2.19 shows the stress distributions derived from Equation 2.5 in cases of different plate thicknesses.

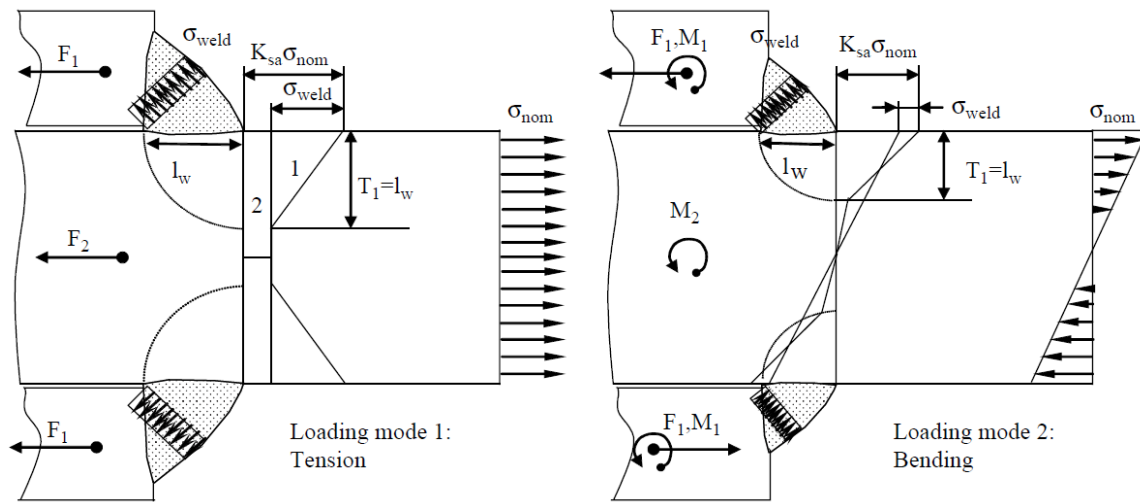


Figure 2.18 Definition of the modified through-thickness structural stress method (Poutiainen, 2006a)

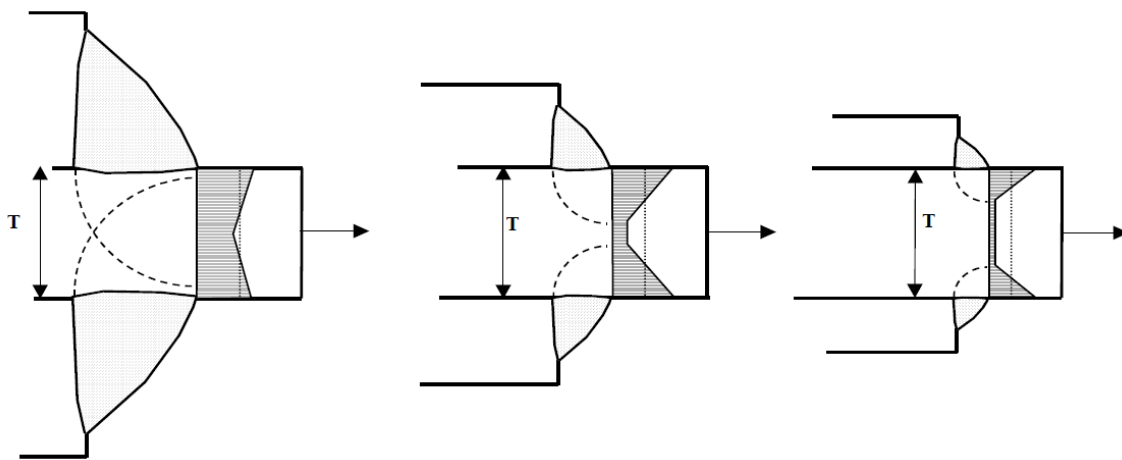


Figure 2.19 Multi-linear stress distribution for different plate thickness and weld size (Poutiainen, 2005)

The effectiveness of this approach was further verified by LEFM predictions based on the

fatigue test data. Poutiainen (2005, 2006a) demonstrated that this method showed very good agreement with the LEM predictions and the modified structural stress also correlated well with previous fatigue test data on a single S-N curve.

Doerk (2003) compared the LSE procedure recommended by the IIW with Dong's method for four different structural details to assess mesh sensitivity. The results indicated that Dong's method was relatively mesh-insensitive for 2D problems but there were problems applying it to 3D cases. This was attributed to the fact that shear stress acting on the transverse element sides is neglected in the equilibrium equations. Hence the stress predicted by Dong's method showed larger scatter for cases where the neglected shear stresses are high. The LSE procedure generally exhibited sensitivity to both element type and size. Element type and size limitations should be applied to different cases based on the IIW recommendations. Mesh-insensitivity was observed in some cases, as long as the mesh is not too coarse, but did not show up with high local effect such as a bracket toe. Nonetheless, the two LSE extrapolation methods (0410 and 0515) produced essentially the same results for most of the cases. A similar comparison was made by Fricke (2005) including Xiao and Yamada's method together with the LSE and Dong's methods. It was concluded that all three methods provided similar fatigue life predictions for the three structural details analyzed. In general, Xiao and Yamada's method predicted slightly longer fatigue lives and Dong's method predicted slightly shorter fatigue lives.

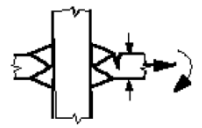
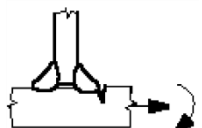
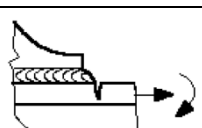
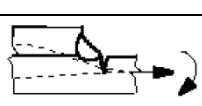
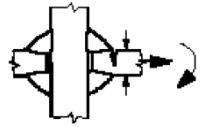
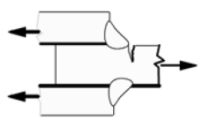
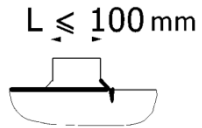
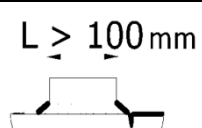
Another comparison between LSE, TTWT, and Dong's method was performed by Poutiainen (2004) with an emphasis on evaluating the finite element mesh. Four different mesh arrangements were studied for 2D models and two different mesh arrangements (coarse and fine) were considered in the 3D models. A correction was made to Dong's equilibrium equations to add the shear stress on the transverse element sides. It was found that all three methods worked well for 2D structural details. The TTWT and Dong's method were more insensitive to different mesh configurations compared to the LSE method. For the 3D models, the TTWT and Dong's method required nodal averaging to obtain accurate results, while the LSE method did not require any additional post-processing beyond that used for the 2D models. The distance from the weld toe to

the reference cross section, δ , was also determined to influence the results from Dong's method.

2.2.2 Hot-spot Stress S-N Curves

One of the advantages of using the structural stress over the nominal stress is that a single master S-N curve can be used instead of a series of S-N curves for different detail categories. Different hot-spot stress based master S-N curves have been proposed but there is little difference between them. A major Joint Industry Project (JIP), "FPSO — Fatigue Capacity", evaluated the different master curves. Lotsberg (2001) and Maddox (2001) summarized the resulting recommendations for hot-spot stress design S-N curves for type a) and c) hot spots shown in Figure 2.13. The FAT 90 curve was conservatively recommended by the IIW for application of the LSE procedure (Hobbacher, 2008). The data tends to support use of the FAT 100 curve. The FAT 80 curve was recommended when the hot-spot stress was directly read at the plate surface 0.5t away from the weld toe. Fricke (2001a) recommended the FAT 100 and FAT 90 curves for the aforementioned two cases, respectively. Fricke (2005) further recommended the FAT 90 curve for the edges of longer attachments (>100 mm) and for load-carrying fillet welds. Lotsberg (2006) later narrowed down the selection to the FAT 90 curve based on the S-N data from both small scale and full scale fatigue tests. Similar recommendations were made by DNV RP C203 (2008). They proposed the DNV D curve, which corresponds to the FAT 90 curve, for hot-spot fatigue analysis. The IIW currently allows both the FAT 100 and FAT 90 curves depending on the structural detail type as shown in Table 2.6. All of the above mentioned curves have a log-log slope of -3.0.

Table 2.6 Fatigue resistance against structural hot spot stress (IIW-1823-07)

No.	Structural Detail	Description	Requirements	FAT Steel	FAT Alu.
1		Butt Joint	As welded, NDT	100	40
2		Cruciform or T-joint with full penetration K-butt welds	K-butt welds, no lamellar tearing	100	40
3		Non load-carrying fillet welds	Transverse non-load carrying attachment, not thicker than main plate, as welded	100	40
4		Bracket ends, ends of longitudinal stiffeners	Fillet welds welded around or not, as welded	100	40
5		Cover plate ends and similar joints	As welded	100	40
6		Cruciform joints with load-carrying fillet welds	Fillet welds, as welded	90	36
7		Lap joint with load-carrying fillet welds	Fillet welds, as welded	90	36
8		Type "b" joint with short attachment	Fillet or full penetration weld, as welded	100	40
9		Type "b" joint with long attachment	Fillet or full penetration weld, as welded	90	36

2.2.3 Approaches Based on Fracture Mechanics

To overcome the singularity problem when applying classical elastic solid mechanics on crack tips, Griffith invoked the First Law of Thermodynamics to formulate a fracture

theory based on energy balance (Anderson, 1994; Griffith, 1920). This theory, for the first time, successfully explained the relationship between fracture strength and flaw size for a given material. The basic concept was that a crack becomes unstable (fractures) when the strain energy released during fracture surpasses the surface energy of the material. Unfortunately Griffith's theory only worked well on ideally brittle materials such as glass because it assumes that surface energy was the only type of energy that a fracture needed to overcome.

To extend Griffith's theory to metals, Irwin (1948) accounted for the energy dissipated by local plastic flow. Several years later in 1956, Irwin developed the concept of the energy release rate, which became the foundation of LEFM. Irwin (1957) described the crack tip stress state by a single characterizing parameter, the stress intensity factor. Both the energy release rate and stress intensity factor methods provide equivalent results for some cases.

As a simple illustration, take an infinite-size plate with a through-thickness crack under a remote tensile stress perpendicular to the crack. The energy release rate can be expressed as:

$$G = \frac{\pi\sigma^2 a}{E} \quad (\text{Equation 2.6})$$

Where G is defined as the energy release rate, a is half-length of the crack, σ is the applied stress, and E is Young's modulus of the material. When the energy release rate generated by the applied stress exceeds the critical energy release rate, G_c , of the material, fracture initiates at the crack tip. The critical energy release rate, G_c , is a constant material property, thus the fracture-inducing stress is inversely proportional to the crack size.

The same problem can be explained in terms of the stress intensity factor. The stress state at any point near the crack tip is a function of the location vector (defined in polar coordinates) and the mode-I stress intensity factor K_I . For a through-thickness crack in an infinite plate, the stress intensity factor K_I , at the crack tip is defined based on the

crack size and the far-field stress perpendicular to the crack:

$$K_I = \sigma\sqrt{\pi a} \quad (\text{Equation 2.7})$$

When the stress intensity caused by the applied stress σ exceeds the critical stress intensity of the material K_{Ic} , fracture occurs at the crack tip. Equating equations 2.6 and 2.7 shows that G and K_I are related by:

$$G = \frac{K_I^2}{E} \quad (\text{Equation 2.8})$$

As shown above, the two approaches are essentially equivalent, but this is only true for linear elastic material. Irwin's LEFM theory is no longer valid when significant plastic deformation precedes failure (Anderson, 1994). Irwin developed plasticity correction factors to extend LEFM beyond brittle materials. Rice (1968) proposed a new parameter, the J integral, to solve the strain concentration problem at a crack tip for elastic-plastic material. This became the theoretical foundation of Elastic-Plastic Fracture Mechanics (EPFM).

Rice (1968) found that a path-independent line integral around the crack tip could be established for linear or nonlinear elastic materials (J-integral). Since the J-integral has the same value for any arbitrary path, it is a path independent single parameter that describes the crack tip energy. This approach was demonstrated to be effective in evaluating elastic-plastic fractures and converged to Griffith's energy balance method for elastic brittle fracture.

Paris (1960, 1961) extended the stress intensity factor concept to analyzing fatigue crack growth rates in terms of the stress intensity factor range ΔK . Measurements in fracture mechanics specimens showed that the fatigue crack growth rate is proportional to the stress intensity factor range (Paris, 1960):

$$\frac{da}{dN} = C(\Delta K)^m \quad (\Delta K_{th} < \Delta K < \Delta K_c) \quad (\text{Equation 2.9})$$

Where a is the crack size; N is the number of cycles; $\frac{da}{dN}$ hence refers to the crack growth per loading cycle, in other words the crack propagation rate; C and m are assumed to be constants depending on the material; and ΔK is the range of the stress intensity factor, which is defined as:

$$\Delta K = K_{\max} - K_{\min} \quad (\text{Equation 2.10})$$

Where K_{\max} and K_{\min} are the maximum and minimum values of the stress intensity factor in the loading cycle, corresponding to the upper and lower limit of the stress history.

Assuming all fatigue starts at a microscopic initial crack-like flaw, the Equation 2.9 can be integrated to determine the number of cycles needed to grow the crack to a failure size. This approach has often been used in research, but practical application is difficult unless the initial crack size is accurately known. Relevant guidelines for application can be found in the latest version of both IIW and DNV documents (Hobbacher, 2008; DNV-RP-C203, 2008).

In general, the process of fatigue failure can be divided into three stages, crack initiation, stable crack propagation, and unstable final rupture. The crack initiation stage involves development of very small separations in the material, usually smaller than the grain size. This tends to occur at locations with high stress concentrations such as notches and defects. The stable crack propagation phase begins once the microcrack reaches a size approximately equal to the grain size. Under cyclic loading, the microcrack slowly grows into a macrocrack at a rate predicted by Equation 2.9. Unstable rupture occurs when the crack size approaches the structural limit load for the cracked member. The crack initiation phase has different duration but represents only a very small portion of the overall fatigue life for welded joints (Gurney, 2006). Since fatigue in weldments usually initiates at weld toes or weld roots; the notch defects typically cause microcracks due to the welding process that begin to grow almost immediately under cyclic load. As cracks grow larger, the crack growth rate accelerates and most of the fatigue life is exhausted once a macrocrack forms. As a result, most of the total fatigue life of a welded

joint is expended in the stable crack propagation phase.

As mentioned previously, the stress state at a crack tip can be solely described by the stress intensity factor, which is defined in Equation 2.7. In general, the equation becomes more complicated for realistic geometries and crack shapes. For cases other than mode I fracture for a through thickness crack in an infinite plate, a more general form, can be rewritten as (Gurney, 2006):

$$K = Y\sigma\sqrt{\pi a} \quad (\text{Equation 2.11})$$

Where Y is a correction factor that accounts for the structural geometry and crack geometry (DNV-RP-C203, 2008). (Equation 2.11) is valid for both plane stress and plane strain condition.

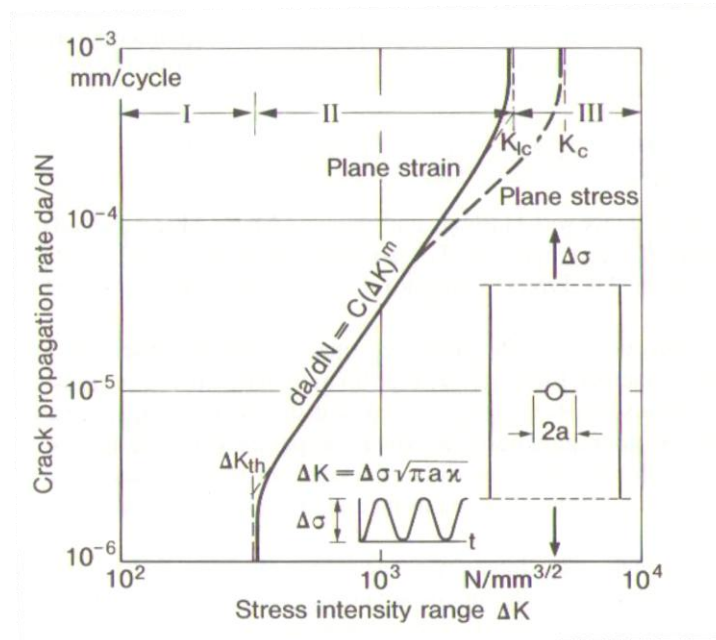


Figure 2.20 Relationship Between Crack Propagation Rate and Range of Stress Intensity Factor (Radaj, 1990)

The basic crack growth rate relationship is illustrated in Figure 2.20. The middle portion of the curve indicates stable crack growth governed by the Paris law. At low values of ΔK a threshold is reached (ΔK_{th}) where crack propagation stops. At the upper end of the

curve ΔK approaches the critical value (ΔK_c) and the crack growth rate rapidly accelerates before failure. The slope of the Paris law straight line varies somewhat depending on whether plane strain or plane stress conditions dominate around the crack. Typical weldments are sufficiently constrained to create plane strain conditions; therefore plane strain curve is typically used. The constants in Equation 2.9 (C and m) are material properties that must be determined before performing fatigue analysis using crack growth rates. However, the values of C and m also depend on the load ratio (R-ratio) and the ambient conditions (corrosiveness, temperature) present at the growing crack. For data collected from tests in air under plane strain conditions with tensile loading (R=0), steel exhibits a linear relationship between $\log(C)$ and m as in SI units (Gurney, 1979):

$$C = \frac{1.315 \times 10^{-4}}{895.4^m} \quad (\text{Equation 2.12})$$

This yields Equation 2.9 to (in SI units):

$$\frac{da}{dN} = 1.315 \times 10^{-4} \left(\frac{\Delta K}{895.4} \right)^m \quad (\Delta K_{th} < \Delta K < \Delta K_c) \quad (\text{Equation 2.13})$$

At this moment it is still not clear the inherent mechanism in the material that determines the value of m, but based on experimental observation $m=3.0$ is frequently assumed for structural steel, which yields C as 1.83×10^{-13} in SI units. Once the value of m is selected, the crack propagation rate can be determined from Equation 2.13. Further the fatigue life can be integrated from the assumed initial flaw size to the designated crack size that is considered as a fatigue failure. Substituting ΔK in Equation 2.9 from Equation 2.11, it can be obtained:

$$\int_{a_0}^{a_f} \frac{da}{C(Y\sqrt{\pi a})^m} = (\Delta\sigma)^m N \quad (\text{Equation 2.14})$$

It can be observed from Equation 2.14 that for a given type of structural detail (a given value of Y), initial flaw size and fatigue failure criterion (given values of a_0 and a_f), the value of the integral is constant, so that:

$$(\Delta\sigma)^m N = \text{Constant} \quad (\text{Equation 2.15})$$

The above equation is equivalent to the equation for S-N curves. The value of m that assumed to be 3.0 is also in good agreement with experimental S-N data. Evaluation of the integral in Equation 2.14 gives the following expression (Wang, 1996):

$$N_f = \begin{cases} \frac{2a_0}{(m-2)C(Y\Delta\Delta\sqrt{\pi a})^m} \left[1 - \left(\frac{a_0}{a_f} \right)^{\frac{m}{2}-1} \right] & \text{for } m \neq 2 \\ \frac{a_0}{CY^2\Delta\sigma^2\pi a} \ln \frac{a_f}{a_0} & \text{for } m = 2 \end{cases} \quad (\text{Equation 2.1})$$

Therefore the fatigue life based on crack propagation approach can be predicted from Equation 2.16. More information such as the evaluation of initial flaw size, calculation of stress intensity factors, effect of residual stress, and other fracture-mechanics-based approaches can be found in Radaj (1990, 1998) and Maddox (1991).

Chapter 3. Experimental Study

One of the objectives of this research is to provide recommendations for fatigue design of the rib-to-deck welds in steel orthotropic decks. The traditional stress range analysis methodology is adopted for this purpose. The stress range values at the potential cracking locations can be calculated theoretically or obtained experimentally with strain measurements. The fatigue life, represented by the number of cycles that it takes to fail a specimen, can only be determined by fatigue tests. In this study fatigue tests were conducted in two different laboratories with similar methodology. The details of the instrumentation, test procedure, data acquisition, and post-test processing are introduced in this chapter.

A few considerations need to be made for the fatigue tests performed in this study. Testing needs to be performed at different stress ranges to establish the S-N curves. The test protocol needs to establish a stress distribution at the potential cracking locations that can evoke as many failure modes as possible. Residual stress is a key factor in the fatigue performance of welded joints; therefore tests should be performed at different R-ratios to study their effect on fatigue life. The stress cycle is under full tension when $R=0$; and it is under an equal tension-compression stress reversal when $R=-1$. Comparison of fatigue results from the two test conditions can help determine how much of the compression stress range is being placed in relative tension due to superposition of residual stresses. The $R=0$ test condition will provide a lower bound for fatigue life. Additionally, it was found that the presence of a gap at the weld root influences the cracking locations and failure modes. Specimens with both open and closed root gaps are tested to examine the difference. Last but not the least important, since investigating the effect of different weld dimensions is the primary approach for weld optimization, specimens with a wide range of weld dimensions, such as weld penetration, weld toe size, and weld throat size should be included in the testing matrix.

For the fatigue tests, instead of full-size orthotropic steel deck panels, full-scale single-rib deck segments were used as test specimens. Advantages of this type of testing compared to full-size panels include: 1) Replicate tests sample a larger weld length under identical

conditions and provide multiple data points to establish S-N curves; 2) this type of tests is much more cost-effective compared to full-scale panel tests; and 3) adjusting the specimen geometry and testing setup can trigger different failure modes separately or jointly, while the full-size panel tests usually are biased toward one failure mode.

Following the fatigue tests, the actual dimensions of each weld were measured and recorded. The weld profile was photographed at each edge of the specimens after polishing and etching with hydrochloric acid. In addition, measurements of the “effective length” between the weld toe and test fixture rollers were also taken to compare the hot-spot stress values computed from ideal finite element models to the actual tests.

3.1 Preparation of Specimens

Overall, 95 fatigue specimens were tested in this study. They were all fabricated at High Steel Structures, Inc. in Lancaster, PA with weld processes and procedures. A full-scale 6 foot long weldment was fabricated from a single rib and portion of a deck plate. Tack welds were placed at intervals to fuse the ribs and decks together before the arc welding during the single-rib deck strip production. Two types of welding techniques were applied on the weldments, which are gas metal arc welding (GMAW) and submerged arc welding (SAW). Both of them were made as partial penetration welds with a designated penetration percentage for each specimen series, except for three series made as fillet welds (FIL, OB and UB) simply following the common practice without particular consideration on the weld penetration (Table 3.1). The welds were produced by automatic welding equipment typically used for full scale fabrication of orthotropic decks. No surface grinding or post-weld profile enhancement was performed. The rib plate and deck plate were forced against each other during the welding process in order to get a tight fit-up between the plates. Figure 3.1 shows the typical appearance of a finished weld. The edges of the rib plate were beveled for GMAW welds to achieve 80% penetration. No bevel preparation was used for the initial series of SAW welds; the rib plate had a square edge. Additional specimens were prepared using the SAW process where the rib plate edge was either over beveled (OB) or under beveled (UB) to control the root gap for testing purposes.

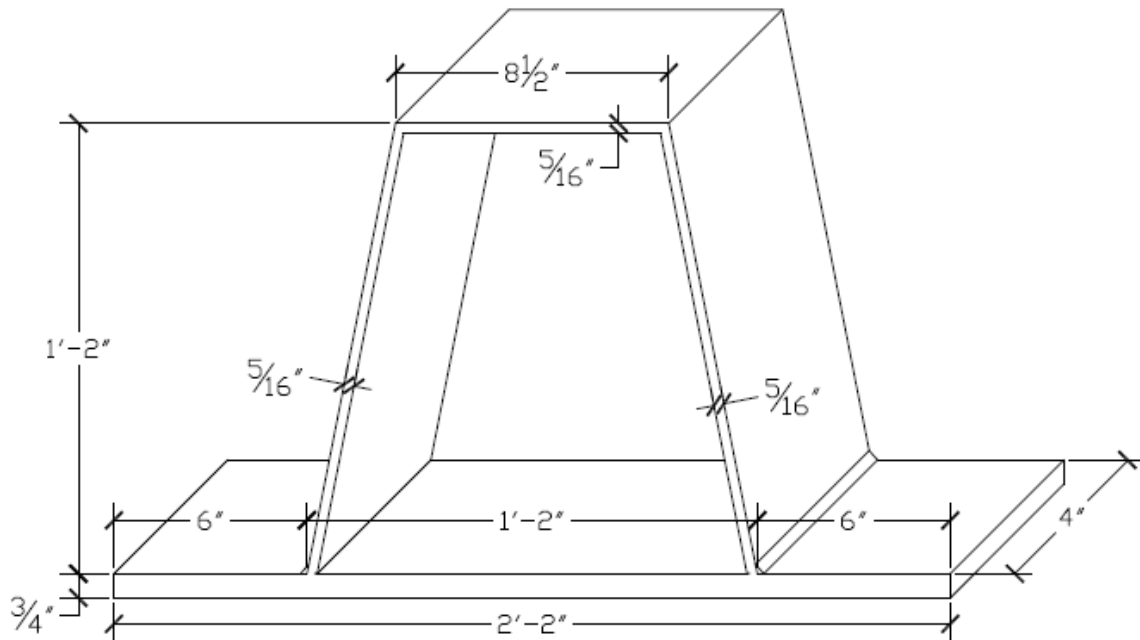


Figure 3.3 Dimensions of specimens

An additional 41 specimens were fabricated using the hybrid laser arc welding (HLAW) process to produce full penetration welds from one side. The HLAW welding was performed at Applied Thermal Sciences, Inc. in Sanford, Maine. The results from these tests are not included in this thesis because it remains an experimental technique.

To investigate the influence of weld penetration on fatigue performance, the welding procedures were designed to produce different target penetration values. The target values were 80%, 60%, 40%, and 20% of the rib plate thickness. Typical profiles of welds in each series are illustrated in Figure 3.4. However, the measured penetration values differed substantially from the target values. The thin 5/16" rib plate thickness made it impossible to produce penetrations below about 50%. Measurements of the actual penetration values were recorded for each specimen after fatigue tests. The actual measurements showed that the target penetration values in fact were not achieved for most of the welds. It is noted that the specimen series names do not reflect the measured penetration percentage. The specimen edges were polished and etched using hydrochloric acid to highlight the weld and heat affected zone (HAZ) profile as discussed in Section 3.5.



Figure 3.4 Typical weld profile in each series

As mentioned before, the last two specimen series were designed to investigate the influence of the weld root gap. Both the over beveled (OB) and under beveled (UB) specimen weld profiles are shown in Figure 3.5. The OB specimens are prepared with a bevel angle greater than the rib angle, resulting in a root gap that is held open before welding. The UB series have a bevel angle less than the rib angle resulting in a closed root gap before welding. Despite this bevel preparation, weld shrinkage due to cooling of the weld metal caused the root gaps to close after welding. The shrinkage forced the rib plate into contact with the deck plate, even for the OB series as shown in Figure 3.6. However, the different bevel preparation resulted in different amounts of contact pressure at the root. The UB series showed definite plastic distortion where the two plates were pressed together. This was less evident in the OB series where the root gap had to close before pressure could develop. Since the OB series did not result in the desired open root gap, half of the specimens in both the OB and UB series were saw-cut at the root to open the gap before testing. The saw-cuts were performed carefully to avoid contact with the weld, thereby preserving the natural situation at the tip of the root notch. Figure 3.7 shows typical saw-cuts on both the OB and UB specimens.

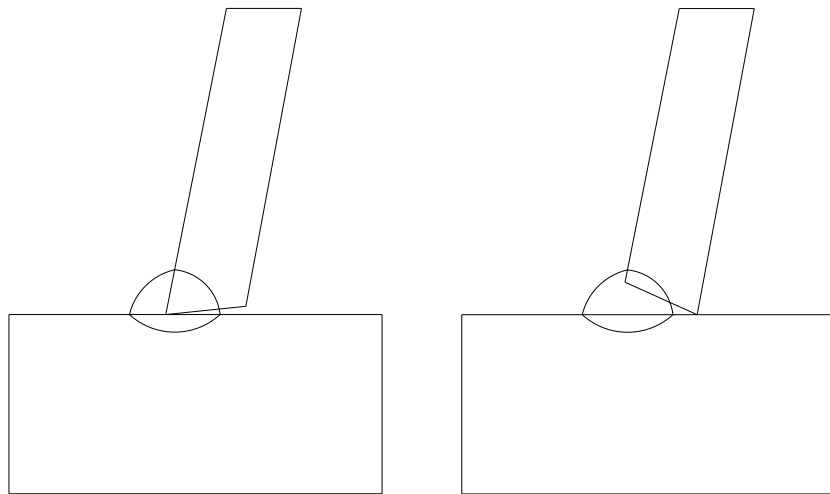


Figure 3.5 Over-beveled (OB) and under-beveled (UB) rib plate preparation

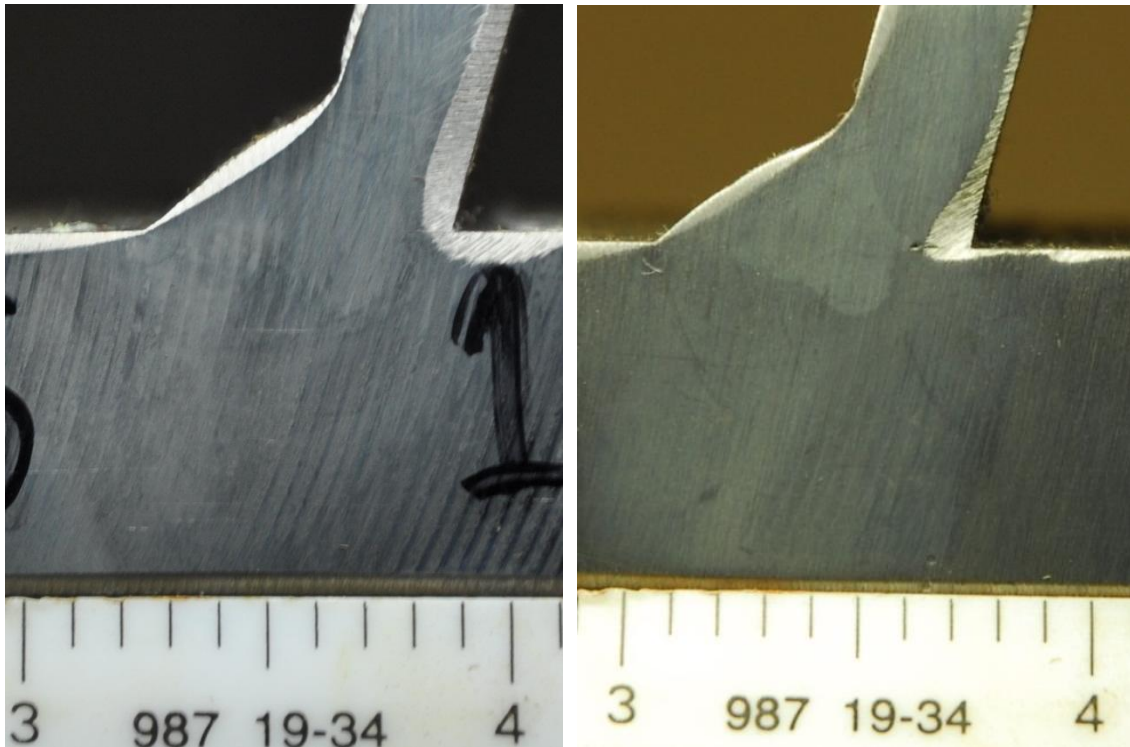


Figure 3.6 Typical over-beveled (OB) and under-beveled (UB) specimens after welding

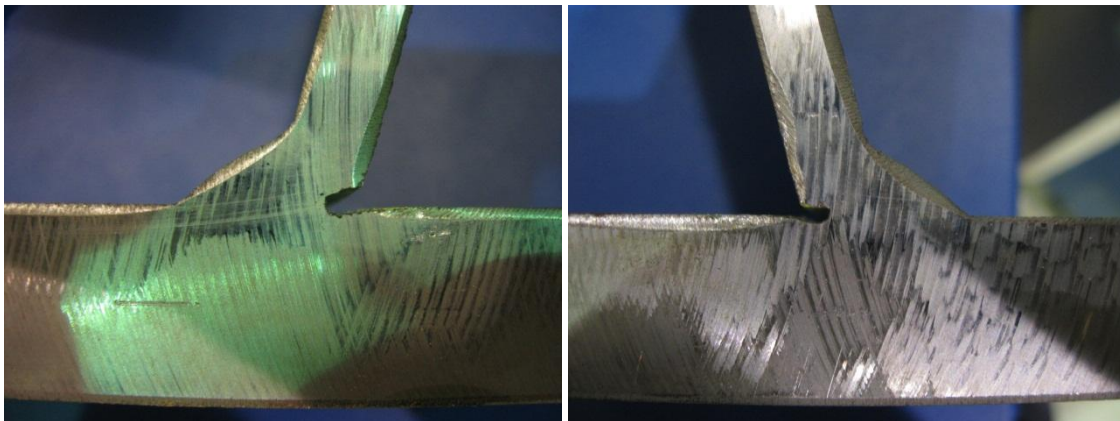


Figure 3.7 Saw-cuts introduced at the weld roots on the OB (Left) and UB (Right) specimens

Overall, there were eight different specimen series with two different welding processes, different target weld penetrations, and different root gap opening conditions. The conditions used to fabricate each specimen series and the number of replicate specimens is listed in Table 3.1. The name of each series is a combination of the welding process (GMAW or SAW) and the target penetration percentage (80% to FIL). The FIL series

was targeted to have minimal penetration expected for a fillet weld. For example, “GMAW-80”, or “GM-80”, indicates that this series of welds were made by gas metal arc welding with a target penetration of 80% into the rib plate. The last two specimen series (OB and UB) were fillet welded with the different bevel preparations.

Table 3.1 Test specimen series.

Series Name	Welding Process	Target Penetration	Rib Plate Beveling	Number of Specimens
GM-80	Gas Metal Arc Welding	80%	Normal	16
SA-80	Submerged Arc Welding	80%	None	15
SA-60	Submerged Arc Welding	60%	None	8
SA-40	Submerged Arc Welding	40%	None	8
SA-20	Submerged Arc Welding	20%	None	8
FIL	Submerged Arc Welding	None	None	8
OB	Submerged Arc Welding	None	Over-beveled	16
UB	Submerged Arc Welding	None	Under-beveled	16

3.2 Test Matrix

Fatigue tests were carried out in two locations; Turner-Fairbank Highway Research Center (TFHRC) and the structures lab in Virginia Tech. Forty-eight specimens were tested at TFHRC including the GMAW-80, SAW-60, SAW-40, SAW-20 and FIL series. Forty-seven specimens were tested in the Virginia Tech Structures Laboratory including the SAW-80, OB, and UB series. The specimens were tested at different stress ranges at two different R-ratios as shown in Table 3.2. With the exception of two specimens tested at 16.67 ksi, all specimens were tested at higher stress ranges to avoid effects of the constant amplitude fatigue limit threshold (CAFL).

Table 3.2 Test matrix

Series	16.67 ksi, R=-1	26.67 ksi, R=-1	33.33 ksi, R=-1	36.67 ksi, R=-1	18.33 ksi, R=0	33.33 ksi, R=0	40 ksi, R=0	Total
GM-80	2	1	5	3	1	3	1	16
SA-80	-	-	8	4	-	3	-	15
SA-60	-	-	-	5	-	3	-	8
SA-40	-	-	-	5	-	3	-	8
SA-20	-	-	-	5	-	3	-	8
FIL	-	-	-	5	-	3	-	8
OB	-	-	8	4	-	4	-	16
UB	-	-	8	4	-	4	-	16

3.3 Equipment

The fatigue tests at Virginia Tech were performed on an MTS servo-hydraulic load frame with an integrated data acquisition system. A customized testing fixture allowed application of both positive and negative bending moments that were developed at the TFHRC also used for the VT testing. This section includes descriptions of the three key parts of the testing equipment: the MTS servo-hydraulic load frame; the MTS integrated controller/data acquisition system; and the customized loading fixture.

3.3.1 MTS Servo-hydraulic Test System

A 110 kip MTS Landmark™ Servo-hydraulic Test System was used for all fatigue testing at VT. It consists of a floor-standing MTS Landmark loading frame connected to a MTS Hydraulic Power Unit (HPU) and a MTS FlexTest® controller with a computer workstation. Figure 3.8 shows the MTS load frame used at Virginia Tech; similar MTS test systems were used at TFHRC.



Figure 3.8 MTS servohydraulic test system at VT

Table 3.3 Floor-standing load frame specifications (model: 370.50)

Load Frame Specifications	U.S. Units	SI Units
Force Capacity (rated dynamic force)	110 kips	500 kN
Servo-valve Flow Rating	30 GPM	114 LPM
Available Actuator Ratings	55, 110 kips	250, 500 kN
Actuator Dynamic Stroke	6 in	150 mm

A FlexTest 40 controller with a capacity of up to 4 control channels on one test station was used in the fatigue tests performed at VT. It consists of a Series 494 Hardware chassis that contains controller hardware as shown in Figure 3.9, and a computer workstation that runs MTS controller applications



Figure 3.9 Flextest 40 controller (series 494) and handset (model: 494.05)

Figure 3.10 shows the capability to monitor both the computer command and load cell response signals using the MTS application software. The software continuously monitors the test response and “tunes” the command signal to make sure the desired load range is achieved on the specimen. This allows the command signal to “over drive” the test to achieve higher cyclic frequencies without compromising accuracy of the loading.

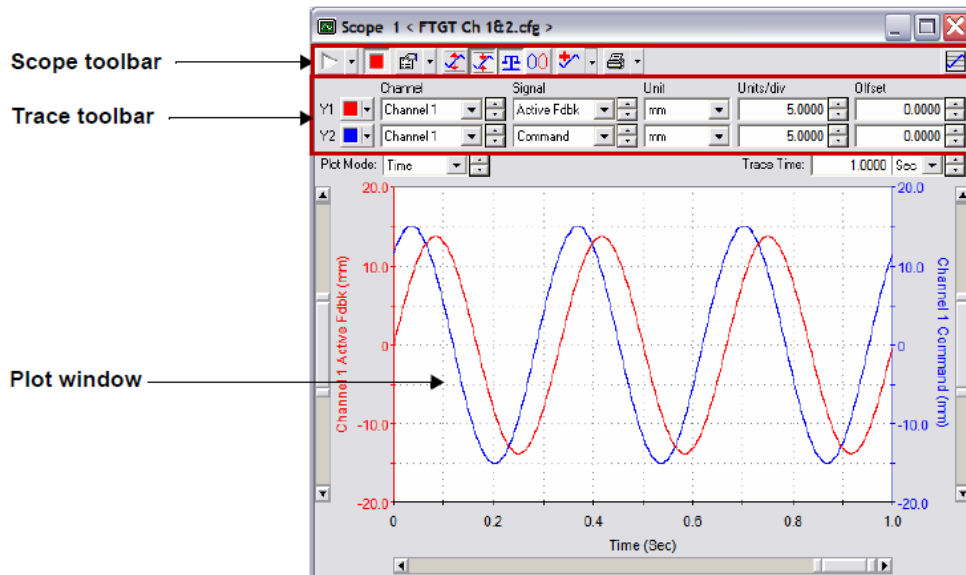


Figure 3.10 Comparison of command and response signals at a 4 Hz test speed showing “over-driving” of the command signal

3.3.2 Customized Fixture

A customized fixture was designed and fabricated to provide boundary conditions and stabilize the specimens during the tests. It consists of a steel spreader beam with high stiffness and four steel columns used to attach rollers. Figure 3.11 shows the two rollers mounted on each column to facilitate the application of load reversal on the test specimens. Each of the rollers is supported by two adjustable threaded rods to allow the rollers to be adjusted to fit the test specimens. The pillow blocks used to support the rollers have bearings that allow for some angle adjustment so the rollers can be adjusted perfectly parallel to the test specimen surface. The rollers can tilt to make tight contact with the specimen thereby providing evenly distributed clamping forces along the length of the roller. The welded test specimens have a certain amount of plate distortion induced by welding. The angular adjustment capability of the rollers is essential to allow the rollers to adapt to the specimen and prevent distortional twisting that can cause error in the applied stress range.

The bottom flat of the specimen rib plate is positively attached to the hydraulic actuator by bolting. Since the bottom of the rib is not typically flat or parallel to the deck plate, two spherical bearing washers are placed between the specimen and hydraulic actuator to allow specimen alignment. The washers can be rotated when the specimen is installed to level the deck plate in two directions. The spherical washers are shown in Figure 3.12. Some of the early tests performed at TFHRC did not utilize the spherical washers in the test set-up.

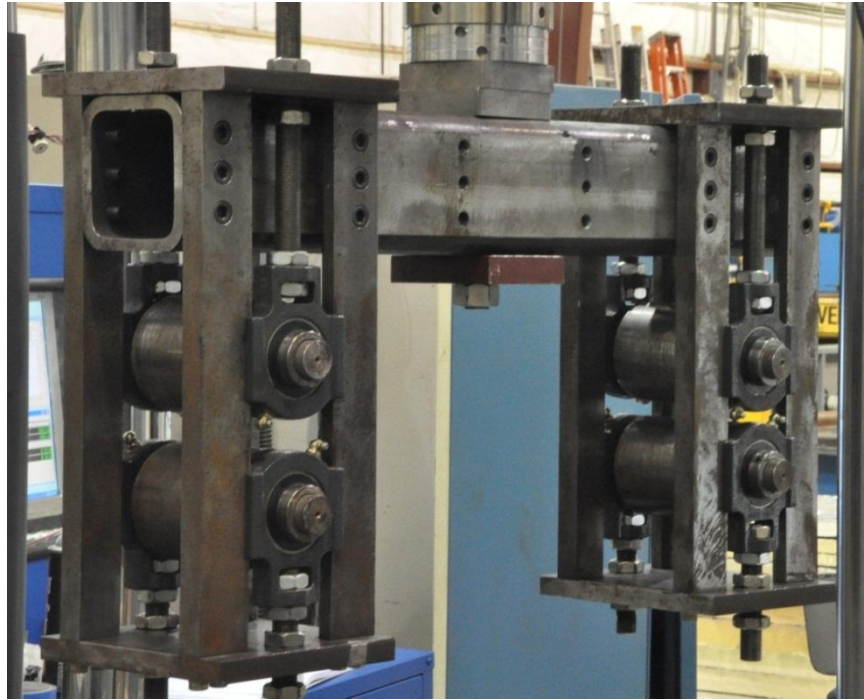


Figure 3.11 Customized fixture



Figure 3.12 Spherical bearing washers

3.4 Test Setup and Procedure

3.4.1 Test Setup

The testing fixture applies load and roller boundary conditions to the test specimens as shown in Figure 3.13. The strip of deck plate is simply supported by rollers at each end resulting in a 24 in. bending span length. The loads were applied through the bottom flat

surface of the rib plate. The top and bottom rollers allowed both positive and negative loads to be applied to the specimens resulting in both positive and negative bending of the deck plate. Large bearing plate washers were placed above and below the rib flat to prevent distortional flexing.

The test fixtures essentially create 4-point bending in the deck plate. However, since the rib walls are not perpendicular to the deck plate, the bending stress distribution in the deck plate is altered by the presence of axial forces. The idealized moment and axial force distribution in the rib and deck plates is shown in Figure 3.14 . This represents the results from 1st-order structural analysis. Additional 2nd-order moments are also induced in the rib plate walls since the rib plate flexes under load. It is noted that the size of the bearing plate has an effect on the rib stress distribution. Figure 3.14 shows the scenario for tests at VT where 3.75” wide bearing plates were used. The moment and axial force diagrams for the rib plate are slightly different for the tests performed at TFHRC since 5” wide bearing plates were used. These 2nd-order effects are considered further in the finite element analysis performed in Section 4.2.5.

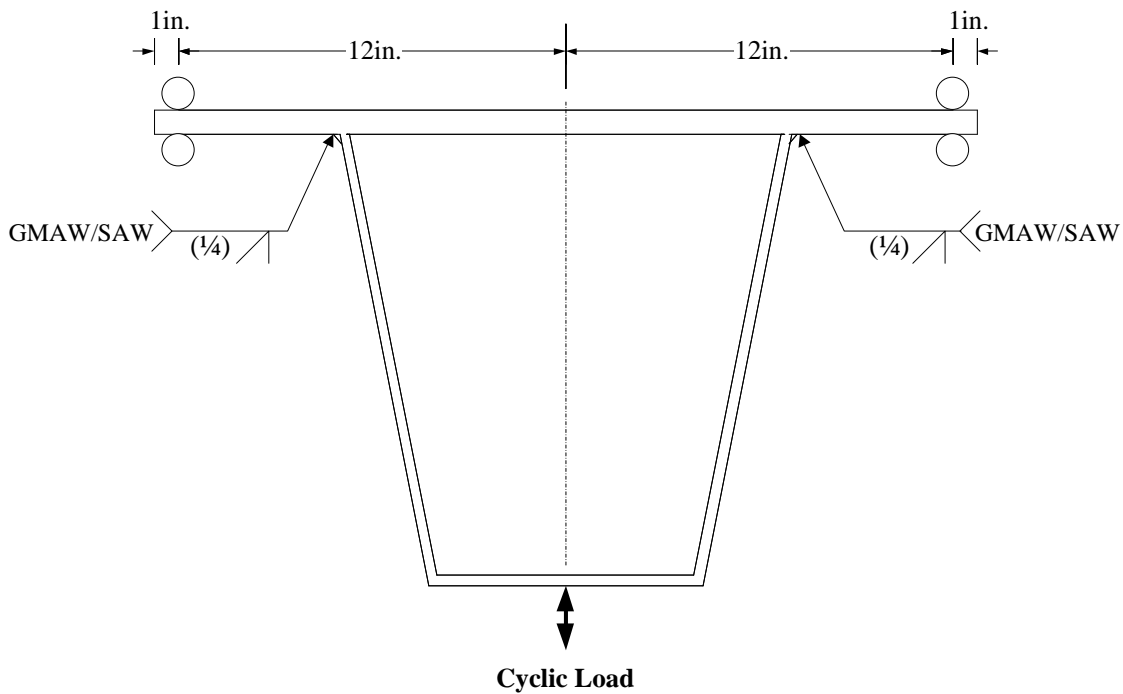


Figure 3.13 Test setup

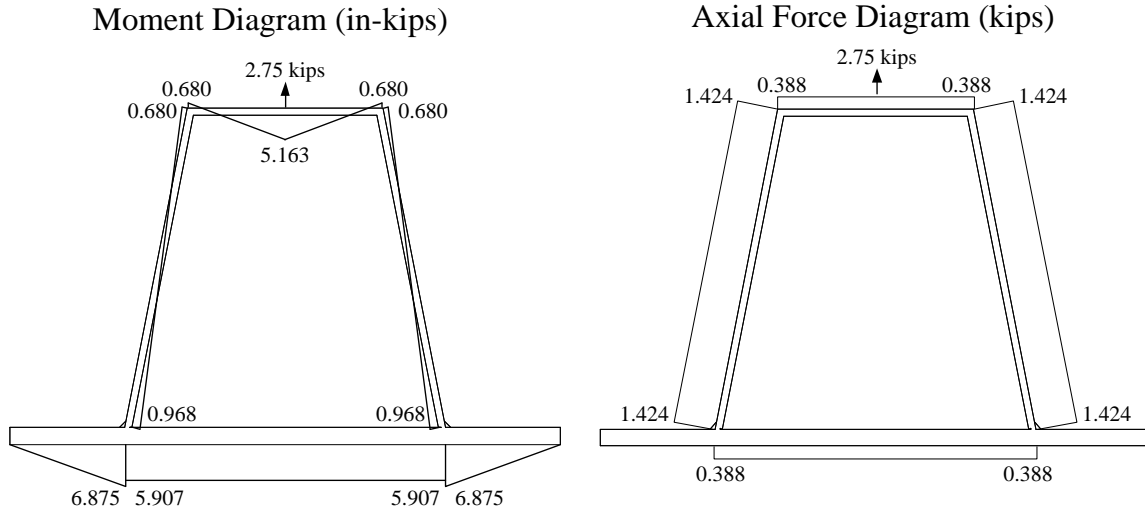


Figure 3.14 Moment and axial diagrams for the tests at VT

3.4.2 Test Procedure

Identical procedures were followed when installing the test specimens to minimize any testing bias due to the fixturing. Figure 3.15 and Figure 3.16 show typical test specimens mounted in the loading fixture at VT and TFHRC, respectively. The distance between the roller supports is precisely 24 in. while the specimen length is 26", leaving one in. extension beyond the rollers. The installation procedure is as follows:

- 1) The specimen is first bolted to the hydraulic actuator and the deck plate is leveled about two axes using the spherical washers. The rollers are not in contact with the specimen at this stage.
- 2) The lower rollers are adjusted up so they just contact the bottom surface of the deck plate. Each side of the roller is adjusted individually so the roller is in even contact across the width of the deck plate. This procedure exactly adapts the test fixture to the specimen geometry so the rollers do not impart any twisting to the specimen.
- 3) The top rollers are adjusted to contact the top surface of the deck plate. A modest pre-tension force is applied to the top roller to prevent slip in the test fixtures when the specimen is subjected to load reversal.



Figure 3.15 Test Setup at VT



Figure 3.16 Test Setup at TFHRC

Consistent boundary conditions between specimens are essential to minimize scatter in the test results. Ideally, the top and bottom rollers should provide ideal boundary conditions. However, excessive clamping force between the two rollers potentially can add some fixity. The stress state at the potential cracking locations is expected to change dramatically if fixed end conditions exist instead of the ideal rollers. Too much clamping force from the rollers on the deck plate can cause roller friction that effectively creates a semi-fixed boundary condition. Too little clamping force would introduce slip in the load path and allow the specimen to bang and vibrate in the test fixture under load reversal. Therefore, procedures were imitated to measure and limit the clamping force to insure that the ideal roller boundary condition is present. After a few trials, the clamping force was set to be 70 lbs on each side, 140 lbs in total. The force was measured by monitoring the load cell output during the clamping procedure. It was observed that the rollers were still able to rotate freely at this clamping force level.

Since only one load cell is used to measure the summation of both roller reactions; the clamping forces on both roller supports should be equalized. The load cell is not capable of detecting differential clamping forces between the different supports as long as they balance each other out. Different clamping forces between the supports could alter the stress state between the two welds which is a divergence away from the ideal boundary conditions used in the FEM. Care was taken in the specimen installation procedure to ensure equal clamping force on each side of the specimen.

The key steps described below were followed for the specimen installation:

- 1) Tightly bolt the specimen to the actuator through the bottom of the rib. Use a level to make sure the deck plate is horizontal before tightening the bolt.
- 2) Manually raise the actuator under displacement control to raise the specimen into the desired test position.
- 3) Take a zero load reading with no roller contact with the specimen.
- 4) With the actuator still under displacement control, apply the equal 70 lb clamping force from the four rollers to the deck plate individually one after another by adjusting the height for both tips of each roller. Also make sure the rollers tilt

- along with the specimen for evenly distributed clamping forces along the roller lines. This can be done by applying half of the clamping force for each roller, in this case 35 lbs, from each tip of the rollers. To determine how much clamping force is being applied, access the real-time feedback from the load cell through the computer workstation.
- 5) After applying the clamping forces from all the rollers, the reading from the load cell should be back to zero. Though small error within tolerance may exist. In this case turn the actuator to load control mode and manually command the force back to zero. However this action is not suggested if the error is considered to be out of tolerance since differential clamping forces may be caused by this action. Instead, step 4 and step 5 should be performed again.
 - 6) After the specimen is clamped tight with zero reading from the load cell, offset the displacement reading from the LVDT to zero as well. Turn off the manual control then initiate the cyclic load in the MPT application with the corresponding test procedure and environmental variables.

A test procedure was designed and programmed in the MPT application through the Procedure Editor. It acquired data from the sensors and controlled the action of the actuator and HPU. The loading function was specified as a sine wave with the peak/valley levels corresponding to the target stress range and R-ratio listed in the test matrix in Table 3.2. Two data limit detectors were enabled to stop the test if either one of them were triggered. The first data limit would be triggered if the peak/valley displacement exceeds a preset limit. The second data limit detector monitors the difference between the peak/valley displacements of two successive cycles and would be triggered if the difference were out of the specified tolerance. This detector was usually triggered when fatigue crack initiation occurred and displacement increased. Three data acquisition commands were programmed during testing. The first recorded the peak and valley values of load and displacement for the first 2000 cycles after testing was initiated or resumed following a pause. The second recorded the same values for the last 2000 cycles before the cyclic load was terminated or paused. These two data logs showed the behavior of the specimen during the stabilization of the sine wave loads and before the failure. The third data acquisition command recorded the peak/valley values of load and

displacement at one hour intervals during the test. This data logging provides assurance that the stress range remained constant over the entire test. The test procedure in the Multi-Purpose Testware (MPT) is shown in Figure 3.17.

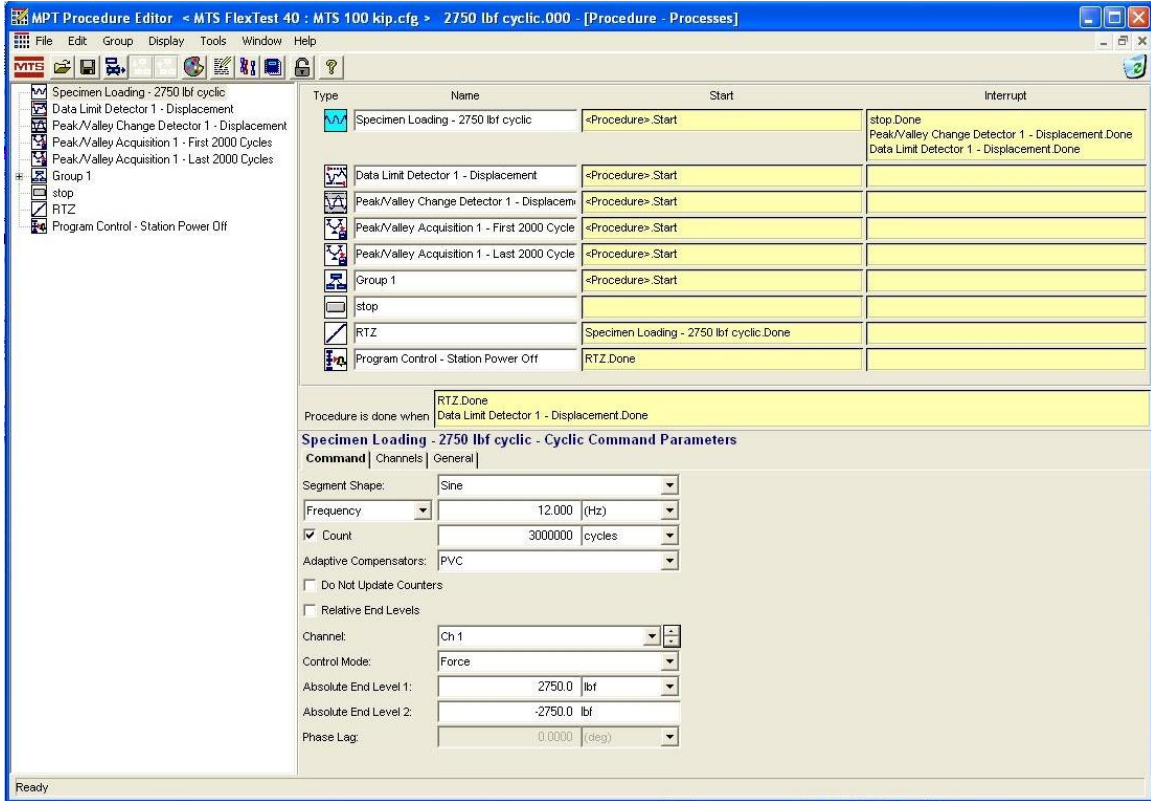


Figure 3.17 Test procedure in the MPT

3.5 Post-Test Processing

3.5.1 Measurement of the Weld Profile

Each of the test specimen series was produced with a different welding procedures resulting in different geometric weld profiles. There was also a certain amount of profile variability along the length of the welds within a given series. Therefore, detailed measurements were made of the weld profile at both exposed edges of each test specimen. This data was statistically analyzed after testing to determine the effect of various geometric features on fatigue life. The specimens were sanded and polished on each specimen edge at the rib-to-deck weld location. An etching solution of concentrated hydrochloric acid was applied on the surfaces to mark the weld metal and heat affected

zone (HAZ). High resolution digital photographs were taken of each etched weld along with a reference scale. The photographs were then imported into AutoCAD, scaled to the drawing scale, and curved lines were traced along the weld outlines. Additional straight measurement lines were then drawn to record features of the weld profile. Figure 3.18 shows typical AutoCAD drawings for each measurement location. The measurement locations were assigned with reference numbers as shown in Figure 3.19 relative to the side where the specimen failed. Locations 1 and 3 are on the cracked side, while locations 2 and 4 are on the un-cracked side. For cases where cracks occurred on both sides, locations 1 and 3 are on the side with the larger crack.



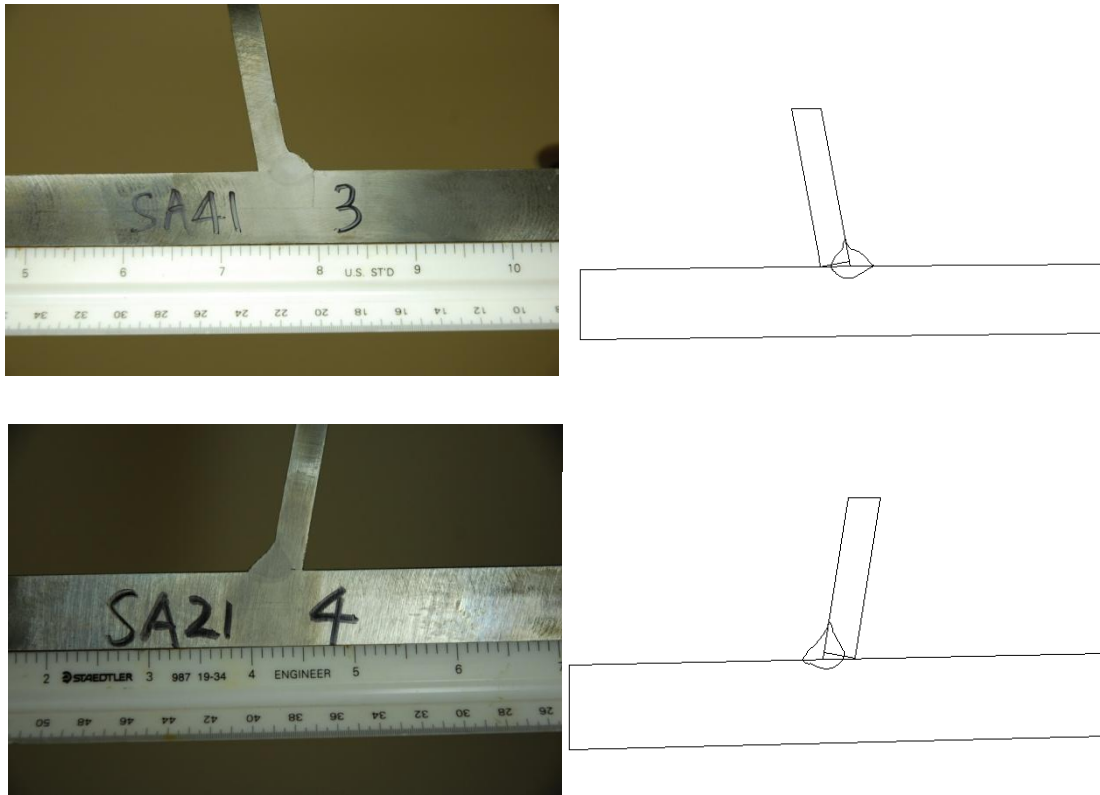


Figure 3.18 AutoCAD drawings of weld profiles

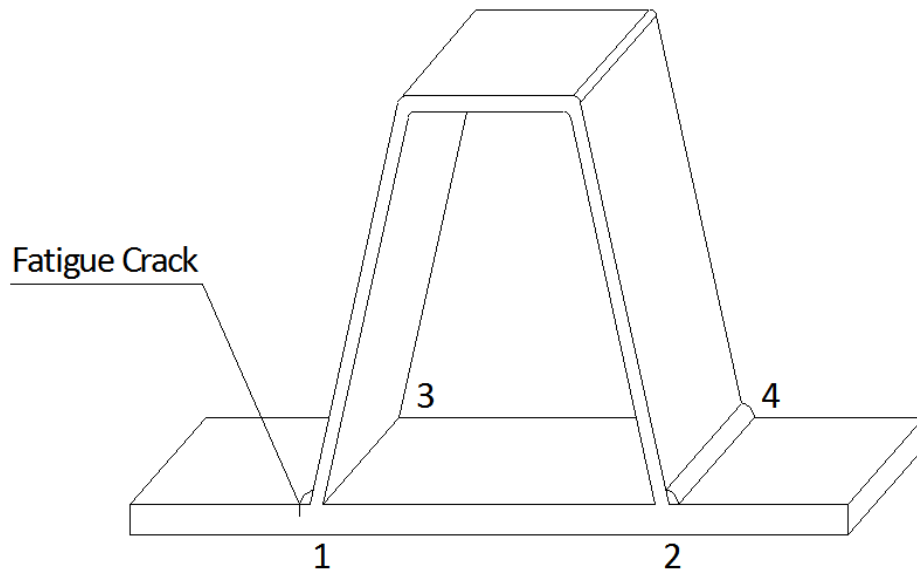


Figure 3.19 Denotation of weld locations

A number of numerical measurements were taken from the AutoCAD drawings for each

weld profile, as shown in Figure 3.20. These measurements included the weld toe size, weld penetration, weld throat size, weld area, etc. Tables listing all the measurements can be found in Appendix D.

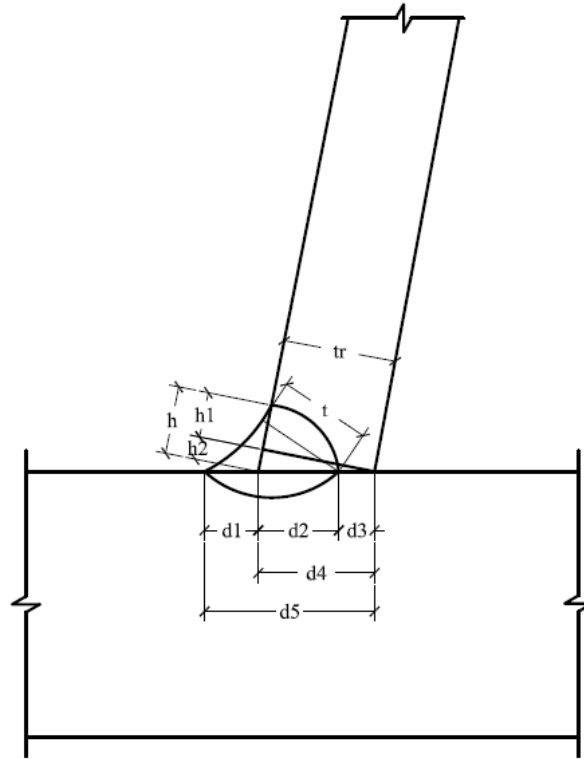


Figure 3.20 Measured dimensions

The measured weld dimensions are defined as follows:

- d_1 – weld toe size (on the deck plate)
- d_2 – size of the weld penetration (into the rib plate)
- d_2/d_4 – percentage of the weld penetration
- d_3 – size of the gap behind the weld
- d_1+d_2 – total size of the weld
- h – weld height, essentially the weld toe size on the rib plate
- t – weld throat size, defined as the distance from the weld root on the deck plate to the nearest point on the curved weld surface
- A_w – weld area
- t_r – thickness of the rib plate

The measurements indicated that the target weld penetration for each series was not achieved. As shown in Appendix D, the welds with 80% target penetration had larger penetration compared to the other specimen series, but the penetration values did not significantly change among other specimen series. The average penetration achieved for the fillet welds and partial penetration welds with 20%~60% target penetration was between about 60%~70%. As a result, the target penetration values were no longer taken as a relevant factor. Although the names of the specimens and series were kept, they had no relation with the penetration of the welds in that series.

3.5.2 Measurement of the Effective Length (L_e)

The effective length, L_e , is defined as the distance from the fatigue crack at the weld toe on the deck plate to the line of roller support in the fixture, as shown in Figure 3.21. The moment within this length varies linearly from zero at the support to certain value at the weld toe, as shown in Figure 3.14. Therefore, the L_e value directly affects the actual stress range at the weld toe on the deck plate, which is the primary crack location.

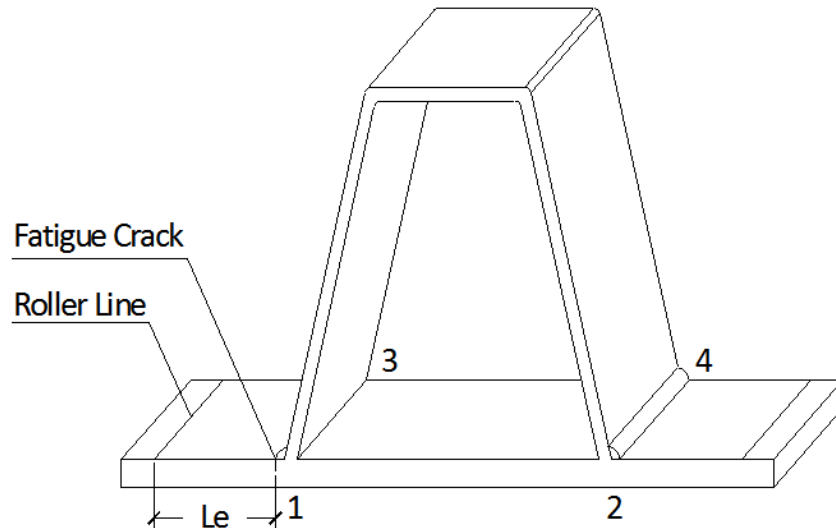


Figure 3.21 Definition of L_e

L_e was designed as 5" for all the tests. However this does not include the presence of the weld. Variations in weld toe size, fabrication tolerance, and test specimen mounting tolerances, cause variations in L_e . This affects the stress range at the location of fatigue

cracking at the weld toe. To quantify this effect and get accurate stress ranges, the actual L_e values were measured on each specimen after testing. The rollers left clear marks on the deck plate at the points of contact. The distance between these marks and the weld toe could be accurately measured. The results are tabulated in Appendix E.

3.5.3 Record of the Tack Weld Locations

Tack welds were made on the specimens to hold the rib plate and deck plate in place before the continuous welds were placed. The continuous welds passed over and re-melted the tack welds during the welding procedure. This results in increased weld metal volume at the tack weld locations and a corresponding enlargement of the weld size. A possible concern is that the geometry discontinuity at the tack weld locations would result in premature fatigue cracking in that area. The tack weld locations were marked on the specimens during fabrication. These locations were compared with the fatigue crack initiation locations observed in the test specimens. Forty-four specimens tested at the TFHRC were examined for this investigation. The specimens were loaded to open up the fatigue crack and expose the crack surface as shown in Figure 3.22. The tack weld locations and fatigue crack initiation points were recorded and compared in Appendix F. A few observations were made during the recording:

- 1) The cracks were predicted to initiate around the mid-width location along the weld toe as shown in Figure 3.23. This is based on stress analysis of the specimens and the fact that the stress state varies from plane-strain at mid-width to plane stress at the edges. Therefore, no conclusions can be made if the fatigue cracks initiate at tack welds located at the mid-width location. Only the fatigue cracks initiating from the tack welds located away from the mid-width location can provide information useful to assess the effect of tack welds.
- 2) The middle $\frac{1}{4}$ width of the deck plate can be assumed to have an equal probability of fatigue crack initiation at any point. Since there is little variation in stress range across this region, the "weak-link" point of crack initiation can occur at any location. In cases where both the tack welds and crack initiation points were located in this region, it was identified as "close to center".
- 3) For the cases where tack welds and cracks occurred at different locations, either with

one of them or neither at the center, it should be regarded as negative evidence to any relationship between them.



Figure 3.22 Setup for breaking specimens from fatigue cracks

After recording 44 specimens (Appendix F), it showed an inconclusive relationship between tack welds and crack initiation locations. Eleven specimens were regarded as having a relation between them, while 12 of them were regarded as not having such relation. The rest of the specimens could not be confirmed for a conclusion because either both locations occurred at the center, or no tack weld was present. As a result, it can be concluded that tack weld locations were not more susceptible to fatigue cracking compared other locations along the weld.

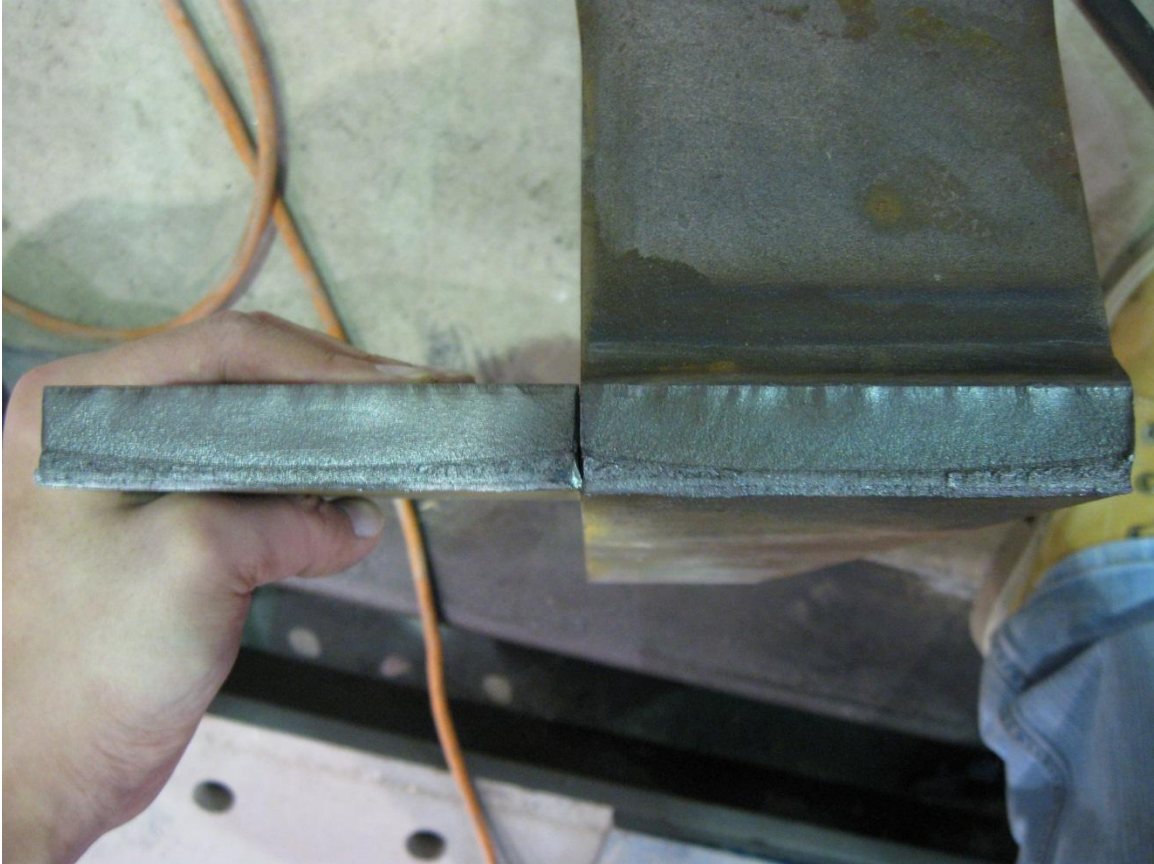


Figure 3.23 Typical crack surface

3.6 Test Results and Discussion

Three failure modes were observed after fatigue testing 95 specimens as shown in Figure 3.24. The failure modes are labeled to indicate the point of fatigue crack initiation as follows: WT@DECK refers to cracks that initiate at the weld toe on the deck plate and propagate through the deck plate thickness; WT@RIB refers to cracks that initiate at the weld toe on the rib plate and propagate through the rib wall thickness; and WR indicates cracks that initiate at the weld root notch and propagate through the weld throat. All three failure modes were observed in this testing program.

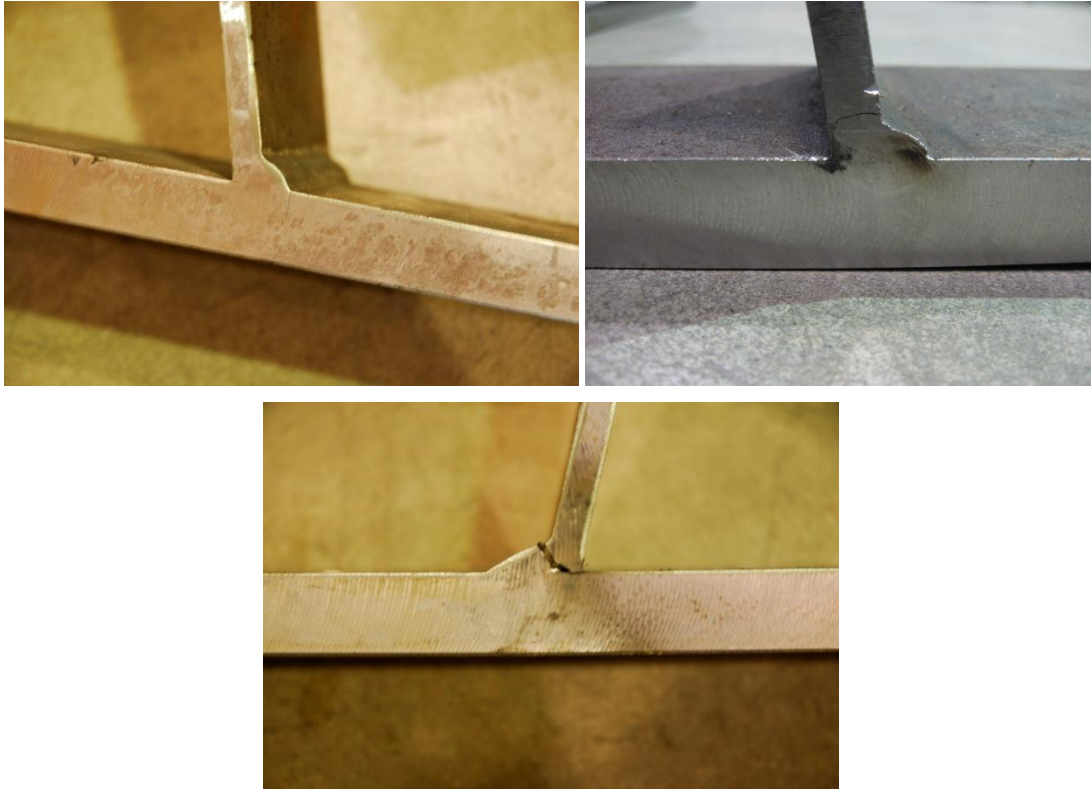


Figure 3.24 Failure modes: WT@DECK, WT@RIB, and WR

For the initial test specimen series, only the WT@DECK and WT@RIB failure modes were observed. Among the tests conducted at the TFHRC, only the WT@DECK failure mode was observed. Both the WT@DECK and WT@RIB failure modes were observed in the initial test series performed at VT. This can be explained by the difference in test fixtures between the two sites. The TFHRC tests used larger bearing plates to support the bottom surface of the rib where it was attached to the actuator. The larger support area reduced the amount of bending occurring in the rib wall. This slightly reduced the stress range occurring at the weld toe on the rib wall and biased the failure to the weld toe on the deck plate. The VT tests with the reduced size bearing plates came closer to having an equal probability of cracking at the rib plate and deck plate weld toes. The effect of the bearing plate on rib bending is discussed further in Chapter 4.

A noticeable difference was found between the fatigue test results performed at the two different R-ratios ($R=0$ and $R=-1$). For the $R=0$ tests, the entire stress range applies tensile loading at the deck plate weld toe. The $R=-1$ tests apply a complete stress reversal

cycle where the stress range alters between tension and compression. It is generally known that significant tensile residual stresses are present at weldments. When added to the applied stress cycle, a portion of the compressive part of the load cycle is converted to tension. Therefore, a portion of the compressive load cycle can be added to the tension part of the load cycle to calculate the stress range that causes fatigue damage.

The AASHTO bridge code only requires fatigue design for details that are located in regions of tensile stress. The exception is details in regions of stress reversal where the compressive portion of the live load stress cycle is added to the tensile portion to define the stress range for fatigue design. Consistent with this methodology, the stress range for the $R=-1$ tests is calculated assuming the compressive portion of the load cycle causes tensile stress at the detail. This is based on the assumption that the residual tensile stress in most cases is as high as close to the yield stress, therefore the entire compressive stress cycle, as long as it remains elastic, is shifted to tensile cycle.

Using this definition of stress range, the fatigue test results show that the $R=-1$ tests have noticeably longer fatigue lives compared to the $R=0$ tests. If the assumption is correct that the entire compressive portion of the load cycle is converted to tension, the two different R -ratios should show equivalent fatigue resistance. The fact that the $R=-1$ tests show longer fatigue lives indicates that only a portion of the compressive load cycle is converted to tension due to residual stresses. This indicates that the residual stress for the weldments tested is lower in magnitude than the maximum compression stress induced by the load cycle.

The residual stress magnitude at weldments depends on many variables such as the plate thickness, weld size, and welding procedure. Residual stress magnitude cannot be readily calculated. Therefore, the $R=0$ tests where the entire load cycle is guaranteed to produce a tensile stress range should be used to determine the fatigue resistance. When calculating the stress range through structural analysis, both the tensile and compressive portions of the stress cycle should have the same sign and should be added.

Overall, 15 fatigue specimens failed in the WR mode. Only one of the 15 had a closed root notch, the others had open root notches. A total of 24 specimens were tested with

open root gaps. Seventeen of them were tested under $R=-1$. Fourteen failed from root cracks while three failed at the weld toes; and the other one ran out over 4 million cycles without failure. The rest 6 specimens with open root gaps under $R=0$ also failed at weld toes but due to the fact that they were tested under compressive cycles at weld roots. There is strong evidence that the open root gaps enable the root gap failure mode to occur prior to weld toe cracking for the specimen geometry tested. There is a clear increase in fatigue resistance of the rib-to-deck joint when the root gap is closed by the combination of joint design and weld shrinkage.

Among the 95 specimens from the seven test series, no distinguishable difference was found in the fatigue resistance. The effect of weld penetration and other geometric variables is studied in more depth in 0. The weld dimension measurements shows that the average penetration achieved the target value at 80% for GMAW series, but is 65% to 70% for all of the submerged arc welds (SAW series) and 60% to 65% for the fillet welds (FIL, OB & UB series), representing the typical penetration that can be achieved without special technique. The lower bound penetration with 95% confidence is 64% for GMAW series, and 50.2% for SAW series and fillet welds, which is used in 0 to derive the requirement for the minimum weld toe sizes.

Chapter 4. Finite Element Modeling and Hot-Spot Stress Analysis

The purpose of hot-spot stress concept is to provide structural stress values for different weld toe details that can be compared to a single S-N curve. It is “typically used where there is no clearly defined nominal stress due to complicated geometric effects or where the structural discontinuity is not comparable to a classified structural detail” (Hobbacher, 2008). The hot-spot approach is very useful for fatigue analysis of tubular joints because nominal stress is usually very hard to calculate. It has similar advantages for plate-type structures where detail specific S-N curves are unavailable. Ideally the hot-spot stress values calculated using FEA should be mesh insensitive because the stress magnitude depends on the global geometry of the structure. It should not be different from one finite element model to another. However, in the currently available structural stress approaches discussed in Section 2.2.1, the goal of absolute mesh insensitivity is still not achieved. Even though stresses are calculated at reference points located away from the weld toe, there is still some dependence on mesh size. Therefore, modeling rules are still necessary in order to get consistent hot-spot stress values from finite element models built from different sources. Among the different recommended finite element modeling guidelines for structural stress evaluation, the DNV-RP-C203 (2008) and IIW-1823-07 (Hobacher, 2008) are used in this study since they have been validated in the literature.

Since the notch effect (stress concentration effect) is intended to be excluded from the hot-spot stress values, the reference points used for the extrapolation should be located outside of the region that is considered to be under the influence of notch effect.

However, they also should be close enough to capture the stress gradient approaching the weld toe. Locations are specified in both the DNV and IIW recommendations for different cases. Hot-spot stresses are calculated assuming linear elastic material behavior with an idealized structural model that contains no fabrication-related misalignment.

Only the linear stress distribution through the plate thickness needs to be evaluated to define hot-spot stress as shown in Figure 4.1. However, the finite element model should still have element types, shapes, and mesh size capable of capturing the stress gradients

and effects of plate bending (DNV-RP-C203, 2008).

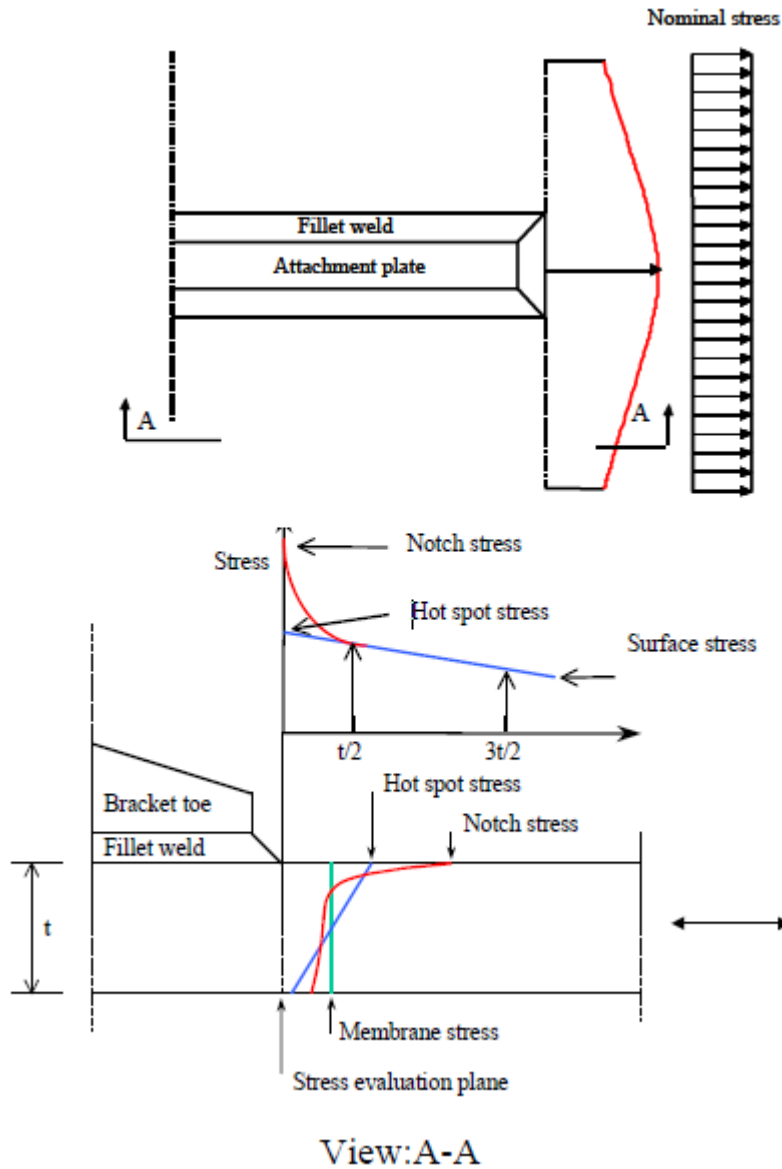


Figure 4.1 Schematic of the hot-spot stress distribution (DNV CN-30.7)

It should be noted that the hot-spot stress method, at least the methods defined by DNV and IIW, is limited to the assessment of fatigue at weld toes. The hot-spot methodology may be extended to other fatigue cracking locations such as the weld root, but this is further complicated since the master S-N curve used for hot-spot fatigue evaluation was developed based on the geometric and dimensional parameters of weld toe geometries.

4.1 Recommended Procedures

4.1.1 DNV Recommendations

Det Norske Veritas (DNV) adopted the procedures introduced in Section 2.2.1 as described in DNV-RP-C203 “Fatigue Design of Offshore Steel Structures”, DNV CN-30.7 “Fatigue Assessment of Ship Structures”, and DNV-RP-C206 “Fatigue Methodology of Offshore Ships”. All three documents contain similar recommendations regarding element type, mesh size, reference point locations, and extrapolation methods. These documents are widely used and are considered to be a very important reference for this research.

Both DNV CN-30.7 and DNV-RP-C206 suggest that both global and local models should be developed for fatigue analysis purposes. Global models help to find the potential critical locations for fatigue while the local models enable calculation of hot-spot stress values at the critical locations. DNV-RP-C203 states that the extent of the local model should be chosen so that the influence of the boundary conditions is minimized. In this study, since the test specimens are relatively small, only one model was required to capture both the global and local effects.

Three weld toe types are identified as illustrated in Figure 2.13. Either 2D shell elements or 3D solid elements can be used in the finite element models. Thin shell elements located at the mid-plane of the structural component should be used if shell elements are chosen. Caution is needed when modeling type b) weld toes to prevent under-estimation of the stress. In shell element models, the welds are usually not explicitly modeled except for special cases where high local bending effects are present. Such cases include fabrication misalignment and offsets between plates. In these cases the weld can be modeled as transverse plate/shell elements with appropriate stiffness or by assigning displacement constraints between the appropriate nodes. If the weld is modeled using transverse shell elements, the weld element thickness may be defined as twice of the base plate thickness. Eight node elements with a quadratic shape function (Q8) are preferred, especially in regions with high stress gradients. The 4-node linear elements may be prone to shear locking problems.

Alternatively, 3D solid elements are recommended for more complex geometries. The solid elements should also have quadratic shape functions capable of capturing steep stress gradients and a linear bending stress distribution through the base plate thickness. Isoparametric 20-node elements with quadratic shape functions along the edges (Q20) are recommended. These elements enable evaluation of both the membrane and bending stress components using reduced integration from as few as two integration points through the thickness of the base plate. Eight-node solid elements with linear shape functions could also be used but a finer mesh size is required. The weld should be explicitly modeled in the 3D solid models to accurately capture the local stiffness of the geometry.

The requirements for mesh density and element size vary depending on the element types used in the models. General finite element modeling rules should be followed to obtain accurate results, such as limiting the corner angles of quadrilateral and hexahedral elements to between 45° to 135° , and limiting the element aspect ratio to less than five. For the Q8 shell elements and the L4 shell elements with additional internal degrees of freedom a mesh size between $t \times t$ and $2t \times 2t$ may be used, where t is the thickness of the base plate. Larger mesh sizes may produce non-conservative results in the hot-spot region. For the Q20 solid elements, only one element is required through the plate thickness. The first few element rows in front of the weld toe in the hot-spot region should have the following dimensions: 1) the element length can be selected as the plate thickness t with the limit of $2t$; 2) the element width in the transverse direction can be again selected as t ; and 3) the element width should not exceed the attachment width for type c) weld toes, where the attachment width is defined as the plate width plus twice the weld toe size. For the 8-node solid elements with linear shape functions, a finer mesh size should be modeled. In this case, at least 4 elements are recommended through the base plate thickness. Both the length and width of the elements should be reduced proportionally.

The hot-spot stress values are obtained by linear extrapolation as illustrated in Figure 4.1. The extrapolation is based on read-out points located at $0.5t$ and $1.5t$ away from the weld toe following the DNV-RP-C203 recommendations. The extrapolation lines are shown in

Figure 4.2 for both the shell and solid element models. When a $t \times t$ element size is used in the hot-spot region, the extrapolation can be performed as follows for both the shell and solid elements:

- If shell elements are used as shown in Figure 4.2 (left), the surface stress calculated in the model can be directly used as read-out points at the $0.5t$ and $1.5t$ locations.
- If solid elements are used, the surface stress needs to be extrapolated from the integration points; then linearly interpolated to $0.5t$ and $1.5t$ locations as shown in Figure 4.3.

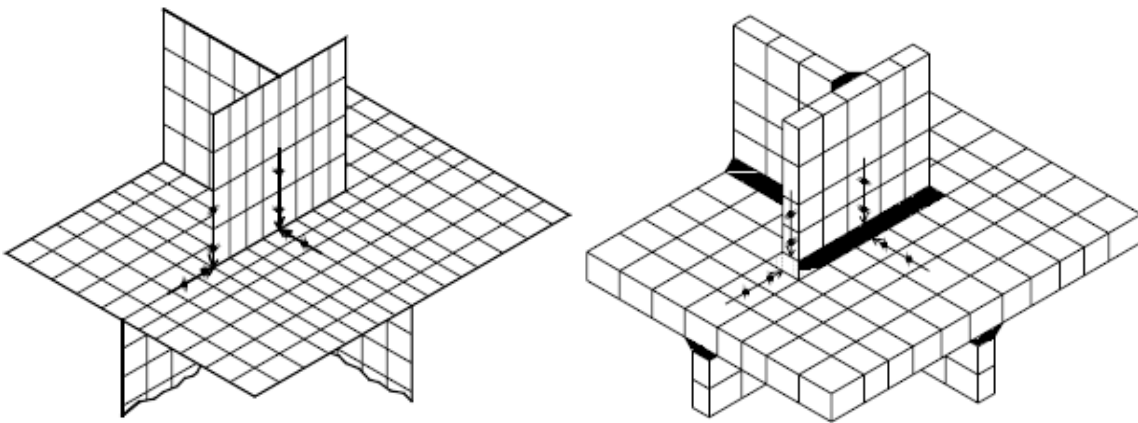


Figure 4.2 Stress extrapolation in 3D FE Models (DNV-RP-C203)

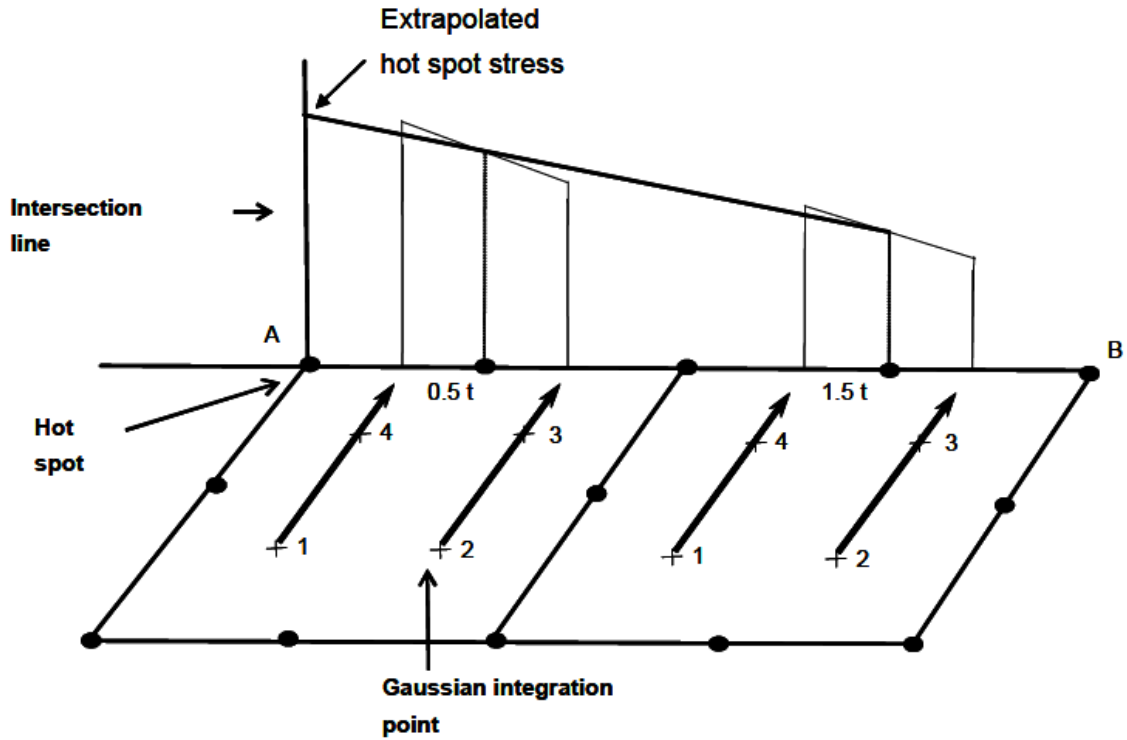


Figure 4.3 Interpolation of stress from the element integration points to the read-points (DNV-RP-C203)

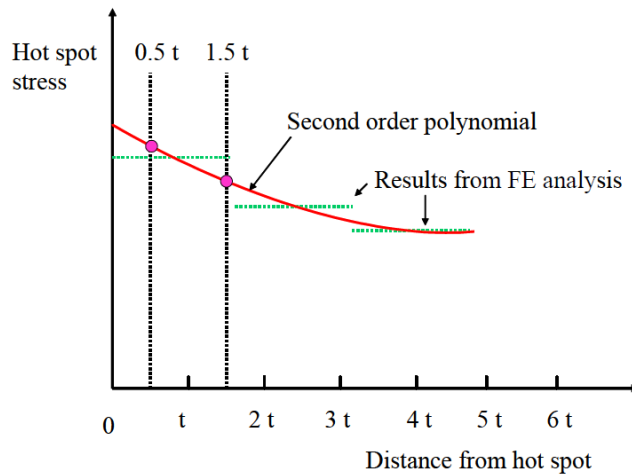


Figure 4.4 Hot-spot stress derivation for element sizes larger than $t \times t$ (DNV-RP-C203)

If the model is built using 4-node shell elements with a mesh size larger than $t \times t$, the stress values at the read-out points should be derived from a quadratic curve fit to the corner point by stress values of the first three elements adjacent to the weld toe. For

models built using 8-node elements with a mesh size larger than $t \times t$, the stress values on the mid-side nodes of the first three elements adjacent to the weld toe should be used for quadratic curve fitting. The stress values at $0.5t$ and $1.5t$ in front of the weld toe can then be determined from the quadratic curve. The extrapolation and curve fitting procedures are shown in Figure 4.4. For the models built in this study the elements size was much smaller than $t \times t$ so this calculation did not need to be performed.

The DNV recommendations provide alternative methods for hot-spot stress determination in addition to the 0515 extrapolation. For both methods, the “effective hot-spot stress” is calculated based on correction factors accounting for different fatigue crack orientations that alter the direction of the principal stresses. The first method, “Method A”, calculates the hot-spot stress components extrapolated from the 0515 read-out points as follows:

$$\sigma_{\text{Eff}} = \max \begin{cases} \sqrt{\Delta\sigma_{\perp}^2 + 0.81\Delta_{\parallel}^2} \\ \alpha\Delta\sigma_1 \\ \alpha|\Delta\sigma_2| \end{cases} \quad (\text{Equation 4.1})$$

where $\alpha = 0.90, 0.80,$ or 0.72 for the DNV C2, C1, and C details, respectively. The principal stresses, $\Delta\sigma_1$ and $\Delta\sigma_2$, are calculated as follows:

$$\Delta\sigma_1 = \frac{\Delta\sigma_{\perp} + \Delta\sigma_{\parallel}}{2} + \frac{1}{2}\sqrt{(\Delta\sigma_{\perp} - \Delta\sigma_{\parallel})^2 + 4\Delta\Delta_{\parallel}^2} \quad (\text{Equation 4.2})$$

$$\Delta\sigma_2 = \frac{\Delta\sigma_{\perp} + \Delta\sigma_{\parallel}}{2} - \frac{1}{2}\sqrt{(\Delta\sigma_{\perp} - \Delta\sigma_{\parallel})^2 + 4\Delta\Delta_{\parallel}^2} \quad (\text{Equation 4.3})$$

The notation of $\Delta\sigma_{\perp}$, $\Delta\sigma_{\parallel}$ and $\Delta\tau_{\parallel}$ refer to the normal and shear stress components perpendicular and parallel to the weld toe as illustrated in Figure 4.5. This method is applicable to either shell or solid elements, with or without inclusion of the weld in the model.

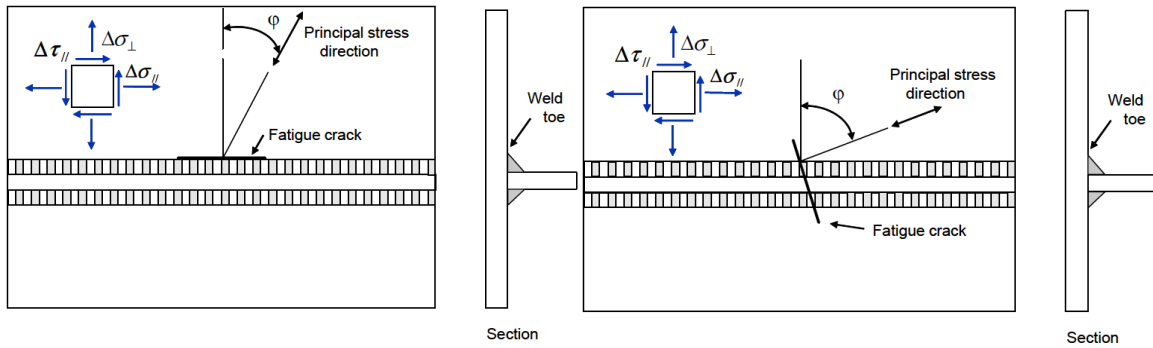


Figure 4.5 Principal stress components and potential fatigue crack orientations (DNV-RP-C203)

“Method B” allows the hot-spot stress to be read as the stress at a single read-out point located 0.5t in front of the weld toe in either the shell or solid element models. The effective hot-spot stress is calculated as follows:

$$\sigma_{\text{Eff}} = \max \begin{cases} 1.12\sqrt{\Delta\sigma_{\perp}^2 + 0.81\Delta\sigma_{//}^2} \\ 1.12\alpha \cdot 1 \\ 1.12\alpha|\Delta\sigma_2| \end{cases} \quad (\text{Equation 4.4})$$

In the present study, only the crack pattern shown on the left in Figure 4.5 occurred. The values of $\Delta\sigma_{//}$ and $\Delta\tau_{//}$ were regarded as zero because they were very small compared to the magnitude of $\Delta\sigma_{\perp}$, therefore Equation 4.2 calculates the principal stress equal to $\Delta\sigma_{\perp}$. The effective hot-spot stress was also calculated as $\Delta\sigma_{\perp}$ according to Method A (Equation 4.1).

For fatigue life prediction, the calculated hot-spot stress is compared to the DNV category D fatigue resistance S-N curve.

4.1.2 IIW Recommendations

The IIW-1823-07 (Hobbacher, 2008) document defines two different weld toe classifications compared to three in the DNV documents. DNV types a) and c) are combined into a single classification as shown in Figure 4.6. Different assessment procedures are proposed for these two weld-type classifications. The hot-spot stress can be determined either by calculation or direct measurement, both following essentially the

same equations and procedures.

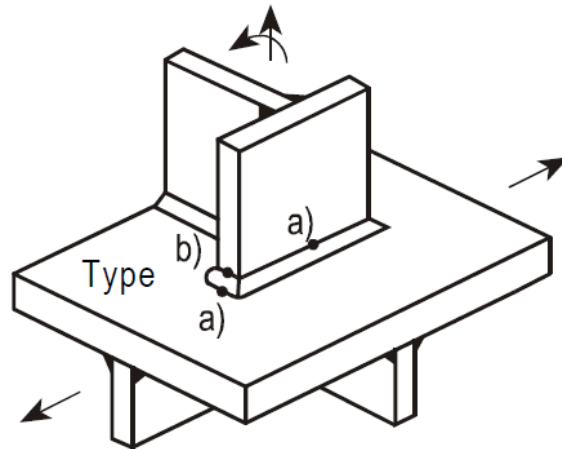


Figure 4.6 Weld toe type classifications (IIW-1823-07)

The IIW recommends essentially the same guidelines for finite element modeling as the DNV. Eight-node thin shell elements are recommended without explicit modeling of the weld and 20-node quadratic solid elements are recommended if the weld is included in the model. Any possible joint misalignment should be explicitly modeled in the geometry because the hot-spot stress methodology assumes idealized, perfectly aligned welded joints. While the modeling recommendations are essentially the same between the IIW and DNV guides, different hot-spot stress assessment methods involving different extrapolation schemes are recommended by the IIW.

For type a) weld toes, if the model has a relatively fine mesh with element size less than $0.4t$, linear extrapolation should be used from reference points located at $0.4t$ and $1.0t$ away from the weld toe, as calculated below:

$$\sigma_{hs} = 1.67 \cdot \sigma_{0.4t} - 0.67 \cdot \sigma_{1.0t} \quad (\text{Equation 4.5})$$

For hot spots with pronounced nonlinear structural stress gradients, or sharp direction changes of the applied force, or thick plates, quadratic extrapolation from the $0.4t$, $0.9t$, and $1.4t$ reference points is recommended. For fine mesh sizes the hot spot stress is calculated as follows:

$$\sigma_{hs} = 2.52 \cdot \sigma_{0.4t} - 2.24 \cdot \sigma_{0.9t} + 0.72 \cdot \sigma_{1.4t} \quad (\text{Equation 4.6})$$

For coarser mesh sizes with higher-order elements and element sizes equal to the plate thickness at the hot spot, linear extrapolation from reference points located at 0.5t and 1.5t away from the weld toe is recommended. In this case the stress values can be read directly from the mid-side points on the elements, as calculated below:

$$\sigma_{hs} = 1.50 \cdot \sigma_{0.5t} - 0.50 \cdot \sigma_{1.5t} \quad (\text{Equation 4.7})$$

A correction for plate thickness is required to perform the surface extrapolation for type a) weld toes, especially when the plate thickness is greater than the reference thickness. For thinner plates, the thickness may be ignored, but this should be verified by component tests. The thickness reduction factor is calculated as follows:

$$f(t) = \left(\frac{t_{ref}}{t_{eff}} \right)^n \quad (\text{Equation 4.8})$$

The reference thickness should be taken as 25mm. The thickness correction exponent n depends on the effective thickness t_{eff} and the joint category, as listed in Table 4.1.

Table 4.1 Thickness Correction Exponents (IIW-1823-07)

Joint Category	Condition	n
Cruciform joints, transverse T-joints, plates with transverse attachments, ends of longitudinal stiffeners	As-welded	0.3
Cruciform joints, transverse T-joints, plates with transverse attachments, ends of longitudinal stiffeners	Toe ground	0.2
Transverse butt welds	As-welded	0.2
Butt welds ground flush, base material, longitudinal welds or attachments to plate edges	Any	0.1

For type b) weld toes, it is believed that the stress distribution in the hot-spot region is independent from the plate thickness. Therefore the reference points are given as the

absolute value of the distance from the weld toe. For relatively fine mesh sizes with element lengths less than 4mm, the reference points should be located at 4mm, 8mm, and 12mm away from the weld toe and the quadratic extrapolation method should be used to derive hot-spot stress, as calculated below:

$$\sigma_{hs} = 3 \cdot \sigma_{4mm} - 3 \cdot \sigma_{8mm} + \sigma_{12mm} \quad (\text{Equation 4.9})$$

For relatively coarse mesh sizes using higher-order elements and element lengths exceeding 10mm in the hot-spot region, the hot-spot stress should be linearly extrapolated from reference points located at 5mm and 15mm away from the weld toe as calculated below:

$$\sigma_{hs} = 1.5 \cdot \sigma_{5mm} - 0.5 \cdot \sigma_{15mm} \quad (\text{Equation 4.10})$$

The hot-spot stress can be also derived from strain measurements taken during fatigue tests. The placement and number of strain gauges recommended by IIW-1823-07 depends on the extent of shell bending stress, plate thickness, and the hot-spot type. It is recommended that the center point of the first strain gauge should be placed at 0.4t away from the weld toe. The length of the gauge should be not more than 0.2t. If the plate thickness is too small to achieve this, the first gauge should be placed with its leading edge 0.3t away from the weld toe. The number of gauges and extrapolation procedure are different for type a) and b) weld types as described below:

For the type a) weld toes, two extrapolation methods can be applied. Two strain gauges can be attached at reference points located at 0.4t and 1.0t in front of the weld toe then the hot-spot strain can be linearly extrapolated from the reference points, as calculated below:

$$\varepsilon_{hs} = 1.67 \cdot \varepsilon_{0.4t} - 0.67 \cdot \varepsilon_{1.0t} \quad (\text{Equation 4.11})$$

Alternatively, three strain gauges can be placed at reference points located at 0.4t, 0.9t and 1.4t in front of the weld toe from which quadratic extrapolation is used to derive the hot-spot strain, as calculated below:

$$\varepsilon_{hs} = 2.52 \cdot \varepsilon_{0.4t} - 2.24 \cdot \varepsilon_{0.9t} + 0.72 \cdot \varepsilon_{1.4t} \quad (\text{Equation 4.12})$$

For the type b) weld toes, it is recommended that the strain gauges should be placed at distances of 4mm, 8mm and 12mm away from the weld toe. Quadratic extrapolation should be used to derive the hot-spot strain, as calculated below:

$$\varepsilon_{hs} = 3 \cdot \varepsilon_{4mm} - 3 \cdot \varepsilon_{8mm} + \varepsilon_{12mm} \quad (\text{Equation 4.13})$$

In this study, both the DNV and IIW recommendations were considered. Finite element models with very fine mesh were built; therefore linear 0410 extrapolation and 0515 extrapolation were performed. As a first step, 2D models with planar elements under plain strain assumption were built to verify the accuracy of the boundary conditions and investigate the influence of the local geometry. The effects of element type, element size, and mesh configuration are studied with or without including the root gap and weld shape in the model. Based on the results from the 2D models, 3D models with solid elements were constructed. The hot-spot stress values obtained from the 3D models, adjusted to account for the variability in L_c values, were used in this study as discussed in Section 3.5.2.

4.2 2D Modeling

Both two-dimensional and three-dimensional models were built in this study. Though the final stress results were obtained from 3D models, 2D models were still useful to investigate different modeling options such as boundary conditions, element type, and mesh density, since they take less computation time compared to the 3D models. Since the cross-sectional dimensions of the weld were much smaller than its transverse length dimension, out-of-plane strains were not expected to be significant. Plane strain conditions were assumed for the 2D elements; this was later verified as appropriate by the 3D model results.

Considering that the transverse weld dimension (4") is much larger than the in-plane dimensions (~0.3"), plane strain elements with 4" thickness were adopted in 2D models. The traditional modeling technique employs 2D shell elements representing the mid-

surface of the plates to form 3D models. This option is especially useful when modeling complex structures with interaction between different components. 3D solid element models are usually too computationally intensive for this purpose. However, in this study shell element models were not used for the following reasons. First, the stress distribution around the weld cross section and the effect of local weld geometry are of interest for this study. However neither can be investigated using shell elements. Second, shell elements only allow one element through the thickness of the plate. Though one quadratic element is enough for the purpose of hot-spot stress extraction according to both the DNV and IIW recommendations, a finer mesh size with multiple elements through the thickness is desirable to capture the nonlinear stress gradient close to the weld toes. Therefore, the linear region for read-out points is better defined. This was later proven by a mesh density study, which showed a considerable disparity between the $t \times t$ mesh and finer mesh sizes. The mesh density study was performed using 2D plain strain elements. Third, shell elements do not differentiate between the two weld toes on the deck and the rib plate because the weld generally is not explicitly modeled with shell elements. In the fatigue tests conducted at VT, fatigue cracks were observed initiating from both the rib and deck plate weld toes. Therefore it is necessary to investigate the different stress states occurring at each weld toes separately. The weld can be included in the model using either 3D solid elements or 2D plain strain elements. For the aforementioned reasons, the hot-spot stress modeling was performed using 3D solid elements in this study.

4.2.1 Construction of 2D Models

The 2D models were built assuming plane strain behavior. The primary purpose of 2D models was to quickly investigate a number of modeling options. Considerably more time would have been required to investigate modeling options using 3D solid elements. The modeling options include the element shape, element type, mesh density, and the presence of a root gap in the local weld geometry. The boundary conditions, effects of load application, influence of the load bearing plate were also investigated using the 2D models.

The specimen was supported by two rollers on each end and fixed on the piston that

applied the load. So ideally the boundary conditions should allow both ends of the specimen to translate horizontally and rotate within a small angle. In reality this is somewhat compromised by the clamping force applied on the rollers against the specimen. The clamping force is necessary to stabilize the specimen under the cyclic load reversals during testing. However, excessive clamping force causes friction against the horizontal translation and restrains the end rotation of the specimen, thereby creating a partially fixed boundary condition. The effect of clamping force on the boundary conditions depends on the ratio of the applied load and clamping force. A clamping force of 140 lbs was found to be sufficient for the tests performed at VT where the fatigue loads were at least ± 2.5 kips. At this level, the effect of clamping force was minimal. Therefore, pin-roller end boundary conditions were assumed in this study.

Even though the fatigue tests were conducted under different loads, it is unnecessary to apply different loads to the FE models since the tests remained linear-elastic under all load levels. A representative load can be selected to calculate one stress state in the model and the stresses at other levels can be calculated by multiplying by the load ratio. As shown in Table 3.2, most tests were performed under either 33.33 ksi or 36.67 ksi stress ranges, corresponding to loads of ± 2.5 kips/5 kips and ± 2.75 kips; only the load of ± 2.75 kips was applied to all specimen series. Therefore an upward load of 2.75 kips was selected to apply to all models.

The exact global geometry of the test specimens was modeled except for the radius at the corners of the rib, which were not locations of interest. The 2D model geometry is shown in Figure 4.7. The deck plate length was taken as exactly 24 in. between the roller supports ignoring the extra 1 in. overhang at each end.

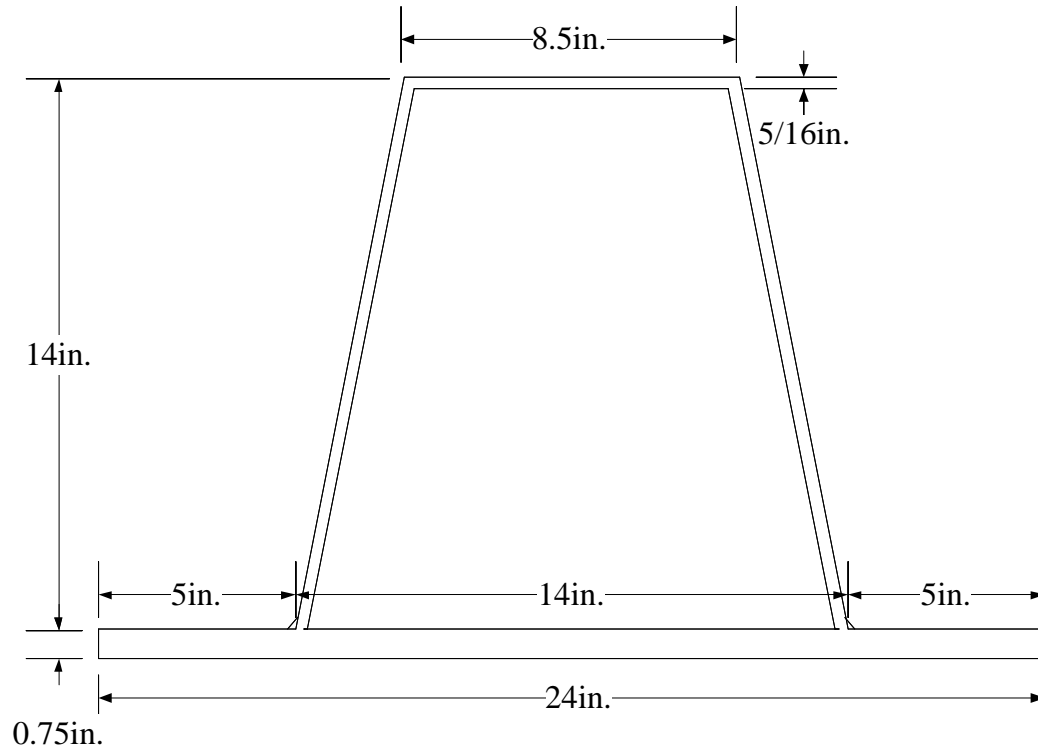


Figure 4.7 Global geometry of the 2D FE models

Welds were included in both the 2D and 3D models. The weld geometry used in the majority of the models was based on the average weld dimensions measured for each specimen series as listed in Table 4.2. The weld outlines were approximated as straight lines instead of the rounded edges present in the actual welds. These simplifications were justified by the following FE study on the local geometry that concluded that the deviation of individual weld dimensions had little influence on the hot-spot stresses magnitude.

The weld geometry adopted for the generic models is shown in Figure 4.8. The weld toe size on the deck plate (d_1) was taken as 0.2 in.; the weld height on the rib plate (h) was taken as 0.3 in.; and the root gap size (d_3) was taken as 0.075 in.. These dimensions were based on the average values in the specimen series. The small weld geometry variations were taken into account in a follow-on study using the actual weld dimensions from one specimen; however the differences were found to be trivial. The influence of the root gap was also investigated and will be discussed later.

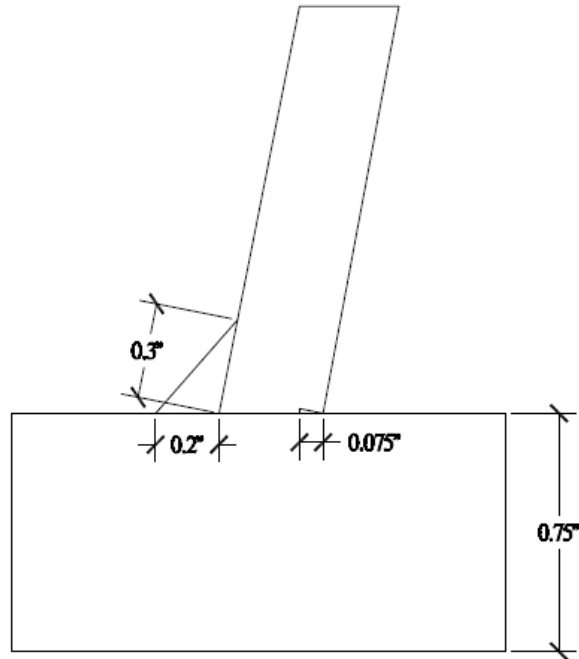


Figure 4.8 Local weld geometry in the 2D FE models

Table 4.2 Average weld dimensions throughout the specimen series

Series	d_1 Average (in)	d_3 Average (in)	h Average (in)
GM-80	0.187	0.060	0.326
FIL	0.266	0.123	0.368
SA-20	0.195	0.104	0.285
SA-40	0.253	0.136	0.282
SA-60	0.231	0.105	0.283
SA-80	0.320	0.116	0.241
OB	0.336	0.122	0.310
UB	0.284	0.122	0.337
Average	0.266	0.109	0.304

Another important issue was the presence and size of bearing plates used to distribute the

load to the bottom flat surface of the rib plate during the test. The bearing plate effect was not recognized until some of the tests performed at VT failed at the weld toe on the rib plate. Briefly speaking, the bearing plates restrained the flat section of the rib plate from bending. This restraint affected the amount of bending deformation in the rib walls and affected the stress range at the rib weld toe. Smaller bearing plates were used in the tests performed at VT compared to those performed at TFHRC. This elevated the hot-spot stress at the rib weld toe in the VT tests and explains why some of the specimens failed in the rib plate (WT@RIB). Since the bearing plates were 1 in. thick; compared to the 5/16 in. rib plate thickness, the portion of the rib plate clamped between the bearing plates behaved nearly as a rigid body. Thus in both 2D and 3D models, the flat portion of the rib under the bearing plates was kinematically constrained to the center point, where the load was applied. The quantitative analysis of the bearing plate effect is presented in Section 4.2.5.

4.2.2 Element Type and Mesh Density

It is generally recommended by both DNV and IIW that quadratic elements should be used when modeling for hot-spot stress analysis purposes. Linear elements could be used in global models to identify potential cracking locations; however higher-order elements, even sometimes with a coarser mesh, are preferred for the local models.

The recommended maximum mesh density is $t \times t$ if the LSE method is applied. However a finer mesh is useful to investigate the stress pattern through the plate thickness which is necessary for application of the TTWT method. A mesh density study was performed to make sure that the read-out points are well located in the linear stress region and the hot-spot stresses converge beyond a certain mesh density level.

The influence of element type and mesh density was investigated using 2D plane strain models. Models with 4-node linear quadrilateral elements (Q4), 6-node quadratic triangular elements (T6), or linear strain triangles (LST), and 8-node quadratic quadrilateral elements (Q8) built on 5 different mesh density levels were compared for their accuracy and effectiveness. The normal stress predicted by both the LSE and TTWT methods was included in the comparison.

First, models with isoparametric Q4 or Q8 elements were built with the same mesh shown in Figure 4.9. These models were built based on the 5 in. bearing plates used at TFHRC. Regions between $0.4t$ to $2t$ away from the weld toes were modeled with a fine mesh ($0.1t \times 0.1t$) for the convenience of locating the read-out points. A finer mesh ($t/30$) was used for the welds to provide higher resolution in that region. The weld root gap was included but regarded as closed in the models. A further mesh refinement ($t/300$) was used around the root gap. The region between the first read-out point ($0.4t$) to the weld toe on the deck plate was also meshed as a transition area with isoparametric quadrilateral elements with sizes ranging between $t/10$ to $t/30$.

The model with the T6 or LST elements was built based upon the previous models with the modification of using T6 elements in the transition regions instead of isoparametric Q4/Q8 elements. The mesh elsewhere in the model was identical to the previous Q4/Q8 models, as shown in Figure 4.10. The bearing plate width was also taken as 5 in. in this model.

Normal stresses on the surface and through the plate thickness near weld toes, as well as on the back of the rib plate toward the weld root, were outputted from the three models. The locations of stress read-out lines are shown in Figure 4.11. The normal stress values are plotted in Figure 4.12 through 4.18.

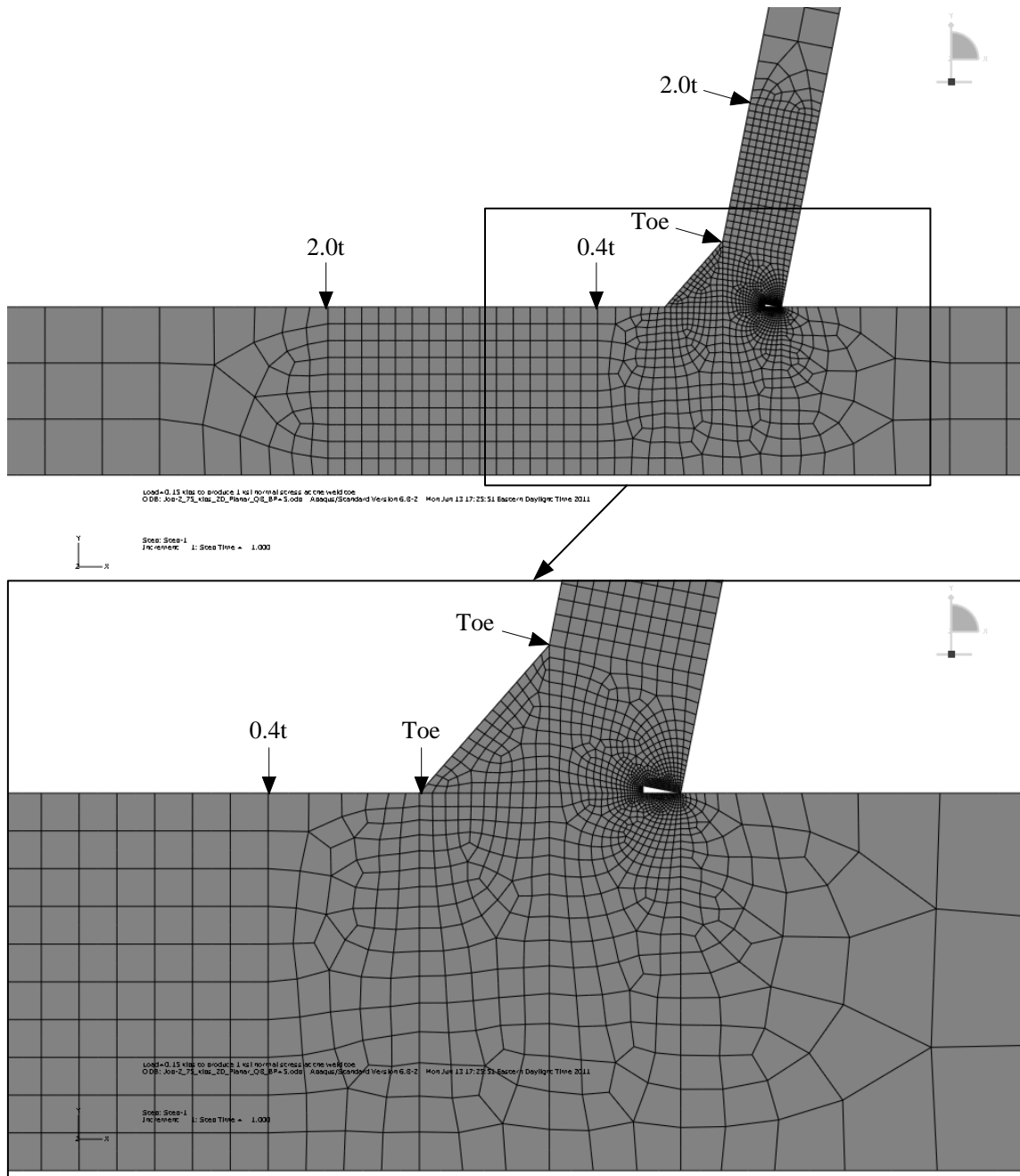


Figure 4.9 Mesh for models with Q4/Q8 elements

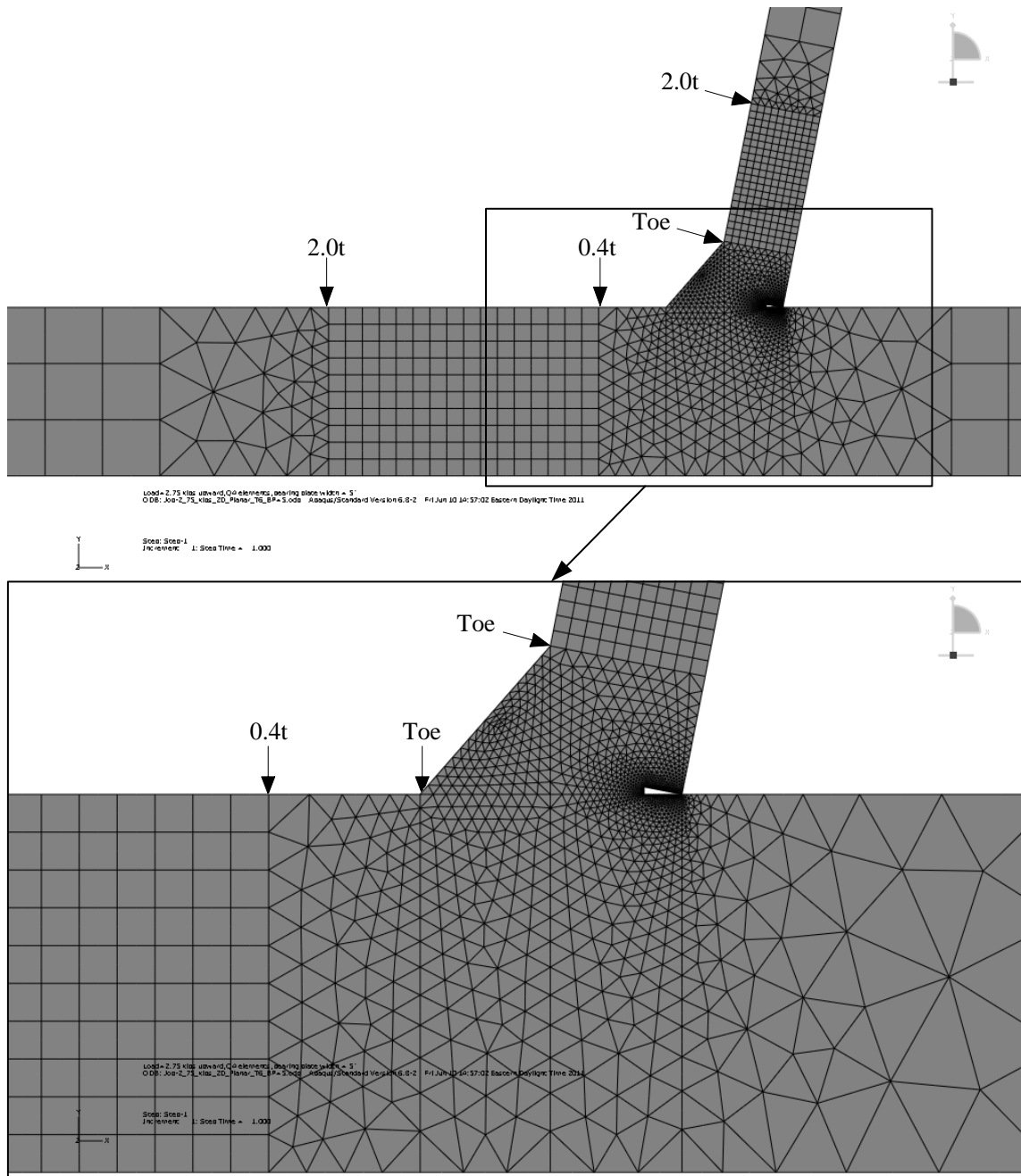


Figure 4.10 Mesh for the model with T6 Elements

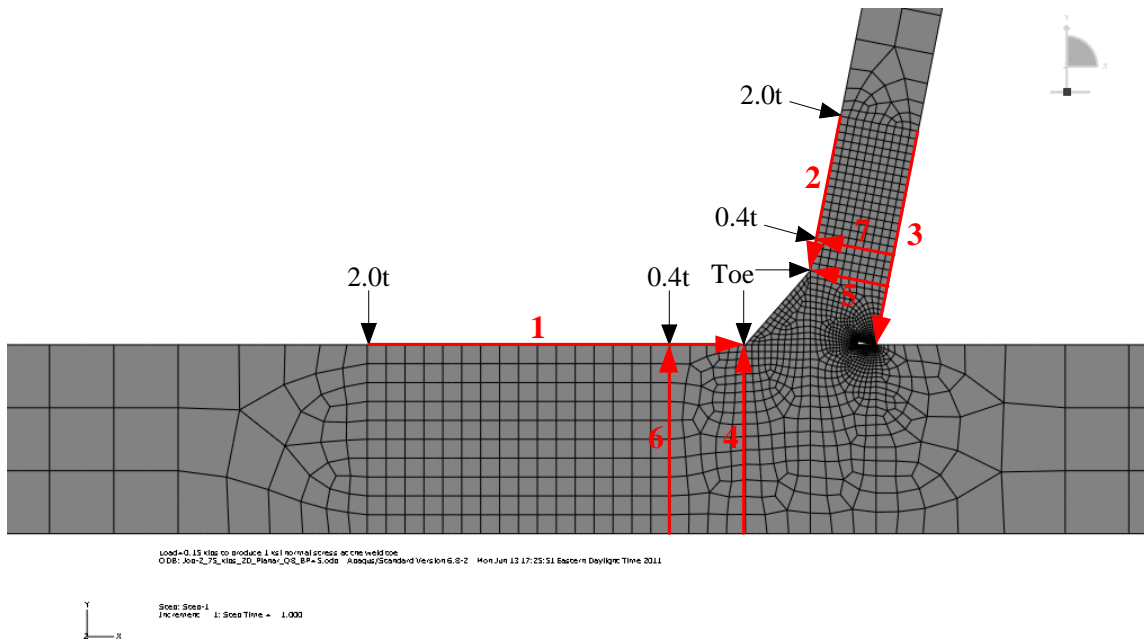


Figure 4.11 Stress read-out lines in the 2D models

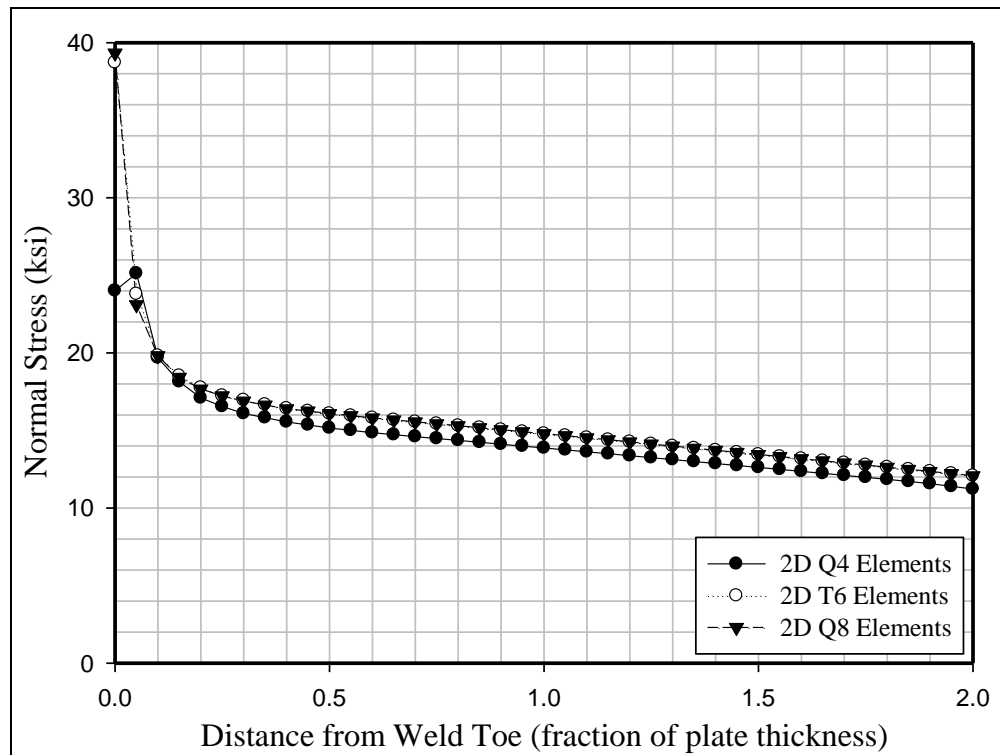


Figure 4.12 Normal stress on line 1 from different element types

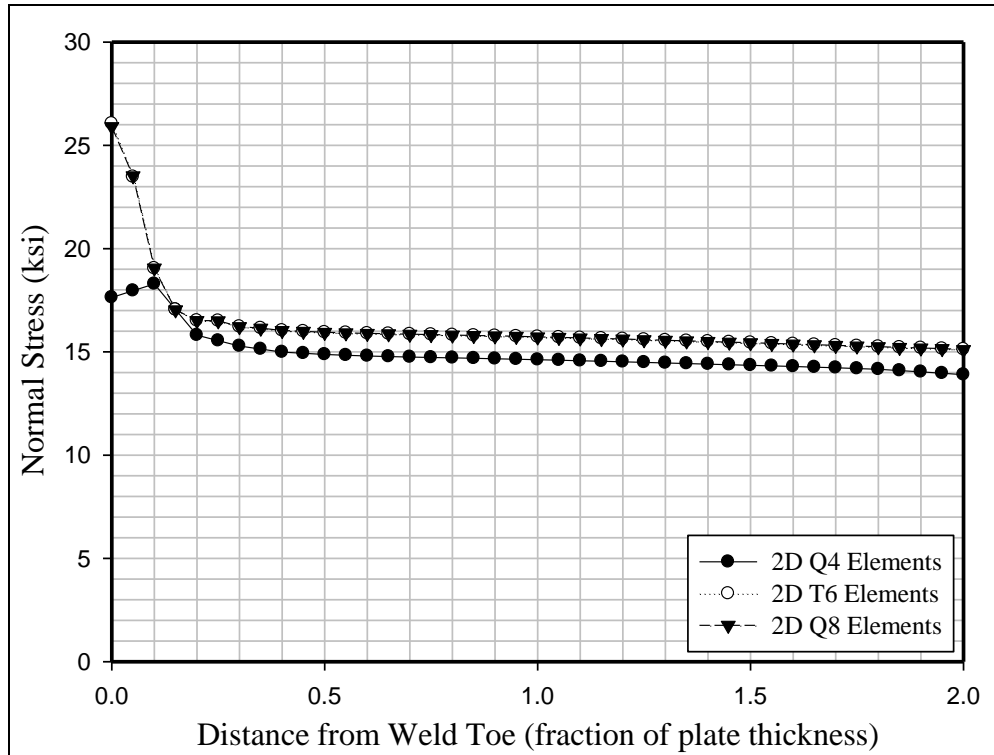


Figure 4.13 Normal stress on line 2 from different element types

As shown in Figure 4.12 and 4.13, quadratic elements (T6 & Q8) predict almost identical stress values with very noticeable nonlinear peaks starting about $0.25t$ away from the weld toe. The linear elements (Q4) consistently predict a lower stress (1 ksi) and a much lower nonlinear peak. It can be seen that the first element adjacent to the weld toe is still capable of depicting the peak stress due to the notch effect for both the T6 and Q8 elements, but fails to capture the peak for Q4 elements due to nodal averaging. Both the linear and quadratic elements give well-defined linear stress distributions away from the weld toes where the read-out points are located.

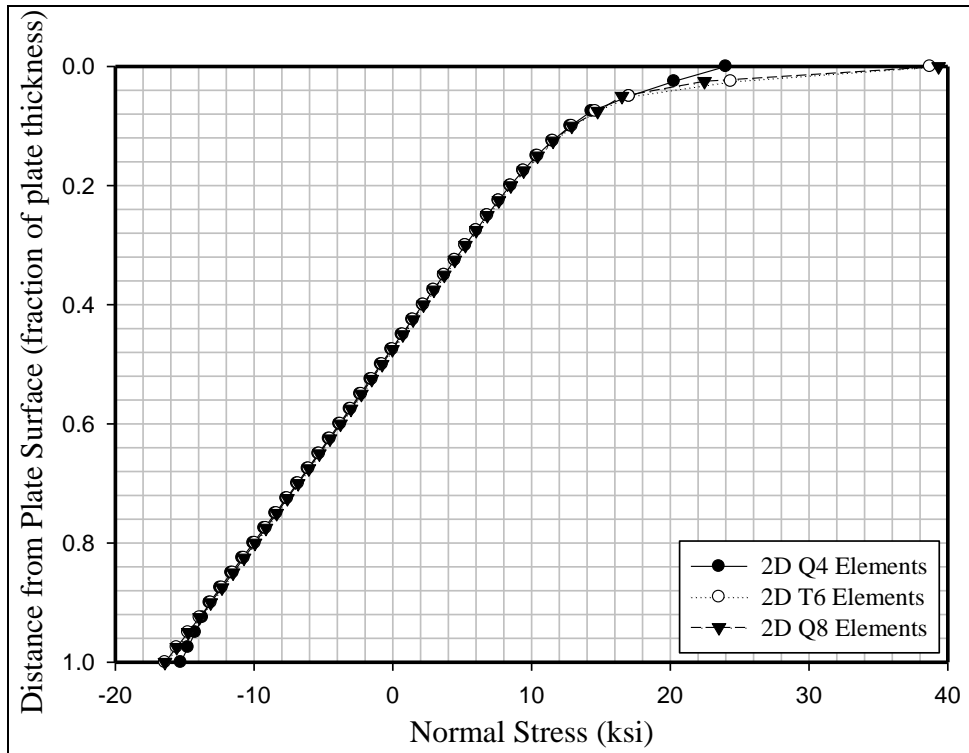


Figure 4.14 Normal stress on line 4 from different element types

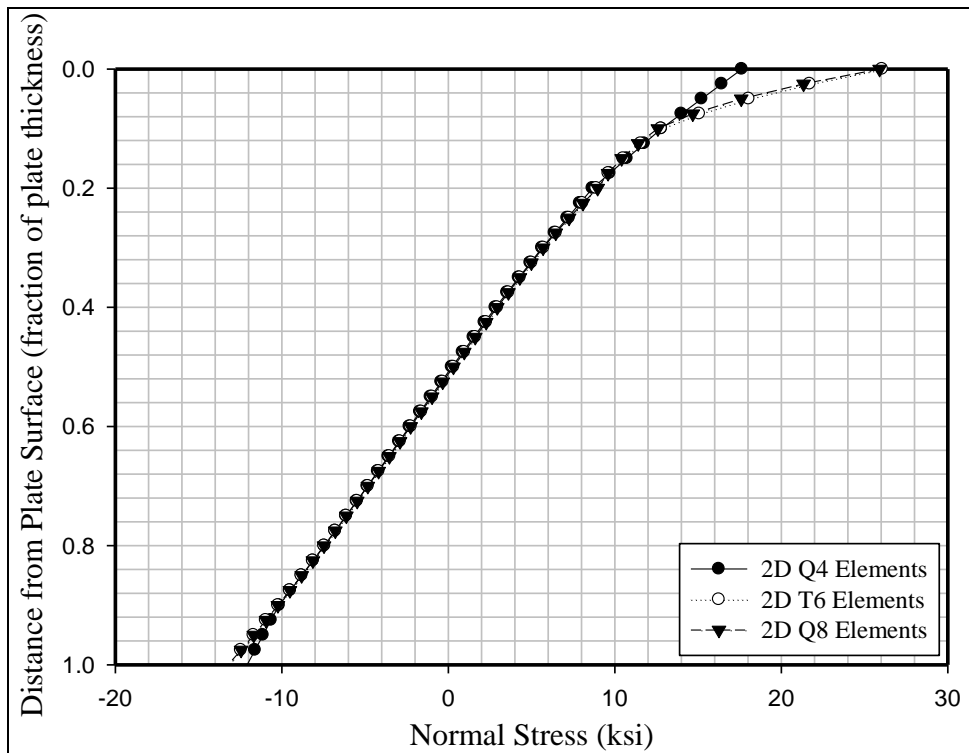


Figure 4.15 Normal stress on line 5 from different element types

The stress pattern through the thickness at the weld toe also shows that higher nonlinear peaks are predicted by the quadratic elements. According to the TTWT methodology, the hot-spot stress should be taken as a linearization of the nonlinear stress pattern through the plate thickness. As shown in Figure 4.14 and 4.15, the T6 and Q8 elements again provide almost identical stress results capturing the high stress peak at the plate surface. The Q4 element cannot capture the notch effect at the surface resulting in an almost linear pattern through the plate thickness. Therefore, the Q4 element underestimates the contribution from the nonlinear stress distribution and underestimates the hot-spot stress calculated by TTWT method. It is noted that the depth of the nonlinear region predicted by the T6 and Q8 models also corresponds well with Xiao's assumption. Xiao predicts that the nonlinear effect diminishes about 1mm below the plate surface, which is about $0.0525t_{deck}$ and $0.126t_{rib}$ for the test specimen geometry (see Figure 4.14 and 4.15).

As previously discussed, the read-out points in the LSE method should be located outside of the region affected by notch effect. This implies that the normal stress should have a linear pattern through the plate thickness under the read-out points. The normal stresses through the thickness at the first read-out point at $0.4t$ from the weld toe are plotted in Figure 4.16 and 4.17. As shown in the plots, all three models predict similar stress results with nearly linear stress distributions.

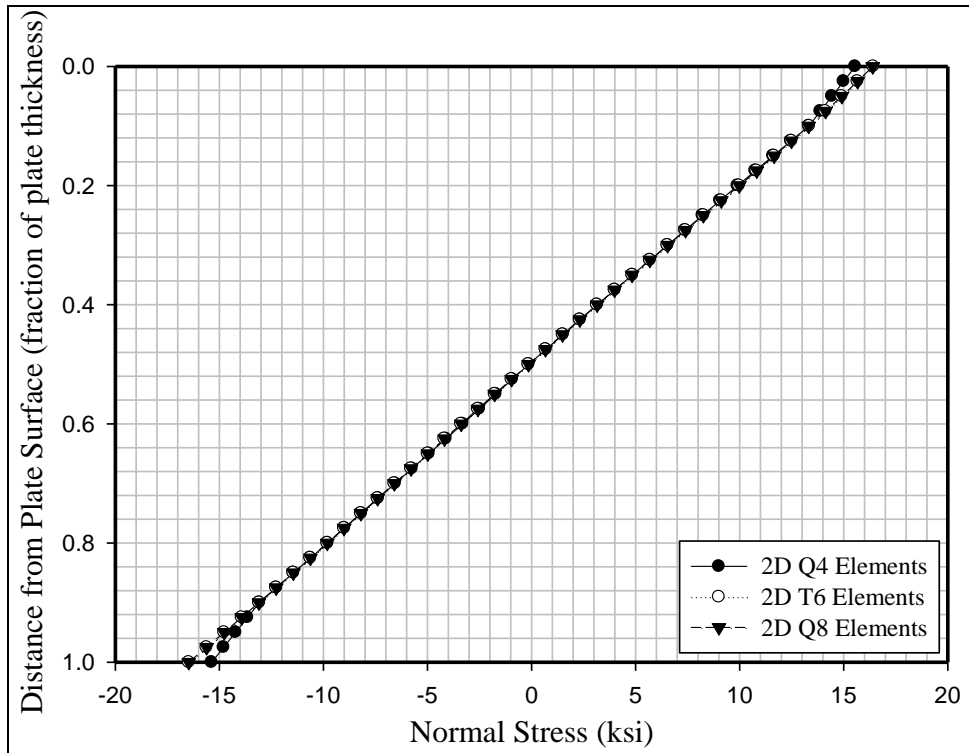


Figure 4.16 Normal stress on line 6 from different element types

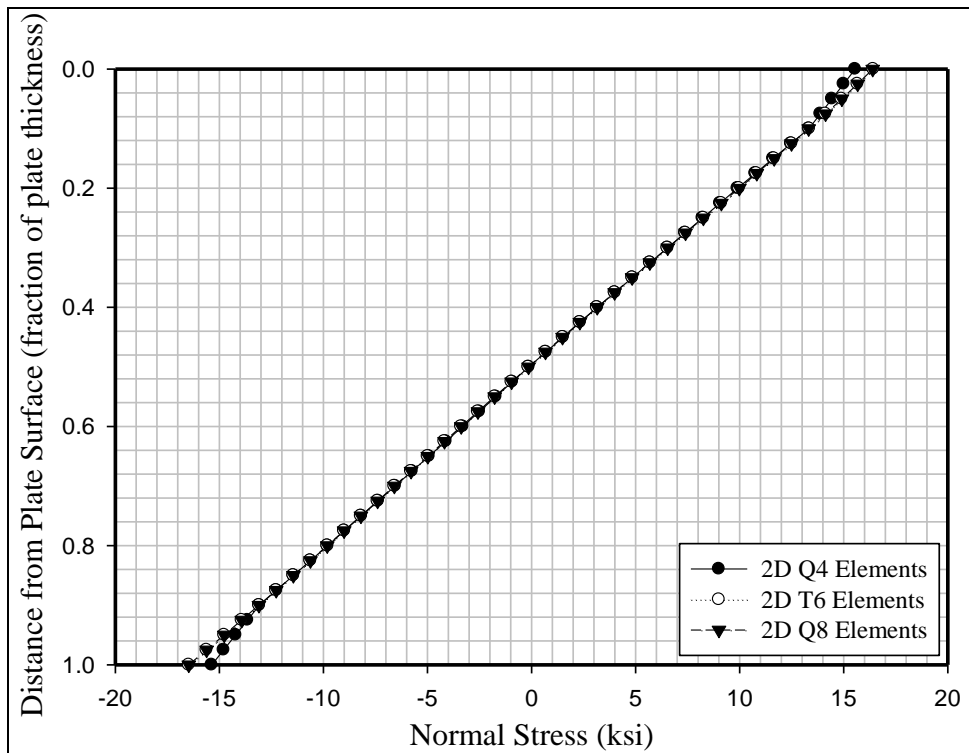


Figure 4.17 Normal stress on line 7 from different element types

Hot-spot stress calculations were not performed for the weld roots, however the stress results from FE models were plotted for reference purposes. The rib plate has a double-curvature deflected shape with a stress reversal in the middle. The normal stress along the inside surface of the rib plate near the weld root is plotted in Figure 4.18. As shown, the local effects of the root gap diminish at distances greater than $1.0t$ from the weld root. Approaching the root gap, the stress drops and should theoretically reduce to zero at the notch edge. The model shows a spike in normal stress within $0.2t$ from the weld root. This is an artificial modeling effect caused by the mesh size and the singularity that exists at the crack tip node. Therefore, the stress distribution within $0.2t$ from the weld root should not be used for fatigue life prediction. Again, the linear elements under-predict the stress magnitude compared to the quadratic elements.

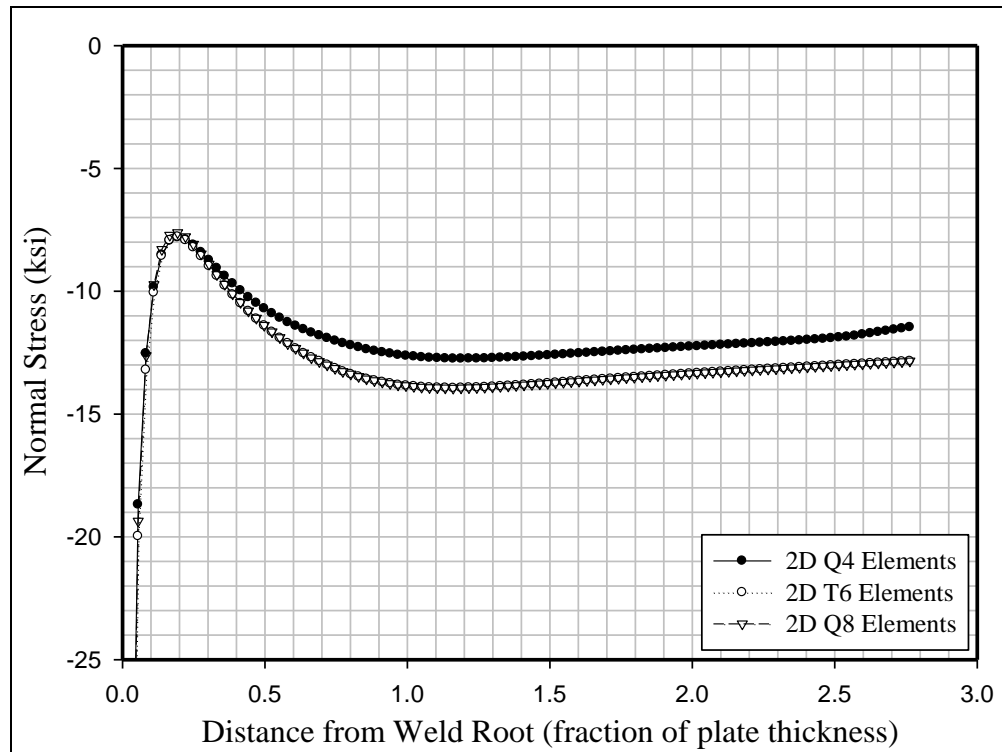


Figure 4.18 Normal stress on line 3 from different element types

In summary, the quadratic elements exhibited better ability to capture the nonlinear effects near the weld detail and showed better agreement with the 3D model results shown in Section 4.3. The extra computation time required for quadratic versus linear elements was trivial for the 2D models. The T6 and Q8 elements showed similar results.

Since the triangular T6 elements are cumbersome to mesh and require more DOFs in the 3D cases, the Q8 elements were adopted for FE analysis in this study.

Although the $0.1t \times 0.1t$ seems to work well for the initial 2D model, A mesh density study was still performed to establish the mesh density level where the results started to converge. This is not very important for 2D modeling since the computation time, even with a fine mesh, takes only seconds on a PC. However, the need for mesh optimization becomes more important for the 3D models since they have about 100 times more DOFs compared to the 2D models with a corresponding increase in computational time.

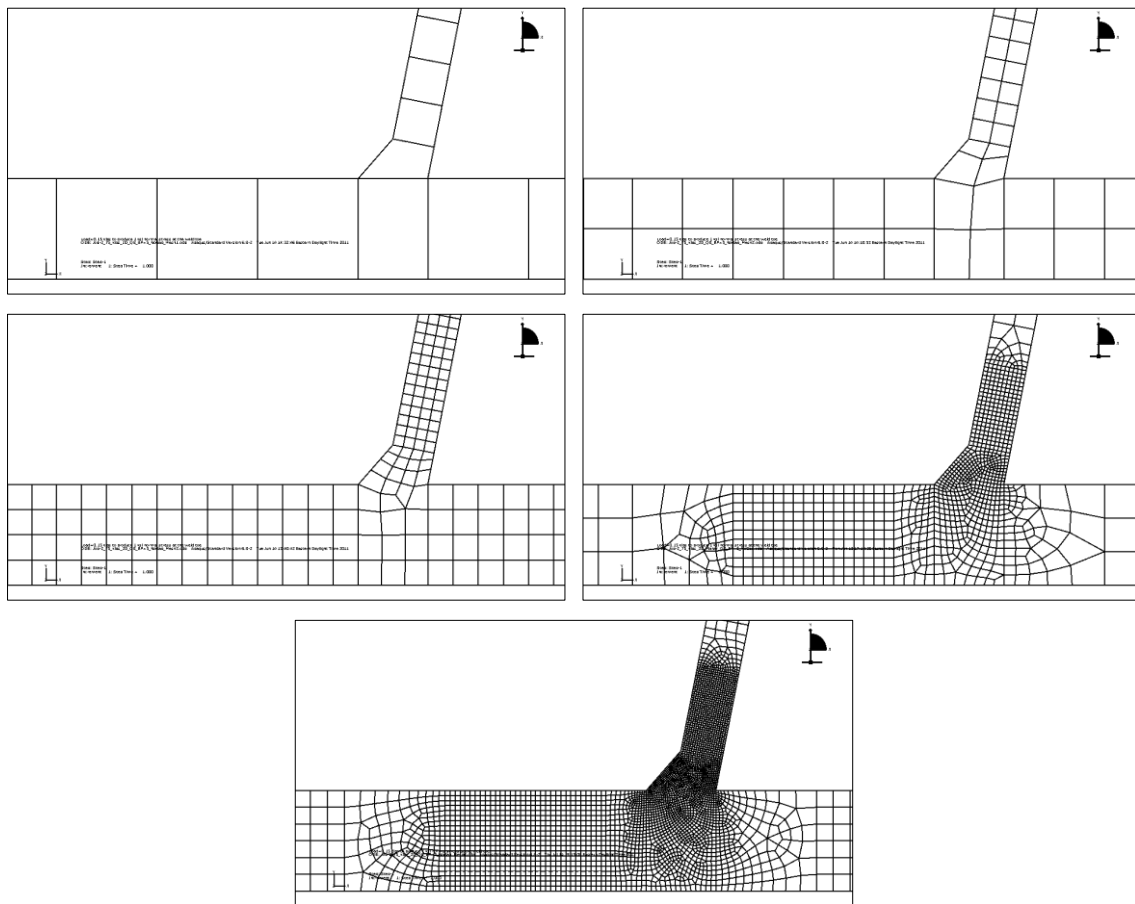


Figure 4.19 Meshing schemes for each model

Models were built with five different mesh densities ($t \times t$, $0.5t \times 0.5t$, $0.25t \times 0.25t$, $0.1t \times 0.1t$, and $0.05t \times 0.05t$) as shown in Figure 4.19. The weld root gap was not included in the models since it has almost no effect on the weld toes stress. The normal stress

distribution along the plate surface is shown in Figure 4.20 and 4.21. All of the mesh sizes predict similar normal stress results at distances greater than $1.0t$ from the weld toe. Closer to the weld toe, the results diverge with the finer meshes doing a better job of capturing the stress concentration effect. The largest difference in results occurs in the first element in front of the weld toe due to the nodal averaging including lower stress from elements in the weld. As shown in Figure 4.20 and Figure 4.21, the mesh 1 and 2 results diverge from the finer mesh size results at distances greater than $0.4t$ in the regions where the hot spot extrapolation points are defined. The mesh 4 and 5 results converge well in this region and will provide similar hot spot stress predictions. The mesh 3 results start to diverge from the mesh 4 and 5 results within the hot-spot extrapolation region, but the differences appear to be minor.

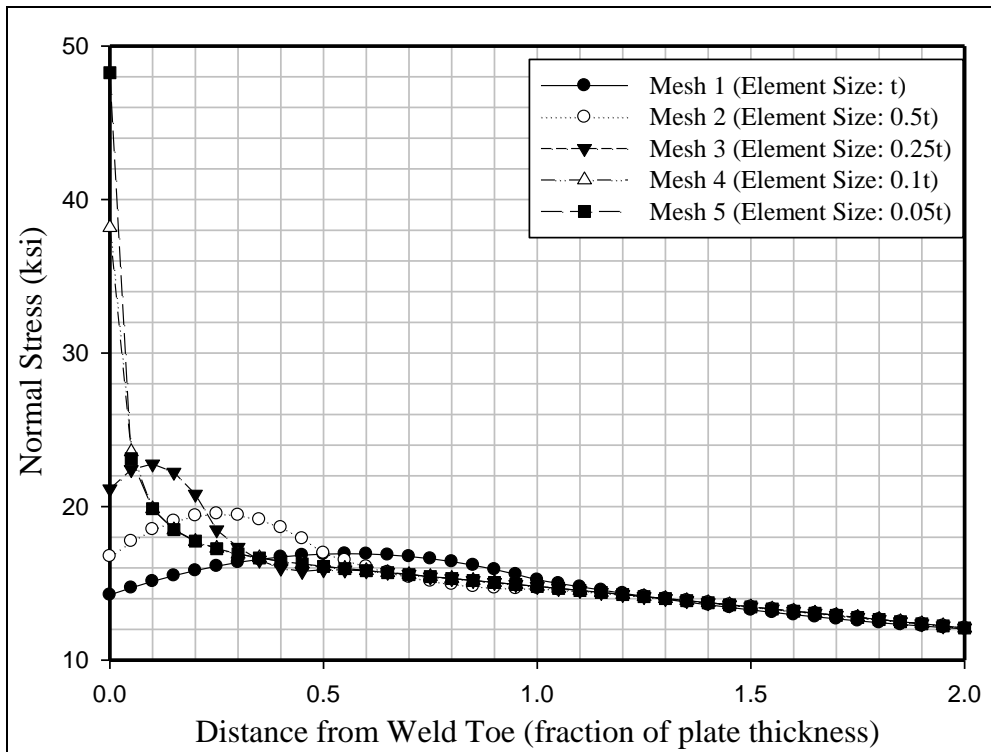


Figure 4.20 Normal stress on line 1 from different meshing schemes

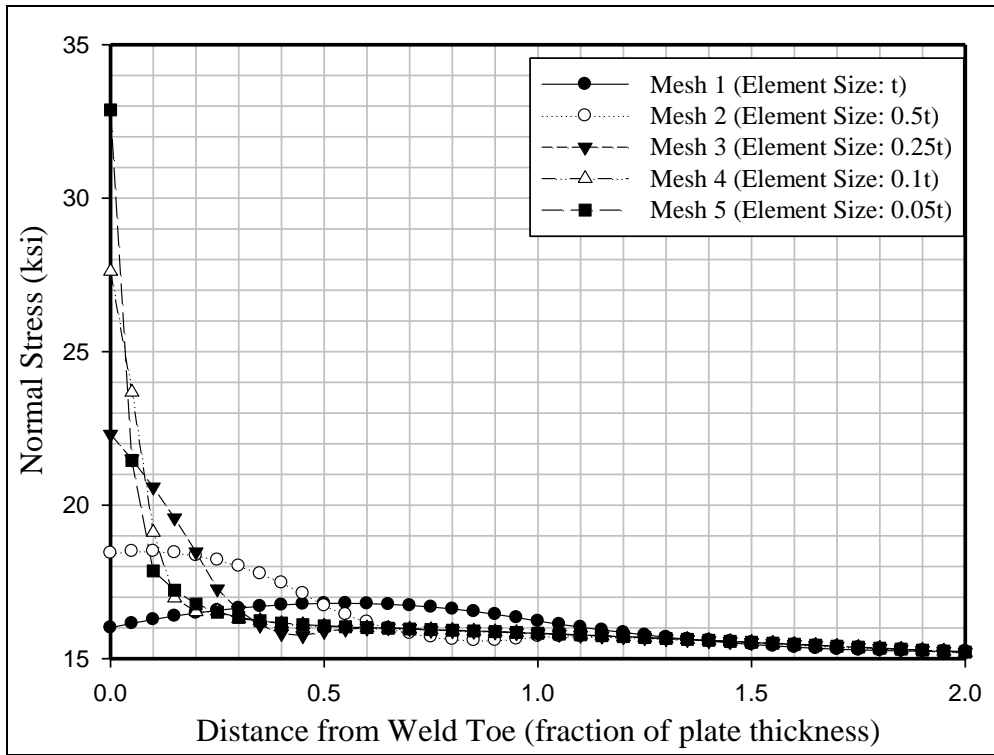


Figure 4.21 Normal stress on line 2 from different meshing schemes

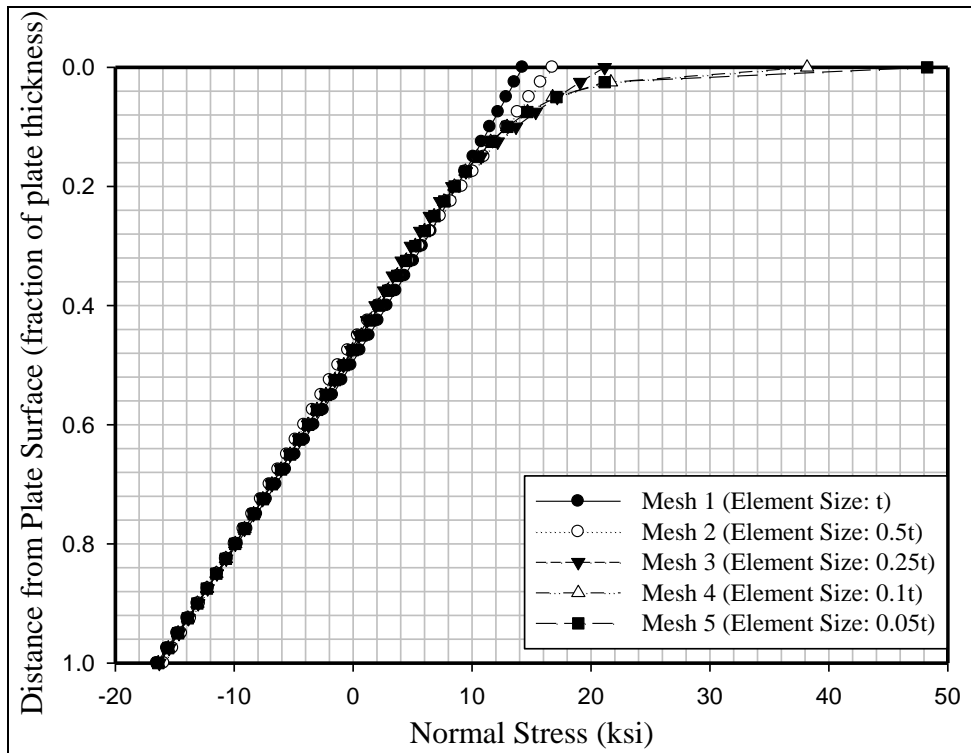


Figure 4.22 Normal stress on line 4 from different meshing schemes

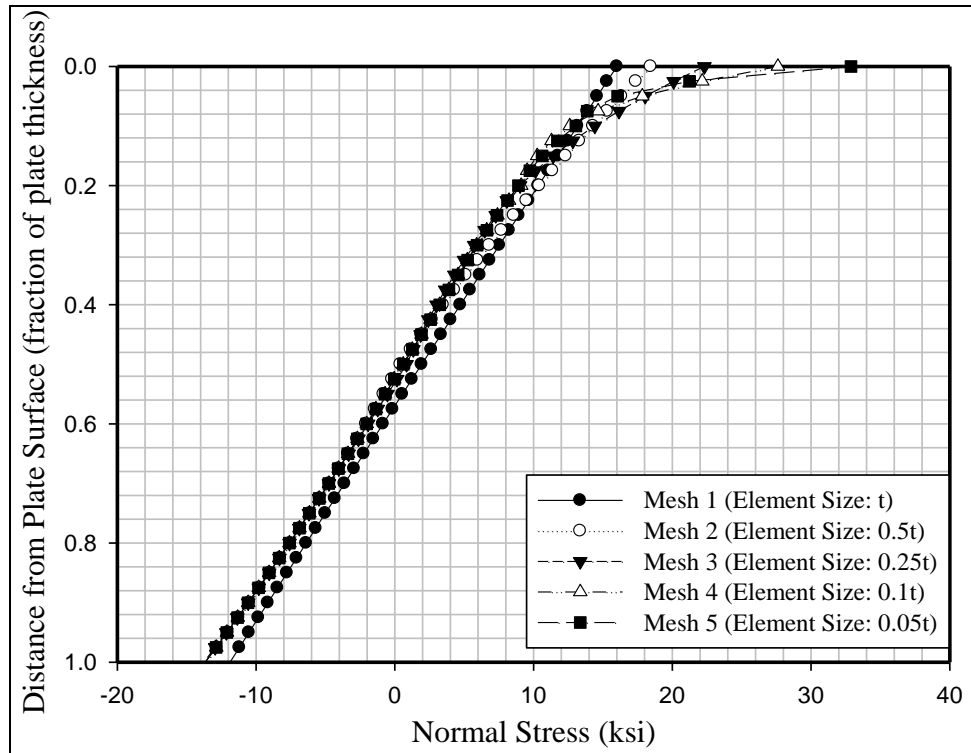


Figure 4.23 Normal stress on line 5 from different meshing schemes

The through thickness normal stress distributions at the hot-spot extrapolation points are shown in Figure 4.22 and 4.23 for all five mesh densities. As shown, all models predict nearly linear stress distributions through most of the plate thickness. There is a notable difference, however, between the nonlinear peak stress values near the plate surface. As expected, mesh 1 predicts a linear stress distribution all the way to the plate surface since the Q8 elements can only predict a linear stress distribution across a given element. The nonlinear surface stress only emerges when more elements are added through the plate thickness. As previously discussed, the area affected by the nonlinear notch effect is limited to about 1mm below the plate surface. It is noted that although different mesh densities predict the stress gradient differently, better mesh-insensitivity is shown for TTWT method compared to the LSE method.

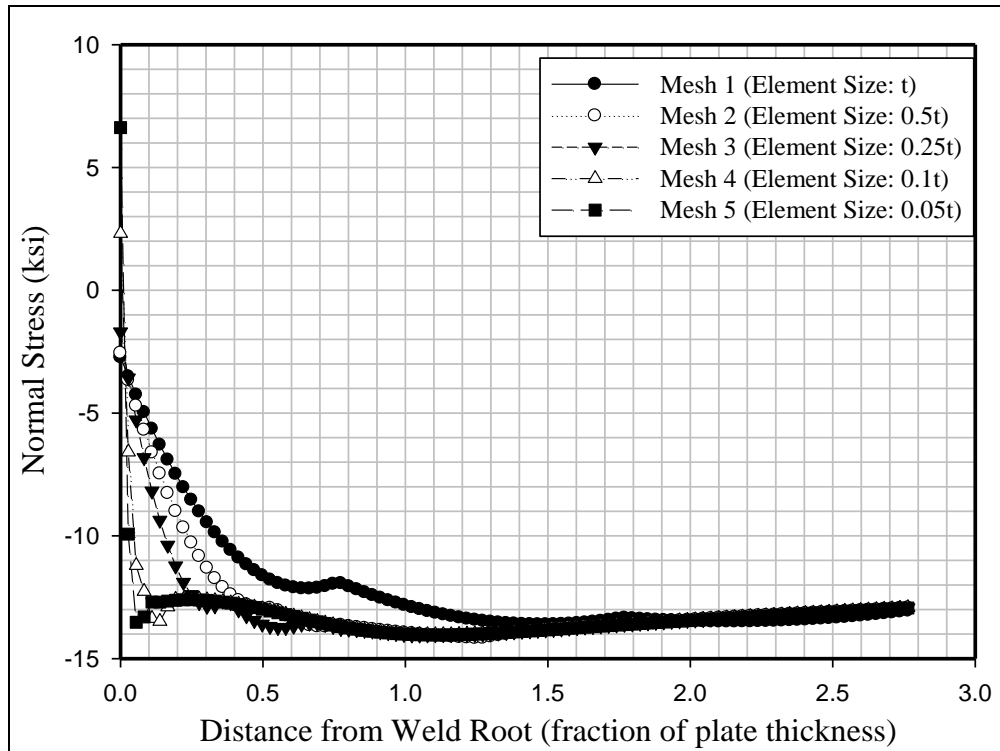


Figure 4.24 Normal stress on line 3 from different meshing schemes

The stress distribution along the inside surface of the rib plate (line 3 in Figure 4.11) is shown in Figure 4.24. Similar to the deck plate results, the divergence of results from the different mesh sizes is greatest close to the weld root. The results diverge at a greater distance from the weld root compared to the weld toe results. The notch effect at the weld root is much more severe than the notch effect at the weld toe. The influence of shear stress changes the direction of the maximum principal stress close to the root. The maximum principal stress, not the normal stress, will drive the development of fatigue cracks. In summary, mesh options 1 and 2 can be expected to introduce errors predicting normal stress within the hot-spot extrapolation region. Mesh options 3, 4, and 5 are expected to provide similar hot-spot stress calculation results. However, mesh3 has problems capturing the nonlinear behavior near the weld toe. Mesh options 4 and 5 gave essentially the same results except for the peak value of the notch stress. Therefore, mesh 4 was selected for use in this study as the ideal compromise between accuracy and computation time.

4.2.3 Modeling of the Weld Root Gap

Both open and closed root gaps were observed in the test specimens. In many cases, the rib plate and deck plate were pressed against each other during fabrication to eliminate root gaps. However, due to straightness imperfections along the rib plate edge and flatness imperfections in the deck plate, it is difficult to consistently achieve tight fit-up conditions for the entire weld length. This tended to be overcome, however, by weld shrinkage that occurs when the weld metal cools. The rib plate edge was pressed into the deck plate in most cases, thereby closing any root gap that may have existed due to plate tolerances. Hairline cracks could still be observed, but they were being held closed due to residual stress effects. This essentially pre-compressed the root notch in many cases.

The stress state around the weld root is rather complicated due to contact effects and the presence of the root gap. Compared to the weld toes, the inside corner at the weld root creates a much higher notch effect that cannot be predicted by the hot-spot stress method. The root gap produces a crack-like defect with a stress singularity that can only be properly dealt with by fracture mechanics. The residual stress state causes compressive pre-stressing of the weld root crack that prevents the crack from opening through part of the fatigue loading cycle. Therefore part of the applied load cycle does not contribute to fatigue damage at the root crack tip where fatigue cracks typically initiate. The residual stress magnitude varies depending on the initial gap tolerance and the welding process. Considering these issues, the notch stress at the weld root can be calculated following the procedure recommended by the IIW (Hobbacher, 2008) involving fictitious rounding of the crack tip. The stress state at the weld root and its influence on the weld toes stress was investigated in this study.

Models with three different root gap conditions, no gap, closed gap, and open gap, were built using $0.1t \times 0.1t$ Q8 quadratic elements in the hot-spot region as shown in Figure 4.25. According to IIW-1823-07 (Hobbacher, 2008), fictitious rounding with a 1mm radius was introduced at the two weld toes and root crack tip in all three models. The rounding at the weld root for the no gap and open gap conditions was placed so the radius center point coincided with the crack tip. For the closed gap model, the arc was made tangent to both crack edges as shown in Figure 4.25. This represents the squashing effect on the weld root due to weld shrinkage and avoids the singularity problem encountered in

previous models. Root gaps were assumed to extend 0.1” at the back of the weld based on the average measured dimension of d_3 shown in Table 4.2. This resulted in a weld penetration about 68.6% through the rib plate thickness. The open gap in the third model was modeled as a keyhole as recommended by Fricke (2008). The gap was left with a 0.02” wide open end, representing the tolerance that can be typically achieved in the fabrication. The element size in the effective notch stress region, as recommended by IIW-1823-07, should be less than $\frac{1}{4}$ of the radius if quadratic elements are used. Therefore the mesh size was set at 0.0075” on the perimeter of the rounding, equal to about $\frac{1}{5}$ of the radius. The bearing plate width for all three models was 5 in.

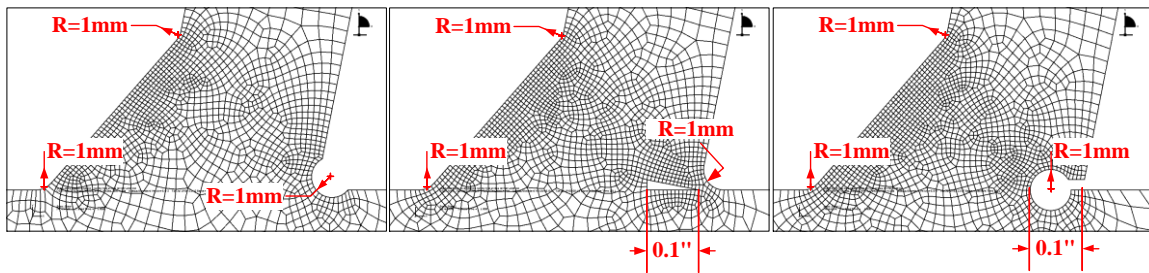


Figure 4.25 Modeling of root gaps

The maximum principal stress contours near the weld toes are shown in Figure 4.26 with the same scale of 0~50 ksi (dark grey represents compressive stress). For all three models, the maximum stress occurs at the deck plate weld toe, which helps explain why none of the specimens tested at TFHRC failed at the weld root. Tests performed in VT used a 3.75 in. wide bearing plate which changed the stress distribution especially at the weld toe on the rib plate and at the weld root, as will be discussed in Section 4.2.5.

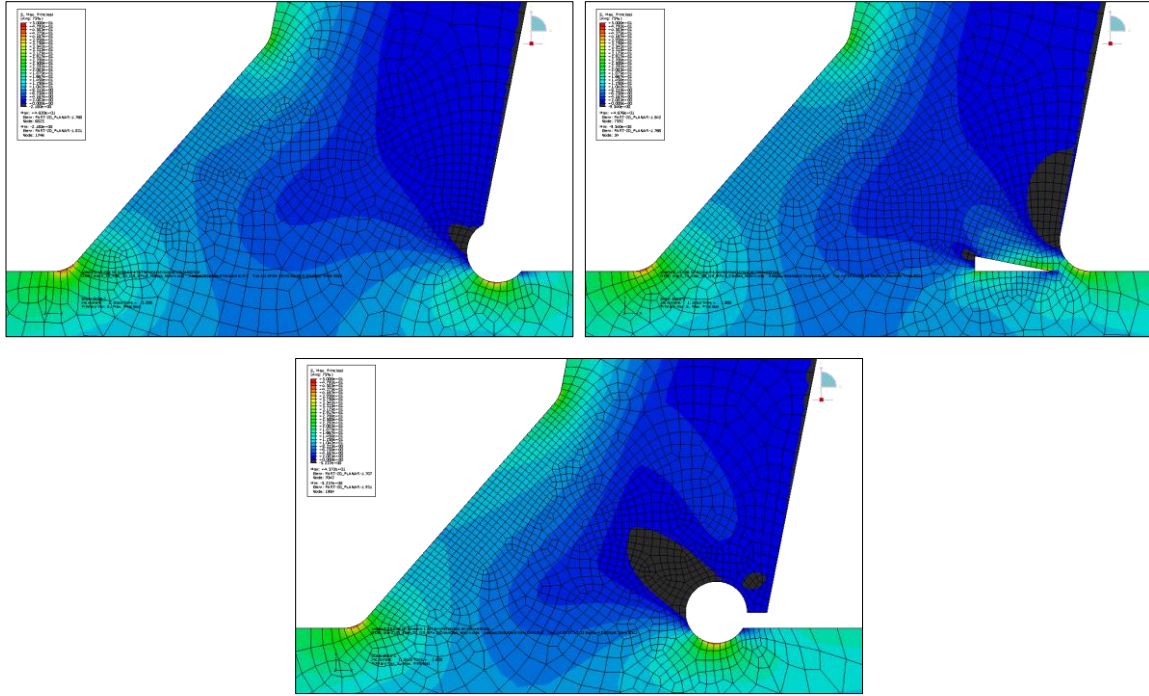


Figure 4.26 Distributions of maximum principal stress near weld toes

The stress distributions near weld toes are plotted in Figure 4.27 through 4.30. It is noted that in Figure 4.27 and 4.28, the normal stresses are plotted in the hot-spot region ($0.4t \sim 2.0t$) while maximum principal stresses are plotted within $0.4t$ where the stress state is strongly influenced by the notch effect. This was done since the maximum principal stress drives the formation of fatigue cracks. Theoretically the principal stress is equal to the normal stress on free plate surfaces where the other stress components vanish under the plane strain assumptions. As shown in the figures, the weld toe stress distributions are essentially identical, on both the surface and throughout the thickness, for all three gap models. Therefore, similar stress results can be obtained using LSE, TTWT or effective notch stress method.

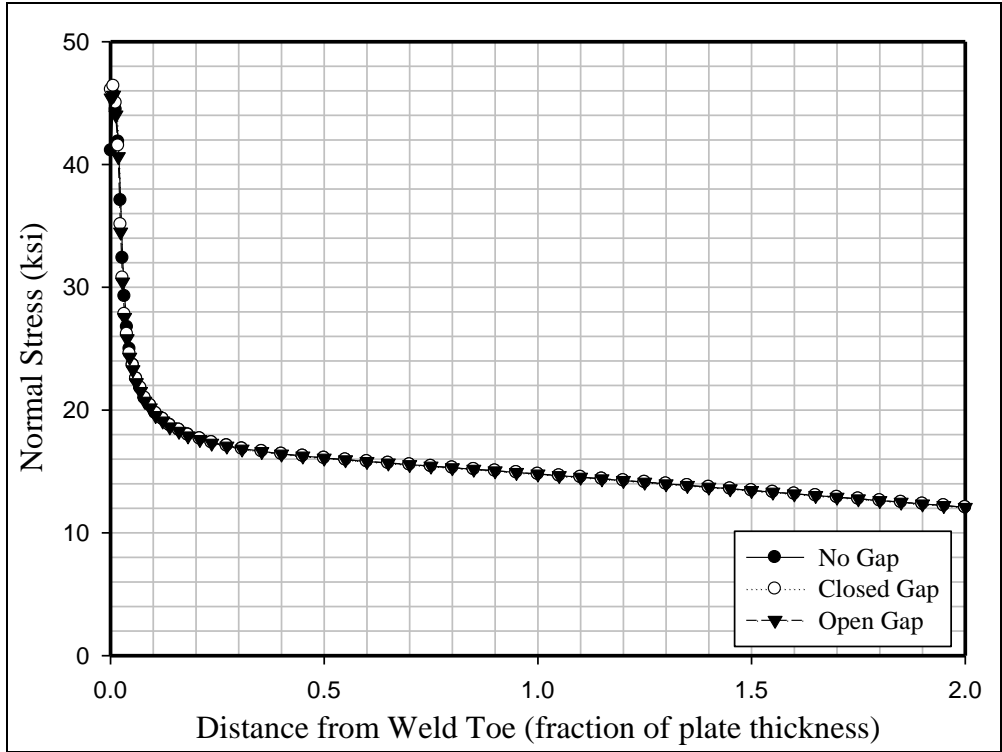


Figure 4.27 Normal stress on line 1 from different root gap conditions

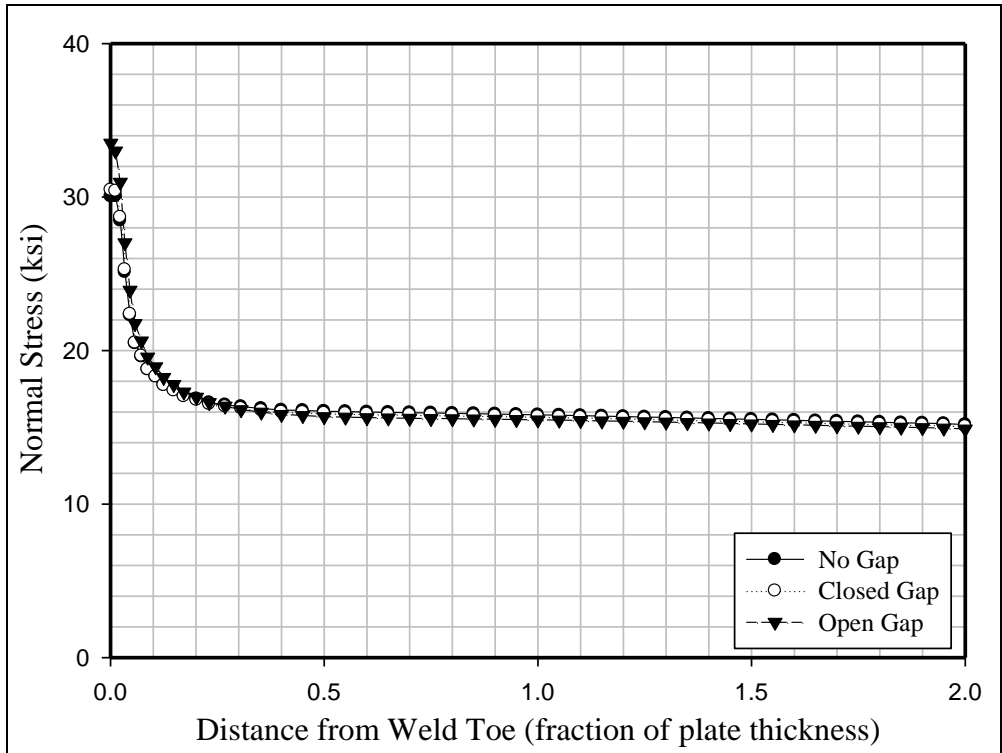


Figure 4.28 Normal stress on line 2 from different root gap conditions

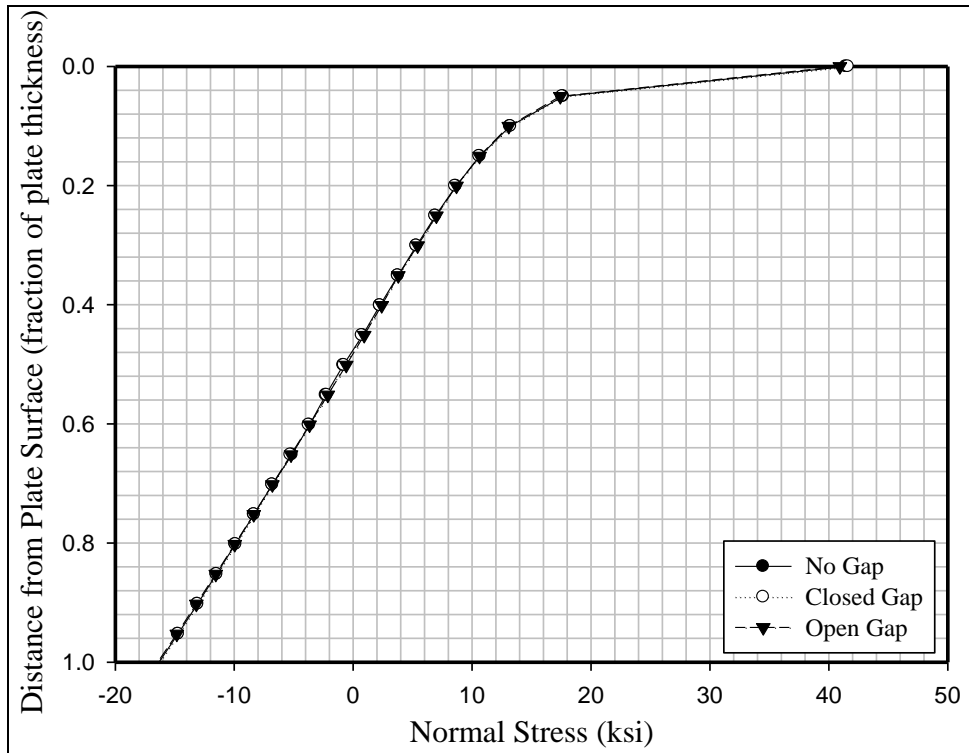


Figure 4.29 Normal stress on line 4 from different root gap conditions

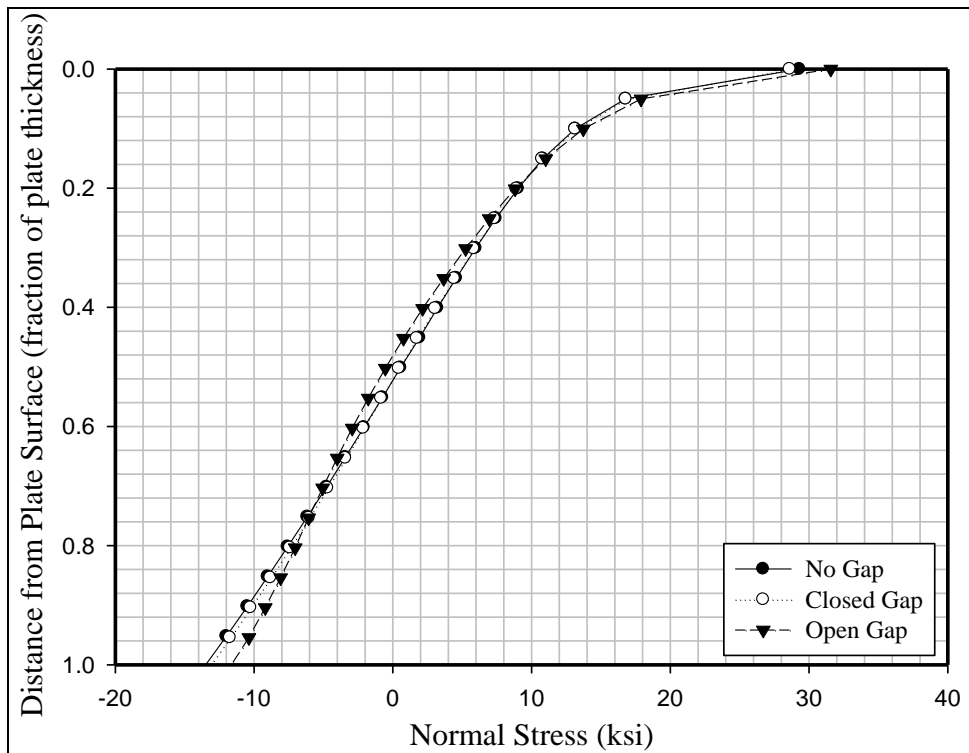


Figure 4.30 Normal stress on line 5 from different root gap conditions

The only difference caused by root gap conditions occurs near the weld root. Maximum principal stress is plotted within approximately $0.2t$ from the weld root and normal stress is plotted further away from the weld root on the inner surface of the rib plate (Figure 4.31). The zero gap and closed gap models produce similar results except at around $0.2t$ where the rounding is abruptly connected with the rib wall in the no root gap model. However, it should be noted that the closed gap model assumes the root gap does not open under tensile load, while in reality the compressive prestress might not be sufficient to hold the material together under all loading. The compressive prestress magnitude is assumed to be sufficient to keep the crack closed under all loading. The open gap condition causes the highest stress at the root notch radius represented by the part of the curve with a negative distance to the weld root. Nonetheless, the hot-spot method is no longer effective in this case since the stress is not linear in the read-out region. The notch effect is dominant and overwhelms the structural stress. If extrapolation is intended to be performed, it seems that the read-out points should be located at least $1.0t$ away from the weld root. It is also noted that the weld root undergoes stress reversal at the weld toes, which explains why none of the specimens failed at the weld root under $R=0$ loading. The weld root experienced a compressive stress range ignoring the contribution of residual stress

The maximum principal stress contours inside the root gaps (Figure 4.32) show the upper corner is the location with the highest stress. This corresponds to the location where fatigue crack initiation was observed in specimens that failed at the root gap. The contours have the same scale of 0~50 ksi with areas in compression in dark grey. The stress distributions are caused by a downward 2.75-kip load.

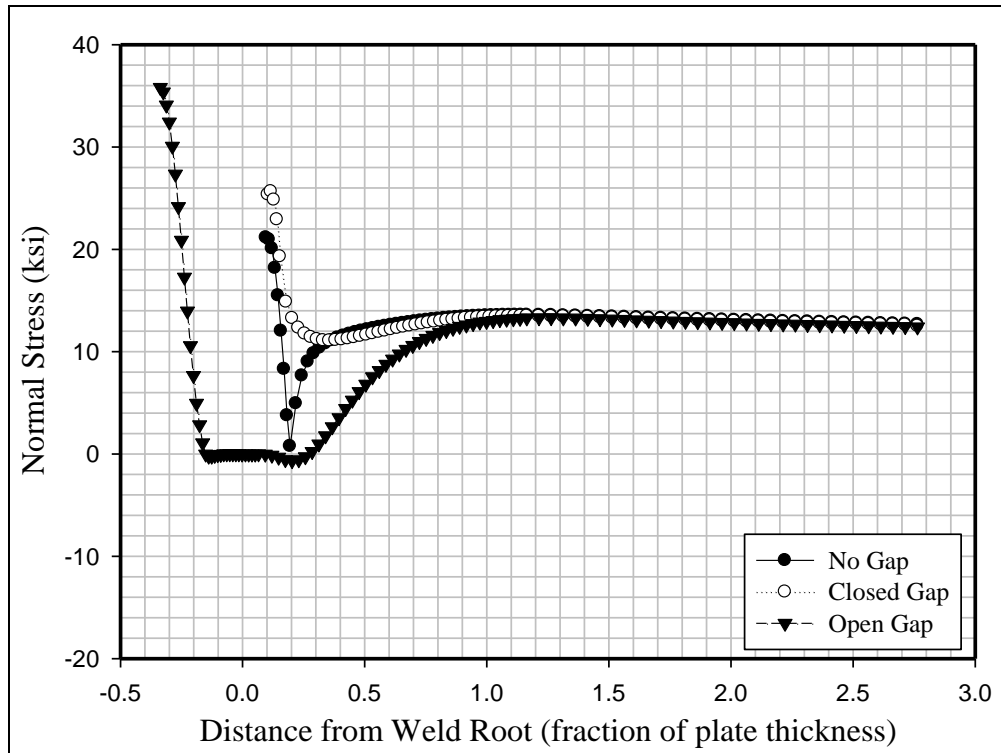


Figure 4.31 Normal stress on line 3 from different root gap conditions

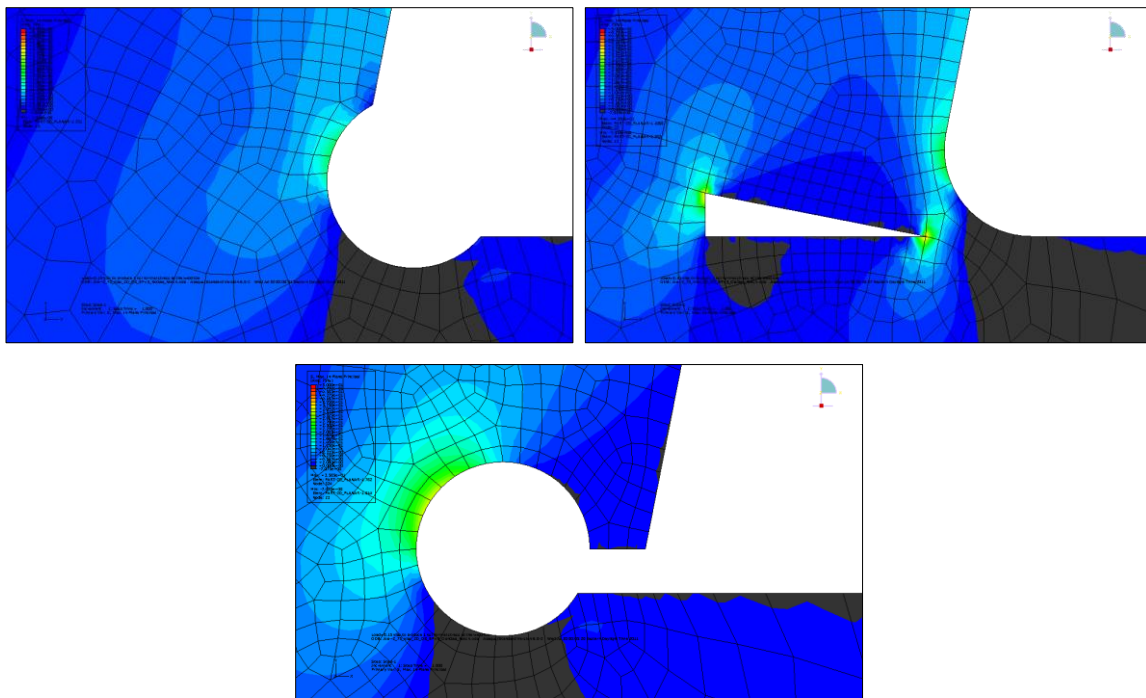


Figure 4.32 Distributions of maximum principal stress near weld roots

The FE modeling and the subsequent hot-spot stress and notch stress analysis shows that the root notch modeling method has little effect on the stress state at the weld toes. As long as the stress state at the weld root is lower than the weld toe stress, the root gap does not need to be explicitly modeled to obtain accurate fatigue life prediction. However, this is not always the case because there are plenty of scenarios where the weld root is more fatigue-critical than weld toes. As an example, the tests conducted at VT show different stress distributions at the weld root due to the change of bearing plate size. Still the root gap was not included in the 3D models because the extremely small element size required to model the root gap significantly increases the time required to build and run the models. For fatigue analysis, the stress range carried by the weld root is determined using the traditional nominal stress method.

4.2.4 Local Geometry Influence

Small variations exist in the weld dimensions of the test specimens that might have an influence on the fatigue resistance. To quantify this effect, a model with the actual weld profile from specimen GM-83 was built and analyzed (Figure 4.33). The weld dimension can be found in Appendix D. Using the same element type, mesh size, and bearing plate size, the GM-83 model was compared to the generic model. Since the root gap was not open in GM-83, the detailed model was compared with generic models without root gaps, both with and without the fictitious rounding. The two welds on the specimen were modeled differently with their individual dimensions; therefore the stresses near both welds were included in the comparison.

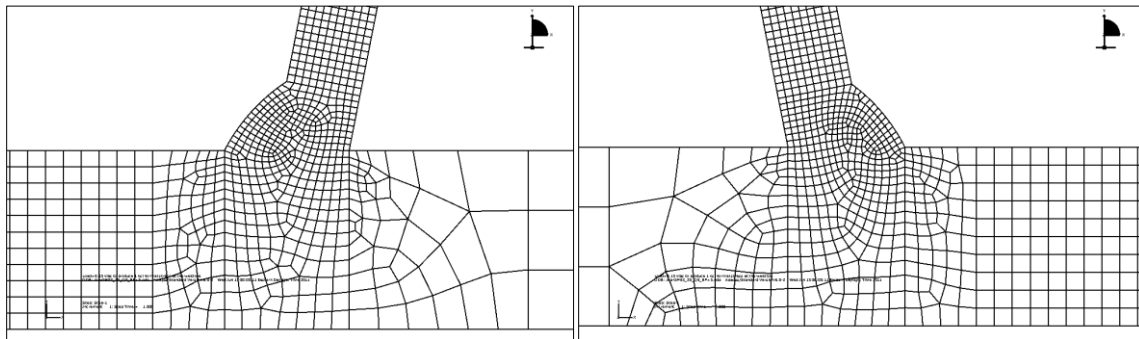


Figure 4.33 GM-83 model

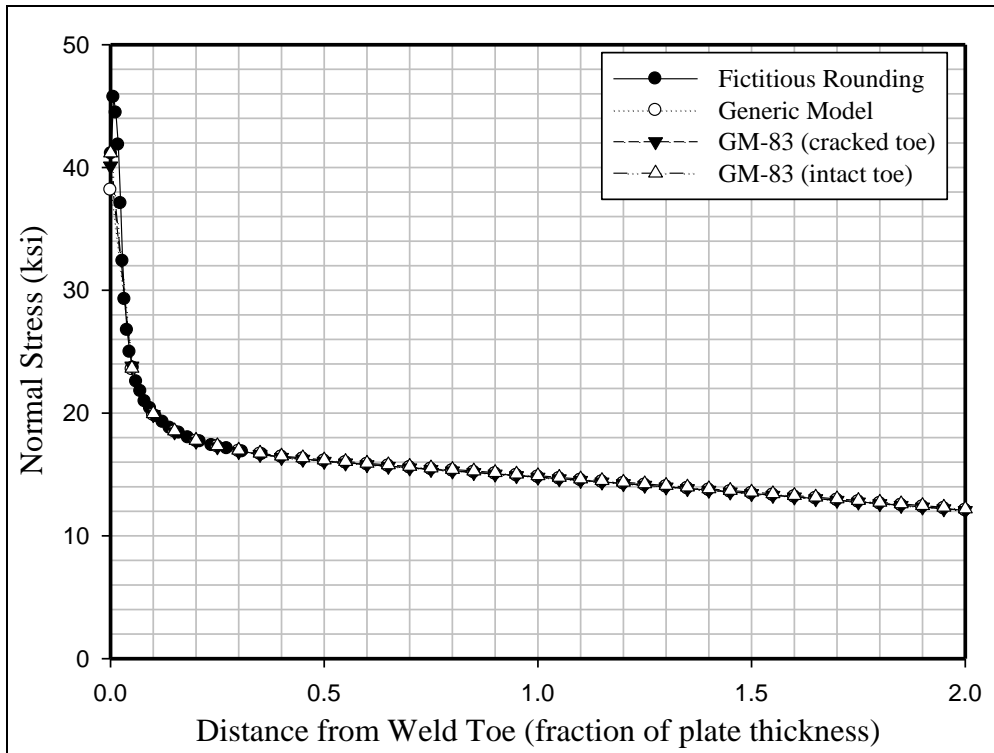


Figure 4.34 Normal stress on line 1 from different local geometries

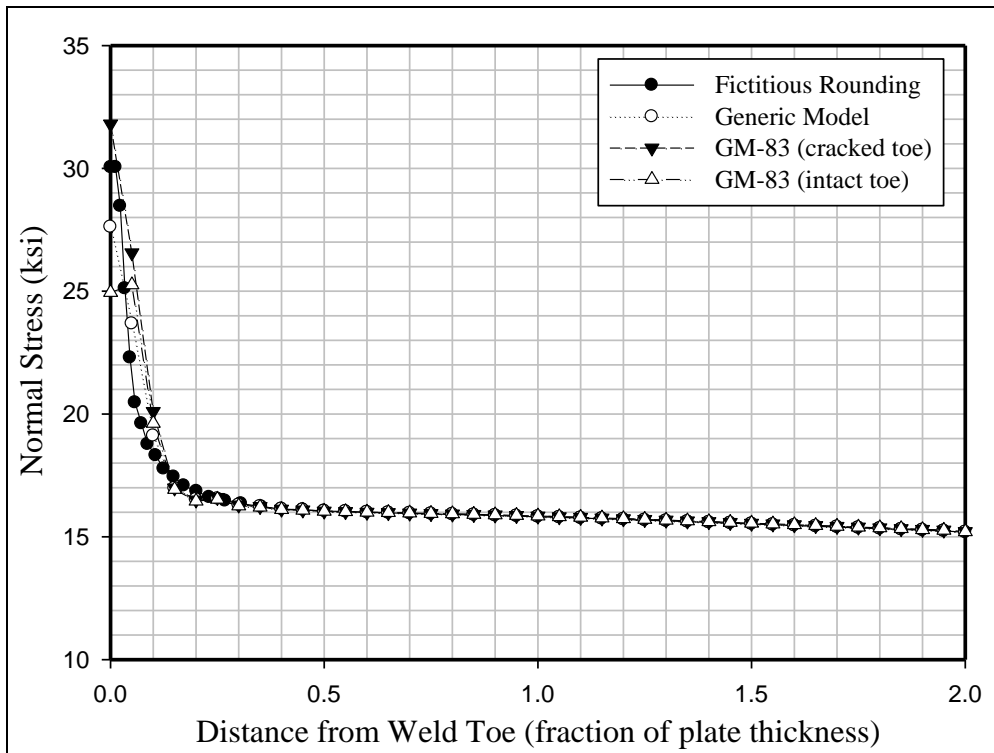


Figure 4.35 Normal stress on line 2 from different local geometries

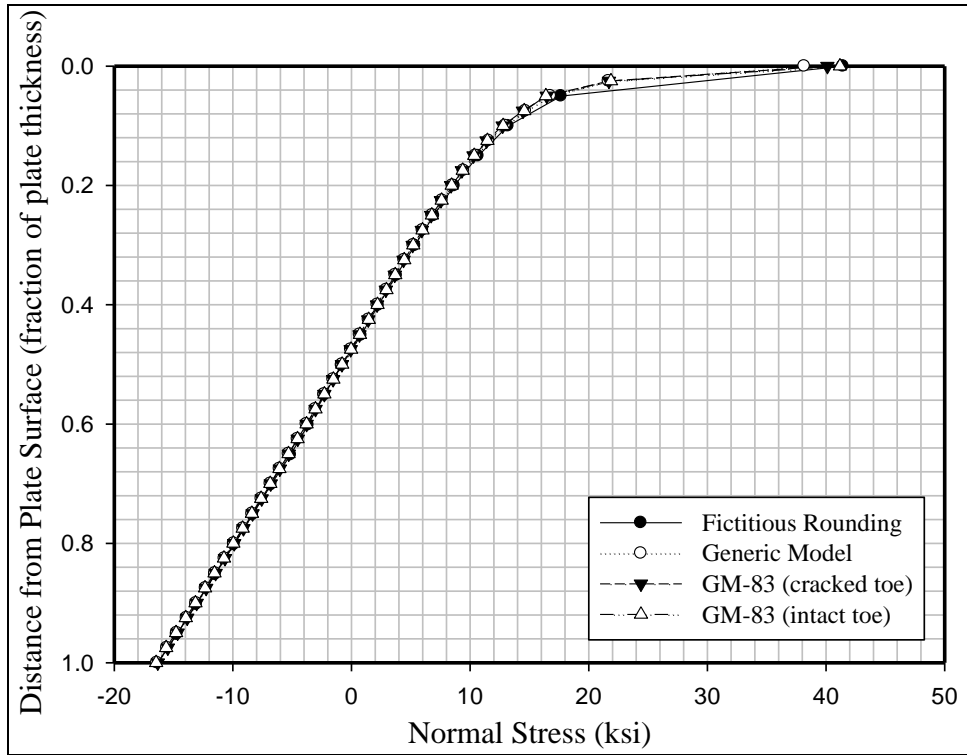


Figure 4.36 Normal stress on line 4 from different local geometries

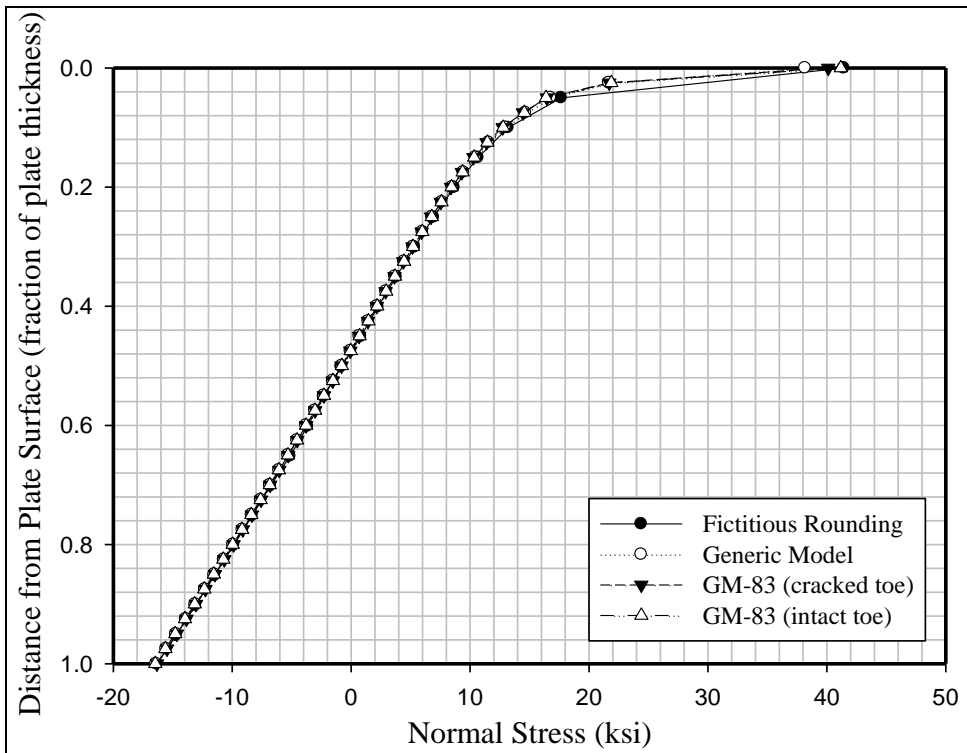


Figure 4.37 Normal stress on line 5 from different local geometries

It can be seen in Figure 4.34 through 4.37 that all models give identical results except for small variations in the notch affected zone. Here the model with fictitious rounding predicts the notch stress more effectively. Therefore, the generic 3D models were used to predict all hot-spot stresses in this study. However, it should be noted that the hot-spot stress methodology inherently excludes the notch effect which is highly influenced by the local geometry. While in reality it is impossible to calculate notch stress for each actual weld profile, it is impractical to calculate the notch stress for each specimen. Therefore the generic 2D models with fictitious rounding are used to predict the effective notch stress. The influence of individual weld dimensions is studied statistically in Section 4.2.4.

4.2.5 Influence of the Bearing Plate Size

The influence from the bearing plate was not realized until the fatigue tests performed at VT showed different failure modes compared to those tested at TFHRC. The bearing plate was not modeled in the early stages of the FE analysis but was added when its importance was recognized. The bearing plate size caused different stress distributions in the rib wall as illustrated by the moment diagrams for both the TFHRC (left) and VT (right) specimens as shown in Figure 4.38. The moment diagrams are computed using first-order elastic structural analysis.

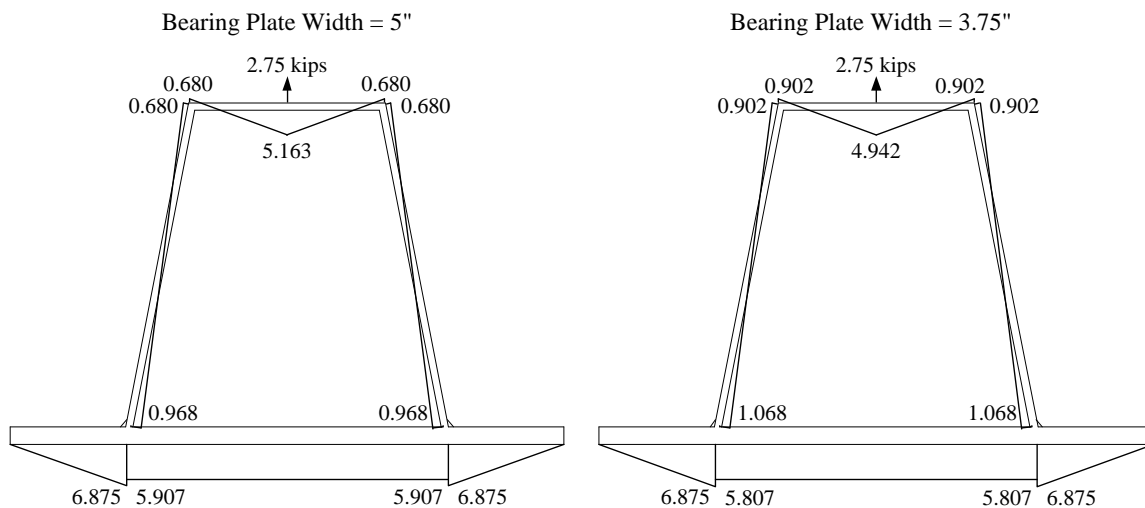


Figure 4.38 Moment Diagrams for Different Bearing Plate Sizes (in-kips)

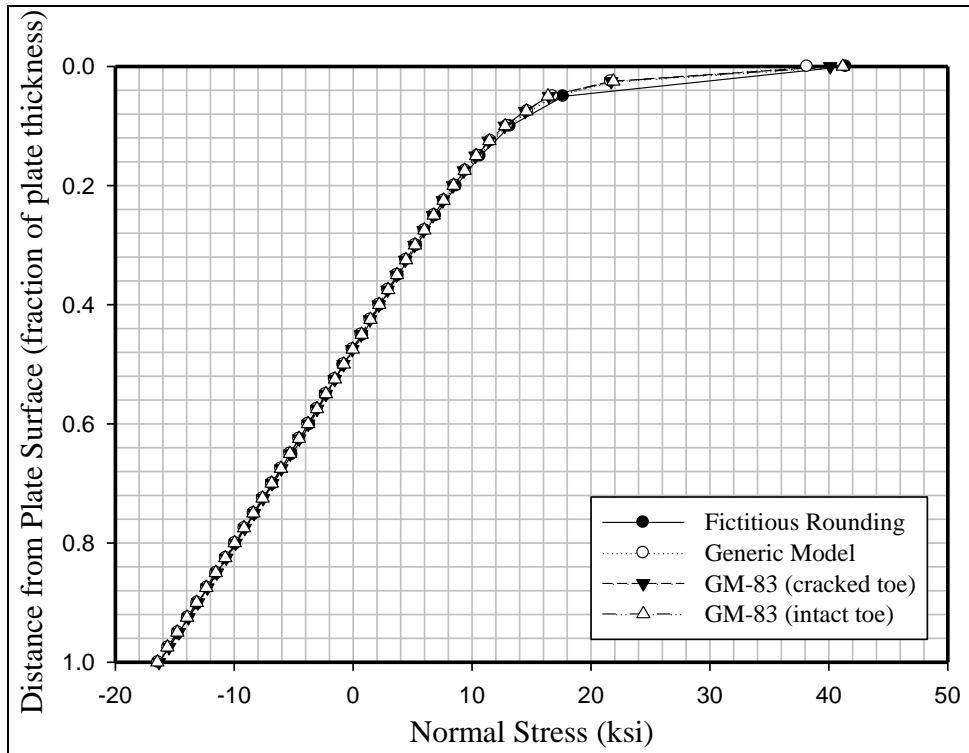


Figure 4.39 Normal Stress on Line 1 from Different Bearing Plate Sizes

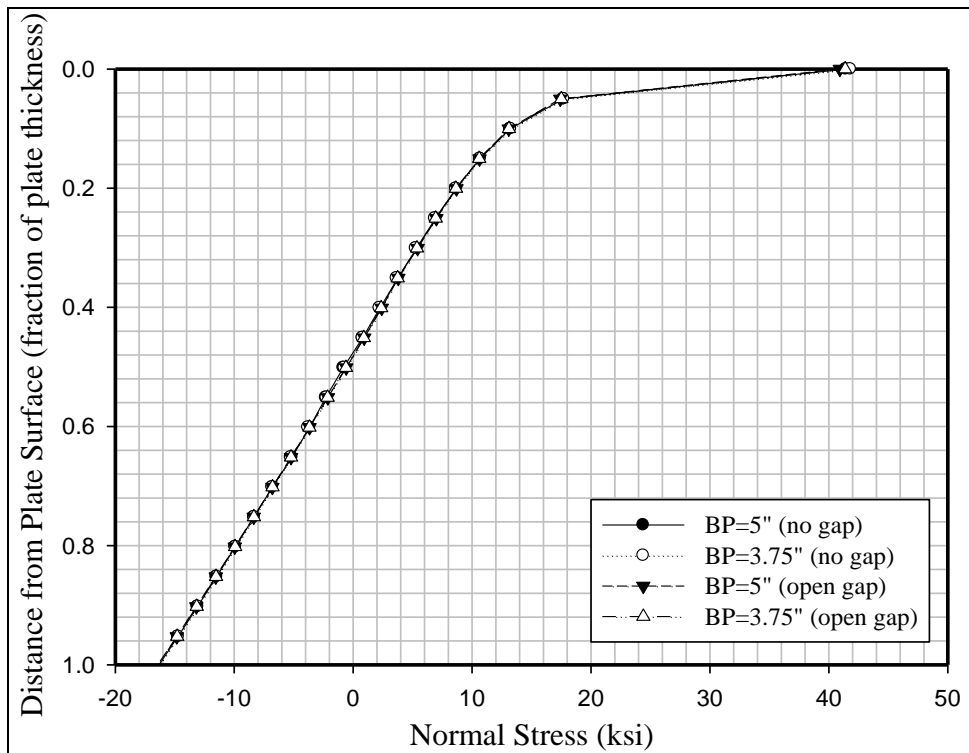


Figure 4.40 Normal stress on line 4 from different bearing plate sizes

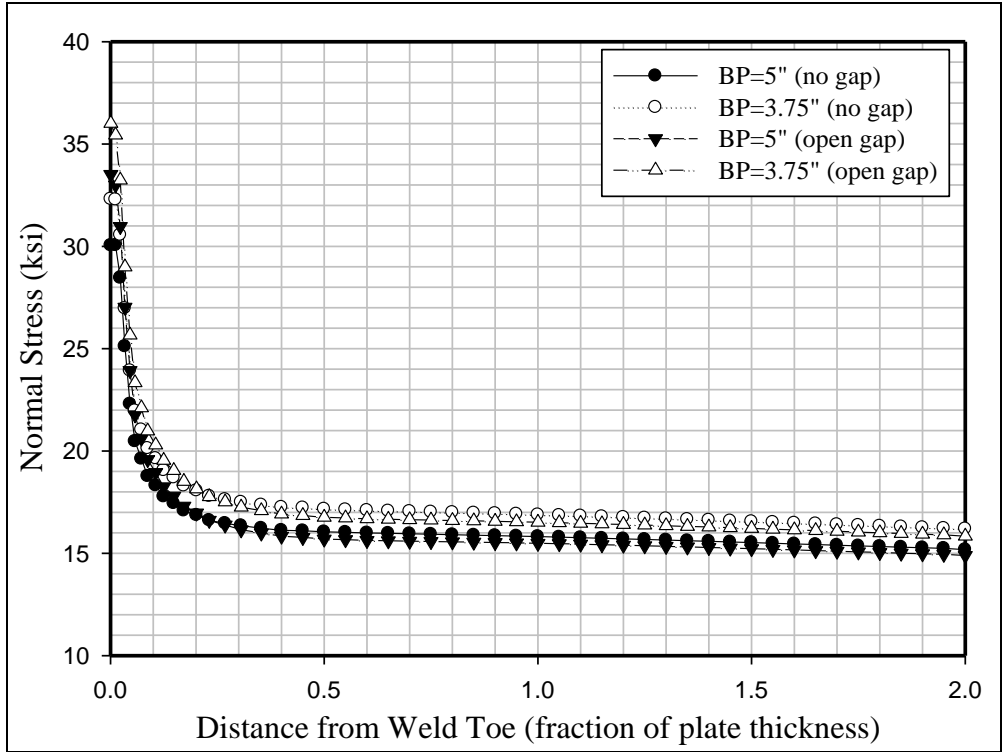


Figure 4.41 Normal stress on line 2 from different bearing plate sizes

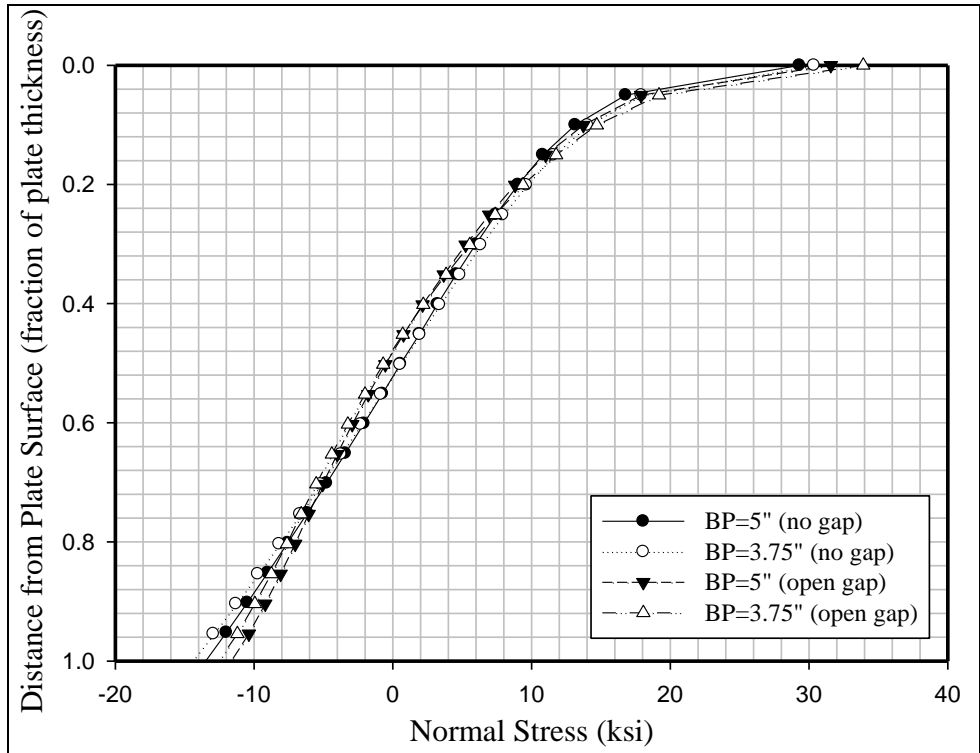


Figure 4.42 Normal stress on line 5 from different bearing plate sizes

Models were built including both bearing plate sizes with both no gap and open gap scenarios. As shown in Figure 4.39 and 4.40, the bearing plate size has little effect on the deck plate weld toe stress. However, the smaller bearing plate causes higher bending stresses in the rib walls raising the stress range by approximately 1 ksi throughout the hot-spot region (Figure 4.41). The notch stresses at both the weld toe and weld root increase as well. 4.42 shows the stress pattern at the weld toe through the thickness of the rib wall plate. After taking out the notch effect by linearization of the curves, the structural stresses calculated by the TTWT method are plotted in Figure 4.43. This shows the higher structural stress induced by the smaller bearing plate.

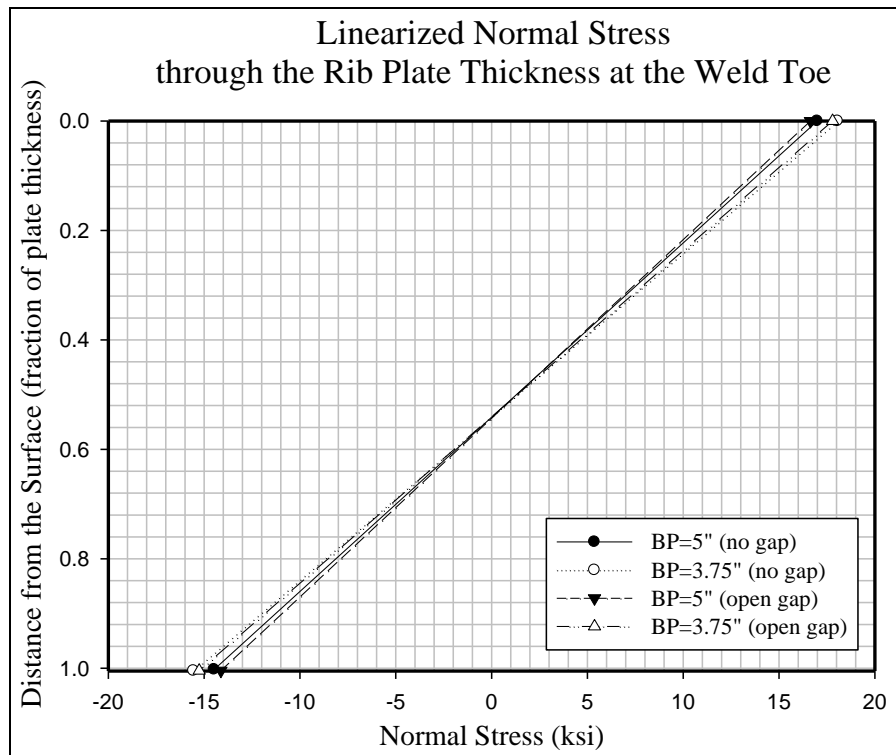


Figure 4.43 Structural stresses according to ttwt method

In summary, a number of different 2D FE models were built and compared to optimize the element type, mesh density, root gap condition, and the local geometry to provide the basis for 3D modeling. It was decided to use generic models with $0.1t \times 0.1t$ quadratic elements. It was also decided to use average weld dimensions for the following analysis. 2D models are used for effective notch stress determination to study the fatigue performance of weld roots.

4.3 3D Modeling

Two 3D solid models were built using the same planar mesh as 2D models with 50 layers of quadratic 20-node (Q20) elements across the specimen width. Root gaps were not included in these models since very small element sizes would be required, thereby dramatically increasing the computation time. The root gap mesh would also be awkward to control since a mesh size transition is required. The bearing plates were modeled as 5" and 3.75" wide by constraining the nodes in the clamped part between bearing plates to have identical vertical displacement. The stress results were read along similar lines for comparison with the 2D models. The mesh size and stress read-out lines are illustrated in Figure 4.44. Lines 3 through 7 are not visible in the picture but their in-plane locations on the center plane are the same as those shown in Figure 4.11 for the 2D models.

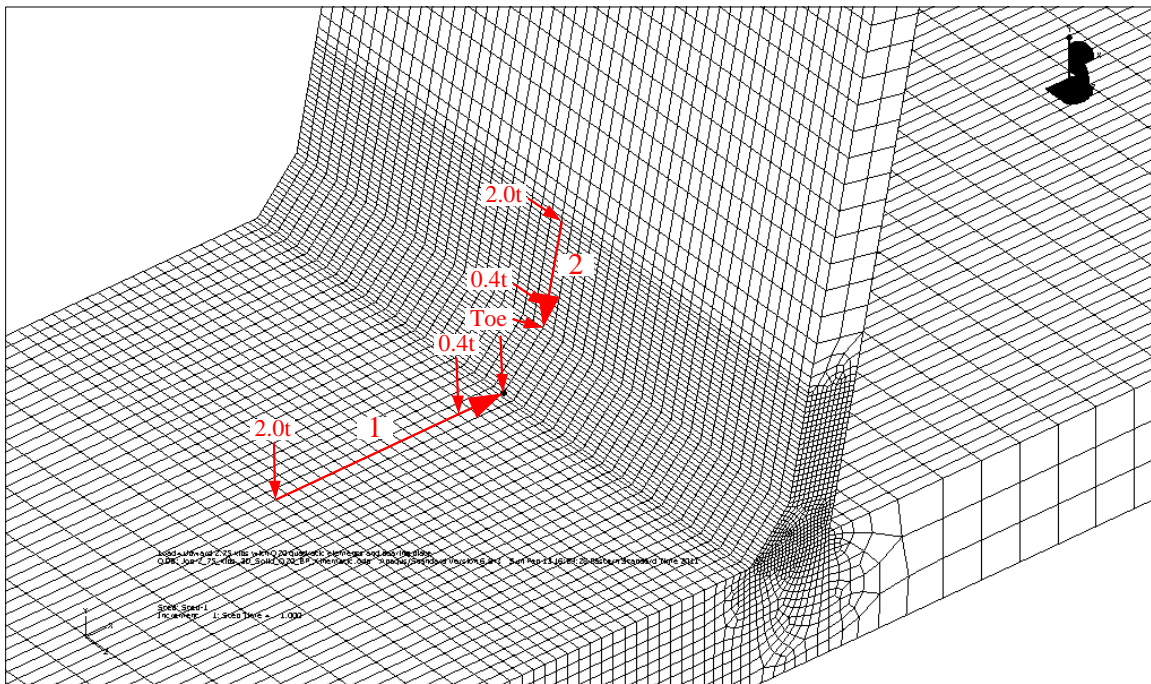


Figure 4.44 Stress read-out lines in 3D models

The maximum principal stress distributions are shown in Figure 4.45 with a scale of 0~50 ksi. Compared to the weld toe on the deck plate, the stress at the weld toe on the rib plate shows a higher stress concentration towards the center of the specimen. This makes the

3D stress results somewhat higher than those predicted by the 2D models. The smaller bearing plate size does not make much difference to the stresses at the weld toe on the deck plate, but it raises the stress along the weld toe on the rib plate. However, the FE stress values on the weld toes cannot be regarded as the true notch stresses since weld toe rounding is not included in the 3D models.

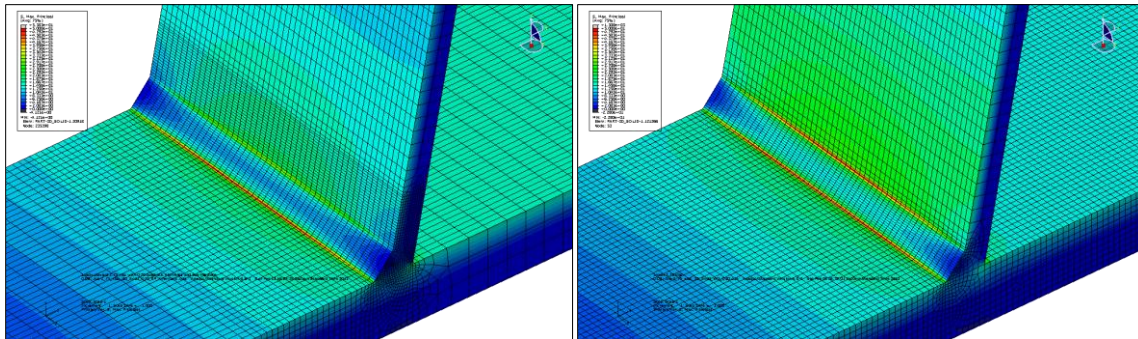


Figure 4.45 Maximum principal stress distribution for BP = 5" (left) and BP = 3.75" (right)

The validity of the plane strain assumption used for the 2D models can be illustrated by the stress contours through the deck and rib plate thicknesses as shown in Figure 4.46. Plane strain behavior assumes the out-of-plane strains (ϵ_z , γ_{xz} and γ_{yz}) to be zero, thus the in-plane stresses should be uniformly distributed in the transverse direction. As shown, the normal stress is almost even along the weld on the deck plate, but there is some concentration at the center along the weld toe on the rib plate. The weld root also exhibits plane strain behavior as shown in Figure 4.49 (the notch stress near the weld root predicted by the models without the fictitious rounding should be ignored). Therefore, to account for the out-of-plane bending effect in the rib, the hot-spot stresses are derived from the 3D models. However, since the corners are not rounded in 3D models, the notch stresses are still read from 2D models but an amplification factor can be applied to account for the stress concentration towards the center plane.

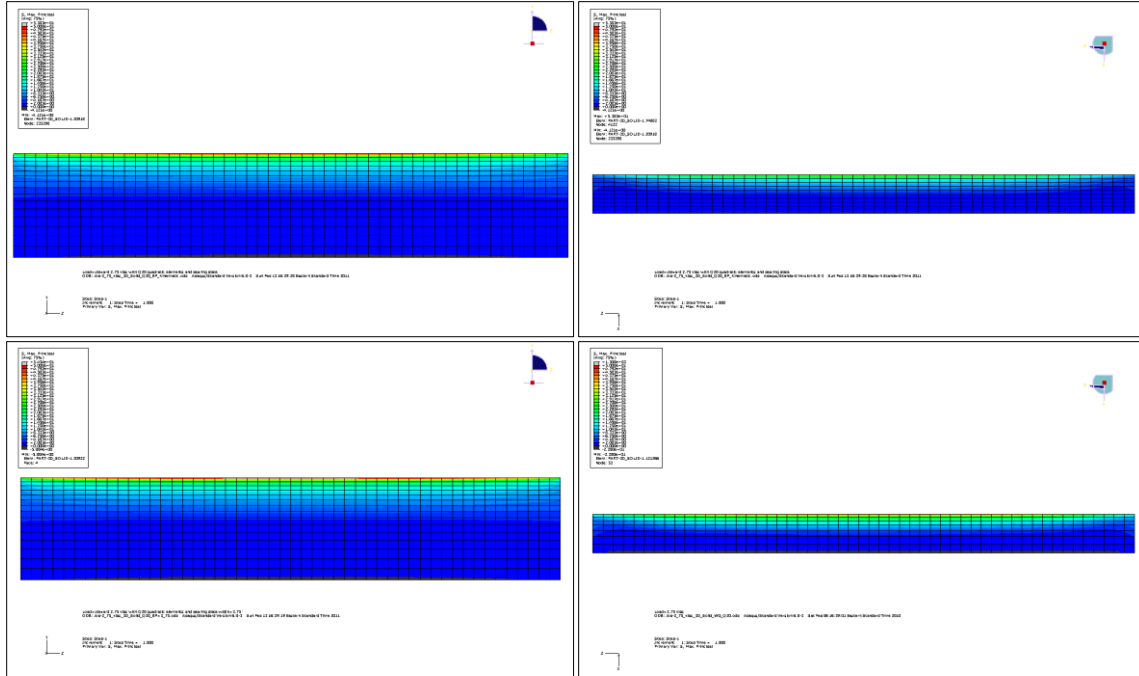


Figure 4.46 Maximum principal stress distributions through deck plates (left) and rib plates (right) with 5" wide bearing plate (top) and 3.75" wide bearing plate (bottom) at weld toes

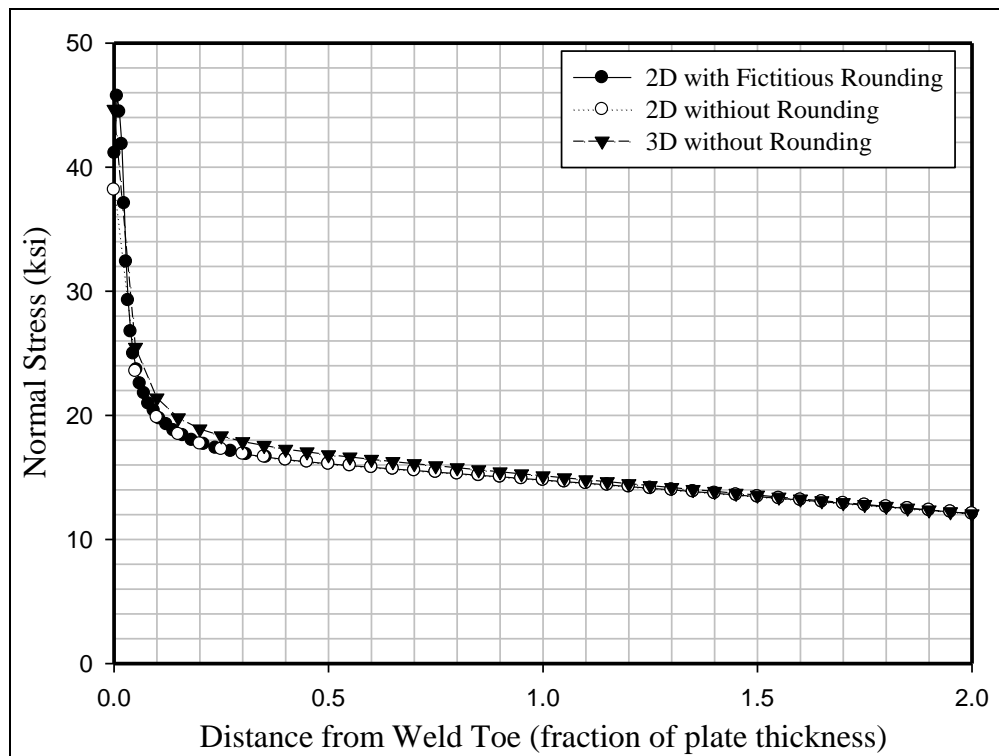


Figure 4.47 Normal stress on line 1 with 5" bearing plate

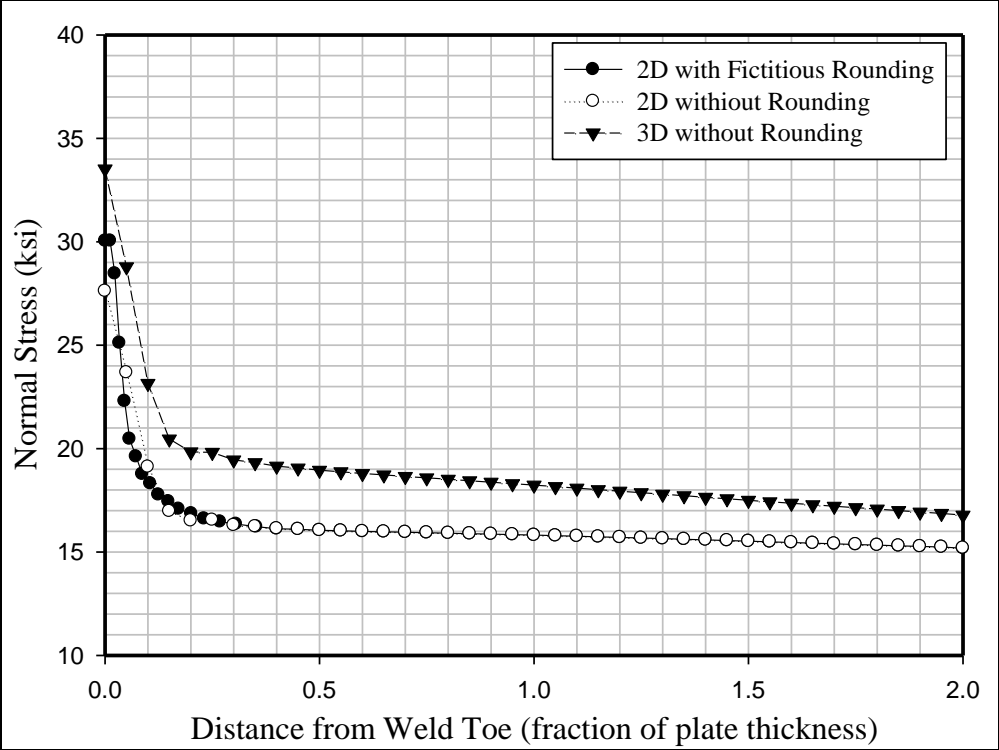


Figure 4.48 Normal stress on line 2 with 5" bearing plate

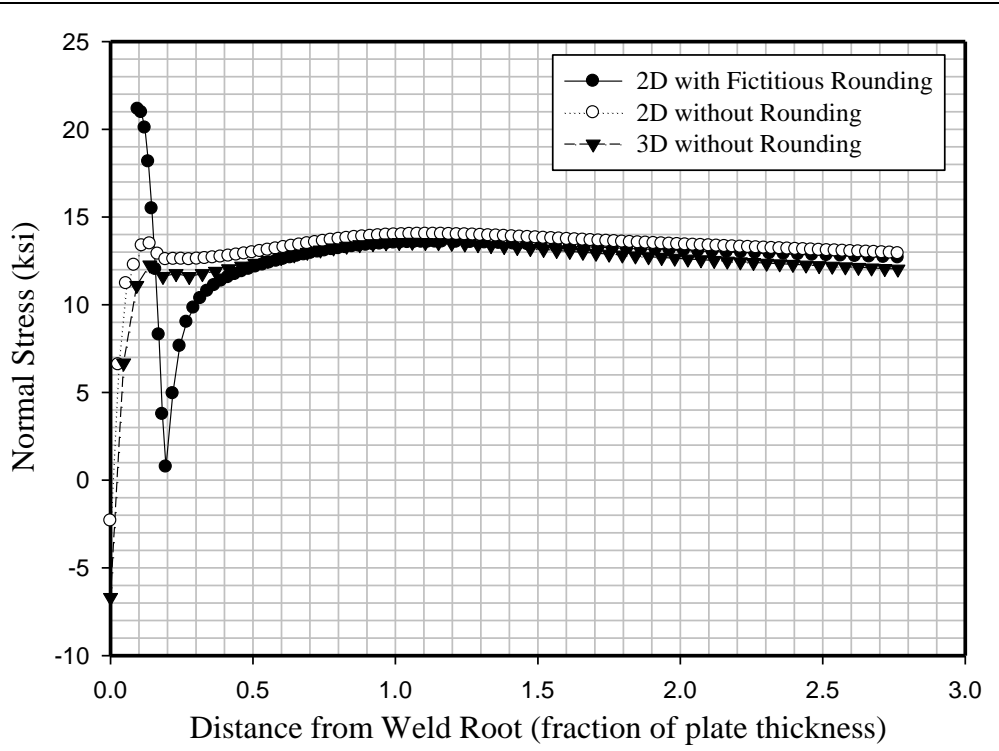


Figure 4.49 Normal stress on line 3 with 5" bearing plate

4.4 Hot-Spot Stress Analysis

The hot-spot stresses were calculated from 3D models using both the LSE and TTWT methods with similar results. The read-out points for LSE method were located on the lines shown in Figure 4.44 at 0.4t and 1.0t from weld toes (0410 extrapolation), or at 0.5t and 1.5t from weld toes (0515 extrapolation). Because all tests were carried out within elastic range, all models were run using an upward load of 2.75 kips. The results were proportioned to correspond with the individual specimen loads. To account for the different possible failure modes, the stress ranges at the cracked locations were calculated for each specimen. Since the average weld dimensions were modeled, the L_e distances (Figure 3.21) for both models (with 3.75" & 5" wide bearing plates) were taken as 4.8" indicating a 0.2 in. weld toe size. As addressed in Section 3.5.2, there was a small variation of L_e values caused by the misalignment of the rib plate during fabrication. This caused slight changes in the stress values at the weld toe. Therefore the extrapolated stresses from the FE models were proportioned by the actual L_e distance for each failure at the weld toe on the deck plate (WT@DECK). The L_e distance is not directly related to the stress range on the rib plate so proportioning was not performed for specimens that exhibited other failure modes (WT@RIB & WR).

Table 4.3 Hot-Spot Stress Results

Specimen Series	Specimen ID	Load Ratio	Load Range (kips)	Experimental Stress Range (ksi)	Root Gap	Failure Mode	L_e (in)	SHS @ WT 0410 Extrapolation	SHS @ WT 0515 Extrapolation	Cycles to Failure
FIL	FIL-1	0	5.00	33.33	Close	WT @ DECK	4-7/8	34.5057	34.0765	308,351
FIL	FIL-2	0	5.00	33.33	Close	WT @ DECK	4-3/4	33.6209	33.2028	352,981
FIL	FIL-3	0	5.00	33.33	Close	WT @ DECK	4-3/4	33.6209	33.2028	302,927
FIL	FIL-4	-1	5.50	36.67	Close	WT @ DECK	4-15/16	38.4429	37.9647	698,763
FIL	FIL-5	-1	5.50	36.67	Close	WT @ DECK	4-7/8	37.9563	37.4842	855,918
FIL	FIL-6	-1	5.50	36.67	Close	WT @ DECK	4-3/4	36.9830	36.5230	2,179,319
FIL	FIL-7	-1	5.50	36.67	Close	WT @ DECK	4-15/16	38.4429	37.9647	870,418
FIL	FIL-8	-1	5.50	36.67	Close	WT @ DECK	4-7/8	37.9563	37.4842	529,113
GM-80	GM-81	-1	5.50	36.67	Close	WT @ DECK	5-1/8	39.9028	39.4064	888,807
GM-80	GM-82	0	5.00	33.33	Close	RUNOUT	5-3/16	36.7176	36.2609	20,000,655
GM-80	GM-83	0	2.75	18.33	Close	WT @ DECK	5-1/4	20.4380	20.1838	18,253,515
GM-80	GM-84	-1	5.00	29.11	Close	WT @ RIB	5-1/16	35.9264	35.7750	6,060,816
GM-80	GM-85	-1	5.50	36.67	Close	WT @ DECK	5-1/4	40.8760	40.3676	770,672
GM-80	GM-86	-1	5.00	33.33	Close	WT @ DECK	5	35.3905	34.9503	1,517,705
GM-80	GM-87	-1	5.50	36.67	Close	WT @ DECK	5-5/16	41.3626	40.8481	751,609

Specimen Series	Specimen ID	Load Ratio	Load Range (kips)	Experimental Stress Range (ksi)	Root Gap	Failure Mode	L _e (in)	SHS @ WT 0410 Extrapolation	SHS @ WT 0515 Extrapolation	Cycles to Failure
GM-80	GM-88	0	5.00	33.33	Close	WT @ DECK	5-3/16	36.7176	36.2609	302,451
GM-80	GM-89	-1	2.50	16.67	Close	RUNOUT	5-1/16	17.9164	17.6936	10,000,000
GM-80	GM-810	0	5.00	33.33	Close	WT @ DECK	5	35.3905	34.9503	296,571
GM-80	GM-811	-1	5.00	33.33	Close	WT @ DECK	5-1/8	36.2752	35.8240	1,390,062
GM-80	GM-812	-1	4.00	26.67	Close	WT @ DECK	5	28.3124	27.9602	2,112,094
GM-80	GM-813	-1	2.50	16.67	Close	RUNOUT	5-7/16	19.2436	19.0042	10,000,000
GM-80	GM-814	0	6.00	40.00	Close	WT @ DECK	5-1/8	43.5303	42.9888	146,635
GM-80	GM-815	-1	5.00	33.33	Close	WT @ DECK	5-1/16	35.8328	35.3872	863,459
GM-80	GM-816	-1	5.00	33.33	Close	WT @ DECK	5-1/8	36.2752	35.8240	1,657,918
SA-20	SA-21	-1	5.50	36.67	Close	WT @ DECK	4-3/4	36.9830	36.5230	750,996
SA-20	SA-22	-1	5.50	36.67	Close	WT @ DECK	5-3/16	40.3894	39.8870	2,690,351
SA-20	SA-23	-1	5.50	36.67	Close	WT @ DECK	4-15/16	38.4429	37.9647	708,693
SA-20	SA-24	-1	5.50	36.67	Close	WT @ DECK	5-1/8	39.9028	39.4064	381,990
SA-20	SA-25	-1	5.50	36.67	Close	WT @ DECK	5-1/16	39.4161	38.9259	534,364
SA-20	SA-26	0	5.00	33.33	Close	WT @ DECK	5-1/8	36.2752	35.8240	258,639
SA-20	SA-27	0	5.00	33.33	Close	WT @ DECK	5-1/16	35.8328	35.3872	222,741
SA-20	SA-28	0	5.00	33.33	Close	WT @ DECK	5-1/8	36.2752	35.8240	238,136

Specimen Series	Specimen ID	Load Ratio	Load Range (kips)	Experimental Stress Range (ksi)	Root Gap	Failure Mode	L _e (in)	SHS @ WT 0410 Extrapolation	SHS @ WT 0515 Extrapolation	Cycles to Failure
SA-40	SA-41	-1	5.50	36.67	Close	WT @ DECK	5	38.9295	38.4453	643,413
SA-40	SA-42	-1	5.50	36.67	Close	WT @ DECK	5	38.9295	38.4453	540,472
SA-40	SA-43	-1	5.50	36.67	Close	WT @ DECK	5-1/16	39.4161	38.9259	607,547
SA-40	SA-44	-1	5.50	36.67	Close	WT @ DECK	4-7/8	37.9563	37.4842	840,760
SA-40	SA-45	-1	5.50	36.67	Close	WT @ DECK	4-15/16	38.4429	37.9647	649,093
SA-40	SA-46	0	5.00	33.33	Close	WT @ DECK	5-1/8	36.2752	35.8240	294,621
SA-40	SA-47	0	5.00	33.33	Close	WT @ DECK	5	35.3905	34.9503	300,716
SA-40	SA-48	0	5.00	33.33	Close	WT @ DECK	4-15/16	34.9481	34.5134	407,819
SA-60	SA-61	0	5.00	33.33	Close	WT @ DECK	4-15/16	34.9481	34.5134	317,140
SA-60	SA-62	0	5.00	33.33	Close	WT @ DECK	5-3/16	36.7176	36.2609	257,016
SA-60	SA-63	0	5.00	33.33	Close	WT @ DECK	5-3/16	36.7176	36.2609	286,626
SA-60	SA-64	-1	5.50	36.67	Close	WT @ DECK	5	38.9295	38.4453	629,917
SA-60	SA-65	-1	5.50	36.67	Close	WT @ DECK	5	38.9295	38.4453	2,074,221
SA-60	SA-66	-1	5.50	36.67	Close	WT @ DECK	4-15/16	38.4429	37.9647	860,759
SA-60	SA-67	-1	5.50	36.67	Close	WT @ DECK	4-15/16	38.4429	37.9647	588,156
SA-60	SA-68	-1	5.50	36.67	Close	WT @ DECK	5	38.9295	38.4453	521,486
SA-80	SA-81	-1	5.00	29.11	Close	WT @ RIB	4-7/8	35.9264	35.7750	689,134

Specimen Series	Specimen ID	Load Ratio	Load Range (kips)	Experimental Stress Range (ksi)	Root Gap	Failure Mode	L _e (in)	SHS @ WT 0410 Extrapolation	SHS @ WT 0515 Extrapolation	Cycles to Failure
SA-80	SA-83	-1	5.00	29.11	Close	WT @ RIB	4-3/4	35.9264	35.7750	3,732,998
SA-80	SA-84	-1	5.00	29.11	Close	WT @ RIB	5	35.9264	35.7750	2,321,046
SA-80	SA-85	-1	5.00	33.33	Close	WT @ DECK	4-7/8	34.4780	34.0597	3,332,973
SA-80	SA-86	-1	5.00	33.33	Close	WT @ DECK	4-3/4	33.5940	33.1864	2,623,398
SA-80	SA-87	-1	5.00	29.11	Close	WT @ RIB	4-11/16	38.5983	38.4205	3,399,577
SA-80	SA-88	-1	5.00	29.11	Close	WT @ RIB	4-25/32	38.5983	38.4205	2,743,534
SA-80	SA-89	-1	5.50	32.02	Close	WT @ RIB	4-27/32	42.4581	42.2625	283,556
SA-80	SA-810	-1	5.00	29.11	Close	WT @ RIB	4-5/8	35.9264	35.7750	869,732
SA-80	SA-811	-1	5.50	32.02	Close	WT @ RIB	4-7/8	42.4581	42.2625	617,702
SA-80	SA-812	-1	5.50	36.67	Close	WT @ DECK	4-31/32	38.6551	38.1862	1,930,296
SA-80	SA-813	-1	5.50	36.67	Close	WT @ DECK	4-11/16	36.4671	36.0247	1,782,037
SA-80	SA-814	0	5.00	33.33	Close	WT @ DECK	4-7/8	34.4780	34.0597	1,417,734
SA-80	SA-815	0	5.00	33.33	Close	WT @ DECK	4-11/16	33.1519	32.7497	943,434
SA-80	SA-816	0	5.00	33.33	Close	WT @ DECK	4-27/32	34.2570	33.8414	927,241
OB	OB-1	-1	5.00	24.93	Open	WR	4-13/32	27.7492	27.7492	647,879
OB	OB-10	-1	5.00	24.93	Open	WR	4-9/16	27.7492	27.7492	1,056,726
OB	OB-11	-1	5.00	24.93	Open	WR	4-1/2	27.7492	27.7492	996,626

Specimen Series	Specimen ID	Load Ratio	Load Range (kips)	Experimental Stress Range (ksi)	Root Gap	Failure Mode	L _e (in)	SHS @ WT 0410 Extrapolation	SHS @ WT 0515 Extrapolation	Cycles to Failure
OB	OB-12	-1	5.00	24.93	Open	WR	4-5/8	27.7492	27.7492	1,316,952
OB	OB-15	-1	5.50	32.02	Open	WT @ RIB	4-17/32	42.4581	42.2625	660,272
OB	OB-16	-1	5.50	27.42	Open	WR	4-17/32	30.5242	30.5242	768,171
OB	OB-2	-1	5.00	24.93	Open	WR	4-19/32	27.7492	27.7492	981,142
OB	OB-3	-1	5.00	24.93	Open	WR	4-15/32	27.7492	27.7492	2,385,939
OB	OB-4	-1	5.00	24.93	Open	WR	4-5/8	27.7492	27.7492	1,376,487
OB	OB-7	-1	5.50	27.42	Open	WR	4-19/32	30.5242	30.5242	1,076,871
OB	OB-8	-1	5.50	27.42	Open	WR	4-3/4	30.5242	30.5242	618,383
OB	OB-9	-1	5.00	24.93	Open	WR	4-5/8	27.7492	27.7492	2,451,238
UB	UB-1	-1	5.00	33.33	Close	WT @ DECK	4-5/8	32.7099	32.3131	1,359,570
UB	UB-10	-1	5.00	33.33	Open	RUNOUT	5	35.3905	34.9503	4,725,868
UB	UB-11	-1	5.00	24.93	Open	WR	4-7/8	27.7492	27.7492	1,483,203
UB	UB-12	-1	5.00	24.93	Open	WR	4-11/16	27.7492	27.7492	1,590,018
UB	UB-15	-1	5.50	27.42	Open	WR	4-5/8	30.5242	30.5242	856,676
UB	UB-16	-1	5.50	32.02	Open	WT @ RIB	4-1/2	42.4581	42.2625	1,177,345
UB	UB-2	-1	5.00	24.93	Close	WR	4-5/8	27.7492	27.7492	694,734
UB	UB-3	-1	5.00	29.11	Close	WT @ RIB	4-5/8	38.5983	38.4205	2,011,029

Specimen Series	Specimen ID	Load Ratio	Load Range (kips)	Experimental Stress Range (ksi)	Root Gap	Failure Mode	L _e (in)	SHS @ WT 0410 Extrapolation	SHS @ WT 0515 Extrapolation	Cycles to Failure
UB	UB-4	-1	5.00	33.33	Close	WT @ DECK	4-9/16	32.2679	31.8764	1,372,641
UB	UB-7	-1	5.50	36.67	Close	WT @ DECK	4-5/8	35.9809	35.5444	1,292,525
UB	UB-8	-1	5.50	36.67	Close	WT @ DECK	4-3/4	36.9534	36.5050	1,182,601
UB	UB-9	-1	5.00	33.33	Open	WT @ DECK	4-11/16	33.1519	32.7497	2,024,920
OB	OB-13	0	5.00	33.33	Open	WT @ DECK	4-9/16	32.2679	31.8764	990,806
OB	OB-14	0	5.00	33.33	Open	WT @ DECK	4-5/8	32.7099	32.3131	979,089
OB	OB-5	0	5.00	33.33	Open	WT @ DECK	4-11/16	33.1519	32.7497	574,148
OB	OB-6	0	5.00	33.33	Open	WT @ DECK	4-3/4	33.5940	33.1864	688,273
UB	UB-13	0	5.00	29.11	Open	WT @ RIB	4-7/16	38.5983	38.4205	448,014
UB	UB-14	0	5.00	33.33	Open	WT @ DECK	4-19/32	32.4889	32.0947	591,939
UB	UB-5	0	5.00	33.33	Close	WT @ DECK	4-11/16	33.1519	32.7497	386,829
UB	UB-6	0	5.00	33.33	Close	WT @ DECK	4-9/16	32.2679	31.8764	474,226

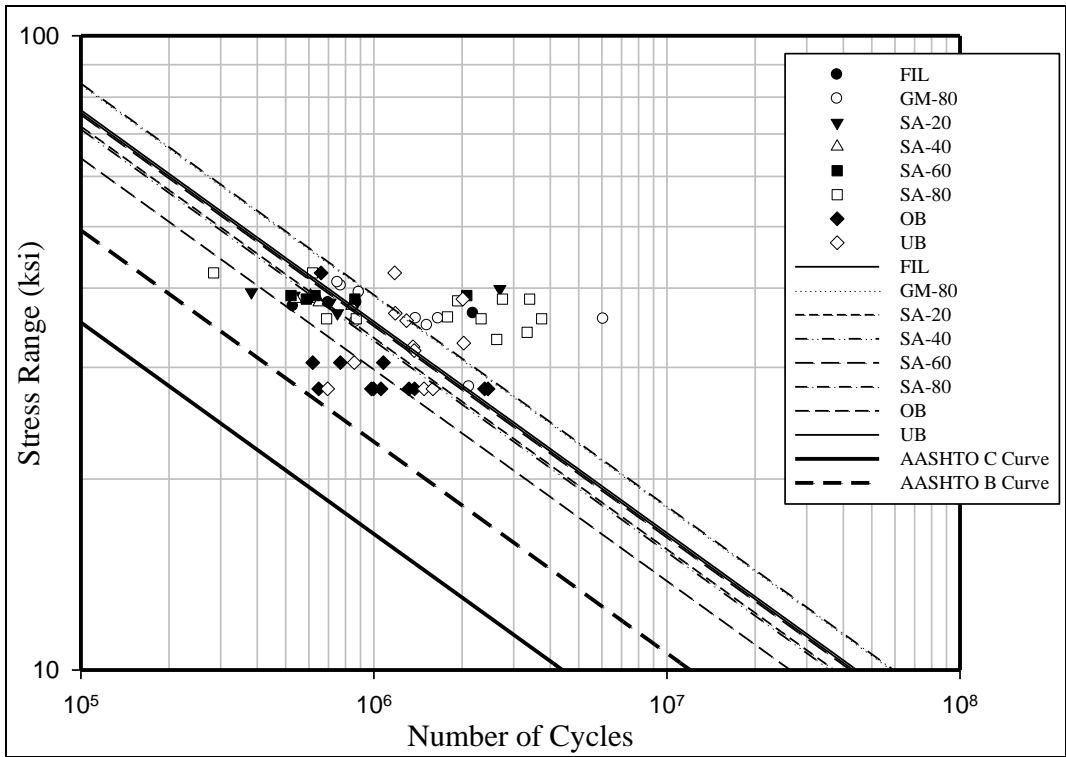


Figure 4.50 S-N curves for specimen series (R=-1)

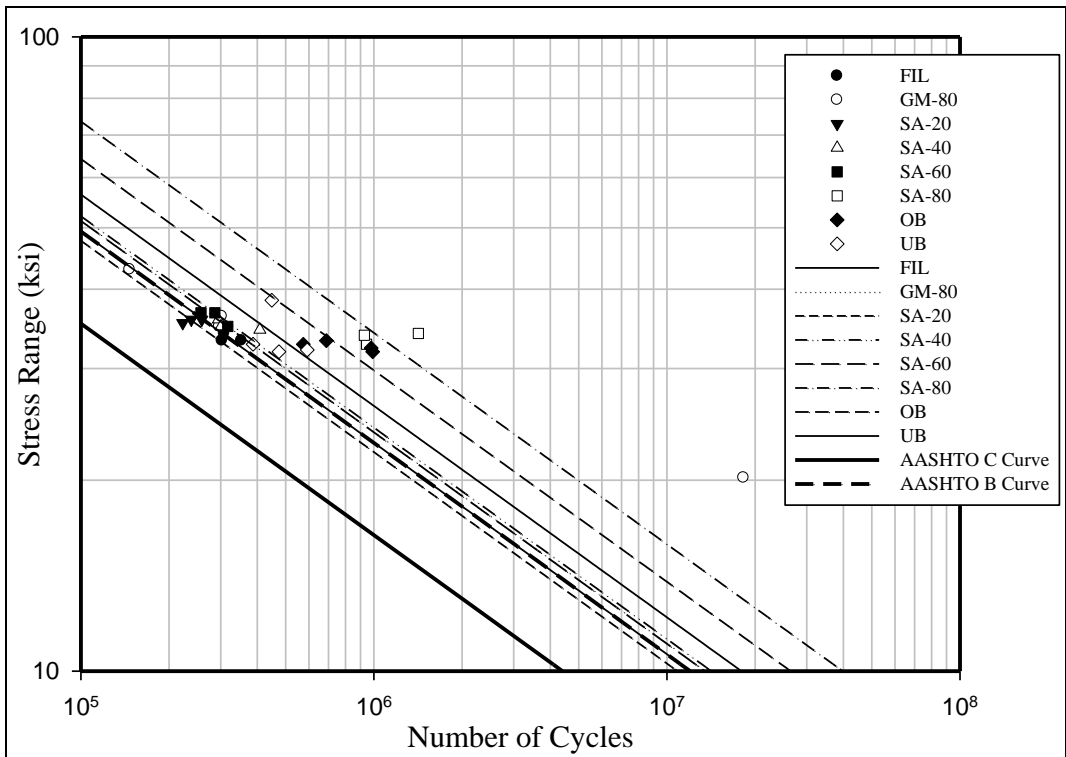


Figure 4.51 S-N curves for specimen series (R=0)

A summary of the derived hot-spot stresses is tabulated in Table 4.3. The experimental stress ranges in the table were calculated based on moment diagrams illustrated in Figure 4.38 using beam theory. The S-N curves for each specimen series are plotted in Figure 4.50 and 4.51. Hot-spot stresses are not available for the failure mode on weld root (WR) therefore nominal stresses are used in the plots. As shown for the $R = -1$ loading, all data points are close together except for the over-beveled (OB) specimen series, since most of the OB specimens failed at weld root where the nominal stresses are higher. For the $R = 0$ tests, the average S-N curves for each specimen series show slightly larger scatter due to fewer replicate specimens were tested under $R=0$. Nonetheless, the curves are not all statistically distinctive from each other, as demonstrated in Figure 4.51. It is also observed that the $R = 0$ data shows shorter fatigue life compared to the $R = -1$ data. This indicates the residual stress magnitude is insufficient to convert the entire compressive stress range into tension that will cause fatigue damage. The residual stress magnitude can be roughly estimated by comparing results from these two loading cases statistically. More detailed analysis of the S-N results is presented in Chapter 5.

Chapter 5. S-N Curve Study and Statistical Analysis

S-N curves are developed combining the results from the fatigue tests and the FE models. In this chapter curves are presented isolating the testing variables such as weld dimensions, specimen series, load ratio, failure mode, and root gap conditions. Initially it is not known if these testing variables affect fatigue performance, therefore the S-N curves might not be properly categorized. Regression analysis is required to investigate the significance of each test variable. Of the different regression analysis methods that are available, the multiple linear regression (MLR) and multi-way analysis of covariance (Multi-way ANCOVA) methods particularly match the needs of this research.

Correlation is the measurement of the relationship between two variables. Correlation analysis gives the level of relevance indicated by the correlation coefficient ranging from +1.0 for a perfect positive correlation to -1.0 for a perfect negative correlation. A value of 0.0 represents a lack of any correlation. The Pearson's r , also called the linear or product-moment correlation, is the most widely-used type of correlation coefficient for linear correlation analysis. When one of the variables is dependent on the other one, or there are more than two variables in the comparison, a generalized linear model (GLM) is generally used for regression analysis. The model fit can be evaluated by the coefficient of determination (R^2) where zero represents a lack of correlation and 1.0 represents a perfect correlation. The value of R^2 equals one minus the ratio of residual variability to the overall variability. For simple linear regression, R^2 yields to the same value as the square of Pearson's r in correlation analysis.

Linear regression analysis determines the extent to which the dependent (criterion) variable is linearly related to one or more independent (predictor) variable(s). This indicates how well the data pairs can be captured by a straight line as long as both variables are numerical. The regression line is usually established using the least squares method. For simple linear regression, the method calculates the regression line equation such that the sum of the squared residuals of all data points from the predicted regression line is minimized. Note that the least squares method is not only limited to simple linear regression but is also applicable to many other types of regression analysis including the

MLR and multi-way ANCOVA methods.

The different analysis methods are summarized in Table 5.1. The general procedure involves determination of a regression line using the least squares method (if all independent variables are numerical) and performing hypothesis tests on individual independent variables to determine their level of statistical significance.

Table 5.1 Types of regression analysis

Independent Variable(s)	Numerical	Categorical	Both
Single	Simple Linear Regression	Analysis of Variance (ANOVA)	Analysis of Covariance (ANCOVA)
Multiple	Multiple Linear Regression	Multi-way ANOVA	Multi-way ANCOVA

ANOVA is the underlying hypothesis test involved the regression analysis. It determines if the means of different variable groups differ from each other by comparing their variance to the overall variance across all groups. The null hypothesis (H_0) assumes all group population means are equal and there is no difference between the groups. In other words, the effect of the factor (independent variable) is NOT statistically significant. The alternative hypothesis (H_1) means the opposite, indicating the factor is statistically significant to the result. The level of statistical significance is indicated by the p-value, which is the probability that an outcome of the data (for example, the sample mean) will happen purely by chance when the null hypothesis is true (Illowsky, 2010). Smaller p-values suggest there is less likelihood of an outcome that contradicts the null hypothesis. If the p-value is small enough, an inferential decision can be made to reject the null hypothesis thereby supporting the alternative hypothesis.

The null hypothesis (true or false) can be either accepted or rejected depending on the efficiency of the statistical model. There are four possible outcomes that could occur as listed in Table 5.2. Note that two types of errors can occur. The possibility of a Type I error (α), is conventionally more rigidly controlled and referred as the basis for either

accepting or rejecting the null hypothesis. The p-value is also called the computed α and is compared with the preset α value. If the p-value is smaller than α , it suggests the possibility of getting a Type I error is less than α , therefore it is reasonable to reject the null hypothesis if α is small enough. The α value is generally taken as 0.05 in engineering fields. If the computed p-value is greater than α , there is not enough evidence to reject the null hypothesis. Either the null hypothesis is true or a Type II error occurs. The probability of occurrence of Type II errors is measured by the β value. In this case, a power analysis is helpful to evaluate the outcome. The statistical power is equal to $1-\beta$ where higher statistical power indicates that the null hypothesis is more likely to be correctly accepted.

Table 5.2 Outcomes of a hypothesis test

	H ₀ is true (H ₁ is false)	H ₀ is false (H ₁ is true)
Accept H ₀ (Reject H ₁)	Correct Acceptance	Type II Error (β)
Reject H ₀ (Accept H ₁)	Type I Error (α)	Correct Rejection

It is clear that the stress range is the dominant factor affecting fatigue life but the effect of the other factors is not obvious. Some factors, such as the failure mode and load ratio (R ratio) seem to have a clearly significant effect on fatigue life. Other factors, such as the specimen series and weld dimensions, are more difficult to quantify because of possible correlation between multiple variables. Therefore, a statistical model that includes all possible factors was used for a preliminary study to determine the potential independent variables that need to be considered in the MLR and ANCOVA analyses.

The model fitting is summarized in Table 5.3. A detailed report from the statistical software package JMP can be found in Appendix G. As shown, the failure mode and R-ratio are considered significant to the response in addition to the stress range. This is demonstrated by the low p-values (<0.05) and high statistical powers. The high p-values for the other factors indicate that there is insufficient evidence to indicate they affect fatigue life. However, the low power of the hypothesis tests for the other factors

indicates there is a high chance that a Type II error is occurring meaning that the correlation might exist but cannot be detected by the particular model or sample size. Therefore, two additional analyses were performed, MLR to determine the effect of weld dimensions and multi-way ANCOVA to determine the effect of the test scenarios.

Table 5.3 Summary of Model Fitting—All Potential Factors

Response (Dependent Variable)	Overall Model Fitness	
	R ² =0.6519	R ² (Adjusted)=0.5517
Factors (Independent Variables)	p-value	Power
Specimen Series	0.7827	0.2285
Failure Mode	<0.0001*	0.9993
Root Gap	0.5580	0.0895
R-ratio	<0.0001*	0.9998
Weld Toe Size (d _i)	0.1099	0.3586
Weld Penetration	0.7430	0.0622
Weld Throat (t)	0.1800	0.2669
Weld Height (h)	0.3868	0.1380
Weld Area (A _w)	0.9624	0.0502
Lg (SHS-0515 extrapolation)	0.0001*	0.9790

5.1 Multiple Linear Regression (MLR)

In this section, the effect of weld dimensions are studied in more depth since the preliminary model indicates their effect may be overwhelmed by other factors such as the failure mode and R-ratio which affect the response on a much higher level. MLR models that only include the weld dimensions as factors were built. This excludes the influence from other factors by eliminating them from the model. For example, separate MLR models were constructed for the data with different experimental stress ranges. The

stress range is still included in the models to account for the small stress variance caused by the differing L_e values.

Since the dimensions taken from a weld profile are not completely independent from each other, the factors in the MLR models need to be carefully selected to avoid multicollinearity between the factors. For example, consider the interdependence of the dimensions d_1 , d_2 , d_3 , d_4 , d_5 and the weld penetration, dimension d_4 , the projection of the rib wall thickness on the deck plate, is not dependent on weld size. Dimension d_5 is completely redundant with d_1 since $d_5=d_1+d_4$. Dimension d_2 and the weld penetration are the same measurement and d_3 can be derived from d_2 or the weld penetration ($d_3=d_4-d_2$). Therefore only one factor between d_1 and d_5 can enter the model. Dimension d_1 was selected because it excludes the error from d_4 . Similarly, only one factor can be selected from among d_2 , d_3 and the weld penetration. The weld penetration is chosen because it can be calculated as the ratio of d_2/d_4 , thereby canceling out possible measurement errors. Therefore 5 predictors are chosen as independent variables, the weld toe size d_1 , weld penetration, weld throat t , weld height h , and the weld area A_w . However, it is still difficult to completely suppress the statistical correlation among the variables since larger welds tend to proportionally increase all dimensions and vice versa.

5.1.1 Preliminary Simple Linear Regression

MLR analyses are conducted separately for several data groups, each with identical stress range, failure mode, and R ratio. Preliminary plots of the simple linear regression lines for each individual factor are made for each data group first; statistical models with different factor combinations are then built to account for the possible collaborative effect among factors. The results of the preliminary simple linear regression are summarized in Table 5.4 and full reports are provided in Appendix H through Appendix K.

Table 5.4 Summary of Simple Linear Regressions

Model Response: Cycles to Failure			
Data Group	Factor	R²	p-value
R-ratio = -1 Experimental Stress Range = 36.67 ksi Failure Mode: WT@DECK Number of Samples: 24	Weld Toe Size (d ₁)	0.139767	0.0547
	Weld Penetration	0.007093	0.6762
	Weld Throat (t)	0.011237	0.5987
	Weld Height (h)	0.005336	0.7173
	Weld Area (A _w)	0.219426	0.0137*
R-ratio = -1 Experimental Stress Range = 33.33 ksi Failure Mode: WT@DECK Number of Samples: 9	Weld Toe Size (d ₁)	0.630527	0.0106*
	Weld Penetration	0.135236	0.3302
	Weld Throat (t)	0.485763	0.0369*
	Weld Height (h)	0.566106	0.0193*
	Weld Area (A _w)	0.442688	0.0505
R-ratio = 0 Experimental Stress Range = 33.33 ksi Failure Mode: WT@DECK Number of Samples: 24	Weld Toe Size (d ₁)	0.523656	<0.0001*
	Weld Penetration	0.006951	0.6985
	Weld Throat (t)	0.008631	0.6659
	Weld Height (h)	0.087336	0.1609
	Weld Area (A _w)	0.657158	<0.0001*
R-ratio = 0 Experimental Stress Range = 24.93 ksi Failure Mode: WR Number of Samples: 11	Weld Toe Size (d ₁)	0.02864	0.6189
	Weld Penetration	0.208138	0.1584
	Weld Throat (t)	0.236645	0.1292
	Weld Height (h)	0.627773	0.0036*
	Weld Area (A _w)	0.106694	0.3269

Four data groups were analyzed as shown in the Table 5.4. It is observed that the weld

toe size (d_1) and the weld area (A_w) generally show a correlation with the number of fatigue cycles indicated by p-values less than 0.05. The weld height (h) also exhibits significance in the second and fourth data groups but with a negative correlation to fatigue life, meaning the fatigue life declines with increasing weld height. Different from first three data groups with the WT@DECK failure mode, none of the dimensions had a significant effect on fatigue life for the fourth data group with the weld root failure mode. None of the regressions indicate that the weld penetration has a significant effect on the fatigue life. It should be noted that the second and fourth data groups are less statistically stable due to their smaller sample sizes (9 and 11).

5.1.2 MLR for All Possible Models

MLR analyses were performed including multiple factors simultaneously to enhance the model fit. The “Root Mean Squared Error” (RMSE) indicating the model fit was calculated for all possible factor combinations which is equal to the square root of the variance of the residuals. This provides a measure to indicate how close the predicted response matches the observed data; therefore it indicates the absolute fit of the model. Lower RMSE values indicate a better fit. The R^2 values are no longer used for models with more than one factor because the R^2 value is dependent on the number of factors in the model. The R^2 value increases as more factors are added to the model, therefore the value is artificially biased. Instead, an adjusted R^2 value is used as a relative measurement of model fit that is independent from the number of predictors and can be interpreted as the proportion of total variance that is explained by the regression model. The overall performances of all possible models are sorted by their RMSE values in ascending order. Then the models with high global fitness are analyzed and compared to indicate the effect of individual factors.

Since MLR allows the stress range to be a predictor in every model, the samples are rearranged in four data groups disregarding the stress range. The MLR results later prove the stress range to be significant in nearly all models. For each data group, the three models with the highest RMSE value are listed in Table 5.5. It can be seen that every factor has some contribution to the overall model fit. Further investigation shows that not all factors have statistical significance in the model. Some factors predict too little

response variance to be regarded as influential on the response. The following stepwise model fitting analysis reveals the effect of each factor.

Table 5.5 Models with high overall fit

Data Group	Model	Adjusted R ²	RMSE
R-ratio = -1 Failure Mode: WT@DECK Sample Size: 37	d ₁ , weld penetration, Lg(stress range)	0.4531	0.1804
	d ₁ , weld penetration, h, Lg(stress range)	0.4404	0.1825
	d ₁ , weld penetration, t, Lg(stress range)	0.4373	0.1830
R-ratio = 0 Failure Mode: WT@DECK Sample Size: 27	h, A _w , Lg(stress range)	0.9192	0.1128
	d ₁ , t, h, A _w , Lg(stress range)	0.9175	0.1140
	d ₁ , h, A _w , Lg(stress range)	0.9165	0.1147
R-ratio = -1 Failure Mode: WT@RIB Sample Size: 12	d ₁ , h, A _w , Lg(stress range)	0.5996	0.2523
	t, Lg(stress range)	0.5856	0.2566
	d ₁ , h, Lg(stress range)	0.5757	0.2597
R-ratio = -1 Failure Mode: WR Sample Size: 15	weld penetration, t, h, Lg(stress range)	0.6828	0.1051
	d ₁ , weld penetration, t, h, Lg(stress range)	0.6764	0.1062
	weld penetration, t, h, A _w , Lg(stress range)	0.6657	0.1079

5.1.3 Stepwise Model Fitting Analysis

Stepwise analysis only keeps the statistically significant factors in the model. Depending on the screening criteria, there are two types of stepwise analysis, forward and backward. Forward stepwise analysis adds the most significant predictor in the model at every step among the remaining predictors. Backward stepwise analysis first includes all factors in the model and eliminates the least significant factor at each step, leaving the significant factors at the end. Criteria can be set for the p-value to determine if a factor should be added or removed from the model. For this work, the p-value was set at 0.05, consistent with the preset significance level α . A factor is regarded as significant and entered in the

model if its p-value is less than 0.05 and is regarded as insignificant and removed from the model if its p-value is greater than 0.05.

Table 5.6 Stepwise model fitting analysis

Response (Criterion): Lg(Cycles to Failure)				
Data Group	Stepwise Method	Model Fitness	Factor	p-value
R-ratio = -1 Failure Mode: WT@DECK Sample Size: 37	Forward	Adjusted $R^2 = 0.4289$	A_w	0.00377*
			Lg(Stress Range)	0.00221*
	Backward	Adjusted $R^2 = 0.4531$	d_1	0.00146*
			Weld Penetration	0.001189*
			Lg(Stress Range)	0.00431*
R-ratio = 0 Failure Mode: WT@DECK Sample Size: 27	Forward	Adjusted $R^2 = 0.9192$	h	0.00043*
			A_w	0.00018*
			Lg(Stress Range)	1.1×10^{-13} *
	Backward	Adjusted $R^2 = 0.9147$	d_1	0.00028*
			Weld Penetration	0.02427*
			h	0.0015*
			Lg(Stress Range)	1.4×10^{-12} *

Due to potential correlation between the factors, the significance level of each individual factor is affected by the other factors. Hence the forward and backward techniques do not always generate the same model. For the analyses performed, the cases with the WT@DECK failure mode result indifferent models using forward and backward methods as shown in Table 5.6. As expected, the stress range is included in all models. The forward method predicts that the weld area (A_w) is significant, while the backward method predicts that d_1 and the weld penetration are significant. The weld height h is also selected for the R=0 case however with a negative correlation. For the R=-1 case it

also shows a negative correlation although this effect has insufficient significance to allow h to be entered into the model. Multiple models are suggested is due to the difference in correlation between factors as demonstrated below.

5.1.4 Bivariate Regression Analysis for Relationships between Factors

As discussed previously, the R^2 value in a multiple regression model indicates the combined proportion of variance that is predicted by all factors. When some of the factors are correlated with each other, their combined effect in the model can be either enhanced or decreased. It was observed in the stepwise analyses that the A_w factor considerably reduces the significance of d_1 (increases the p-value) when it enters into the model. The d_1 factor also decreases the significance of A_w slightly (Table 5.7). This is due to the variance predicted by these two factors has a large overlap area correlated with the response, especially for d_1 since it predicts less variance than A_w . Therefore, the d_1 factor is redundant in this case. As illustrated in Figure 5.1, both d_1 and A_w individually predict a statistically significant variance in the response (number of fatigue cycles). However, once combined, d_1 is no longer significant since a major portion of variance is explained by A_w . The significance level of A_w is also reduced but remains above the threshold $p\text{-value} < 0.05$.

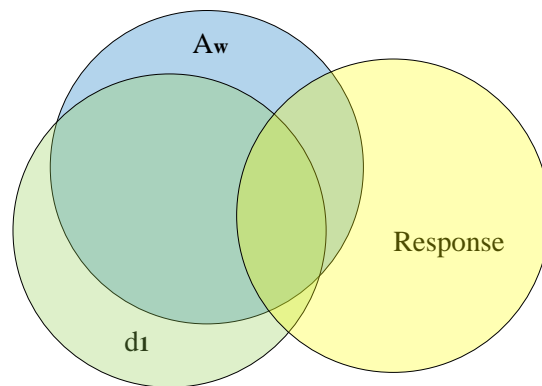


Figure 5.1 d_1 as a redundant factor to A_w

Table 5.7 Combined effect of d_1 and A_w

Response (Criterion): Lg(Cycles to Failure)				
Data Group	Model	R²	Factor	p-value
R-ratio = -1 Failure Mode: WT@DECK Sample Size: 37	d_1 , Lg(Stress Range)	0.3910	d_1	0.03775*
	A_w , Lg(Stress Range)	0.4607	A_w	0.00377*
	d_1 , A_w , Lg(Stress Range)	0.4608	d_1	0.91895
			A_w	0.04655*
R-ratio = 0 Failure Mode: WT@DECK Sample Size: 27	d_1 , h , Lg(Stress Range)	0.9086	d_1	0.00356*
	A_w , h , Lg(Stress Range)	0.9285	A_w	0.00018*
	d_1 , h , A_w , Lg(Stress Range)	0.9293	d_1	0.61499
			A_w	0.01858*

The relationship between d_1 and the weld penetration is more complex. As shown in Table 5.8, the weld penetration alone is barely correlated with fatigue life. However, its significance is drastically enhanced if d_1 is included in the model. The significance level of d_1 is also increased but to a lesser extent. This is a typical indication that d_1 is a suppressor of the weld penetration, meaning that d_1 is highly correlated to the weld penetration in the area that is NOT correlated to the response as illustrated in Figure 5.2. Hence inclusion of d_1 suppresses the portion of variance that is irrelevant to the response from weld penetration and the remaining variance becomes the significant predictor. In a classical suppression situation one of the factors has nearly zero correlation with the response. It only acts as a suppressor to enhance the significance of the other factor on the response, its own correlation to the response cannot be increased by any means. In fact, simple correlation coefficient of the suppressor is often negative. In this case, both factors (d_1 and the weld penetration) act as suppressors and enhance each other's significance levels. This qualifies a cooperative suppression situation where the suppression effect is predominant on the weld penetration. A major part of its irrelevant variance can be suppressed by d_1 . The negative correlation between d_1 and the weld

penetration is also a sign of cooperative suppression (Lewis, 1986).

Table 5.8 Combined effect of d_1 and weld penetration

Response (Criterion): Lg(Cycles to Failure)				
Data Group	Model	R²	Factor	p-value
R-ratio = -1 Failure Mode: WT@DECK Sample Size: 37	d_1 , Lg(Stress Range)	0.3910	d_1	0.03775*
	Weld Penetration, Lg(Stress Range)	0.3156	Weld Penetration	0.52428
	d_1 , Weld Penetration, Lg(Stress Range)	0.4987	d_1	0.00146*
			Weld Penetration	0.01189*
R-ratio = 0 Failure Mode: WT@DECK Sample Size: 27	d_1 , h, Lg(Stress Range)	0.9086	d_1	0.00356*
	Weld Penetration, h, Lg(Stress Range)	0.8667	Weld Penetration	0.96425
	d_1 , Weld Penetration, h, Lg(Stress Range)	0.9278	d_1	0.00028*
			Weld Penetration	0.02427*

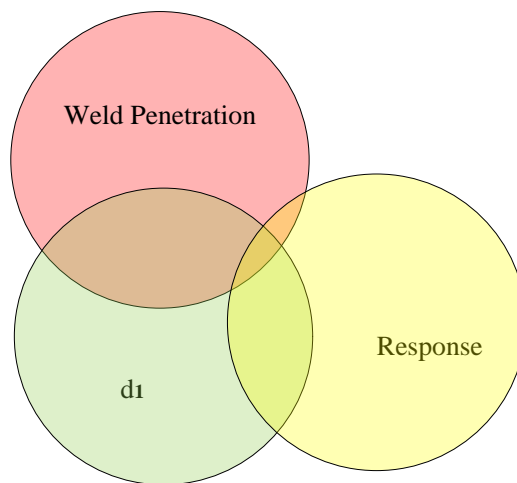


Figure 5.2 Factor d_1 as a suppressor to the weld penetration factor

The redundancy and suppression relationships can be further validated mathematically by the following calculations. Suppose the correlation coefficients between the response y and factor 1, y and factor 2, and between factors 1 and 2, are denoted as r_{y1} , r_{y2} and r_{12} , respectively. According to Lewis (1986), the following conditions need to be satisfied to qualify a redundancy relationship:

$$\begin{aligned} |r_{y1}| &> |r_{y2}| |r_{12}| > 0 \\ |r_{y2}| &> |r_{y1}| |r_{12}| \end{aligned} \quad (\text{Equation 5.1})$$

The resulting effect on the regression coefficients can be expressed as:

$$0 < |\text{Partial}| < |\text{Simple}| \quad (\text{Equation 5.2})$$

The condition for suppression is as the follows:

$$r_{y1}r_{y2}r_{12} < 0 \quad (\text{Equation 5.3})$$

The resulting effect on the regression coefficients can be expressed as:

$$|\text{Simple}| < |\text{Partial}| \quad (\text{Equation 5.4})$$

Knowing the r_{y1} , r_{y2} and r_{12} values from simple linear regression defined as the square root of the regression coefficient R^2 , semi-partial correlation coefficients can be calculated as follows (Pedhazer, 1982):

$$\begin{aligned} r_{y(1,2)} &= \frac{r_{y1} - r_{y2}r_{12}}{\sqrt{1 - r_{12}^2}} \\ r_{y(2,1)} &= \frac{r_{y2} - r_{y1}r_{12}}{\sqrt{1 - r_{12}^2}} \end{aligned} \quad (\text{Equation 5.5})$$

The overall regression coefficient (R^2) is calculated as:

$$R_{y,12}^2 = \frac{r_{y1}^2 + r_{y2}^2 - 2r_{y1}r_{y2}r_{12}}{1 - r_{12}^2} \quad (\text{Equation 5.6})$$

Such calculations were performed on the first and third data groups in Table 5.4 to exclude the effect of stress range, thereby simplifying models as bivariate. The results are tabulated below:

Table 5.9 Redundancy within d_1 (1) and A_w (2)

Data Group	Response (y): Cycles to Failure					
R-ratio = -1 Experimental Stress Range = 36.67 ksi Failure Mode: WT@DECK	R^2_{y1}	R^2_{y2}	R^2_{12}	$R^2_{y(1,2)}$	$R^2_{y(2,1)}$	$R^2_{y,12}$
	0.139767	0.219426	0.488805	0.004203	0.083862	0.223629
	r_{y1}	r_{y2}	r_{12}	$r_{y(1,2)}$	$r_{y(2,1)}$	$R^2_{y(1,2)} + R^2_{y(2,1)}$
	0.373854	0.468429	0.699146	0.064832	0.28959	0.088065
R-ratio = 0 Experimental Stress Range = 33.33 ksi Failure Mode: WT@DECK	R^2_{y1}	R^2_{y2}	R^2_{12}	$R^2_{y(1,2)}$	$R^2_{y(2,1)}$	$R^2_{y,12}$
	0.523656	0.657158	0.568468	0.029294	0.162796	0.686452
	r_{y1}	r_{y2}	r_{12}	$r_{y(1,2)}$	$r_{y(2,1)}$	$R^2_{y(1,2)} + R^2_{y(2,1)}$
	0.723641	0.810653	0.753968	0.171156	0.40348	0.192091

Table 5.10 Cooperative suppression between d_1 (1) and the weld penetration (2)

Data Group	Response (y): Cycles to Failure					
R-ratio = -1 Experimental Stress Range = 36.67 ksi Failure Mode: WT@DECK	R^2_{y1}	R^2_{y2}	R^2_{12}	$R^2_{y(1,2)}$	$R^2_{y(2,1)}$	$R^2_{y,12}$
	0.139767	0.007093	0.126057	0.186533	0.053859	0.193626
	r_{y1}	r_{y2}	r_{12}	$r_{y(1,2)}$	$r_{y(2,1)}$	$R^2_{y(1,2)} + R^2_{y(2,1)}$
	0.373854	0.08422	-0.35505	0.431894	0.232075	0.240392
R-ratio = 0 Experimental Stress Range = 33.33 ksi Failure Mode: WT@DECK	R^2_{y1}	R^2_{y2}	R^2_{12}	$R^2_{y(1,2)}$	$R^2_{y(2,1)}$	$R^2_{y,12}$
	0.523656	0.006951	0.116518	0.640255	0.12355	0.647206
	r_{y1}	r_{y2}	r_{12}	$r_{y(1,2)}$	$r_{y(2,1)}$	$R^2_{y(1,2)} + R^2_{y(2,1)}$
	0.723641	0.083373	-0.34135	0.80016	0.351497	0.763806

Simple calculations from Table 5.9 demonstrate that the redundancy relationships specified by Equation 5.1 are satisfied for both data groups. The semi-partial correlation coefficients ($r_{y(1,2)}$ and $r_{y(2,1)}$) are less than the corresponding simple correlation coefficients (r_{y1} and r_{y2}) defined by Equation 5.2, especially for the d_1 factor. The variance predicted by d_1 and A_w reduces simultaneously by 0.135564 and 0.494362 for the first and second data groups as they combined ($R^2_{y(1,2)} - R^2_{y1}$ or $R^2_{y(2,1)} - R^2_{y2}$). The response variance uniquely predicted by both factors reduces by the same amount ($R^2_{y(1,2)} + R^2_{y(2,1)} - R^2_{y,12}$) as the total correlated variance, indicating the size of the redundant overlap area.

The condition required by Equation 5.3 is valid due to the negative correlation between d_1 and the weld penetration. As shown in Table 5.10, the two semi-partial correlation coefficients are uniformly enhanced for both data groups. The correlation between the weld penetration and number of fatigue cycles is enhanced to a much larger extent indicating that the suppressed irrelevant variance is a greater portion in the weld penetration variance compared to the variance of d_1 (Figure 5.2). Due to the enhancement of semi-partial correlations when the two factors are combined, the sum of the variance correlated with each factor exceeds the overall variance correlated with both factors together:

$$R^2_{y(1,2)} + R^2_{y(2,1)} > R^2_{y(1,2)} + R^2_{y2} = R^2_{y1,2}$$

The weld height (h) factor is also included with high significance level for the specimen group with $R=0$ (Table 5.6) but it has a negative effect on fatigue life when the specimen failed from the weld toe on the deck plate. Stepwise analysis concludes that the significance level of h is not strongly affected by the other factors. Correspondingly, simple linear regressions between the factors show that the weld height is not significantly correlated with any other factors. The weld throat (t) does not present high significance in any models; however, the weld throat is largely correlated with the weld penetration. Therefore, it is anticipated that the weld throat may also exhibit cooperative suppression behavior with the weld toe d_1 if the sample size is large enough.

Linear regressions performed on the weld dimensions to one another further support their

interactions found previously. Among all the interrelationships, weld penetration and weld throat t are positively correlated with the highest R^2 of above 0.65 for both load ratios. Factor d_1 is positively correlated with A_w to a large extent and negatively correlated with weld penetration, implying the redundancy and suppression behavior to those two factors, respectively. Due to the strong positive correlation between weld penetration and throat size t , d_1 is also negatively correlated with t in the case of $R=-1$. It is also found that d_1 and penetration combined can correlate with 80% variance of A_w ($R^2 \approx 0.80$) for both load ratios, explaining similar fitness of the model with d_1 and penetration and the model with A_w .

The interrelationships between weld dimensions can be understood physically as well. Since during the welding process, certain voltage, amp and passing speed are set and maintained for the entire production to achieve the designated penetration percentage; a larger penetration is more likely to leave less welding material out of the rib wall, and vice versa. The weld throat is measured from the weld root to the weld surface. Larger penetration moves the weld root further away from the weld surface thus effectively increases the weld throat (Figure 3.20). Weld area A_w , to a large extent, is determined by the production of d_1 +penetration and weld height h . Therefore d_1 appears to be redundant if A_w is included in the model. The negative effect of weld height h on the fatigue life can be explained by its influence on notch stresses on weld toes. With the same weld toe size, a taller weld creates a sharper corner at the weld toe on the deck plate thus increases the notch stress. The fatigue life is therefore reduced. A smaller weld height however intensifies the notch effect on the other weld toe on the rib plate. It is expected that the fatigue life is positively correlated with the weld height h but negatively correlated with the weld toe size d_1 for the failures occurring at the other weld toe on the rib plate. The relationships among individual weld dimensions can be illustrated as Figure 5.3.

With the knowledge of the interactions between factors, models from stepwise analysis listed in Table 5.6 are selected and analyzed. The reports are attached in Appendix N and Appendix O.

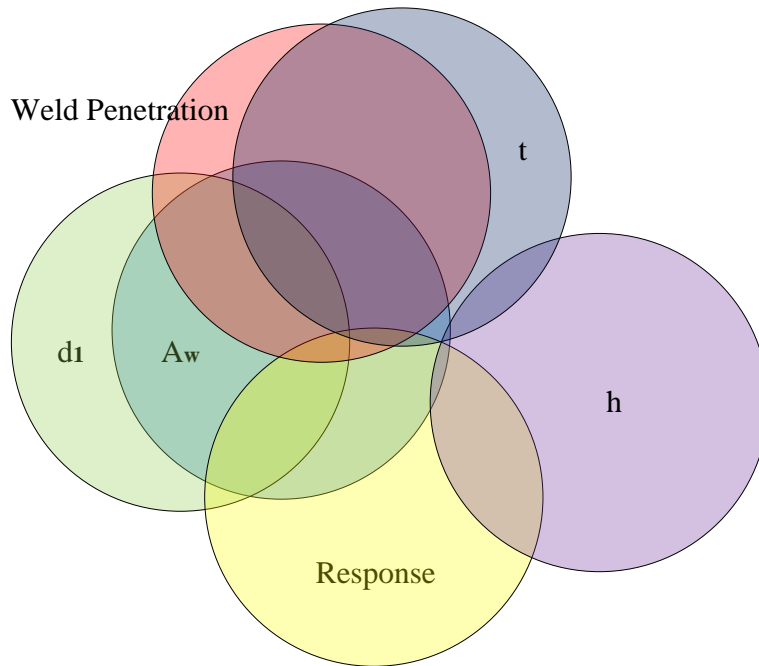


Figure 5.3 Interactions among weld dimensions on predicting the fatigue life

Statistical significance of weld dimensions to the fatigue life is not well presented in MLR analyses for the other two failure modes, WT@RIB and WR, due to smaller sample sizes. For the latter only the weld height h has a p -value lower than 0.05 that can be regarded as statistically significant, with a negative correlation with the fatigue life. The model with the highest overall fit is thus analyzed in detail, see Appendix Q. For the failures occurring at the weld toe on the rib wall, similar effects from factors are found as the failure mode on the deck plate, but with much less significance level (p -values > 0.05) due to smaller sample size. One noticeable difference is that in this case the weld height h is positively correlated with the fatigue life but the weld toe size d_1 is negatively correlated (Appendix P). This is another demonstration that the weld toe sizes on both plates (d_1 & h) influence the fatigue life by affecting the notch stresses on weld toes, as described in the paragraph above.

5.1.5 Summary and Recommendations

The MLR analyses reveal the influential weld dimensions on the fatigue life, as well as their correlations and interactions to one another. It is observed that the weld area A_w affects the fatigue life positively to a large extent with R^2 ranging from 0.3 to 0.68. The

weld toe sizes on the deck and rib plate, d_1 and h , also statistically significant enough to influence the fatigue life, with positive effect on the local weld toe but negative effect on the other weld toe. The weld penetration is significant to the fatigue life only when the weld toe is included in the statistical model as a suppressor, which implies that the weld penetration is not individually correlated to the fatigue life. For the failures that occur at weld roots, the weld height seems to be a relevant factor that is negatively correlated with the fatigue life, however a larger sample size is helpful to reinforce this observation.

To quantify the effects from the factors so that proper limits could be set to the weld dimensions to achieve an optimal fatigue performance, another MLR model is built from stepwise analysis with the effect of stress range leveled out, by including the stress range in the model with a fixed slope of -3, according to AASHTO. The model is built based on the samples with $R=0$ and failure mode of WT@DECK since it is considered to be the worst scenario with full tensile stress range. The idea for the optimization of the weld is making sure the lower bound of the samples is above the current code-specified S-N curve— AASHTO C Curve, DNV D-Curve or IIW FAT-90 Curve.

The model with the best fit in this case includes weld toe size d_1 , weld throat t and weld height h . Assume their regression coefficients are denoted as β_1 , β_2 and β_3 ; the stress range is denoted as σ , the lower bound of the model can be expressed as:

$$\text{Lg(Cycles)} = \beta_1 d_1 + \beta_2 t + \beta_3 h - 3\text{Lg}(\sigma) + \text{Intercept} - 2 \times \text{RMSE} \quad (\text{Equation 5.7})$$

The AASHTO C-Curve follows the equation of:

$$\text{Lg(Cycles)} = 9.643 - 3\text{Lg}(\sigma) \quad (\text{Equation 5.8})$$

The lower bound curve should be above the AASHTO C-Curve, therefore:

$$\beta_1 d_1 + \beta_2 t + \beta_3 h + \text{Intercept} - 2 \times \text{RMSE} \geq 9.643 \quad (\text{Equation 5.9})$$

The combined effect of d_1 , t and h needs to satisfy (Equation 5.9) to maintain the fatigue performance above the AASHTO C-Curve. (Equation 5.9) is calculated for a range of values as listed in Table 5.11. The weld throat values are calculated from the weld

penetration because they are strongly correlated with each other. As shown d_1 and h increase/decrease simultaneously since they have opposite effects in (Equation 5.9). The satisfactory weld dimensions are not exclusive but can be optimized considering the typical penetration and the limit for weld area A_w . A distribution analysis shows that the penetration of the welds among these samples has a mean value of 66.6% and a lower bound of 50.4%, including fillet welds which do not target for a specific penetration but typically reach about 60%. The weld area A_w in this case is again correlated with the fatigue life, from where a value of 0.09063 in^2 is derived in order to maintain the lower bound above C-Curve. Since A_w is highly correlated d_1 , simple linear regression between them suggests a d_1 value of $0.2181''$ corresponding to the minimum weld area requirement. Considering the worst scenario of 50% penetration, this leads to an almost equal weld height of $0.22''$ from Table 5.11, about 70% of the rib thickness.

The weld penetration does not affect the fatigue life as long as failures are not from weld roots. In this sense a certain target penetration is not required thus fillet welds can be directly applied without compromising the fatigue performance of the weld toes, so has the tests proven. However, larger penetrations increases the possibility of the presence of a root gap therefore raise the risk of cracking from the weld root. From the observation to the specimens, it is found, however, almost all specimens did not present an open root gap. It is believed that the shrinkage of the welding material during the cooling process pulled the gap closed. As the test results shows, only one out of 68 closed-gap specimens failed from the weld root; and all the other 14 specimens that failed from weld roots had open root gaps. It is very important to have closed gaps to avoid root failures. However, because full penetration is not achievable for rib-to-deck welds, a small initial gap size and sufficient welding material are preferred to close the root gap by the shrinkage. Since the specimens with closed gaps have average penetrations of 66.6%, it is recommended to require the weld penetration not less than 70% in the fabrication, which reduces the probability of getting a melt-through defect, as well as ensures closed root gaps. An initial gap size of less than $0.02''$ is also recommended to further help achieve closed gaps.

Table 5.11 Minimum Dimensions for d_1 (in)

Weld Penetration	0	0.1	0.2	0.3	0.4	0.5	0.6	0.7	0.8	0.9	1
h \ t	0.0605	0.0982	0.1359	0.1736	0.2113	0.2490	0.2866	0.3243	0.3620	0.3997	0.4374
0	0.3502	0.2790	0.2078	0.1367	0.0655	-0.0057	-0.0768	-0.1480	-0.2192	-0.2903	-0.3615
0.02	0.3714	0.3002	0.2290	0.1579	0.0867	0.0155	-0.0556	-0.1268	-0.1979	-0.2691	-0.3403
0.04	0.3926	0.3214	0.2502	0.1791	0.1079	0.0368	-0.0344	-0.1056	-0.1767	-0.2479	-0.3191
0.06	0.4138	0.3426	0.2715	0.2003	0.1291	0.0580	-0.0132	-0.0844	-0.1555	-0.2267	-0.2979
0.08	0.4350	0.3638	0.2927	0.2215	0.1503	0.0792	0.0080	-0.0632	-0.1343	-0.2055	-0.2767
0.1	0.4562	0.3850	0.3139	0.2427	0.1715	0.1004	0.0292	-0.0420	-0.1131	-0.1843	-0.2555
0.12	0.4774	0.4062	0.3351	0.2639	0.1927	0.1216	0.0504	-0.0208	-0.0919	-0.1631	-0.2342
0.14	0.4986	0.4274	0.3563	0.2851	0.2140	0.1428	0.0716	0.0005	-0.0707	-0.1419	-0.2130
0.16	0.5198	0.4487	0.3775	0.3063	0.2352	0.1640	0.0928	0.0217	-0.0495	-0.1207	-0.1918
0.18	0.5410	0.4699	0.3987	0.3275	0.2564	0.1852	0.1140	0.0429	-0.0283	-0.0995	-0.1706
0.2	0.5622	0.4911	0.4199	0.3487	0.2776	0.2064	0.1352	0.0641	-0.0071	-0.0783	-0.1494
0.22	0.5834	0.5123	0.4411	0.3699	0.2988	0.2276	0.1564	0.0853	0.0141	-0.0570	-0.1282
0.24	0.6046	0.5335	0.4623	0.3911	0.3200	0.2488	0.1777	0.1065	0.0353	-0.0358	-0.1070

Weld Penetration	0	0.1	0.2	0.3	0.4	0.5	0.6	0.7	0.8	0.9	1
h / t	0.0605	0.0982	0.1359	0.1736	0.2113	0.2490	0.2866	0.3243	0.3620	0.3997	0.4374
0.26	0.6259	0.5547	0.4835	0.4124	0.3412	0.2700	0.1989	0.1277	0.0565	-0.0146	-0.0858
0.28	0.6471	0.5759	0.5047	0.4336	0.3624	0.2912	0.2201	0.1489	0.0777	0.0066	-0.0646
0.3	0.6683	0.5971	0.5259	0.4548	0.3836	0.3124	0.2413	0.1701	0.0989	0.0278	-0.0434
0.32	0.6895	0.6183	0.5471	0.4760	0.4048	0.3336	0.2625	0.1913	0.1201	0.0490	-0.0222
0.34	0.7107	0.6395	0.5683	0.4972	0.4260	0.3549	0.2837	0.2125	0.1414	0.0702	-0.0010
0.36	0.7319	0.6607	0.5896	0.5184	0.4472	0.3761	0.3049	0.2337	0.1626	0.0914	0.0202
0.38	0.7531	0.6819	0.6108	0.5396	0.4684	0.3973	0.3261	0.2549	0.1838	0.1126	0.0414
0.4	0.7743	0.7031	0.6320	0.5608	0.4896	0.4185	0.3473	0.2761	0.2050	0.1338	0.0626

5.2 Multi-way ANCOVA

From the preliminary analysis it is shown that factors of the failure mode and R ratio are significant to the fatigue life. To confirm this conclusion, as well as to discover potential influential factors that were not found before, other ANCOVA analyses are conducted more in depth.

As suggested by the preliminary ANCOVA summarized in Table 5.3, the failure mode and R-ratio were significant to the fatigue life. None of the weld dimensions were effective since they were entered in the model altogether. Therefore two other ANCOVA analyses are performed to confirm the effects of test scenarios and to isolate the significant weld dimensions.

The first ANCOVA has four categorical factors: specimen series, failure mode, root gap openness and R-ratio, with only Lg(stress range) as the covariant. The analysis resulted in similar findings as in the preliminary analysis, as summarized in Table 5.12. Further analyses show that the model with only factors of failure mode and R-ratio has an improved model fit; the model with factors of specimen series and root gap exhibits a lack of fit. Therefore these two factors are not included in the following analyses.

Table 5.12 Summary of Model Fitting — Fatigue Test Scenarios

Response (Dependent Variable)	Overall Model Fitness	
Lg (Cycles to Failure)	R ² =0.62622	R ² (Adjusted)=0.56623
Factors (Independent Variables)	p-value	Power
Specimen Series	0.0667	0.7428
Failure Mode	<0.0001*	0.9987
Root Gap	0.4323	0.1221
R-ratio	<0.0001*	0.9999
Lg (SHS-0515 Extrapolation)	0.0001*	0.9837

The second ANCOVA further investigates the effects of fatigue test scenarios with the weld dimensions taken into account, to build the model with the highest fit and interactions of significant factors. The stepwise analysis shows that the best model includes weld toe size d_1 , weld throat t and weld height h , besides the failure mode and R-ratio, as summarized in Table 5.13. The model fitting report can be found in Appendix R. As shown below, similar weld dimensions are again attributed to the variance of fatigue life. According to the model fitting report, fatigue failures occurred the weld roots have noticeably shorter fatigue lives than failures occurred at weld toes since nominal stress is calculated for weld roots. Failures occurred at both weld toes have statistically the same fatigue resistance. Specimens tested under $R=0$ have the lowest fatigue resistance with a lower bound S-N curve right above AASHTO Category C. No root failure is found in this test scenario since the weld root undergoes reverse stress state as weld toes. All test results are re-grouped into four categories considering failure modes and R-ratios, the average and lower bound S-N curves are shown in Figure 5.4 and 5.5. Note that the specimens failed at two weld toes with $R=-1$ actually follow the same S-N curve, indicated by their individual curves very close to each other. The majority of specimens under $R=0$ failed at WT@DECK with only one exception of WT@RIB; therefore their S-N curves are plotted jointly as the one labeled as $R=0$.

Table 5.13 Summary of Model Fitting — All Significant Factors

Response (Dependent Variable)	Overall Model Fitness	
Lg (Cycles to Failure)	$R^2=0.630118$	R^2 (Adjusted)=0.595711
Factors (Independent Variables)	p-value	Power
Weld Toe Size d_1	0.0035*	0.8425
Weld Throat t	0.0007*	0.9378
Weld Height h	0.0416*	0.5342
Failure Mode	<0.0001*	1.0000
R-ratio	<0.0001*	1.0000
Lg (SHS-0515 Extrapolation)	<0.0001*	0.9920

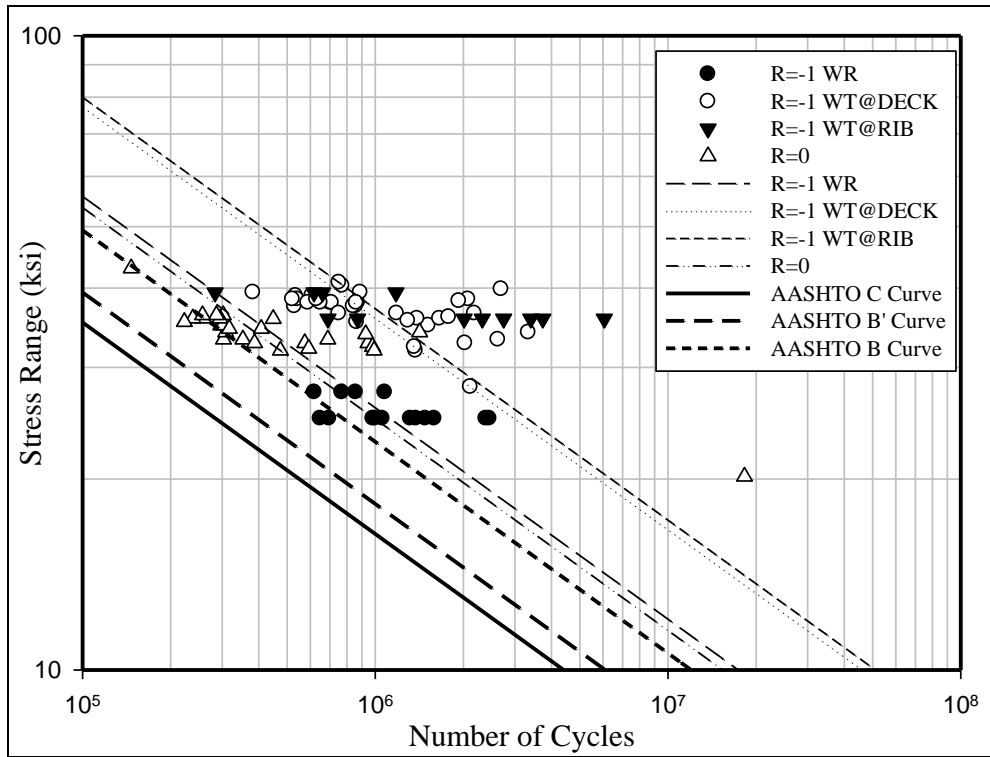


Figure 5.4 Mean S-N curves for all specimens

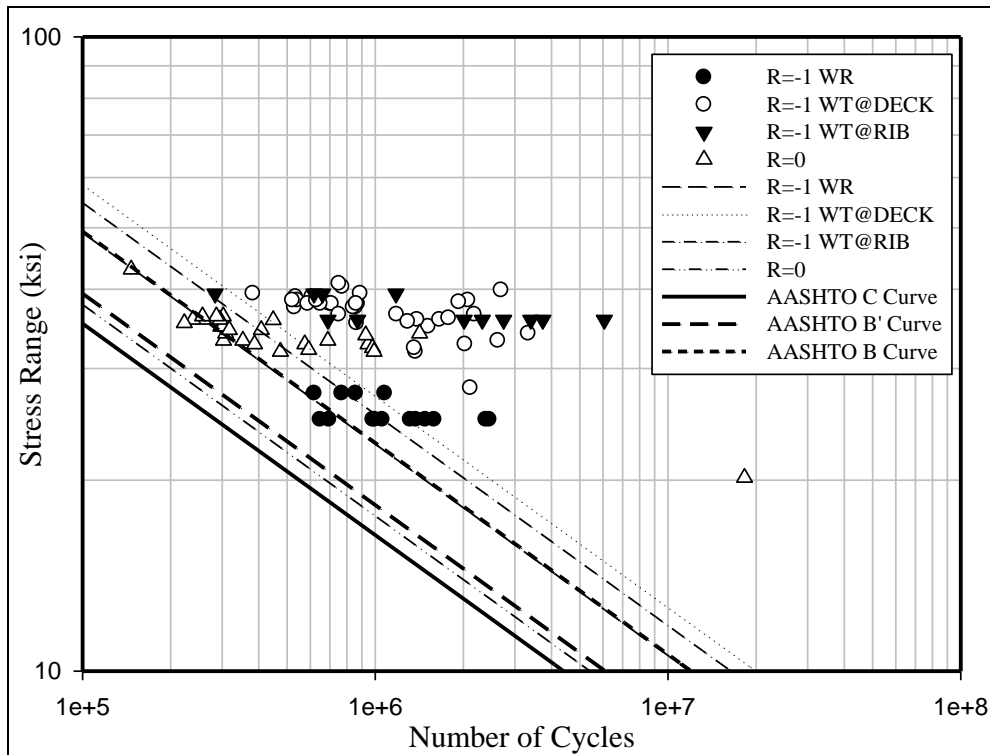


Figure 5.5 Lower bound S-N curves for all specimens

As shown Figure 5.4 all the mean curves fall way above the AASHTO C Curve however the lower bound curve for the worst scenario (R=0) falls above AASHTO C Curve but below AASHTO B' Curve. Considering full tensile stress cycle is not a rare event during the life time of a bridge, AASHTO C Curve should be used in engineering design for rib-to-deck welds to guarantee a 95% probability of survival. This corresponds to the DNV and IIW recommendations, where DNV D Curve and IIW FAT-90 Curve are proposed. The comparison is shown in Figure 5.6. Thickness correction is performed for DNV D Curve. As can be seen, three proposed curves are essentially the same.

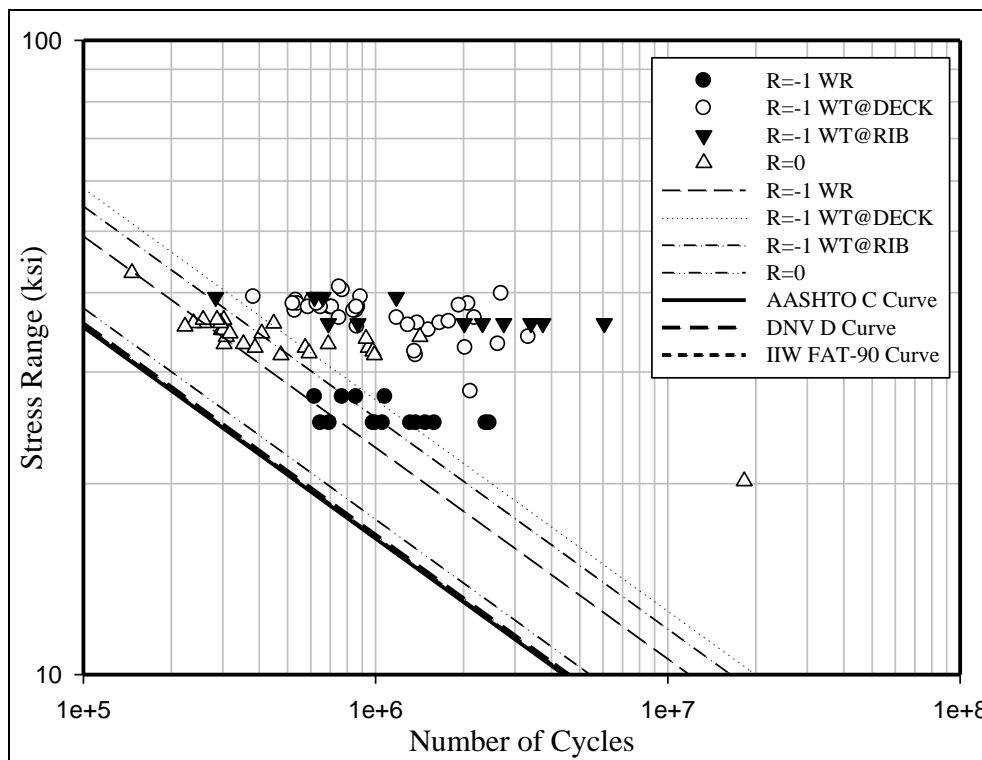


Figure 5.6 Lower bound S-N curves in comparison with proposed curves

By obtaining the mean S-N curves for both R ratios, it is possible to estimate the level of residual stress involved in the tests under R=-1 by comparing the two mean curves, regarding the curve for R=0 as unbiased. Most of the specimens with R=-1 are tested under 36.67 ksi, corresponding to a fatigue life of 1172373 cycles on the mean curve for R=-1. However, this amount of fatigue cycles are in fact caused by a stress range of 25.094 ksi, according to the mean curve for R=0. This leads to the residual stress as $25.094 - 36.67/2 = 6.761$ ksi.

Chapter 6. Conclusions and Recommendations

6.1 Summary

This research performed in Virginia Tech aimed to provide recommendations on both design and detailing levels concerning the fatigue issues of rib-to-deck welds on steel orthotropic decks. For this purpose the effects of different test scenarios and weld dimensions were studied theoretically, experimentally and statistically, in order to propose the proper S-N curve as the reference for design, as well as to optimize the shape and size of the welds.

To establish S-N curves for this structural detail under different test scenarios, both fatigue cycles and the stress state at the potential crack locations needed to be evaluated. By fatigue testing 95 specimens with rib-to-deck welds produced by three different types of welding processes across seven specimen series with different target weld penetrations, the fatigue cycles were recorded under different load ratios and root gap conditions. To study the stress state at the fatigue critical locations, a method called hot-spot stress analysis was applied, which evaluated all weld toes altogether by using a single S-N curve. Finite element modeling was employed to derive the hot-spot stresses at weld toes. Since the method is currently only limited to weld toes, traditional nominal stresses calculated from first-order elastic structural analysis were still used for weld roots. Notch stresses were also calculated using fictitious rounding method to study the effect of the presence of an open root gap.

From the fatigue tests three failure modes were found: fatigue cracks at the weld toe into the deck plate (WT@DECK), at the weld toe into the rib wall (WT@RIB) and from the weld root through the weld (WR). Only the first failure mode presented in the first stage of the tests conducted in TFHRC but all three failure modes were found in the tests performed in VT. The presence of the second failure mode was attributed to the different sizes of the bearing plates involved. Since the bearing plates used in VT were narrower (3.75") than the ones used in TFHRC (5"), more bending effect was induced which raised the stress range at the weld toe on the rib plate, so has demonstrated by FE analysis.

Fatigue cracks from weld roots were attributed to the presence of open root gaps. Strong correlation between the root gap condition and the third failure mode was shown from the test results that suggested the open gaps directly caused fatigue cracks to occur from weld roots. Similar findings were also obtained from notch stress analysis that showed a stress range increase at the inner tip of the open root gap.

To investigate the effect of different weld dimensions on the fatigue resistance for detailing requirements, statistical analysis was adopted under the circumstance without any available theoretical equations. Multiple linear regression (MLR) analyses were performed for this purpose accounting for the possible interactions among individual dimensions. The findings were then explained physically from a structural point of view. Recommendations were made regarding to the detailing requirements. Another statistical analysis, multi-way analysis of covariance (ANCOVA) was also performed to investigate the effect of parameters involved in fatigue tests such as the specimen series, failure mode, load ratio, and root gap condition. This analysis resulted in re-categorizing test data based on their failure modes and R-ratios so that the worst case could be found and the lower bound S-N curve could be established.

6.2 Conclusions and Recommendations

The validity of hot-spot stress analysis for weld toes has been demonstrated by its corresponding S-N curve being consistent with the proposed curves (AASHTO C, DNV D and IIW FAT-90) as shown in Figure 5.6. It is found through the finite element analysis, though, that LSE method generally exhibited a higher mesh-sensitivity than TTWT method. The first element in front of the weld toe is recommended to be limited out of the region of read-out points since the stress prediction within that element is heavily affected by the notch effect. A transition region between the first read-out point and the weld toe is very helpful to capture a better stress peak, but in any case the notch stress should be calculated with more elaborate methods, for example, the fictitious rounding method.

Certain requirements are recommended for the detailing of the weld dimensions. Although it is very difficult to completely isolate one dimension from the others due to

the correlations among them, it was found that generally the weld toe sizes of both weld toes are significant to the fatigue resistance of the weld. The weld toe size positively affects the fatigue resistance of the local weld toe but negatively on the other weld toe. Both toe sizes need to be increase/decrease simultaneously to ensure balanced fatigue resistance on both weld toes. The weld area is also significant to the fatigue performance and is referred to set the lower limits of toe sizes. In other words, comparable toe sizes need to be maintained (i.e., one toe should not be excessively larger than the other); also both weld toes should be large enough to make sure the weld area is sufficient, so that the lower bound curve can be guaranteed above AASHTO C Curve. Through statistical calculations, it is recommended that both toes should be not less than 0.7 times of the rib plate thickness.

Weld penetration is found to be generally not related to the fatigue performance of the weld toes, which are the primary cracking locations. However, excessive lack of penetration may leave a large initial root gap that is difficult to be pulled closed by the weld shrinkage during the cooling process. It is found in the test results that open root gaps directly caused fatigue cracks occurring from weld roots. Since the design philosophy is to completely eliminate root failures due to its inaccessibility for inspection and catastrophic consequences, all root gaps should be closed. From the measurements of the tested specimens, it is found that with an average of 66.6% penetration, all the root gaps were closed by the shrinkage unless the root gap was intended to be made open (OB series and saw-cut specimens). Therefore a penetration of not less than 70% and an initial gap size of not more than 0.02" are recommended to close the root gaps during the cooling process.

Failure modes and R-ratios are found to be influential to the fatigue performance. Among the three failure modes, the one at weld roots has lower fatigue resistance while the other two at weld toes have statistically the same fatigue resistance. Specimens tested under $R=0$ have much lower fatigue resistance than the ones tested under $R=-1$. This is attributed to that the residual stress is not high enough to offset the entire compressive stress cycle into tensile for the case of $R=-1$. By comparing the two mean S-N curves corresponding to $R=0$ and $R=-1$, the residual stress is calculated as 6.761 ksi for the

specimens tested under 36.67 ksi experimental stress range with $R=-1$.

The specimens that failed from weld toes with $R=0$ appear to be the worst scenario with the lowest S-N curve. The lower bound curve with a 95% possibility of survival for this scenario falls above AASHTO C Curve but below B' Curve, so as found by other researchers. Considering full tensile stress cycle is likely to happen during the lifetime of a bridge, AASHTO C curve is recommended for the fatigue design of rib-to-deck welds.

6.3 Future Research

Currently the hot-spot stress method is limited to weld toes only. The reason is that the hot-spot stress method assumes the disparity between the predicted structural stress and the actual stress is uniform throughout all weld toes. Hence the fatigue resistance for all weld toes follows the same S-N curve. However this assumption no longer holds for weld roots since the notch effect is much more severe thus it follows a different S-N curve; especially for open root gaps since it creates a crack-like defect, whose fatigue resistance highly depends on the local geometry thus difficult to be captured by a single S-N curve. A more comprehensive methodology to determine the stress range including for weld roots is needed to be developed so that a unified S-N curve can be achieved. In this study such method is not available so conservatism is involved that the root gap is required to be closed to prevent any root failures.

It is observed in the test results that specimens failed at weld toes under full tensile stress range ($R=0$) have the lowest fatigue resistance. Specimens failed at weld roots have a lower S-N curve than the ones failed at weld toes with $R=-1$; but failures at weld roots were not found under $R=0$ since the weld root in this case experienced full compressive stress cycles (ignoring the residual stress). The fatigue performance for the weld root under more severe circumstances is not investigated. Nevertheless, root failures are aimed to be completely avoided by following the recommended detailing requirements.

It is concluded that the R-ratio has a significant effect on the fatigue resistance, while only two R-ratios are involved in the tests. It is possible to obtain more realistic R-ratio values for actual bridges by long-term monitoring or extensive full-scale bridge modeling

so that design requirements can be improved accordingly. Before acquiring this information, the design curve is recommended as AASHTO C to account for the worst scenario ($R=0$). The residual stress calculation can also be improved by including a range of different R-ratios.

An initial tight fit for the weld root is preferred to help eliminate root gaps after the weld fabrication. However zero initial gap size raises very high requirement to the straightness of the rib edge and flatness of the deck plate and is often very difficult to achieve. It is observed in the specimens that all the root gaps are closed by the shrinkage of the weld with the presented weld toe size, penetration and initial gap size of 0.02", which is claimed by the fabricator to be achievable. Such requirements are then recommended accordingly. However, further research is appreciated on this matter including welds from different fabricators, or finite element modeling accounting for the heat transfer and shrinkage during the cooling process; so that requirements for sizes of the weld and the initial gap can be established with higher rationality.

References

“Bronx-Whitestone Bridge Rehabilitation (tie).”

<http://newyork.construction.com/projects/TopProjects06-07/TPComplete16-20.pdf>

“Williamsburg Bridge Rehabilitation Contract 8— 100-year-old Steel Bridge Ready for 100 Years More.” <http://www.siny.org/media/projects/wbrc8.pdf>

American Association of State Highway and Transportation Officials (AASHTO), (2007). “AASHTO LRFD Bridge Design Specifications.” American Association of State Highway and Transportation Officials. Washington, D.C.

Anderson, T.L. (1994). “Fracture mechanics—fundamentals and applications.” Second Edition, CRC Press, 1994.

Burdekin, F.M. (1981). “Fatigue cracks in some steel bridges.” Proceedings International Conference on: Gestion des Ouvrages d’Art, Inspection, Maintenance and Repair of Road and Railway Bridges, pp. 163-167, Paris, France

Connor, R.J. and Fisher, J.W., (2000). “In-service response of an orthotropic steel deck compared with design assumptions.” 5th International Bridge Engineering Conference, Theme: Performance Based Design and Long-Span Bridges, pp. 100-108.

Dijkstra, O. D. and de Back, J. (1980). “Fatigue Strength of Welded Tubular T- and X-Joints.” Proceedings Offshore Technology Conference (OTC 3639). Houston.

DNV (1984). “Fatigue Strength Analysis for Mobile Offshore Units.” CN 30-2. Det Norske Veritas, Høvik, Norway. August, 1984.

DNV (2006). “Fatigue Methodology of Offshore Ships.” DNV-RP-C206. Det Norske Veritas, Høvik, Norway. October, 2006.

DNV (2008). “Fatigue Assessment of Ship Structures.” CN 30-7. Det Norske Veritas, Høvik, Norway. October, 2008.

DNV (2005). "Fatigue Design of Offshore Steel Structures." DNV-RP-C203. Det Norske Veritas, Høvik, Norway. 2005.

DNV (2008). "Fatigue Design of Offshore Steel Structures." DNV-RP-C203. Det Norske Veritas, Høvik, Norway. April, 2008.

Doerk, O. (2003). "Comparison of Different Calculation Methods for Structural Stresses at Welded Joints." International Journal of Fatigue. Vol. 25(5): pp. 359-369.

Dong, P. (2001a). "A Structural Stress Definition and Numerical Implementation for Fatigue Analysis of Welded Joints." International Journal of Fatigue. Vol. 23(10): pp. 865-876.

Dong, P., Hong, J. K., et al. (2001b). "A Mesh-Insensitivity Structural Stress Procedure for Fatigue Evaluation of Welded Structures." IIW Doc. XIII-1902-01 / XV-1089-01. International Institute of Welding.

Dong, P., Hong, J. K., et al. (2004). "Master S-N Curve Development and Validations for Aluminium MIG and Laser Welds." IIW Doc. XIII-2035-04 / XV-1172-04. International Institute of Welding.

Dong, P., Hong, J. K., et al. (2007). "Analysis of Recent Fatigue Data Using the Structural Stress Procedure in ASME Div 2 Rewrite." Journal of Pressure Vessel Technology. Vol. 129: pp. 355-362.

ENV 1991-3 (1995) "Eurocode 1 – Basis of design and actions on structures – Part 3: Traffic loads on bridges", European Committee for Standardization, Brussels, Belgium

ENV 1993-1-9 (2005) "Eurocode 3: Design of steel structures – Part 1-9: Fatigue", European Committee for Standardization, Brussels, Belgium

Fricke, W. (2001a). "Recommended Hot Spot Analysis Procedure for Structural Details of FPSOs and Ships Based on Round-Robin FE Analyses." Proceedings of the Eleventh (2001) International Offshore and Polar Engineering Conference. Stavanger, Norway. The International Society of Offshore and Polar Engineers: pp. 89-96.

Fricke, W. and Bogdan, R. (2001b). "Determination of Hot Spot Stress in Structural Members with in-Plane Notches Using a Coarse Element Mesh." IIW Doc. XIII-1870-01. International Institute of Welding.

Fricke, W. (2003). "Fatigue Analysis of Welded Joints: State of Development." Marine Structures. Vol. 16(3): pp. 185-200.

Fricke, W. and Kahl, A. (2005). "Comparison of Different Structural Stress Approaches for Fatigue Assessment of Welded Ship Structures." Marine Structures. Vol. 18(7-8): pp. 473-488.

Fricke, W. (2006). "Round-Robin Study on Stress Analysis for the Effective Notch Stress Approach." IIW Doc. XIII-2129-06 / XV-1223-06. International Institute of Welding (German Delegation).

Fricke, W. and Kahl, A. (2007). "Local Stress Analysis and Fatigue Assessment of Bracket Toes Based on Measured Weld Profile." IIW Doc. XIII-2166-07 / XV-1253-07. International Institute of Welding (German Delegation), Hamburg, Germany.

Fricke, W. (2008). "Guideline for the Fatigue Assessment by Notch Stress Analysis for Welded Structures." IIW-Doc. XIII-2240-08/XV-1289-08. International Institute of Welding (German Delegation), June, 2008.

Griffith, A.A. (1920) "The phenomena of rupture and flow in solids." Philosophical Transactions, Series A, Vol. 221, 1920, pp. 163-198.

Gurney, T. R. (1979). "An Analysis of Some Fatigue Crack Propagation Data for Steels Subjected to Pulsating Tension Loading." Welding Research Institute. Vol. 9(4): pp. 45-52.

Gurney, T.R., Maddox, S.J. (1987) "Fatigue tests on joints in orthotropic decks", Proceedings International Conference on Welded Structures, P64/1-20, Cambridge, United Kingdom

Gurney, T. R. (1991). "The Fatigue Strength of Transverse Fillet Welded Joints."

Cambridge. Abington Publishing.

Gurney, T. (2006). "Cumulative Damage of Welded Joints." Cambridge. Woodhead Publishing.

Haibach, E., De Back, J., Bruls, A., Carracilli, J., Jacob, B., Kolstein, M.H., Page, J., Pfeifer, M.R., Sanpaolesi, I., Tilly, G., Zachel, J.M. (1991), "Measurements and interpretation of dynamic loads on bridges", report EUR 9759, Brussels, Belgium

Hill, T., Lewicki, P. (2007). "STATISTICS Methods and Applications." StatSoft. Tulsa, OK.

Hobbacher, A. (2008) "Recommendations for fatigue design of welded joints and components", IIW document IIW-1823-07, International Institute of Welding.

Hobbacher, A. (2009). "The New IIW Recommendations for Fatigue Assessment of Welded Joints and Components – A Comprehensive Code Recently Updated." International Journal of Fatigue. Vol. 31(1): pp. 50-58.

Illowsky, B., Dean, S. (2010). "Collaborative Statistics." Houston, Texas.
<http://cnx.org/content/col10522/1.38/>

Irwin, G.R., (1948) "Fracture dynamics." Fracturing of Metals, American Society for Metals, Cleveland, 1948, pp. 147-166.

Irwin, G.R., (1957) "Analysis of stresses and strains near the end of a crack traversing a plate." Journal of Applied Mechanics, Vol. 24, 1957, pp. 361-364.

Janss, J. (1988), "Fatigue of welds in orthotropic bridge deck panels with trapezoidal stiffeners", Journal of Constructional Steel Research 9, pp. 147-154

Kang, H., Dong, P., et al. (2007). "Fatigue Analysis of Spot Welds Using a Mesh-Insensitive Structural Stress Approach." International Journal of Fatigue. Vol. 29(8): pp. 1546-1553.

Kolstein, M.H. (2007). "Fatigue Classification of Welded Joints in Orthotropic Steel

Bridge Decks”. Ph.D. Dissertation. Delft University of Technology. The Netherlands. ISBN 978-90-9021933-2.

Leendertz, J.S., Jong de, F.B.P. (2003) “Fatigue aspects of orthotropic steel decks”, Proceedings Lightweight Bridge Decks, COBRAE, pp. 1-13, Leusden, The Netherlands

Lewis, J.W., Escobar, L.A. (1986). “Suppression and Enhancement in Bivariate Regression”. The Statistician, Vol. 35, No. 1. (1986), pp. 17-26.

Lotsberg, I. (2001). “Overview of the FPSO-Fatigue Capacity JIP.” 20th International Conference on Offshore Mechanics and Arctic Engineering. Rio de Janeiro, Brazil. Proceedings of OMAE 2001.

Lotsberg, I. and Sigurdsson, G. (2006). “Hot Spot Stress S-N Curve for Fatigue Analysis of Plated Structures.” Journal of Offshore Mechanics and Arctic Engineering. Vol. 128(4): pp. 330-336.

Maddox, S.J. (1974a) “Fatigue of welded joints loaded in bending”, Supplementary Report 84UC, Transport and Road Research Laboratory, Structures Department, Bridges Division, Crowthorne, Berkshire, United Kingdom

Maddox, S.J. (1974b). “The fatigue behaviour of trapezoidal stiffener to deck plate welds in orthotropic bridge decks”, Supplementary Report 96UC, Transport and Road Research Laboratory, Structures Department, Bridges Division, Crowthorne, Berkshire, United Kingdom

Maddox, S. J. (1991). "Fatigue Strength of Welded Structures." Cambridge. Abington Publishing.

Maddox, S.J. (2001) “Recommended hot-spot stress design S-N curves for fatigue assessment of FPSOs”, Proceedings of the Eleventh International Offshore and polar Engineering Conference, pp. 97-104, Stavanger, Norway

Mehue, P. (1981) “Steel decks in road bridges”, Proceedings International Conference on: “Gestion des ouvrages d’art”, Inspection, Maintenance and Repair of Road and

Railway Bridges, pp. 609-612, Bruxelles, Belgium, Paris, France.

Mehue, P. (1990) "Cracks in steel orthotropic decks", Proceedings International Conference on Bridge Management, pp. 633-642, Surrey, United Kingdom.

Mehue, P. (1992) "Repair procedures for cracks in steel orthotropic decks", Proceedings 3rd International Workshop on Bridge Rehabilitation, pp. 159-163, Darmstadt, Germany.

Mori, T. (2009). "Assessment of Fatigue Strength of Cruciform Welded Joints Failing from Weld Roots under Out-of-Plane Bending." IIW Doc. XIII- 2287-09. International Institute of Welding (Japanese Delegation).

MTS Systems Corporation. "MTS Landmark Testing Solutions."
http://www.mts.com/ucm/groups/public/documents/library/dev_004324.pdf

Niemi, E. (1995a). "Recommendations Concerning Stress Determination for Fatigue Analysis of Welded Components." Cambridge. Abington Publishing.

Niemi, E. (1995b). "Stress Determination for Fatigue Analyses of Welded Components." IIW Doc. XIII-1221-93. International Institute of Welding, Cambridge, UK.

Niemi, E., Fricke, W., et al. (2001). "Structural Stress Approach to Fatigue Analysis of Welded Components--Designer's Guide." IIW Doc. XIII-1819-00/XV-1090-01. International Institute of Welding, Paris.

Niemi, E. and Marquis, G. (2002). "Introduction to the Structural Stress Approach to Fatigue Analysis of Plate Structures." Proceeding of The IIW Fatigue Seminar. IIW-Commission XIII: pp. 73-90.

Paris, P.C. and Erdogan, F., (1960) "A critical analysis of crack propagation laws." Journal of Basic Engineering, Vol. 85, 1960, pp. 528-534.

Paris, P.C., Gomez, M.P. and Anderson, W.P., (1961) A rational analytic theory of fatigue." The Trend in Engineering, Vol. 13, 1961, pp. 9-14.

Partanen, T. and Niemi, E. (1996). "Hot Spot Stress Approach to Fatigue Strength

Analysis of Welded Components: Fatigue Test Data for Steel Plate Thickness up to 10 mm.” *Fatigue & Fracture of Engineering Materials & Structures*. Vol. 19(6): pp. 709-722.

Pedersen, M. M., Mouritsen, O. Ø., et al. (2010). “Re-Analysis of Fatigue Data for Welded Joints Using the Notch Stress Approach.” *International Journal of Fatigue*. Vol. 32(10): pp. 1620-1626.

Pedhazur, E. J. (1982). *Multiple regression in behavioral research* (2nd ed.). New York: Holt, Rinehart, & Winston.

Poutiainen, I. (2004). “Finite Element Methods for Structural Hot Spot Stress Determination—a Comparison of Procedures.” *International Journal of Fatigue*. Vol. 26(11): pp. 1147-1157.

Poutiainen, I. and Marquis, G. (2005). “A Modified Hot Spot Stress Method Based on Weld Stresses.” IIW Doc. XIII-2087-05 / XV-1205-05. International Institute of Welding (Delegation of Finland), Lappeenranta, Finland.

Poutiainen, I. and Marquis, G. (2006a). “A Fatigue Assessment Method Based on Weld Stress.” *International Journal of Fatigue*. Vol. 28(9): pp. 1037-1046.

Poutiainen, I. and Marquis, G. (2006b). “Comparison of Local Approaches in Fatigue Analysis of Welded Structures.” IIW Doc. XIII-2105-06. International Institute of Welding (Delegation of Finland), Lappeenranta, Finland.

Radaj, D. (1990). “Design and Analysis of Fatigue Resistant Welded Structures.” Cambridge. Abington Publishing.

Radaj, D. and Sonsino, C. M. (1998). “Fatigue Assessment of Welded Joints by Local Approaches.” Cambridge. Abington Publishing.

Rice, J.R., (1968). “A Path Independent Integral and the Approximate Analysis of Strain Concentration by Notches and Cracks.” *Journal of Applied Mechanics*, Vol. 35, 1968, pp. 379-386.

Sedlacek, G. (1992). "Orthotropic Plate Bridge Decks, Constructional Steel design – An International Guide", Edited by P.J. Dowling, J.E. Harding, R. Björhovde, Elsevier, ISBN 1 851668950, pp. 227-245

Sim, H. and Uang, C. (2007). "Effects of Fabrication Procedures and Weld Melt-Through on Fatigue Resistance of Orthotropic Steel Deck Welds." Report No. SSRP-07/13. University of California, San Diego. August.

StatSoft, Inc. (2011). "Electronic Statistics Textbook." Tulsa, OK: StatSoft. WEB: <http://www.statsoft.com/textbook/>.

Tsakopoulos, P.A. and Fisher, J.W. (2003). "Full-Scale Fatigue Tests of Steel Orthotropic Decks for the Williamsburg Bridge." Journal of Bridge Engineering, Vol. 8(5), 2003, pp. 323-333.

Tsakopoulos, P.A. and Fisher, J.W. (2005). "Fatigue Performance and Design Refinements of Steel Orthotropic Deck Panels Based on Full-scale Laboratory Tests." Steel Structures, Vol. 5, 2005, pp. 211-223.

Wang, C. H. (1996). "Introduction to Fracture Mechanics." DSTO-GD-0103. DSTO Aeronautical and Maritime Research Laboratory, Melbourne, Victoria, Australia. July 1996.

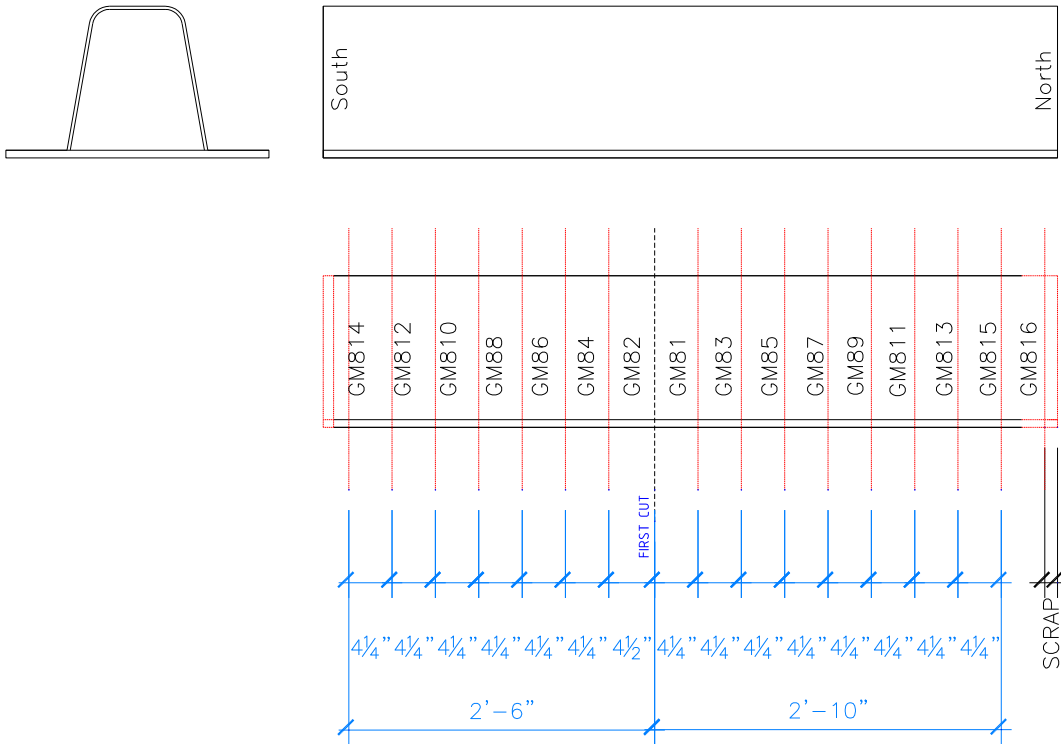
Wolchuk, R. (2001) "The use of orthotropic decks in redecking of bridges", Engineering Journal, Vol. 38, No. 1, pp. 2-10, American Institute of Steel Construction, USA

Xiao, Z.-G. and Yamada, K. (2004). "A Method of Determining Geometric Stress for Fatigue Strength Evaluation of Steel Welded Joints." International Journal of Fatigue. Vol. 26(12): pp. 1277-1293.

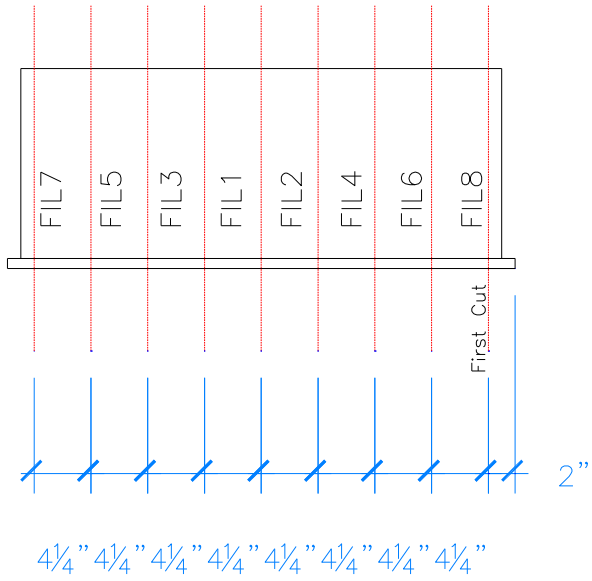
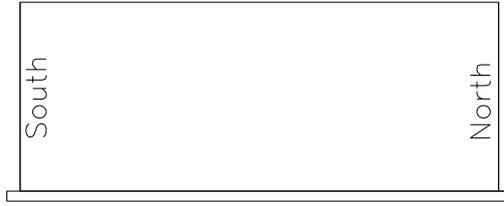
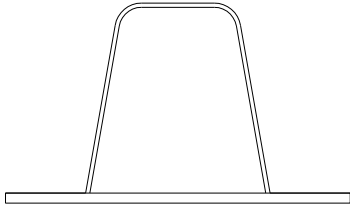
Yamada, K. and Xiao, Z. (2004). "A New Method of Evaluating Fatigue Strength of Weld Toe Failures." IIW Doc. XIII-2022-04 / XV-1175-04. International Institute of Welding (Japanese Delegation), Nagoya, Japan.

Appendix A Arrangement of Specimens on Full-Scale Deck Strips from TFHRC

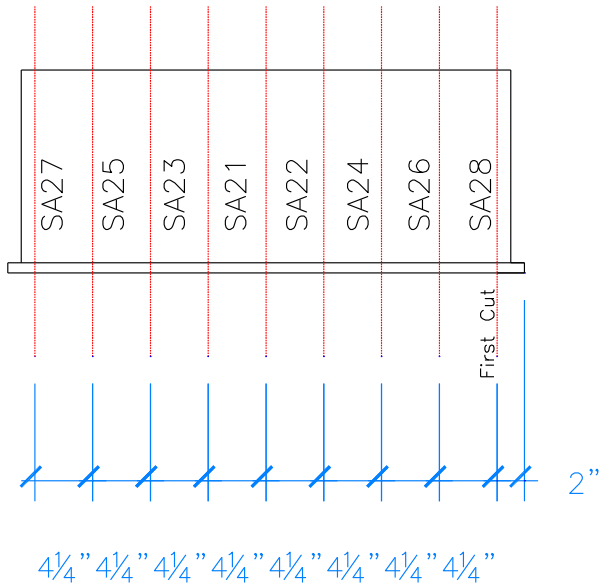
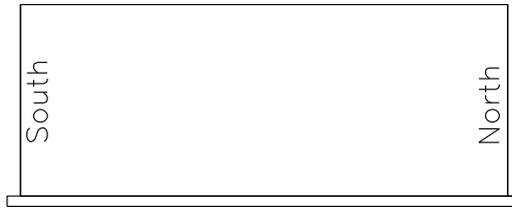
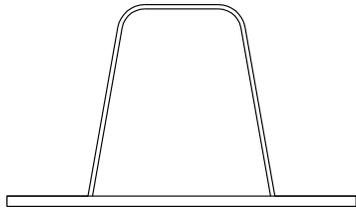
GM-80 Series



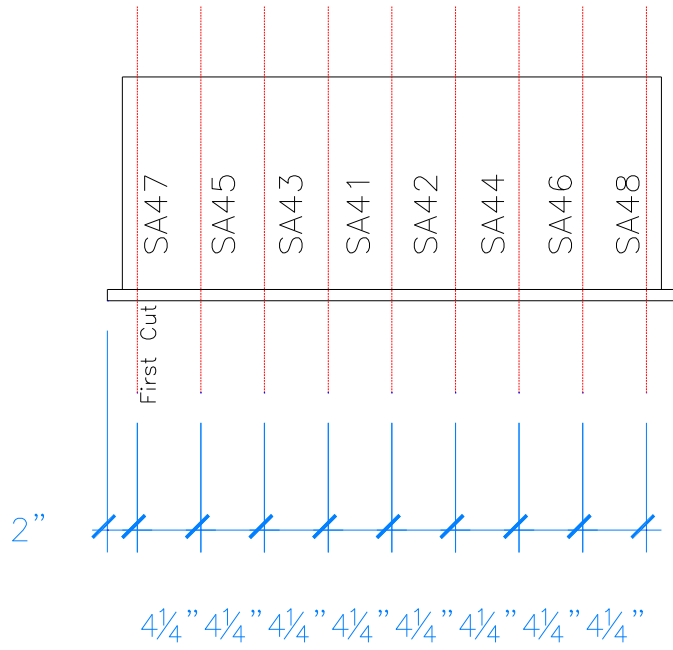
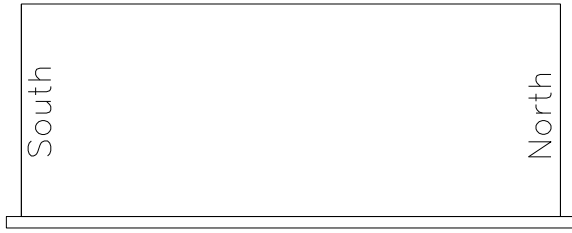
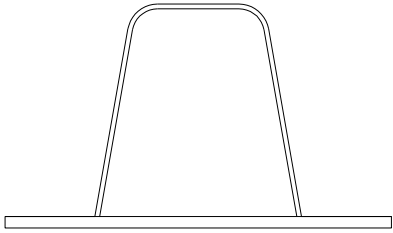
FIL Series



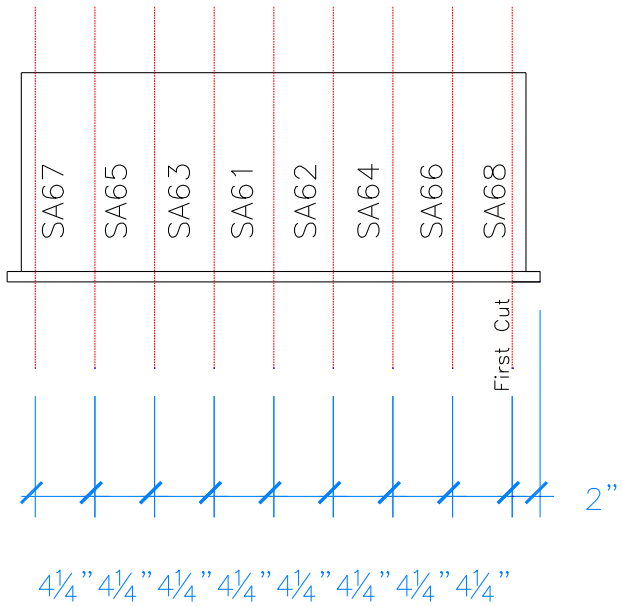
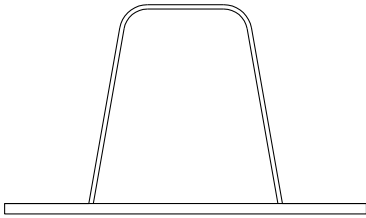
SAW-20 Series



SAW-40 Series



SAW-60 Series



Appendix B Test Results from TFHRC

Table B.1 Test Results of GM-80 Series

Specimen	Load Range (lbs)	Experimental Stress Range (ksi)	Load Ratio	Cycles to Failure	Failure Mode
GM-81	2750 / -2750	36.66	-1	888807	Crack in deck plate at east rib leg
GM-82	0 / 5000	33.33	0	20000655	Test stopped without cracking
GM-83	0 / 2750	18.33	0	18253515	Crack in deck plate at east rib leg
GM-84	2500 / -2500	33.33	-1	6060816	Crack through weld throat at east rib leg
GM-85	2750 / -2750	36.66	-1	770672	Crack in deck plate at east rib leg
GM-86	2500 / -2500	33.33	-1	1517705	Crack in deck plate at east rib leg
GM-87	2750 / -2750	36.66	-1	751609	Crack in deck plate at east rib leg
GM-88	0 / 5000	33.33	0	302451	Crack in deck plate at east rib leg
GM-89	1250 / -1250	16.66	-1	10000000	Test stopped without cracking
GM-810	0 / 5000	33.33	0	296571	Cracks in deck plate at both legs, west leg dominate
GM-811	2500 / -2500	33.33	-1	1390062	Crack in deck plate
GM-812	2000 / -2000	26.66	-1	2112094	Crack in deck plate at west rib leg
GM-813	1250 / -1250	16.66	-1	10000000	Test stopped without cracking
GM-814	0 / 6000	40.00	0	146635	Cracks in deck plate at both legs, west leg dominate
GM-815	2500 / -2500	33.33	-1	863459	Crack in deck plate at east rib leg
GM-816	2500 / -2500	33.33	-1	1657918	Crack in deck plate

Table B.2 Test Results of FIL Series

Specimen	Load Range (lbs)	Experimental Stress Range (ksi)	Load Ratio	Cycles to Failure	Failure Mode
FIL-1	0 / 5000	33.33	0	308351	Crack in deck plate at both rib legs, west leg dominate
FIL-2	0 / 5000	33.33	0	352981	Crack in deck plate at both rib legs, east leg dominate
FIL-3	0 / 5000	33.33	0	302927	Crack in deck plate at both rib legs, east leg dominate
FIL-4	2750 / -2750	36.66	-1	698763	Crack in deck plate at east rib leg
FIL-5	2750 / -2750	36.66	-1	855918	Crack in deck plate at west rib leg
FIL-6	2750 / -2750	36.33	-1	2179319	Crack in deck plate at both ribs, east rib most dominate
FIL-7	2750 / -2750	36.66	-1	870418	Crack in deck plate at both rib legs, west leg larger
FIL-8	2750 / -2750	36.66	-1	529113	Crack in deck plate at both rib legs, west leg dominate

Table B.3 Test Results of SA-20 Series

Specimen	Load Range (lbs)	Experimental Stress Range (ksi)	Load Ratio	Cycles to Failure	Failure Mode
SA-21	2750 / -2750	36.66	-1	750996	Crack in deck plate at both rib legs, east leg dominate
SA-22	2750 / -2750	36.66	-1	2690351	Deck plate cracks at both rib legs, west leg dominate
SA-23	2750 / -2750	36.66	-1	708693	Crack in deck plate at both rib legs, east leg dominate
SA-24	2750 / -2750	36.66	-1	381990	Crack in deck plate at west rib leg
SA-25	2750 / -2750	36.66	-1	534364	Crack in deck plate at west rib leg
SA-26	0 / 5000	33.33	0	258639	Crack in deck plate at west rib leg
SA-27	0 / 5000	33.33	0	222741	Crack in deck plate at west rib leg
SA-28	0 / 5000	33.33	0	238136	Crack in deck plate at west rib leg

Table B.4 Test Results of SA-40 Series

Specimen	Load Range (lbs)	Experimental Stress Range (ksi)	Load Ratio	Cycles to Failure	Failure Mode
SA-41	2750 / -2750	36.66	-1	643413	Crack in deck plate at west leg
SA-42	2750 / -2750	36.66	-1	540472	Crack in deck plate at both rib legs, west leg dominate
SA-43	2750 / -2750	36.66	-1	607547	Crack in deck plate at both rib legs, west leg dominate
SA-44	2750 / -2750	36.66	-1	840760	Crack in deck plate at west rib leg
SA-45	2750 / -2750	36.66	-1	649093	Crack in deck plate at west rib leg
SA-46	0 / 5000	33.33	0	294621	Crack in deck plate at both rib legs, west leg dominate
SA-47	0 / 5000	33.33	0	300716	Crack in deck plate at west rib leg
SA-48	0 / 5000	33.33	0	407819	Crack in deck plate at east rib leg. Crack started on north edge, found stripped rod supporting roller and probably affected load distribution

Table B.5 Test Results of SA-60 Series

Specimen	Load Range (lbs)	Experimental Stress Range (ksi)	Load Ratio	Cycles to Failure	Failure Mode
SA-61	0 / 5000	33.33	0	317140	Crack in deck plate at both rib legs, west leg dominate
SA-62	0 / 5000	33.33	0	257016	Crack in deck plate at both rib legs, west leg dominate
SA-63	0 / 5000	33.33	0	286626	Crack in deck plate at both rib legs, west leg dominate
SA-64	2750 / -2750	36.66	-1	629917	Crack in deck plate at both rib legs, east leg dominate
SA-65	2750 / -2750	36.66	-1	2074221	Crack in deck plate at east rib leg
SA-66	2750 / -2750	36.66	-1	860759	Crack in deck plate at west rib leg
SA-67	2750 / -2750	36.66	-1	588156	Crack in deck plate at both rib legs, west leg dominate
SA-68	2750 / -2750	36.66	-1	521486	Crack in deck plate at just west rib leg

Appendix C Test Results from VT

Table C.1 Test Results of SA-80 Series

Specimen	Load Range (kips)	Load Ratio	Nominal Stress Range (ksi)	Number of Cycles	Failure Mode
SA-81	2.5 / -2.5	-1	29.10	689,134	WT-RIB
SA-83	2.5 / -2.5	-1	29.10	3,732,998	WT-RIB
SA-84	2.5 / -2.5	-1	29.10	2,321,046	WT-RIB
SA-85	2.5 / -2.5	-1	33.33	3,332,973	WT-DECK
SA-86	2.5 / -2.5	-1	33.33	2,623,398	WT-DECK
SA-87	2.5 / -2.5	-1	31.90	3,399,577	WT-RIB
SA-88	2.5 / -2.5	-1	31.90	2,743,534	WT-RIB
SA-89	2.75 / -2.75	-1	35.09	283,556	WT-RIB
SA-810	2.5 / -2.5	-1	29.10	869,732	WT-RIB
SA-811	2.75 / -2.75	-1	35.09	617,702	WT-RIB
SA-812	2.75 / -2.75	-1	36.67	1,930,296	WT-DECK
SA-813	2.75 / -2.75	-1	36.67	1,782,037	WT-DECK
SA-814	0 / 5	0	33.33	1,417,734	WT-DECK
SA-815	0 / 5	0	33.33	943,434	WT-DECK
SA-816	0 / 5	0	33.33	927,241	WT-DECK

Table C.2 Test Results of OB Series

Specimen	Load Range (kips)	R Ratio	Nominal Stress Range (ksi)	Number of Cycles	Failure Mode
OB-01	2.5 / -2.5	-1	27.75	647,879	WR
OB-02	2.5 / -2.5	-1	27.75	981,142	WR
OB-03	2.5 / -2.5	-1	27.75	2,385,939	WR
OB-04	2.5 / -2.5	-1	27.75	1,376,487	WR
OB-05	0 / 5	0	33.33	574,148	WT-DECK
OB-06	0 / 5	0	33.33	688,273	WT-DECK
OB-07	2.75 / -2.75	-1	30.52	1,076,871	WR
OB-08	2.75 / -2.75	-1	30.52	618,383	WR
OB-09	2.5 / -2.5	-1	27.75	2,451,238	WR
OB-10	2.5 / -2.5	-1	27.75	1,056,726	WR
OB-11	2.5 / -2.5	-1	27.75	996,626	WR
OB-12	2.5 / -2.5	-1	27.75	1,316,952	WR
OB-13	0 / 5	0	33.33	990,806	WT-DECK
OB-14	0 / 5	0	33.33	979,089	WT-DECK
OB-15	2.75 / -2.75	-1	35.09	660,272	WT-RIB
OB-16	2.75 / -2.75	-1	30.52	768,171	WR

Table C.3 Test Results of UB Series

Specimen	Load Range (kips)	R Ratio	Nominal Stress Range (ksi)	Number of Cycles	Failure Mode
UB-01	2.5 / -2.5	-1	33.33	1,359,570	WT-DECK
UB-02	2.5 / -2.5	-1	27.75	694,734	WR
UB-03	2.5 / -2.5	-1	31.90	2,011,029	WT-RIB
UB-04	2.5 / -2.5	-1	33.33	1,372,641	WT-DECK
UB-05	0 / 5	0	33.33	386,829	WT-DECK
UB-06	0 / 5	0	33.33	474,226	WT-DECK
UB-07	2.75 / -2.75	-1	36.67	1,292,525	WT-DECK
UB-08	2.75 / -2.75	-1	36.67	1,182,601	WT-DECK
UB-09	2.5 / -2.5	-1	33.33	2,024,920	WT-DECK
UB-10	2.5 / -2.5	-1	N/A	4,725,868	RIB TOP
UB-11	2.5 / -2.5	-1	27.75	1,483,203	WR
UB-12	2.5 / -2.5	-1	27.75	1,590,018	WR
UB-13	0 / 5	0	31.90	448,014	WT-RIB
UB-14	0 / 5	0	33.33	591,939	WT-DECK
UB-15	2.75 / -2.75	-1	30.52	856,676	WR
UB-16	2.75 / -2.75	-1	35.09	1,177,345	WT-RIB

Appendix D Weld Dimensions

Table D.1 Weld Dimensions of GM-80 Series

Specimen	Weld Location	d ₁ (in)	d ₂ (in)	d ₃ (in)	d ₄ (in)	d ₂ /d ₄	d ₅ (in)	T (in)	h ₁ (in)	h ₂ (in)	h (in)	t _r (in)	A _w (in ²)
GM-81	1	0.278	0.241	0.105	0.346	0.698	0.624	0.332	0.317	0.059	0.378	0.307	0.106
	2	0.213	0.262	0.057	0.318	0.822	0.531	0.360	0.330	0.061	0.391	0.313	0.123
	3	0.197	0.247	0.080	0.327	0.756	0.524	0.309	0.201	0.055	0.256	0.318	0.104
	4	0.193	0.256	0.067	0.323	0.792	0.516	0.308	0.286	0.061	0.347	0.319	0.090
	Average 1 & 3	0.237	0.244	0.092	0.336	0.727	0.574	0.321	0.259	0.057	0.317	0.313	0.105
	Average 2 & 4	0.203	0.259	0.062	0.321	0.807	0.523	0.334	0.308	0.061	0.369	0.316	0.106
GM-82	1	0.189	0.251	0.103	0.355	0.709	0.440	0.342	0.227	0.065	0.293	0.325	0.091
	2	0.255	0.219	0.100	0.319	0.687	0.574	0.342	0.286	0.053	0.338	0.315	0.115
	3	0.208	0.244	0.078	0.322	0.757	0.530	0.313	0.288	0.065	0.353	0.315	0.091
	4	0.221	0.252	0.080	0.332	0.759	0.553	0.325	0.255	0.057	0.311	0.327	0.099
	Average 1 & 3	0.198	0.248	0.091	0.338	0.733	0.485	0.328	0.257	0.065	0.323	0.320	0.091
	Average 2 & 4	0.238	0.235	0.090	0.325	0.723	0.563	0.333	0.270	0.055	0.325	0.321	0.107

Specimen	Weld Location	d ₁ (in)	d ₂ (in)	d ₃ (in)	d ₄ (in)	d ₂ /d ₄	d ₅ (in)	T (in)	h ₁ (in)	h ₂ (in)	h (in)	t _r (in)	A _w (in ²)
GM-83	1	0.194	0.257	0.063	0.320	0.805	0.513	0.357	0.248	0.059	0.307	0.314	0.104
	2	0.166	0.245	0.074	0.319	0.768	0.485	0.310	0.190	0.061	0.252	0.313	0.090
	3	0.220	0.249	0.072	0.321	0.775	0.541	0.332	0.227	0.052	0.282	0.317	0.099
	4	0.180	0.256	0.073	0.329	0.778	0.509	0.333	0.223	0.065	0.288	0.322	0.092
	Average 1 & 3	0.207	0.253	0.067	0.321	0.790	0.527	0.344	0.238	0.056	0.295	0.315	0.101
	Average 2 & 4	0.173	0.250	0.073	0.324	0.773	0.497	0.322	0.206	0.063	0.270	0.318	0.091
GM-84	1	0.220	0.226	0.097	0.322	0.700	0.542	0.336	0.295	0.039	0.334	0.320	0.117
	2	0.167	0.225	0.105	0.330	0.681	0.497	0.336	0.252	0.069	0.321	0.323	0.085
	3	0.220	0.205	0.115	0.320	0.640	0.540	0.317	0.275	0.038	0.313	0.318	0.076
	4	0.168	0.273	0.046	0.318	0.857	0.486	0.363	0.254	0.066	0.320	0.312	0.099
	Average 1 & 3	0.220	0.215	0.106	0.321	0.670	0.541	0.327	0.285	0.039	0.324	0.319	0.096
	Average 2 & 4	0.168	0.249	0.075	0.324	0.769	0.492	0.349	0.253	0.067	0.320	0.317	0.092
GM-85	1	0.217	0.252	0.053	0.305	0.828	0.522	0.347	0.222	0.052	0.275	0.300	0.105
	2	0.154	0.274	0.043	0.317	0.863	0.471	0.348	0.226	0.061	0.286	0.311	0.092
	3	0.220	0.246	0.063	0.309	0.797	0.529	0.347	0.245	0.052	0.297	0.305	0.099

Specimen	Weld Location	d ₁ (in)	d ₂ (in)	d ₃ (in)	d ₄ (in)	d ₂ /d ₄	d ₅ (in)	T (in)	h ₁ (in)	h ₂ (in)	h (in)	t _r (in)	A _w (in ²)
	4	0.170	0.248	0.065	0.313	0.792	0.483	0.327	0.206	0.061	0.267	0.307	0.093
	Average 1 & 3	0.219	0.249	0.058	0.307	0.812	0.526	0.347	0.234	0.052	0.286	0.302	0.102
	Average 2 & 4	0.162	0.261	0.054	0.315	0.827	0.477	0.337	0.216	0.061	0.276	0.309	0.092
GM-86	1	0.162	0.265	0.061	0.325	0.814	0.487	0.350	0.224	0.063	0.286	0.319	0.093
	2	0.157	0.254	0.076	0.330	0.770	0.411	0.352	0.256	0.055	0.311	0.225	0.116
	3	0.185	0.262	0.079	0.340	0.768	0.526	0.350	0.222	0.068	0.290	0.334	0.099
	4	0.216	0.195	0.135	0.330	0.592	0.545	0.304	0.230	0.056	0.286	0.325	0.090
	Average 1 & 3	0.174	0.263	0.070	0.333	0.791	0.507	0.350	0.223	0.065	0.288	0.326	0.096
	Average 2 & 4	0.187	0.224	0.105	0.330	0.681	0.478	0.328	0.243	0.056	0.299	0.275	0.103
GM-87	1	0.181	0.268	0.047	0.315	0.851	0.496	0.357	0.251	0.056	0.308	0.310	0.100
	2	0.196	0.256	0.055	0.312	0.822	0.508	0.332	0.206	0.063	0.269	0.305	0.101
	3	0.195	0.255	0.060	0.316	0.809	0.511	0.341	0.235	0.057	0.292	0.310	0.098
	4	0.165	0.267	0.054	0.321	0.831	0.486	0.334	0.222	0.062	0.284	0.315	0.093
	Average 1 & 3	0.188	0.262	0.054	0.315	0.830	0.503	0.349	0.243	0.056	0.300	0.310	0.099

Specimen	Weld Location	d ₁ (in)	d ₂ (in)	d ₃ (in)	d ₄ (in)	d ₂ /d ₄	d ₅ (in)	T (in)	h ₁ (in)	h ₂ (in)	h (in)	t _r (in)	A _w (in ²)
	Average 2 & 4	0.181	0.261	0.055	0.316	0.827	0.497	0.333	0.214	0.062	0.276	0.310	0.097
GM-88	1	0.244	0.219	0.106	0.325	0.674	0.569	0.338	0.243	0.054	0.297	0.320	0.104
	2	0.174	0.255	0.072	0.326	0.780	0.500	0.339	0.241	0.062	0.303	0.320	0.092
	3	0.233	0.229	0.093	0.322	0.711	0.554	0.351	0.274	0.055	0.329	0.317	0.112
	4	0.141	0.276	0.051	0.327	0.844	0.468	0.350	0.218	0.062	0.280	0.321	0.095
	Average 1 & 3	0.238	0.224	0.099	0.323	0.693	0.562	0.344	0.259	0.054	0.313	0.319	0.108
	Average 2 & 4	0.157	0.265	0.061	0.327	0.812	0.484	0.344	0.230	0.062	0.292	0.321	0.094
GM-89	1	0.171	0.253	0.059	0.312	0.810	0.483	0.309	0.308	0.046	0.354	0.340	0.105
	2	0.157	0.314	0.014	0.328	0.957	0.485	0.320	0.285	0.070	0.355	0.392	0.129
	3	0.182	0.271	0.040	0.311	0.871	0.494	0.308	0.351	0.048	0.399	0.367	0.100
	4	0.192	0.253	0.055	0.308	0.822	0.501	0.302	0.289	0.059	0.349	0.349	0.096
	Average 1 & 3	0.176	0.262	0.050	0.312	0.841	0.488	0.308	0.329	0.047	0.376	0.353	0.102
	Average 2 & 4	0.175	0.284	0.035	0.318	0.889	0.493	0.311	0.287	0.065	0.352	0.371	0.113
GM-810	1	0.151	0.272	0.065	0.336	0.808	0.487	0.347	0.225	0.066	0.291	0.330	0.096

Specimen	Weld Location	d ₁ (in)	d ₂ (in)	d ₃ (in)	d ₄ (in)	d ₂ /d ₄	d ₅ (in)	T (in)	h ₁ (in)	h ₂ (in)	h (in)	t _r (in)	A _w (in ²)
	2	0.207	0.255	0.076	0.331	0.770	0.538	0.363	0.272	0.055	0.327	0.327	0.121
	3	0.151	0.292	0.034	0.326	0.897	0.477	0.372	0.244	0.065	0.308	0.319	0.112
	4	0.213	0.214	0.107	0.321	0.666	0.535	0.323	0.244	0.053	0.296	0.317	0.096
	Average 1 & 3	0.151	0.282	0.049	0.331	0.853	0.482	0.360	0.234	0.065	0.300	0.324	0.104
	Average 2 & 4	0.210	0.234	0.092	0.326	0.718	0.536	0.343	0.258	0.054	0.312	0.322	0.108
GM-811	1	0.149	0.303	0.019	0.322	0.940	0.471	0.316	0.312	0.062	0.374	0.385	0.098
	2	0.161	0.262	0.076	0.337	0.776	0.498	0.347	0.316	0.068	0.384	0.330	0.086
	3	0.166	0.270	0.053	0.323	0.836	0.488	0.359	0.357	0.058	0.415	0.318	0.097
	4	0.188	0.259	0.075	0.334	0.776	0.522	0.368	0.307	0.063	0.370	0.328	0.095
	Average 1 & 3	0.157	0.286	0.036	0.322	0.888	0.480	0.337	0.335	0.060	0.394	0.351	0.097
	Average 2 & 4	0.175	0.260	0.075	0.335	0.776	0.510	0.357	0.311	0.066	0.377	0.329	0.090
GM-812	1	0.168	0.298	0.042	0.340	0.878	0.507	0.392	0.262	0.064	0.326	0.334	0.097
	2	0.201	0.262	0.062	0.325	0.808	0.525	0.375	0.262	0.055	0.316	0.320	0.112
	3	0.180	0.298	0.042	0.340	0.878	0.507	0.392	0.232	0.059	0.291	0.311	0.097
	4	0.229	0.241	0.085	0.326	0.738	0.554	0.349	0.276	0.050	0.326	0.322	0.100

Specimen	Weld Location	d ₁ (in)	d ₂ (in)	d ₃ (in)	d ₄ (in)	d ₂ /d ₄	d ₅ (in)	T (in)	h ₁ (in)	h ₂ (in)	h (in)	t _r (in)	A _w (in ²)
	Average 1 & 3	0.174	0.298	0.042	0.340	0.878	0.507	0.392	0.247	0.061	0.308	0.322	0.097
	Average 2 & 4	0.215	0.252	0.074	0.325	0.773	0.540	0.362	0.269	0.052	0.321	0.321	0.106
GM-813	1	0.134	0.308	0.000	0.308	1.000	0.458	0.425	0.346	0.053	0.399	0.303	0.129
	2	0.148	0.278	0.045	0.323	0.861	0.472	0.355	0.275	0.067	0.342	0.316	0.092
	3	0.169	0.283	0.035	0.317	0.890	0.486	0.368	0.268	0.055	0.323	0.313	0.100
	4	0.167	0.264	0.056	0.319	0.825	0.487	0.335	0.285	0.067	0.356	0.312	0.093
	Average 1 & 3	0.151	0.295	0.017	0.313	0.945	0.472	0.396	0.307	0.054	0.361	0.308	0.114
	Average 2 & 4	0.158	0.271	0.050	0.321	0.843	0.479	0.345	0.280	0.067	0.349	0.314	0.092
GM-814	1	0.221	0.220	0.103	0.323	0.682	0.544	0.293	0.190	0.061	0.251	0.317	0.078
	2	0.176	0.273	0.053	0.326	0.837	0.502	0.364	0.250	0.054	0.304	0.322	0.109
	3	0.172	0.277	0.039	0.317	0.876	0.489	0.376	0.276	0.058	0.334	0.311	0.099
	4	0.196	0.277	0.058	0.335	0.826	0.531	0.376	0.274	0.058	0.332	0.330	0.121
	Average 1 & 3	0.197	0.249	0.071	0.320	0.779	0.516	0.334	0.233	0.060	0.293	0.314	0.088
	Average 2 & 4	0.186	0.275	0.056	0.331	0.832	0.516	0.370	0.262	0.056	0.318	0.326	0.115

Specimen	Weld Location	d ₁ (in)	d ₂ (in)	d ₃ (in)	d ₄ (in)	d ₂ /d ₄	d ₅ (in)	T (in)	h ₁ (in)	h ₂ (in)	h (in)	t _r (in)	A _w (in ²)
GM-815	1	0.132	0.315	0.000	0.315	1.000	0.454	0.434	0.355	0.061	0.416	0.309	0.126
	2	0.153	0.265	0.061	0.326	0.814	0.479	0.336	0.310	0.067	0.377	0.319	0.091
	3	0.134	0.293	0.022	0.315	0.930	0.449	0.399	0.348	0.054	0.402	0.311	0.105
	4	0.159	0.266	0.055	0.321	0.827	0.480	0.352	0.226	0.066	0.292	0.314	0.085
	Average 1 & 3	0.133	0.304	0.011	0.315	0.965	0.452	0.416	0.352	0.057	0.409	0.310	0.115
	Average 2 & 4	0.156	0.265	0.058	0.323	0.821	0.479	0.344	0.268	0.066	0.334	0.317	0.088
GM-816	1	0.187	0.244	0.075	0.318	0.765	0.505	0.347	0.242	0.055	0.297	0.313	0.088
	2	0.154	0.243	0.082	0.325	0.748	0.479	0.316	0.216	0.063	0.279	0.319	0.084
	3	0.153	0.286	0.031	0.317	0.901	0.470	0.440	0.309	0.056	0.364	0.312	0.109
	4	0.140	0.257	0.067	0.325	0.793	0.464	0.373	0.231	0.063	0.294	0.318	0.092
	Average 1 & 3	0.170	0.265	0.053	0.318	0.833	0.488	0.393	0.275	0.055	0.331	0.313	0.098
	Average 2 & 4	0.147	0.250	0.075	0.325	0.770	0.472	0.344	0.223	0.063	0.286	0.319	0.088
Average	1 & 3	0.187	0.262	0.060	0.323	0.814	0.507	0.353	0.269	0.056	0.326	0.320	0.101
	2 & 4	0.181	0.256	0.068	0.324	0.790	0.502	0.341	0.256	0.061	0.317	0.319	0.099
	All	0.184	0.259	0.064	0.323	0.802	0.505	0.347	0.263	0.059	0.322	0.320	0.100

Specimen	Weld Location	d₁ (in)	d₂ (in)	d₃ (in)	d₄ (in)	d₂/d₄	d₅ (in)	T (in)	h₁ (in)	h₂ (in)	h (in)	t_r (in)	A_w (in²)
Standard Deviation	1 & 3	0.035	0.028	0.031	0.011	0.092	0.039	0.036	0.048	0.007	0.046	0.017	0.011
	2 & 4	0.028	0.022	0.022	0.007	0.068	0.033	0.021	0.035	0.005	0.036	0.023	0.012
	All	0.031	0.025	0.027	0.009	0.081	0.036	0.030	0.042	0.007	0.042	0.020	0.012

Table D.2 Weld Dimensions of FIL Series

Specimen	Weld Location	d ₁ (in)	d ₂ (in)	d ₃ (in)	d ₄ (in)	d ₂ /d ₄	d ₅ (in)	T (in)	h ₁ (in)	h ₂ (in)	h (in)	t _r (in)	A _w (in ²)
FIL-1	1	0.241	0.248	0.076	0.324	0.767	0.565	0.353	0.290	0.067	0.356	0.317	0.128
	2	0.259	0.226	0.108	0.335	0.675	0.594	0.312	0.230	0.063	0.293	0.329	0.123
	3	0.278	0.184	0.148	0.332	0.555	0.610	0.293	0.310	0.070	0.380	0.325	0.103
	4	0.248	0.218	0.097	0.315	0.691	0.563	0.319	0.316	0.056	0.372	0.310	0.121
	Average 1 & 3	0.259	0.216	0.112	0.328	0.661	0.587	0.323	0.300	0.068	0.368	0.321	0.116
	Average 2 & 4	0.254	0.222	0.103	0.325	0.683	0.579	0.316	0.273	0.059	0.332	0.319	0.122
FIL-2	1	0.269	0.172	0.154	0.326	0.528	0.594	0.300	0.334	0.060	0.334	0.320	0.114
	2	0.262	0.202	0.130	0.332	0.608	0.594	0.314	0.298	0.069	0.366	0.325	0.116
	3	0.263	0.218	0.122	0.340	0.642	0.602	0.318	0.378	0.068	0.445	0.333	0.122
	4	0.240	0.222	0.099	0.321	0.690	0.561	0.310	0.256	0.065	0.321	0.314	0.115
	Average 1 & 3	0.266	0.195	0.138	0.333	0.585	0.598	0.309	0.356	0.064	0.390	0.327	0.118
	Average 2 & 4	0.251	0.212	0.115	0.326	0.649	0.577	0.312	0.277	0.067	0.344	0.319	0.115
FIL-3	1	0.267	0.206	0.119	0.324	0.634	0.591	0.316	0.333	0.060	0.393	0.319	0.116

Specimen	Weld Location	d ₁ (in)	d ₂ (in)	d ₃ (in)	d ₄ (in)	d ₂ /d ₄	d ₅ (in)	T (in)	h ₁ (in)	h ₂ (in)	h (in)	t _r (in)	A _w (in ²)
	2	0.205	0.272	0.044	0.316	0.860	0.521	0.357	0.328	0.065	0.392	0.310	0.121
	3	0.255	0.216	0.116	0.332	0.650	0.587	0.316	0.328	0.060	0.388	0.326	0.118
	4	0.268	0.150	0.181	0.331	0.453	0.599	0.301	0.292	0.070	0.362	0.324	0.112
	Average 1 & 3	0.261	0.211	0.118	0.328	0.642	0.589	0.316	0.331	0.060	0.391	0.323	0.117
	Average 2 & 4	0.237	0.211	0.113	0.324	0.656	0.560	0.329	0.310	0.067	0.377	0.317	0.116
FIL-4	1	0.261	0.225	0.105	0.329	0.682	0.591	0.335	0.336	0.060	0.396	0.324	0.120
	2	0.241	0.211	0.116	0.327	0.646	0.568	0.320	0.301	0.067	0.368	0.320	0.120
	3	0.235	0.213	0.110	0.323	0.661	0.558	0.327	0.355	0.061	0.416	0.317	0.118
	4	0.264	0.334	0.000	0.334	1.000	0.598	0.293	0.246	0.070	0.317	0.326	0.116
	Average 1 & 3	0.248	0.219	0.107	0.326	0.672	0.574	0.331	0.345	0.061	0.406	0.320	0.119
	Average 2 & 4	0.253	0.272	0.058	0.330	0.823	0.583	0.307	0.274	0.069	0.342	0.323	0.118
FIL-5	1	0.269	0.233	0.092	0.325	0.718	0.594	0.328	0.298	0.067	0.365	0.318	0.117
	2	0.284	0.151	0.165	0.315	0.478	0.600	0.273	0.256	0.054	0.311	0.311	0.089
	3	0.301	0.175	0.151	0.326	0.538	0.631	0.310	0.317	0.066	0.384	0.319	0.111
	4	0.275	0.180	0.137	0.316	0.569	0.591	0.289	0.275	0.057	0.331	0.311	0.109

Specimen	Weld Location	d₁ (in)	d₂ (in)	d₃ (in)	d₄ (in)	d₂/d₄	d₅ (in)	T (in)	h₁ (in)	h₂ (in)	h (in)	t_r (in)	A_w (in²)
	Average 1 & 3	0.285	0.204	0.121	0.325	0.628	0.612	0.319	0.308	0.067	0.374	0.318	0.114
	Average 2 & 4	0.280	0.165	0.151	0.316	0.524	0.595	0.281	0.266	0.056	0.321	0.311	0.099
FIL-6	1	0.270	0.208	0.117	0.326	0.640	0.596	0.314	0.304	0.060	0.364	0.320	0.115
	2	0.196	0.265	0.058	0.323	0.821	0.519	0.353	0.286	0.066	0.353	0.316	0.120
	3	0.285	0.215	0.109	0.325	0.663	0.610	0.319	0.331	0.061	0.392	0.319	0.122
	4	0.271	0.164	0.160	0.324	0.507	0.595	0.289	0.267	0.065	0.332	0.318	0.100
	Average 1 & 3	0.278	0.212	0.113	0.325	0.651	0.603	0.317	0.317	0.060	0.378	0.319	0.118
	Average 2 & 4	0.234	0.215	0.109	0.324	0.664	0.557	0.321	0.277	0.065	0.342	0.317	0.110
FIL-7	1	0.324	0.079	0.253	0.332	0.239	0.657	0.235	0.252	0.067	0.318	0.326	0.079
	2	0.326	0.082	0.249	0.331	0.249	0.658	0.244	0.255	0.060	0.315	0.326	0.078
	3	0.265	0.221	0.100	0.321	0.689	0.585	0.304	0.245	0.065	0.310	0.314	0.118
	4	0.286	0.206	0.120	0.326	0.633	0.612	0.300	0.242	0.059	0.301	0.321	0.105
	Average 1 & 3	0.295	0.150	0.176	0.326	0.464	0.621	0.270	0.248	0.066	0.314	0.320	0.098
	Average 2 & 4	0.306	0.144	0.184	0.329	0.441	0.635	0.272	0.248	0.060	0.308	0.323	0.092

Specimen	Weld Location	d₁ (in)	d₂ (in)	d₃ (in)	d₄ (in)	d₂/d₄	d₅ (in)	T (in)	h₁ (in)	h₂ (in)	h (in)	t_r (in)	A_w (in²)
FIL-8	1	0.232	0.232	0.091	0.323	0.720	0.555	0.345	0.253	0.065	0.318	0.316	0.115
	2	0.245	0.194	0.135	0.328	0.589	0.573	0.311	0.278	0.059	0.337	0.323	0.110
	3	0.246	0.220	0.107	0.327	0.672	0.574	0.292	0.265	0.066	0.330	0.321	0.094
	4	0.286	0.161	0.156	0.317	0.507	0.603	0.265	0.257	0.055	0.312	0.312	0.099
	Average 1 & 3	0.239	0.226	0.099	0.325	0.696	0.564	0.319	0.259	0.065	0.324	0.318	0.104
	Average 2 & 4	0.265	0.177	0.146	0.323	0.548	0.588	0.288	0.267	0.057	0.324	0.318	0.104
Average	1 & 3	0.266	0.204	0.123	0.327	0.625	0.594	0.313	0.308	0.064	0.368	0.321	0.113
	2 & 4	0.260	0.202	0.122	0.325	0.624	0.584	0.303	0.274	0.062	0.336	0.318	0.110
	All	0.263	0.203	0.123	0.326	0.624	0.589	0.308	0.291	0.063	0.352	0.320	0.111
Standard Deviation	1 & 3	0.024	0.039	0.041	0.005	0.122	0.026	0.027	0.039	0.004	0.038	0.005	0.012
	2 & 4	0.032	0.058	0.058	0.007	0.177	0.034	0.029	0.028	0.005	0.029	0.007	0.013
	All	0.028	0.049	0.049	0.006	0.150	0.030	0.028	0.037	0.005	0.037	0.006	0.012

Table D.3 Weld Dimensions of SA-20 Series

Specimen	Weld Location	d ₁ (in)	d ₂ (in)	d ₃ (in)	d ₄ (in)	d ₂ /d ₄	d ₅ (in)	T (in)	h ₁ (in)	h ₂ (in)	h (in)	t _r (in)	A _w (in ²)
SA-21	1	0.196	0.289	0.035	0.324	0.891	0.520	0.332	0.179	0.063	0.242	0.318	0.121
	2	0.200	0.210	0.116	0.326	0.643	0.526	0.289	0.217	0.065	0.282	0.319	0.090
	3	0.188	0.255	0.076	0.331	0.771	0.519	0.311	0.232	0.066	0.298	0.324	0.100
	4	0.197	0.206	0.120	0.326	0.632	0.523	0.292	0.223	0.063	0.287	0.320	0.091
	Average 1 & 3	0.192	0.272	0.056	0.327	0.831	0.519	0.322	0.206	0.065	0.270	0.321	0.110
	Average 2 & 4	0.198	0.208	0.118	0.326	0.637	0.524	0.290	0.220	0.064	0.284	0.320	0.090
SA-22	1	0.196	0.217	0.114	0.332	0.654	0.527	0.294	0.204	0.066	0.270	0.325	0.093
	2	0.173	0.279	0.053	0.332	0.840	0.505	0.330	0.325	0.064	0.389	0.322	0.103
	3	0.205	0.224	0.105	0.329	0.681	0.535	0.296	0.206	0.067	0.273	0.322	0.095
	4	0.264	0.202	0.147	0.349	0.580	0.613	0.320	0.475	0.068	0.543	0.342	0.127
	Average 1 & 3	0.200	0.221	0.109	0.331	0.668	0.531	0.295	0.205	0.067	0.272	0.324	0.094
	Average 2 & 4	0.219	0.240	0.100	0.340	0.710	0.559	0.325	0.400	0.066	0.466	0.332	0.115
SA-23	1	0.194	0.269	0.061	0.330	0.814	0.524	0.317	0.190	0.064	0.253	0.324	0.098

Specimen	Weld Location	d ₁ (in)	d ₂ (in)	d ₃ (in)	d ₄ (in)	d ₂ /d ₄	d ₅ (in)	T (in)	h ₁ (in)	h ₂ (in)	h (in)	t _r (in)	A _w (in ²)
	2	0.182	0.210	0.120	0.331	0.636	0.513	0.283	0.216	0.066	0.282	0.324	0.088
	3	0.167	0.208	0.131	0.339	0.614	0.506	0.297	0.280	0.069	0.349	0.332	0.096
	4	0.202	0.206	0.118	0.324	0.636	0.526	0.302	0.269	0.063	0.332	0.318	0.088
	Average 1 & 3	0.181	0.238	0.096	0.334	0.714	0.515	0.307	0.235	0.066	0.301	0.328	0.097
	Average 2 & 4	0.192	0.208	0.119	0.327	0.636	0.519	0.292	0.243	0.064	0.307	0.321	0.088
SA-24	1	0.212	0.208	0.116	0.323	0.643	0.535	0.287	0.237	0.064	0.301	0.317	0.092
	2	0.333	0.194	0.125	0.319	0.609	0.652	0.340	0.443	0.058	0.501	0.314	0.144
	3	0.188	0.221	0.114	0.334	0.661	0.522	0.288	0.205	0.068	0.274	0.327	0.091
	4	0.182	0.242	0.082	0.324	0.747	0.506	0.292	0.212	0.060	0.273	0.318	0.090
	Average 1 & 3	0.200	0.214	0.115	0.329	0.652	0.529	0.288	0.221	0.066	0.287	0.322	0.092
	Average 2 & 4	0.257	0.218	0.103	0.322	0.678	0.579	0.316	0.328	0.059	0.387	0.316	0.117
SA-25	1	0.224	0.193	0.137	0.331	0.585	0.555	0.284	0.184	0.066	0.251	0.324	0.089
	2	0.174	0.264	0.068	0.332	0.796	0.507	0.320	0.193	0.063	0.256	0.326	0.100
	3	0.187	0.219	0.115	0.334	0.656	0.521	0.302	0.219	0.066	0.286	0.328	0.093
	4	0.211	0.183	0.140	0.323	0.566	0.535	0.274	0.243	0.063	0.306	0.317	0.089

Specimen	Weld Location	d ₁ (in)	d ₂ (in)	d ₃ (in)	d ₄ (in)	d ₂ /d ₄	d ₅ (in)	T (in)	h ₁ (in)	h ₂ (in)	h (in)	t _r (in)	A _w (in ²)
	Average 1 & 3	0.205	0.206	0.126	0.332	0.620	0.538	0.293	0.202	0.066	0.268	0.326	0.091
	Average 2 & 4	0.193	0.224	0.104	0.328	0.681	0.521	0.297	0.218	0.063	0.281	0.322	0.094
SA-26	1	0.227	0.212	0.115	0.327	0.649	0.552	0.287	0.204	0.064	0.268	0.321	0.092
	2	0.195	0.268	0.058	0.326	0.823	0.521	0.313	0.202	0.062	0.265	0.320	0.097
	3	0.186	0.208	0.121	0.329	0.634	0.514	0.285	0.200	0.065	0.265	0.322	0.089
	4	0.224	0.216	0.111	0.327	0.662	0.551	0.271	0.171	0.063	0.234	0.321	0.099
	Average 1 & 3	0.206	0.210	0.118	0.328	0.641	0.533	0.286	0.202	0.064	0.267	0.322	0.090
	Average 2 & 4	0.210	0.242	0.084	0.327	0.743	0.536	0.292	0.187	0.063	0.250	0.320	0.098
SA-27	1	0.193	0.235	0.098	0.333	0.707	0.526	0.310	0.210	0.065	0.275	0.326	0.096
	2	0.202	0.199	0.144	0.343	0.582	0.545	0.281	0.236	0.067	0.303	0.336	0.093
	3	0.173	0.235	0.091	0.326	0.722	0.499	0.328	0.260	0.061	0.322	0.320	0.098
	4	0.266	0.150	0.177	0.327	0.459	0.593	0.239	0.160	0.062	0.221	0.321	0.080
	Average 1 & 3	0.183	0.235	0.094	0.329	0.714	0.512	0.319	0.235	0.063	0.298	0.323	0.097
	Average 2 & 4	0.234	0.175	0.160	0.335	0.520	0.569	0.260	0.198	0.064	0.262	0.329	0.086

Specimen	Weld Location	d ₁ (in)	d ₂ (in)	d ₃ (in)	d ₄ (in)	d ₂ /d ₄	d ₅ (in)	T (in)	h ₁ (in)	h ₂ (in)	h (in)	t _r (in)	A _w (in ²)
SA-28	1	0.182	0.231	0.097	0.328	0.704	0.510	0.311	0.246	0.064	0.309	0.322	0.090
	2	0.225	0.260	0.073	0.336	0.773	0.561	0.314	0.205	0.064	0.269	0.330	0.099
	3	0.207	0.192	0.136	0.328	0.586	0.535	0.286	0.267	0.063	0.330	0.322	0.083
	4	0.356	0.283	0.043	0.326	0.869	0.682	0.369	0.256	0.060	0.316	0.321	0.103
	Average 1 & 3	0.194	0.212	0.117	0.328	0.645	0.523	0.298	0.256	0.064	0.320	0.322	0.087
	Average 2 & 4	0.291	0.272	0.058	0.331	0.821	0.622	0.341	0.231	0.062	0.292	0.325	0.101
Average	1 & 3	0.195	0.226	0.104	0.330	0.686	0.525	0.301	0.220	0.065	0.285	0.323	0.095
	2 & 4	0.224	0.223	0.106	0.329	0.678	0.554	0.302	0.253	0.063	0.316	0.323	0.099
	All	0.210	0.225	0.105	0.330	0.682	0.539	0.301	0.237	0.064	0.301	0.323	0.097
Standard Deviation	1 & 3	0.017	0.026	0.027	0.004	0.082	0.015	0.016	0.030	0.002	0.030	0.004	0.008
	2 & 4	0.054	0.038	0.039	0.008	0.116	0.054	0.031	0.090	0.003	0.090	0.007	0.016
	All	0.042	0.032	0.033	0.006	0.099	0.042	0.024	0.068	0.003	0.068	0.006	0.013

Table D.4 Weld Dimensions of SA-40 Series

Specimen	Weld Location	d ₁ (in)	d ₂ (in)	d ₃ (in)	d ₄ (in)	d ₂ /d ₄	d ₅ (in)	T (in)	h ₁ (in)	h ₂ (in)	h (in)	t _r (in)	A _w (in ²)
SA-41	1	0.248	0.199	0.170	0.369	0.540	0.617	0.290	0.224	0.056	0.280	0.318	0.097
	2	0.152	0.333	0.000	0.333	1.000	0.485	0.374	0.226	0.065	0.292	0.326	0.104
	3	0.253	0.209	0.125	0.335	0.626	0.587	0.285	0.242	0.057	0.299	0.323	0.102
	4	0.266	0.236	0.138	0.374	0.630	0.640	0.304	0.211	0.062	0.273	0.312	0.116
	Average 1 & 3	0.251	0.204	0.148	0.352	0.583	0.602	0.288	0.233	0.057	0.290	0.320	0.099
	Average 2 & 4	0.209	0.284	0.069	0.353	0.815	0.562	0.339	0.219	0.063	0.282	0.319	0.110
SA-42	1	0.258	0.195	0.133	0.328	0.593	0.586	0.282	0.223	0.058	0.280	0.323	0.099
	2	0.219	0.333	0.000	0.333	1.000	0.552	0.358	0.150	0.067	0.218	0.326	0.111
	3	0.253	0.219	0.114	0.333	0.658	0.585	0.301	0.238	0.060	0.298	0.327	0.105
	4	0.191	0.290	0.058	0.348	0.834	0.539	0.316	0.130	0.073	0.203	0.340	0.102
	Average 1 & 3	0.255	0.207	0.124	0.330	0.626	0.586	0.292	0.230	0.059	0.289	0.325	0.102
	Average 2 & 4	0.205	0.312	0.029	0.340	0.917	0.546	0.337	0.140	0.070	0.210	0.333	0.107
SA-43	1	0.226	0.190	0.185	0.375	0.506	0.601	0.281	0.234	0.057	0.292	0.322	0.098

Specimen	Weld Location	d ₁ (in)	d ₂ (in)	d ₃ (in)	d ₄ (in)	d ₂ /d ₄	d ₅ (in)	T (in)	h ₁ (in)	h ₂ (in)	h (in)	t _r (in)	A _w (in ²)
	2	0.196	0.320	0.000	0.320	1.000	0.516	0.372	0.272	0.059	0.331	0.314	0.119
	3	0.244	0.207	0.120	0.326	0.634	0.570	0.286	0.221	0.056	0.277	0.321	0.104
	4	0.182	0.323	0.000	0.323	1.000	0.505	0.377	0.426	0.061	0.487	0.317	0.118
	Average 1 & 3	0.235	0.198	0.152	0.351	0.570	0.585	0.284	0.227	0.057	0.284	0.321	0.101
	Average 2 & 4	0.189	0.321	0.000	0.321	1.000	0.510	0.374	0.349	0.060	0.409	0.315	0.118
SA-44	1	0.255	0.200	0.142	0.342	0.586	0.597	0.290	0.256	0.058	0.314	0.324	0.100
	2	0.210	0.276	0.050	0.326	0.846	0.536	0.323	0.207	0.064	0.271	0.320	0.101
	3	0.277	0.193	0.127	0.321	0.603	0.598	0.297	0.255	0.056	0.312	0.316	0.103
	4	0.197	0.200	0.123	0.323	0.618	0.520	0.256	0.193	0.064	0.257	0.317	0.096
	Average 1 & 3	0.266	0.197	0.134	0.331	0.595	0.598	0.293	0.256	0.057	0.313	0.320	0.102
	Average 2 & 4	0.204	0.238	0.087	0.325	0.732	0.528	0.289	0.200	0.064	0.264	0.318	0.098
SA-45	1	0.256	0.194	0.127	0.321	0.605	0.576	0.284	0.193	0.055	0.248	0.248	0.099
	2	0.234	0.284	0.053	0.336	0.844	0.571	0.306	0.191	0.067	0.189	0.330	0.116
	3	0.222	0.213	0.125	0.339	0.630	0.560	0.281	0.171	0.063	0.234	0.234	0.111
	4	0.205	0.284	0.075	0.359	0.792	0.564	0.349	0.302	0.061	0.363	0.317	0.133

Specimen	Weld Location	d ₁ (in)	d ₂ (in)	d ₃ (in)	d ₄ (in)	d ₂ /d ₄	d ₅ (in)	T (in)	h ₁ (in)	h ₂ (in)	h (in)	t _r (in)	A _w (in ²)
	Average 1 & 3	0.239	0.204	0.126	0.330	0.618	0.568	0.283	0.182	0.059	0.241	0.241	0.105
	Average 2 & 4	0.220	0.284	0.064	0.347	0.818	0.567	0.328	0.247	0.064	0.276	0.323	0.124
SA-46	1	0.261	0.200	0.135	0.334	0.597	0.596	0.290	0.230	0.058	0.288	0.319	0.101
	2	0.202	0.221	0.102	0.323	0.684	0.525	0.267	0.186	0.064	0.250	0.317	0.098
	3	0.265	0.185	0.141	0.326	0.568	0.591	0.282	0.241	0.059	0.300	0.321	0.098
	4	0.251	0.177	0.150	0.327	0.542	0.578	0.238	0.166	0.064	0.230	0.321	0.095
	Average 1 & 3	0.263	0.192	0.138	0.330	0.582	0.593	0.286	0.236	0.058	0.294	0.320	0.099
	Average 2 & 4	0.226	0.199	0.126	0.325	0.613	0.552	0.253	0.176	0.064	0.240	0.319	0.096
SA-47	1	0.278	0.143	0.180	0.324	0.443	0.601	0.251	0.213	0.052	0.265	0.320	0.092
	2	0.362	0.085	0.246	0.331	0.255	0.693	0.222	0.187	0.067	0.254	0.324	0.091
	3	0.242	0.196	0.129	0.324	0.604	0.567	0.286	0.237	0.054	0.291	0.320	0.099
	4	0.211	0.256	0.081	0.337	0.759	0.548	0.296	0.176	0.068	0.244	0.330	0.105
	Average 1 & 3	0.260	0.170	0.154	0.324	0.523	0.584	0.269	0.225	0.053	0.278	0.320	0.095
	Average 2 & 4	0.287	0.170	0.164	0.334	0.507	0.620	0.259	0.181	0.068	0.249	0.327	0.098

Specimen	Weld Location	d₁ (in)	d₂ (in)	d₃ (in)	d₄ (in)	d₂/d₄	d₅ (in)	T (in)	h₁ (in)	h₂ (in)	h (in)	t_r (in)	A_w (in²)
SA-48	1	0.245	0.231	0.115	0.346	0.667	0.591	0.304	0.229	0.063	0.291	0.320	0.095
	2	0.278	0.153	0.181	0.334	0.459	0.612	0.253	0.229	0.058	0.287	0.315	0.093
	3	0.271	0.210	0.111	0.320	0.655	0.591	0.280	0.178	0.065	0.244	0.313	0.102
	4	0.250	0.218	0.113	0.331	0.658	0.581	0.294	0.209	0.061	0.270	0.325	0.108
	Average 1 & 3	0.258	0.220	0.113	0.333	0.661	0.591	0.292	0.203	0.064	0.267	0.317	0.098
	Average 2 & 4	0.264	0.185	0.147	0.332	0.559	0.597	0.273	0.219	0.059	0.278	0.320	0.101
Average	1 & 3	0.253	0.199	0.136	0.335	0.595	0.588	0.286	0.224	0.058	0.282	0.310	0.100
	2 & 4	0.226	0.249	0.086	0.335	0.745	0.560	0.307	0.216	0.064	0.276	0.322	0.106
	All	0.239	0.224	0.111	0.335	0.670	0.574	0.296	0.220	0.061	0.279	0.316	0.103
Standard Deviation	1 & 3	0.016	0.019	0.023	0.016	0.059	0.015	0.012	0.025	0.004	0.024	0.027	0.004
	2 & 4	0.049	0.071	0.072	0.014	0.215	0.053	0.050	0.070	0.004	0.071	0.007	0.011
	All	0.038	0.057	0.058	0.015	0.173	0.041	0.037	0.052	0.005	0.052	0.021	0.009

Table D.5 Weld Dimensions of SA-60 Series

Specimen	Weld Location	d ₁ (in)	d ₂ (in)	d ₃ (in)	d ₄ (in)	d ₂ /d ₄	d ₅ (in)	T (in)	h ₁ (in)	h ₂ (in)	h (in)	t _r (in)	A _w (in ²)
SA-61	1	0.227	0.261	0.091	0.353	0.741	0.579	0.320	0.185	0.065	0.250	0.326	0.100
	2	0.256	0.229	0.098	0.328	0.700	0.584	0.310	0.199	0.068	0.267	0.320	0.110
	3	0.253	0.241	0.096	0.337	0.716	0.590	0.313	0.232	0.061	0.293	0.322	0.107
	4	0.226	0.240	0.095	0.336	0.716	0.561	0.310	0.223	0.069	0.292	0.318	0.108
	Average 1 & 3	0.240	0.251	0.093	0.345	0.728	0.584	0.316	0.209	0.063	0.272	0.324	0.104
	Average 2 & 4	0.241	0.235	0.097	0.332	0.708	0.572	0.310	0.211	0.069	0.280	0.319	0.109
SA-62	1	0.235	0.236	0.083	0.319	0.740	0.554	0.314	0.226	0.056	0.282	0.314	0.113
	2	0.185	0.253	0.069	0.321	0.786	0.506	0.319	0.220	0.067	0.287	0.314	0.101
	3	0.222	0.222	0.114	0.337	0.660	0.559	0.302	0.220	0.059	0.279	0.318	0.105
	4	0.256	0.225	0.106	0.331	0.680	0.587	0.307	0.211	0.069	0.280	0.323	0.111
	Average 1 & 3	0.229	0.229	0.099	0.328	0.700	0.557	0.308	0.223	0.057	0.281	0.316	0.109
	Average 2 & 4	0.221	0.239	0.087	0.326	0.733	0.547	0.313	0.216	0.068	0.283	0.319	0.106
SA-63	1	0.241	0.229	0.135	0.363	0.630	0.604	0.321	0.240	0.066	0.306	0.319	0.109

Specimen	Weld Location	d ₁ (in)	d ₂ (in)	d ₃ (in)	d ₄ (in)	d ₂ /d ₄	d ₅ (in)	T (in)	h ₁ (in)	h ₂ (in)	h (in)	t _r (in)	A _w (in ²)
	2	0.245	0.260	0.077	0.337	0.771	0.582	0.320	0.206	0.059	0.265	0.265	0.116
	3	0.220	0.242	0.107	0.349	0.694	0.569	0.305	0.199	0.077	0.275	0.332	0.108
	4	0.219	0.249	0.081	0.329	0.755	0.549	0.315	0.193	0.058	0.252	0.324	0.110
	Average 1 & 3	0.231	0.235	0.121	0.356	0.662	0.586	0.313	0.219	0.071	0.291	0.325	0.108
	Average 2 & 4	0.232	0.254	0.079	0.333	0.763	0.565	0.318	0.200	0.059	0.258	0.295	0.113
SA-64	1	0.229	0.224	0.102	0.326	0.686	0.554	0.302	0.254	0.057	0.312	0.321	0.100
	2	0.247	0.227	0.094	0.321	0.708	0.568	0.284	0.157	0.067	0.223	0.314	0.110
	3	0.223	0.238	0.084	0.321	0.740	0.545	0.315	0.230	0.057	0.286	0.316	0.101
	4	0.171	0.257	0.059	0.315	0.814	0.486	0.311	0.172	0.064	0.237	0.308	0.102
	Average 1 & 3	0.226	0.231	0.093	0.324	0.713	0.549	0.308	0.242	0.057	0.299	0.319	0.100
	Average 2 & 4	0.209	0.242	0.076	0.318	0.761	0.527	0.297	0.164	0.066	0.230	0.311	0.106
SA-65	1	0.279	0.202	0.123	0.325	0.621	0.605	0.280	0.219	0.064	0.284	0.319	0.102
	2	0.416	0.021	0.297	0.318	0.065	0.734	0.185	0.430	0.051	0.480	0.314	0.087
	3	0.236	0.224	0.102	0.326	0.687	0.562	0.306	0.219	0.066	0.285	0.319	0.104
	4	0.222	0.205	0.121	0.326	0.628	0.548	0.274	0.184	0.056	0.240	0.321	0.082

Specimen	Weld Location	d ₁ (in)	d ₂ (in)	d ₃ (in)	d ₄ (in)	d ₂ /d ₄	d ₅ (in)	T (in)	h ₁ (in)	h ₂ (in)	h (in)	t _r (in)	A _w (in ²)
	Average 1 & 3	0.258	0.213	0.113	0.326	0.654	0.583	0.293	0.219	0.065	0.284	0.319	0.103
	Average 2 & 4	0.319	0.113	0.209	0.322	0.347	0.641	0.230	0.307	0.054	0.360	0.317	0.085
SA-66	1	0.243	0.230	0.093	0.323	0.713	0.566	0.303	0.205	0.056	0.262	0.318	0.104
	2	0.236	0.249	0.070	0.319	0.780	0.555	0.309	0.246	0.066	0.312	0.312	0.121
	3	0.231	0.241	0.088	0.329	0.733	0.560	0.316	0.246	0.057	0.303	0.324	0.111
	4	0.235	0.223	0.098	0.321	0.696	0.556	0.297	0.202	0.066	0.268	0.314	0.109
	Average 1 & 3	0.237	0.235	0.090	0.326	0.723	0.563	0.309	0.226	0.057	0.282	0.321	0.108
	Average 2 & 4	0.236	0.236	0.084	0.320	0.738	0.556	0.303	0.224	0.066	0.290	0.313	0.115
SA-67	1	0.231	0.228	0.092	0.320	0.712	0.552	0.301	0.230	0.055	0.285	0.316	0.100
	2	0.251	0.232	0.090	0.322	0.721	0.572	0.314	0.228	0.065	0.293	0.315	0.110
	3	0.206	0.217	0.105	0.321	0.674	0.527	0.296	0.216	0.055	0.270	0.317	0.098
	4	0.268	0.214	0.105	0.319	0.671	0.587	0.307	0.221	0.062	0.283	0.313	0.108
	Average 1 & 3	0.219	0.222	0.099	0.321	0.693	0.540	0.298	0.223	0.055	0.278	0.316	0.099
	Average 2 & 4	0.259	0.223	0.097	0.320	0.696	0.580	0.310	0.225	0.064	0.288	0.314	0.109

Specimen	Weld Location	d ₁ (in)	d ₂ (in)	d ₃ (in)	d ₄ (in)	d ₂ /d ₄	d ₅ (in)	T (in)	h ₁ (in)	h ₂ (in)	h (in)	t _r (in)	A _w (in ²)
SA-68	1	0.219	0.250	0.167	0.417	0.600	0.636	0.324	0.227	0.056	0.283	0.328	0.091
	2	0.297	0.175	0.152	0.327	0.535	0.624	0.250	0.256	0.067	0.325	0.320	0.100
	3	0.196	0.233	0.103	0.335	0.694	0.532	0.296	0.209	0.059	0.268	0.330	0.094
	4	0.214	0.226	0.143	0.369	0.613	0.583	0.287	0.251	0.066	0.317	0.314	0.104
	Average 1 & 3	0.208	0.241	0.135	0.376	0.647	0.584	0.310	0.218	0.057	0.275	0.329	0.093
	Average 2 & 4	0.256	0.201	0.147	0.348	0.574	0.603	0.268	0.253	0.067	0.321	0.317	0.102
Average	1 & 3	0.231	0.232	0.105	0.338	0.690	0.568	0.307	0.222	0.060	0.283	0.321	0.103
	2 & 4	0.246	0.218	0.110	0.327	0.665	0.574	0.294	0.225	0.064	0.289	0.313	0.106
	All	0.239	0.225	0.107	0.332	0.677	0.571	0.300	0.224	0.062	0.286	0.317	0.104
Standard Deviation	1 & 3	0.019	0.014	0.022	0.025	0.044	0.028	0.012	0.018	0.006	0.016	0.005	0.006
	2 & 4	0.054	0.057	0.056	0.013	0.175	0.054	0.035	0.061	0.005	0.059	0.014	0.010
	All	0.041	0.041	0.042	0.020	0.126	0.042	0.026	0.044	0.006	0.042	0.011	0.008

Table D.6 Weld Dimensions of SA-80 Series

Specimen	Weld Location	d ₁ (in)	d ₂ (in)	d ₃ (in)	d ₄ (in)	d ₂ /d ₄	d ₅ (in)	T (in)	h ₁ (in)	h ₂ (in)	h (in)	t _r (in)	A _w (in ²)
SA-81	1	0.374	0.167	0.153	0.320	0.521	0.693	0.263	0.193	0.059	0.252	0.315	0.100
	2	0.083	0.139	0.166	0.305	0.456	0.387	0.154	0.066	0.000	0.066	0.304	0.022
	3	0.436	0.205	0.111	0.315	0.650	0.752	0.275	0.166	0.064	0.231	0.309	0.133
	4	0.348	0.159	0.102	0.261	0.609	0.609	0.278	0.235	0.003	0.238	0.312	0.171
	Average 1 & 3	0.405	0.186	0.132	0.318	0.585	0.723	0.269	0.180	0.062	0.241	0.312	0.116
	Average 2 & 4	0.215	0.149	0.134	0.283	0.532	0.498	0.216	0.151	0.001	0.152	0.308	0.096
SA-83	1	0.359	0.201	0.135	0.336	0.598	0.694	0.296	0.195	0.064	0.260	0.329	0.160
	2	0.290	0.216	0.112	0.329	0.658	0.619	0.277	0.167	0.058	0.226	0.323	0.157
	3	0.351	0.119	0.206	0.325	0.365	0.676	0.207	0.132	0.060	0.192	0.319	0.151
	4	0.299	0.219	0.097	0.316	0.692	0.615	0.282	0.181	0.062	0.242	0.310	0.112
	Average 1 & 3	0.355	0.160	0.171	0.330	0.530	0.685	0.251	0.164	0.062	0.226	0.324	0.155
	Average 2 & 4	0.295	0.218	0.105	0.322	0.675	0.617	0.280	0.174	0.060	0.234	0.317	0.134
SA-84	1	0.245	0.266	0.074	0.340	0.784	0.585	0.305	0.142	0.063	0.206	0.334	0.150

Specimen	Weld Location	d ₁ (in)	d ₂ (in)	d ₃ (in)	d ₄ (in)	d ₂ /d ₄	d ₅ (in)	T (in)	h ₁ (in)	h ₂ (in)	h (in)	t _r (in)	A _w (in ²)
	2	0.312	0.216	0.106	0.321	0.672	0.633	0.295	0.198	0.058	0.256	0.316	0.133
	3	0.265	0.258	0.091	0.349	0.739	0.614	0.313	0.183	0.066	0.249	0.343	0.153
	4	0.337	0.254	0.068	0.323	0.788	0.660	0.328	0.200	0.061	0.261	0.317	0.186
	Average 1 & 3	0.255	0.262	0.082	0.345	0.762	0.599	0.309	0.163	0.065	0.227	0.338	0.152
	Average 2 & 4	0.324	0.235	0.087	0.322	0.730	0.646	0.311	0.199	0.059	0.258	0.317	0.160
SA-85	1	0.289	0.263	0.056	0.319	0.823	0.608	0.325	0.187	0.059	0.246	0.313	0.151
	2	0.312	0.283	0.064	0.347	0.815	0.659	0.339	0.184	0.068	0.252	0.340	0.197
	3	0.322	0.213	0.113	0.326	0.653	0.648	0.279	0.164	0.058	0.222	0.320	0.111
	4	0.321	0.212	0.119	0.331	0.641	0.657	0.284	0.178	0.065	0.243	0.324	0.148
	Average 1 & 3	0.306	0.238	0.085	0.322	0.738	0.628	0.302	0.175	0.059	0.234	0.317	0.131
	Average 2 & 4	0.317	0.247	0.091	0.339	0.728	0.658	0.311	0.181	0.066	0.247	0.332	0.173
SA-86	1	0.319	0.234	0.109	0.343	0.683	0.662	0.303	0.176	0.069	0.245	0.336	0.151
	2	0.297	0.220	0.110	0.330	0.668	0.627	0.306	0.198	0.059	0.257	0.324	0.153
	3	0.389	0.208	0.114	0.322	0.646	0.711	0.307	0.211	0.061	0.273	0.316	0.162
	4	0.253	0.226	0.106	0.332	0.679	0.585	0.289	0.170	0.061	0.231	0.326	0.150

Specimen	Weld Location	d ₁ (in)	d ₂ (in)	d ₃ (in)	d ₄ (in)	d ₂ /d ₄	d ₅ (in)	T (in)	h ₁ (in)	h ₂ (in)	h (in)	t _r (in)	A _w (in ²)
	Average 1 & 3	0.354	0.221	0.111	0.332	0.665	0.686	0.305	0.194	0.065	0.259	0.326	0.157
	Average 2 & 4	0.275	0.223	0.108	0.331	0.674	0.606	0.298	0.184	0.060	0.244	0.325	0.152
SA-87	1	0.313	0.263	0.075	0.338	0.777	0.651	0.326	0.186	0.068	0.254	0.332	0.147
	2	0.322	0.238	0.088	0.325	0.730	0.648	0.313	0.192	0.055	0.247	0.321	0.172
	3	0.375	0.193	0.139	0.331	0.582	0.706	0.292	0.177	0.063	0.239	0.325	0.145
	4	0.275	0.252	0.078	0.331	0.762	0.607	0.310	0.171	0.061	0.232	0.326	0.150
	Average 1 & 3	0.344	0.228	0.107	0.335	0.679	0.679	0.309	0.181	0.065	0.246	0.328	0.146
	Average 2 & 4	0.299	0.245	0.083	0.328	0.746	0.627	0.311	0.182	0.058	0.240	0.323	0.161
SA-88	1	0.324	0.195	0.139	0.334	0.584	0.658	0.290	0.205	0.059	0.264	0.329	0.150
	2	0.348	0.203	0.134	0.337	0.601	0.685	0.289	0.196	0.066	0.262	0.330	0.150
	3	0.276	0.183	0.159	0.342	0.535	0.618	0.263	0.163	0.062	0.225	0.336	0.098
	4	0.331	0.236	0.096	0.332	0.710	0.663	0.293	0.161	0.067	0.228	0.325	0.150
	Average 1 & 3	0.300	0.189	0.149	0.338	0.560	0.638	0.277	0.184	0.061	0.245	0.333	0.124
	Average 2 & 4	0.340	0.219	0.115	0.335	0.656	0.674	0.291	0.179	0.067	0.245	0.328	0.150

Specimen	Weld Location	d ₁ (in)	d ₂ (in)	d ₃ (in)	d ₄ (in)	d ₂ /d ₄	d ₅ (in)	T (in)	h ₁ (in)	h ₂ (in)	h (in)	t _r (in)	A _w (in ²)
SA-89	1	0.311	0.209	0.122	0.331	0.633	0.641	0.282	0.117	0.067	0.184	0.324	0.130
	2	0.377	0.202	0.136	0.339	0.596	0.716	0.282	0.202	0.071	0.273	0.331	0.130
	3	0.166	0.139	0.179	0.319	0.435	0.485	0.151	0.032	0.056	0.088	0.314	0.105
	4	0.405	0.064	0.260	0.323	0.198	0.728	0.219	0.214	0.066	0.280	0.316	0.076
	Average 1 & 3	0.238	0.174	0.150	0.325	0.534	0.563	0.217	0.074	0.062	0.136	0.319	0.117
	Average 2 & 4	0.391	0.133	0.198	0.331	0.397	0.722	0.250	0.208	0.069	0.277	0.324	0.103
SA-810	1	0.330	0.168	0.169	0.337	0.499	0.667	0.253	0.162	0.065	0.226	0.331	0.152
	2	0.366	0.217	0.111	0.328	0.661	0.695	0.306	0.226	0.068	0.294	0.321	0.146
	3	0.344	0.176	0.151	0.327	0.539	0.670	0.265	0.151	0.062	0.212	0.321	0.162
	4	0.350	0.162	0.171	0.333	0.487	0.683	0.259	0.177	0.069	0.247	0.325	0.113
	Average 1 & 3	0.337	0.172	0.160	0.332	0.519	0.669	0.259	0.156	0.063	0.219	0.326	0.157
	Average 2 & 4	0.358	0.189	0.141	0.330	0.574	0.689	0.282	0.202	0.069	0.271	0.323	0.130
SA-811	1	0.315	0.220	0.113	0.333	0.660	0.648	0.291	0.178	0.061	0.240	0.327	0.163
	2	0.375	0.209	0.123	0.332	0.629	0.704	0.305	0.224	0.069	0.293	0.325	0.160
	3	0.349	0.180	0.148	0.327	0.549	0.676	0.259	0.168	0.060	0.228	0.322	0.156

Specimen	Weld Location	d ₁ (in)	d ₂ (in)	d ₃ (in)	d ₄ (in)	d ₂ /d ₄	d ₅ (in)	T (in)	h ₁ (in)	h ₂ (in)	h (in)	t _r (in)	A _w (in ²)
	4	0.313	0.215	0.121	0.336	0.640	0.649	0.296	0.190	0.070	0.259	0.329	0.136
	Average 1 & 3	0.332	0.200	0.130	0.330	0.604	0.662	0.275	0.173	0.061	0.234	0.325	0.160
	Average 2 & 4	0.344	0.212	0.122	0.334	0.634	0.677	0.301	0.207	0.070	0.276	0.327	0.148
SA-812	1	0.280	0.266	0.064	0.330	0.807	0.610	0.333	0.195	0.061	0.256	0.324	0.156
	2	0.354	0.220	0.117	0.337	0.652	0.691	0.315	0.226	0.069	0.295	0.330	0.138
	3	0.302	0.218	0.115	0.333	0.655	0.635	0.291	0.182	0.061	0.243	0.327	0.158
	4	0.304	0.216	0.116	0.332	0.652	0.636	0.302	0.202	0.069	0.271	0.325	0.146
	Average 1 & 3	0.291	0.242	0.089	0.331	0.731	0.622	0.312	0.189	0.061	0.249	0.326	0.157
	Average 2 & 4	0.329	0.218	0.117	0.335	0.652	0.663	0.308	0.214	0.069	0.283	0.327	0.142
SA-813	1	0.305	0.250	0.082	0.332	0.752	0.637	0.338	0.226	0.069	0.295	0.325	0.147
	2	0.270	0.265	0.062	0.327	0.810	0.596	0.333	0.196	0.060	0.255	0.321	0.160
	3	0.364	0.235	0.099	0.334	0.703	0.698	0.321	0.215	0.067	0.282	0.327	0.161
	4	0.283	0.277	0.056	0.333	0.832	0.616	0.338	0.191	0.060	0.250	0.327	0.161
	Average 1 & 3	0.335	0.242	0.091	0.333	0.727	0.668	0.330	0.221	0.068	0.289	0.326	0.154

Specimen	Weld Location	d ₁ (in)	d ₂ (in)	d ₃ (in)	d ₄ (in)	d ₂ /d ₄	d ₅ (in)	T (in)	h ₁ (in)	h ₂ (in)	h (in)	t _r (in)	A _w (in ²)
	Average 2 & 4	0.276	0.271	0.059	0.330	0.821	0.606	0.335	0.193	0.060	0.253	0.324	0.160
SA-814	1	0.306	0.223	0.107	0.330	0.676	0.636	0.299	0.189	0.061	0.250	0.324	0.152
	2	0.349	0.217	0.112	0.329	0.659	0.678	0.300	0.191	0.065	0.256	0.323	0.162
	3	0.265	0.252	0.081	0.334	0.756	0.599	0.326	0.197	0.061	0.259	0.328	0.146
	4	0.354	0.202	0.133	0.335	0.603	0.690	0.302	0.228	0.066	0.294	0.329	0.154
	Average 1 & 3	0.286	0.238	0.094	0.332	0.716	0.618	0.313	0.193	0.061	0.254	0.326	0.149
	Average 2 & 4	0.352	0.209	0.123	0.332	0.631	0.684	0.301	0.209	0.066	0.275	0.326	0.158
SA-815	1	0.354	0.209	0.119	0.329	0.636	0.684	0.295	0.195	0.065	0.260	0.323	0.159
	2	0.315	0.246	0.085	0.331	0.742	0.647	0.338	0.221	0.062	0.283	0.326	0.176
	3	0.367	0.237	0.098	0.336	0.706	0.702	0.323	0.243	0.067	0.309	0.329	0.181
	4	0.311	0.235	0.104	0.339	0.693	0.650	0.317	0.199	0.061	0.260	0.333	0.149
	Average 1 & 3	0.361	0.223	0.108	0.333	0.671	0.693	0.309	0.219	0.066	0.284	0.326	0.170
	Average 2 & 4	0.313	0.240	0.095	0.335	0.718	0.648	0.327	0.210	0.061	0.271	0.329	0.162
SA-816	1	0.282	0.274	0.061	0.336	0.817	0.617	0.342	0.222	0.060	0.282	0.330	0.163

Specimen	Weld Location	d ₁ (in)	d ₂ (in)	d ₃ (in)	d ₄ (in)	d ₂ /d ₄	d ₅ (in)	T (in)	h ₁ (in)	h ₂ (in)	h (in)	t _r (in)	A _w (in ²)
	2	0.325	0.232	0.093	0.325	0.714	0.650	0.313	0.198	0.063	0.260	0.319	0.156
	3	0.334	0.225	0.110	0.335	0.671	0.669	0.309	0.197	0.061	0.258	0.329	0.166
	4	0.343	0.237	0.097	0.334	0.709	0.677	0.318	0.209	0.064	0.274	0.328	0.157
	Average 1 & 3	0.308	0.249	0.086	0.335	0.744	0.643	0.326	0.209	0.060	0.270	0.330	0.164
	Average 2 & 4	0.334	0.235	0.095	0.330	0.712	0.664	0.315	0.204	0.064	0.267	0.323	0.156
Average	1 & 3	0.320	0.215	0.116	0.331	0.651	0.652	0.291	0.178	0.063	0.241	0.325	0.147
	2 & 4	0.317	0.216	0.111	0.328	0.659	0.645	0.296	0.193	0.060	0.253	0.324	0.146
	All	0.319	0.216	0.114	0.330	0.655	0.648	0.293	0.186	0.061	0.247	0.324	0.146
Standard Deviation	1 & 3	0.043	0.032	0.030	0.006	0.087	0.041	0.032	0.035	0.003	0.036	0.006	0.017
	2 & 4	0.042	0.036	0.032	0.013	0.101	0.052	0.030	0.018	0.017	0.032	0.006	0.022
	All	0.042	0.034	0.031	0.010	0.093	0.046	0.031	0.028	0.012	0.034	0.006	0.019

Table D.7 Weld Dimensions of OB Series

Specimen	Weld Location	d ₁ (in)	d ₂ (in)	d ₃ (in)	d ₄ (in)	d ₂ /d ₄	d ₅ (in)	T (in)	h ₁ (in)	h ₂ (in)	h (in)	t _r (in)	A _w (in ²)
OB-1	1	0.448	0.094	0.234	0.328	0.288	0.776	0.262	0.254	0.074	0.328	0.319	0.114
	2	0.213	0.241	0.088	0.329	0.732	0.542	0.342	0.255	0.085	0.341	0.317	0.102
	3	0.364	0.204	0.127	0.331	0.616	0.695	0.314	0.265	0.075	0.341	0.322	0.123
	4	0.238	0.215	0.126	0.341	0.630	0.579	0.312	0.200	0.090	0.290	0.329	0.112
	Average 1 & 3	0.406	0.149	0.180	0.330	0.452	0.736	0.288	0.259	0.075	0.334	0.321	0.119
	Average 2 & 4	0.225	0.228	0.107	0.335	0.681	0.560	0.327	0.227	0.088	0.315	0.323	0.107
OB-2	1	0.361	0.220	0.117	0.337	0.652	0.697	0.329	0.246	0.076	0.321	0.328	0.130
	2	0.264	0.240	0.088	0.329	0.731	0.593	0.337	0.224	0.087	0.311	0.317	0.128
	3	0.345	0.199	0.130	0.329	0.604	0.067	0.325	0.277	0.074	0.351	0.321	0.129
	4	0.267	0.200	0.129	0.329	0.609	0.596	0.320	0.225	0.086	0.311	0.318	0.115
	Average 1 & 3	0.353	0.209	0.124	0.333	0.651	0.382	0.327	0.261	0.075	0.336	0.325	0.129
	Average 2 & 4	0.266	0.220	0.108	0.329	0.670	0.594	0.329	0.225	0.086	0.311	0.317	0.121
OB-3	1	0.356	0.228	0.120	0.348	0.656	0.704	0.322	0.195	0.074	0.269	0.340	0.150

Specimen	Weld Location	d ₁ (in)	d ₂ (in)	d ₃ (in)	d ₄ (in)	d ₂ /d ₄	d ₅ (in)	T (in)	h ₁ (in)	h ₂ (in)	h (in)	t _r (in)	A _w (in ²)
	2	0.285	0.242	0.071	0.313	0.774	0.598	0.348	0.241	0.061	0.302	0.307	0.127
	3	0.332	0.224	0.103	0.327	0.684	0.661	0.319	0.212	0.069	0.281	0.322	0.136
	4	0.310	0.199	0.108	0.307	0.647	0.617	0.314	0.227	0.061	0.287	0.301	0.116
	Average 1 & 3	0.344	0.226	0.111	0.337	0.670	0.682	0.320	0.203	0.072	0.275	0.331	0.143
	Average 2 & 4	0.298	0.220	0.090	0.310	0.711	0.608	0.331	0.234	0.061	0.295	0.304	0.122
OB-4	1	0.306	0.304	0.015	0.319	0.954	0.625	0.356	0.192	0.062	0.254	0.313	0.129
	2	0.307	0.226	0.100	0.327	0.691	0.634	0.324	0.238	0.082	0.320	0.316	0.129
	3	0.349	0.209	0.109	0.318	0.657	0.668	0.328	0.255	0.061	0.316	0.313	0.129
	4	0.253	0.240	0.114	0.354	0.677	0.636	0.326	0.235	0.095	0.330	0.340	0.129
	Average 1 & 3	0.328	0.257	0.062	0.318	0.806	0.646	0.342	0.223	0.061	0.285	0.313	0.129
	Average 2 & 4	0.280	0.233	0.107	0.341	0.684	0.635	0.325	0.236	0.088	0.325	0.328	0.129
OB-5	1	0.296	0.222	0.116	0.337	0.659	0.633	0.320	0.224	0.092	0.316	0.325	0.105
	2	0.338	0.220	0.121	0.341	0.646	0.679	0.323	0.241	0.078	0.319	0.332	0.110
	3	0.290	0.222	0.109	0.332	0.670	0.622	0.324	0.214	0.089	0.303	0.319	0.130
	4	0.332	0.204	0.131	0.335	0.610	0.667	0.313	0.250	0.079	0.329	0.326	0.144

Specimen	Weld Location	d ₁ (in)	d ₂ (in)	d ₃ (in)	d ₄ (in)	d ₂ /d ₄	d ₅ (in)	T (in)	h ₁ (in)	h ₂ (in)	h (in)	t _r (in)	A _w (in ²)
	Average 1 & 3	0.293	0.222	0.113	0.334	0.665	0.628	0.322	0.219	0.090	0.309	0.322	0.118
	Average 2 & 4	0.335	0.212	0.126	0.338	0.628	0.673	0.318	0.245	0.078	0.324	0.329	0.127
OB-6	1	0.305	0.221	0.108	0.330	0.672	0.634	0.305	0.210	0.089	0.299	0.317	0.120
	2	0.326	0.203	0.133	0.336	0.605	0.662	0.307	0.230	0.076	0.306	0.328	0.133
	3	0.288	0.228	0.120	0.348	0.655	0.636	0.327	0.225	0.095	0.320	0.335	0.130
	4	0.351	0.185	0.161	0.345	0.535	0.696	0.306	0.249	0.077	0.327	0.336	0.129
	Average 1 & 3	0.296	0.225	0.114	0.339	0.663	0.635	0.316	0.218	0.092	0.310	0.326	0.125
	Average 2 & 4	0.338	0.194	0.147	0.341	0.570	0.679	0.306	0.240	0.077	0.316	0.332	0.131
OB-7	1	0.339	0.202	0.142	0.344	0.587	0.683	0.307	0.226	0.077	0.303	0.335	0.125
	2	0.293	0.225	0.103	0.328	0.685	0.621	0.310	0.194	0.087	0.281	0.317	0.138
	3	0.328	0.243	0.088	0.331	0.733	0.659	0.341	0.236	0.072	0.308	0.323	0.142
	4	0.310	0.271	0.074	0.345	0.785	0.655	0.338	0.195	0.090	0.285	0.333	0.145
	Average 1 & 3	0.333	0.222	0.115	0.338	0.660	0.671	0.324	0.231	0.075	0.305	0.329	0.133
	Average 2 & 4	0.301	0.248	0.089	0.337	0.735	0.638	0.324	0.195	0.089	0.283	0.325	0.142

Specimen	Weld Location	d ₁ (in)	d ₂ (in)	d ₃ (in)	d ₄ (in)	d ₂ /d ₄	d ₅ (in)	T (in)	h ₁ (in)	h ₂ (in)	h (in)	t _r (in)	A _w (in ²)
OB-8	1	0.332	0.235	0.097	0.332	0.708	0.664	0.333	0.229	0.074	0.303	0.324	0.139
	2	0.313	0.207	0.125	0.332	0.624	0.645	0.299	0.190	0.086	0.276	0.321	0.110
	3	0.366	0.230	0.101	0.332	0.694	0.698	0.329	0.261	0.073	0.333	0.324	0.126
	4	0.340	0.204	0.126	0.330	0.618	0.671	0.307	0.232	0.086	0.318	0.319	0.128
	Average 1 & 3	0.349	0.233	0.099	0.332	0.701	0.681	0.331	0.245	0.074	0.318	0.324	0.133
	Average 2 & 4	0.327	0.206	0.125	0.331	0.621	0.658	0.303	0.211	0.086	0.297	0.320	0.119
OB-9	1	0.338	0.252	0.066	0.319	0.792	0.656	0.328	0.202	0.062	0.264	0.313	0.120
	2	0.311	0.205	0.127	0.332	0.618	0.644	0.345	0.228	0.062	0.320	0.327	0.130
	3	0.371	0.233	0.085	0.318	0.733	0.689	0.329	0.238	0.059	0.297	0.313	0.110
	4	0.327	0.174	0.146	0.320	0.545	0.647	0.282	0.244	0.063	0.307	0.314	0.114
	Average 1 & 3	0.354	0.243	0.076	0.318	0.763	0.673	0.329	0.220	0.061	0.281	0.313	0.115
	Average 2 & 4	0.319	0.190	0.136	0.326	0.581	0.645	0.313	0.236	0.062	0.313	0.320	0.122
OB-10	1	0.339	0.176	0.166	0.341	0.515	0.680	0.278	0.220	0.083	0.303	0.331	0.108
	2	0.309	0.242	0.072	0.314	0.772	0.622	0.346	0.246	0.072	0.317	0.305	0.130
	3	0.329	0.178	0.151	0.329	0.541	0.657	0.293	0.218	0.084	0.302	0.318	0.101

Specimen	Weld Location	d ₁ (in)	d ₂ (in)	d ₃ (in)	d ₄ (in)	d ₂ /d ₄	d ₅ (in)	T (in)	h ₁ (in)	h ₂ (in)	h (in)	t _r (in)	A _w (in ²)
	4	0.308	0.241	0.096	0.337	0.715	0.645	0.340	0.238	0.079	0.317	0.327	0.140
	Average 1 & 3	0.334	0.177	0.158	0.335	0.528	0.668	0.286	0.219	0.083	0.302	0.325	0.105
	Average 2 & 4	0.309	0.241	0.084	0.325	0.743	0.634	0.343	0.242	0.075	0.317	0.316	0.135
OB-11	1	0.350	0.149	0.193	0.342	0.436	0.692	0.279	0.228	0.083	0.310	0.331	0.108
	2	0.290	0.176	0.147	0.323	0.546	0.613	0.295	0.221	0.077	0.298	0.314	0.119
	3	0.345	0.215	0.116	0.331	0.649	0.675	0.313	0.235	0.083	0.318	0.320	0.140
	4	0.299	0.220	0.112	0.332	0.664	0.630	0.326	0.236	0.079	0.314	0.322	0.135
	Average 1 & 3	0.347	0.182	0.154	0.336	0.542	0.683	0.296	0.231	0.083	0.314	0.326	0.124
	Average 2 & 4	0.294	0.198	0.129	0.327	0.605	0.622	0.310	0.228	0.078	0.306	0.318	0.127
OB-12	1	0.341	0.233	0.121	0.355	0.658	0.696	0.321	0.198	0.089	0.286	0.343	0.119
	2	0.339	0.200	0.131	0.331	0.604	0.671	0.309	0.233	0.078	0.311	0.322	0.121
	3	0.354	0.219	0.114	0.333	0.659	0.686	0.319	0.214	0.084	0.298	0.322	0.121
	4	0.323	0.231	0.098	0.329	0.701	0.652	0.325	0.225	0.077	0.302	0.320	0.135
	Average 1 & 3	0.347	0.226	0.117	0.344	0.658	0.691	0.320	0.206	0.086	0.292	0.333	0.120

Specimen	Weld Location	d ₁ (in)	d ₂ (in)	d ₃ (in)	d ₄ (in)	d ₂ /d ₄	d ₅ (in)	T (in)	h ₁ (in)	h ₂ (in)	h (in)	t _r (in)	A _w (in ²)
	Average 2 & 4	0.331	0.215	0.115	0.330	0.652	0.661	0.317	0.229	0.078	0.307	0.321	0.128
OB-13	1	0.345	0.242	0.095	0.336	0.719	0.681	0.323	0.211	0.090	0.301	0.324	0.134
	2	0.327	0.202	0.127	0.329	0.614	0.656	0.301	0.217	0.076	0.292	0.320	0.122
	3	0.331	0.211	0.121	0.332	0.635	0.663	0.310	0.218	0.088	0.306	0.320	0.135
	4	0.346	0.141	0.200	0.342	0.413	0.688	0.279	0.216	0.082	0.298	0.332	0.119
	Average 1 & 3	0.338	0.226	0.108	0.334	0.677	0.672	0.316	0.214	0.089	0.303	0.322	0.134
	Average 2 & 4	0.337	0.172	0.164	0.335	0.514	0.672	0.290	0.217	0.079	0.295	0.326	0.121
OB-14	1	0.339	0.167	0.166	0.333	0.501	0.672	0.300	0.228	0.077	0.305	0.324	0.117
	2	0.339	0.188	0.143	0.331	0.568	0.670	0.299	0.204	0.087	0.290	0.319	0.125
	3	0.290	0.216	0.121	0.337	0.641	0.626	0.332	0.229	0.079	0.307	0.327	0.125
	4	0.335	0.201	0.137	0.338	0.595	0.673	0.308	0.228	0.087	0.314	0.327	0.122
	Average 1 & 3	0.314	0.191	0.144	0.335	0.571	0.649	0.316	0.228	0.078	0.306	0.326	0.121
	Average 2 & 4	0.337	0.194	0.140	0.334	0.582	0.672	0.303	0.216	0.087	0.302	0.323	0.123
OB-15	1	0.257	0.213	0.129	0.342	0.624	0.599	0.315	0.242	0.075	0.317	0.334	0.110

Specimen	Weld Location	d ₁ (in)	d ₂ (in)	d ₃ (in)	d ₄ (in)	d ₂ /d ₄	d ₅ (in)	T (in)	h ₁ (in)	h ₂ (in)	h (in)	t _r (in)	A _w (in ²)
	2	0.325	0.192	0.134	0.327	0.588	0.651	0.297	0.223	0.085	0.308	0.315	0.124
	3	0.253	0.223	0.109	0.332	0.672	0.585	0.307	0.307	0.078	0.385	0.323	0.110
	4	0.318	0.222	0.108	0.330	0.674	0.648	0.315	0.230	0.087	0.317	0.318	0.126
	Average 1 & 3	0.255	0.218	0.119	0.337	0.648	0.592	0.311	0.274	0.077	0.351	0.328	0.110
	Average 2 & 4	0.321	0.207	0.121	0.328	0.631	0.650	0.306	0.227	0.086	0.313	0.317	0.125
OB-16	1	0.376	0.172	0.160	0.332	0.517	0.708	0.291	0.220	0.082	0.302	0.321	0.110
	2	0.213	0.216	0.109	0.326	0.665	0.539	0.353	0.279	0.073	0.351	0.317	0.117
	3	0.391	0.171	0.160	0.331	0.516	0.722	0.336	0.295	0.084	0.379	0.320	0.127
	4	0.248	0.212	0.118	0.329	0.643	0.577	0.319	0.220	0.075	0.295	0.321	0.102
	Average 1 & 3	0.383	0.171	0.160	0.332	0.516	0.715	0.313	0.257	0.083	0.341	0.321	0.119
	Average 2 & 4	0.231	0.214	0.113	0.327	0.654	0.558	0.336	0.249	0.074	0.323	0.319	0.110
Average	1 & 3	0.336	0.211	0.122	0.333	0.636	0.650	0.316	0.232	0.078	0.310	0.324	0.124
	2 & 4	0.303	0.212	0.119	0.331	0.641	0.635	0.318	0.229	0.079	0.309	0.321	0.124
	All	0.319	0.212	0.120	0.332	0.639	0.643	0.317	0.230	0.079	0.309	0.322	0.124
Standard Deviation	1 & 3	0.035	0.029	0.031	0.007	0.092	0.079	0.015	0.021	0.009	0.022	0.006	0.010

Specimen	Weld Location	d₁ (in)	d₂ (in)	d₃ (in)	d₄ (in)	d₂/d₄	d₅ (in)	T (in)	h₁ (in)	h₂ (in)	h (in)	t_r (in)	A_w (in²)
	2 & 4	0.036	0.020	0.022	0.008	0.063	0.038	0.014	0.014	0.009	0.012	0.006	0.009
	All	0.039	0.024	0.027	0.007	0.078	0.062	0.014	0.018	0.009	0.017	0.006	0.009

Table D.8 Weld Dimensions of UB Series

Specimen	Weld Location	d ₁ (in)	d ₂ (in)	d ₃ (in)	d ₄ (in)	d ₂ /d ₄	d ₅ (in)	T (in)	h ₁ (in)	h ₂ (in)	h (in)	t _r (in)	A _w (in ²)
UB-1	1	0.251	0.223	0.113	0.335	0.664	0.587	0.332	0.235	0.087	0.322	0.324	0.112
	2	0.345	0.166	0.166	0.333	0.500	0.678	0.280	0.218	0.083	0.301	0.322	0.116
	3	0.262	0.211	0.120	0.331	0.637	0.593	0.318	0.230	0.082	0.312	0.321	0.110
	4	0.347	0.203	0.129	0.332	0.612	0.679	0.303	0.218	0.079	0.294	0.322	0.114
	Average 1 & 3	0.257	0.217	0.116	0.333	0.651	0.590	0.325	0.232	0.085	0.317	0.322	0.111
	Average 2 & 4	0.346	0.185	0.148	0.332	0.556	0.678	0.291	0.218	0.081	0.297	0.322	0.115
UB-2	1	0.322	0.183	0.151	0.334	0.549	0.656	0.293	0.267	0.078	0.345	0.325	0.110
	2	0.261	0.224	0.110	0.334	0.669	0.595	0.327	0.282	0.083	0.371	0.324	0.122
	3	0.311	0.241	0.094	0.334	0.720	0.645	0.321	0.215	0.083	0.298	0.324	0.115
	4	0.270	0.250	0.086	0.336	0.744	0.606	0.336	0.223	0.080	0.302	0.326	0.112
	Average 1 & 3	0.317	0.212	0.122	0.334	0.688	0.651	0.307	0.241	0.080	0.321	0.325	0.112
	Average 2 & 4	0.266	0.237	0.098	0.335	0.707	0.600	0.332	0.252	0.081	0.336	0.325	0.117
UB-3	1	0.281	0.226	0.080	0.306	0.740	0.587	0.344	0.263	0.063	0.326	0.299	0.109

Specimen	Weld Location	d ₁ (in)	d ₂ (in)	d ₃ (in)	d ₄ (in)	d ₂ /d ₄	d ₅ (in)	T (in)	h ₁ (in)	h ₂ (in)	h (in)	t _r (in)	A _w (in ²)
	2	0.367	0.177	0.157	0.334	0.529	0.701	0.286	0.216	0.081	0.296	0.324	0.126
	3	0.280	0.172	0.134	0.306	0.563	0.586	0.307	0.248	0.063	0.311	0.300	0.105
	4	0.337	0.148	0.183	0.332	0.447	0.669	0.275	0.240	0.078	0.318	0.323	0.113
	Average 1 & 3	0.281	0.199	0.107	0.306	0.651	0.587	0.325	0.256	0.063	0.318	0.300	0.107
	Average 2 & 4	0.352	0.163	0.170	0.333	0.488	0.685	0.280	0.228	0.079	0.307	0.323	0.119
UB-4	1	0.254	0.214	0.117	0.331	0.647	0.585	0.323	0.231	0.082	0.313	0.321	0.106
	2	0.344	0.144	0.169	0.312	0.459	0.656	0.276	0.234	0.077	0.311	0.303	0.116
	3	0.206	0.189	0.144	0.333	0.567	0.539	0.363	0.286	0.081	0.366	0.323	0.111
	4	0.370	0.156	0.176	0.332	0.469	0.702	0.285	0.232	0.083	0.315	0.321	0.111
	Average 1 & 3	0.230	0.201	0.130	0.332	0.607	0.562	0.343	0.258	0.081	0.340	0.322	0.108
	Average 2 & 4	0.357	0.150	0.173	0.322	0.464	0.679	0.281	0.233	0.080	0.313	0.312	0.113
UB-5	1	0.279	0.240	0.103	0.343	0.699	0.622	0.337	0.230	0.085	0.315	0.332	0.117
	2	0.333	0.137	0.192	0.329	0.417	0.662	0.264	0.207	0.083	0.290	0.318	0.106
	3	0.258	0.204	0.129	0.333	0.613	0.591	0.328	0.229	0.084	0.313	0.322	0.110
	4	0.329	0.202	0.129	0.331	0.609	0.660	0.297	0.220	0.080	0.300	0.322	0.114

Specimen	Weld Location	d₁ (in)	d₂ (in)	d₃ (in)	d₄ (in)	d₂/d₄	d₅ (in)	T (in)	h₁ (in)	h₂ (in)	h (in)	t_r (in)	A_w (in²)
	Average 1 & 3	0.269	0.222	0.116	0.338	0.656	0.607	0.332	0.229	0.085	0.314	0.327	0.113
	Average 2 & 4	0.331	0.170	0.161	0.330	0.513	0.661	0.281	0.213	0.081	0.295	0.320	0.110
UB-6	1	0.262	0.251	0.089	0.342	0.732	0.604	0.346	0.304	0.088	0.392	0.331	0.123
	2	0.356	0.175	0.154	0.330	0.532	0.686	0.283	0.214	0.082	0.296	0.319	0.118
	3	0.287	0.201	0.138	0.340	0.593	0.626	0.309	0.209	0.083	0.293	0.329	0.110
	4	0.337	0.193	0.140	0.333	0.580	0.670	0.298	0.222	0.081	0.303	0.323	0.108
	Average 1 & 3	0.274	0.226	0.114	0.341	0.662	0.615	0.327	0.257	0.085	0.342	0.330	0.117
	Average 2 & 4	0.346	0.184	0.147	0.331	0.556	0.678	0.290	0.218	0.081	0.299	0.321	0.113
UB-7	1	0.265	0.241	0.094	0.335	0.719	0.600	0.337	0.315	0.085	0.400	0.324	0.120
	2	0.327	0.191	0.142	0.333	0.573	0.660	0.287	0.205	0.086	0.291	0.322	0.120
	3	0.245	0.247	0.087	0.334	0.739	0.580	0.349	0.329	0.085	0.414	0.323	0.122
	4	0.321	0.179	0.152	0.331	0.541	0.653	0.287	0.225	0.080	0.304	0.322	0.109
	Average 1 & 3	0.255	0.244	0.091	0.335	0.729	0.590	0.343	0.322	0.085	0.407	0.324	0.121
	Average 2 & 4	0.324	0.185	0.147	0.332	0.557	0.657	0.287	0.215	0.083	0.297	0.322	0.115

Specimen	Weld Location	d ₁ (in)	d ₂ (in)	d ₃ (in)	d ₄ (in)	d ₂ /d ₄	d ₅ (in)	T (in)	h ₁ (in)	h ₂ (in)	h (in)	t _r (in)	A _w (in ²)
UB-8	1	0.247	0.224	0.115	0.338	0.661	0.585	0.342	0.277	0.082	0.359	0.328	0.105
	2	0.326	0.191	0.140	0.331	0.577	0.657	0.286	0.258	0.083	0.343	0.320	0.123
	3	0.248	0.254	0.083	0.338	0.753	0.586	0.345	0.321	0.084	0.404	0.327	0.129
	4	0.305	0.200	0.135	0.335	0.597	0.640	0.295	0.279	0.085	0.365	0.324	0.121
	Average 1 & 3	0.248	0.239	0.099	0.338	0.707	0.586	0.344	0.299	0.083	0.382	0.328	0.117
	Average 2 & 4	0.316	0.195	0.138	0.333	0.587	0.648	0.291	0.269	0.084	0.354	0.322	0.122
UB-9	1	0.280	0.249	0.084	0.333	0.747	0.613	0.341	0.316	0.079	0.394	0.324	0.128
	2	0.281	0.205	0.119	0.324	0.633	0.603	0.314	0.288	0.084	0.372	0.313	0.120
	3	0.251	0.259	0.072	0.331	0.782	0.058	0.366	0.303	0.080	0.383	0.322	0.137
	4	0.305	0.198	0.137	0.335	0.590	0.640	0.296	0.219	0.083	0.302	0.325	0.117
	Average 1 & 3	0.266	0.254	0.078	0.332	0.764	0.336	0.353	0.309	0.079	0.388	0.323	0.132
	Average 2 & 4	0.293	0.202	0.128	0.330	0.611	0.622	0.305	0.254	0.084	0.337	0.319	0.119
UB-10	1	0.273	0.244	0.088	0.332	0.734	0.605	0.332	0.285	0.084	0.370	0.321	0.118
	2	0.274	0.227	0.103	0.329	0.688	0.604	0.322	0.231	0.078	0.309	0.320	0.116
	3	0.262	0.221	0.113	0.334	0.662	0.595	0.317	0.228	0.086	0.315	0.322	0.123

Specimen	Weld Location	d ₁ (in)	d ₂ (in)	d ₃ (in)	d ₄ (in)	d ₂ /d ₄	d ₅ (in)	T (in)	h ₁ (in)	h ₂ (in)	h (in)	t _r (in)	A _w (in ²)
	4	0.308	0.225	0.108	0.333	0.677	0.641	0.349	0.280	0.074	0.354	0.324	0.128
	Average 1 & 3	0.267	0.232	0.100	0.333	0.698	0.600	0.325	0.257	0.085	0.342	0.322	0.121
	Average 2 & 4	0.291	0.226	0.105	0.331	0.682	0.622	0.335	0.256	0.076	0.332	0.322	0.122
UB-11	1	0.298	0.187	0.141	0.328	0.571	0.626	0.298	0.243	0.072	0.315	0.320	0.100
	2	0.276	0.211	0.126	0.337	0.626	0.613	0.311	0.225	0.087	0.312	0.325	0.114
	3	0.348	0.175	0.161	0.336	0.521	0.684	0.327	0.231	0.077	0.307	0.327	0.121
	4	0.270	0.203	0.128	0.331	0.614	0.602	0.311	0.239	0.083	0.322	0.321	0.115
	Average 1 & 3	0.323	0.181	0.151	0.332	0.546	0.655	0.312	0.237	0.075	0.311	0.323	0.111
	Average 2 & 4	0.273	0.207	0.127	0.334	0.620	0.607	0.311	0.232	0.085	0.317	0.323	0.115
UB-12	1	0.340	0.176	0.160	0.336	0.523	0.676	0.302	0.271	0.074	0.345	0.328	0.123
	2	0.295	0.193	0.140	0.333	0.581	0.628	0.292	0.205	0.085	0.290	0.322	0.119
	3	0.291	0.192	0.154	0.346	0.556	0.637	0.297	0.206	0.081	0.286	0.336	0.104
	4	0.263	0.157	0.169	0.326	0.482	0.589	0.283	0.225	0.082	0.307	0.315	0.096
	Average 1 & 3	0.316	0.184	0.157	0.341	0.540	0.657	0.300	0.238	0.077	0.316	0.332	0.113

Specimen	Weld Location	d ₁ (in)	d ₂ (in)	d ₃ (in)	d ₄ (in)	d ₂ /d ₄	d ₅ (in)	T (in)	h ₁ (in)	h ₂ (in)	h (in)	t _r (in)	A _w (in ²)
	Average 2 & 4	0.279	0.175	0.154	0.329	0.531	0.608	0.288	0.215	0.083	0.298	0.318	0.107
UB-13	1	0.343	0.148	0.186	0.334	0.444	0.677	0.270	0.212	0.070	0.282	0.326	0.117
	2	0.300	0.228	0.107	0.335	0.679	0.635	0.326	0.234	0.085	0.319	0.324	0.126
	3	0.361	0.157	0.181	0.338	0.465	0.699	0.264	0.237	0.073	0.310	0.330	0.126
	4	0.311	0.205	0.126	0.331	0.620	0.642	0.300	0.214	0.083	0.296	0.321	0.116
	Average 1 & 3	0.352	0.153	0.183	0.336	0.454	0.688	0.267	0.224	0.072	0.296	0.328	0.122
	Average 2 & 4	0.305	0.216	0.117	0.333	0.650	0.638	0.313	0.224	0.084	0.308	0.322	0.121
UB-14	1	0.307	0.218	0.120	0.338	0.644	0.645	0.306	0.222	0.094	0.315	0.325	0.117
	2	0.342	0.215	0.122	0.336	0.638	0.678	0.304	0.207	0.078	0.285	0.326	0.113
	3	0.282	0.216	0.120	0.336	0.643	0.618	0.315	0.233	0.086	0.319	0.325	0.113
	4	0.342	0.187	0.143	0.330	0.567	0.672	0.292	0.225	0.077	0.302	0.320	0.116
	Average 1 & 3	0.295	0.217	0.120	0.337	0.644	0.632	0.310	0.227	0.090	0.317	0.325	0.115
	Average 2 & 4	0.342	0.201	0.132	0.333	0.603	0.675	0.298	0.216	0.078	0.294	0.323	0.114
UB-15	1	0.318	0.243	0.089	0.333	0.731	0.650	0.339	0.267	0.076	0.343	0.324	0.119

Specimen	Weld Location	d₁ (in)	d₂ (in)	d₃ (in)	d₄ (in)	d₂/d₄	d₅ (in)	T (in)	h₁ (in)	h₂ (in)	h (in)	t_r (in)	A_w (in²)
	2	0.275	0.198	0.146	0.344	0.577	0.619	0.316	0.227	0.087	0.314	0.333	0.118
	3	0.343	0.187	0.143	0.330	0.567	0.673	0.290	0.213	0.077	0.290	0.321	0.119
	4	0.295	0.204	0.132	0.336	0.607	0.631	0.310	0.243	0.081	0.324	0.326	0.120
	Average 1 & 3	0.330	0.215	0.116	0.331	0.649	0.662	0.314	0.240	0.077	0.317	0.322	0.119
	Average 2 & 4	0.285	0.201	0.139	0.340	0.592	0.625	0.313	0.235	0.084	0.319	0.330	0.119
UB-16	1	0.268	0.188	0.148	0.336	0.559	0.604	0.315	0.252	0.083	0.335	0.326	0.112
	2	0.311	0.165	0.176	0.341	0.485	0.652	0.299	0.220	0.080	0.300	0.331	0.110
	3	0.254	0.199	0.139	0.339	0.588	0.593	0.298	0.310	0.083	0.393	0.328	0.097
	4	0.420	0.168	0.176	0.344	0.489	0.764	0.316	0.295	0.082	0.377	0.334	0.115
	Average 1 & 3	0.261	0.194	0.144	0.337	0.574	0.599	0.306	0.281	0.083	0.364	0.327	0.105
	Average 2 & 4	0.365	0.167	0.176	0.342	0.487	0.708	0.307	0.257	0.081	0.339	0.333	0.112
Average	1 & 3	0.284	0.212	0.122	0.334	0.639	0.601	0.321	0.257	0.080	0.337	0.324	0.115
	2 & 4	0.317	0.191	0.141	0.333	0.575	0.649	0.300	0.233	0.082	0.315	0.322	0.116
	All	0.300	0.202	0.131	0.333	0.607	0.625	0.311	0.245	0.081	0.326	0.323	0.116
Standard Deviation	1 & 3	0.034	0.026	0.027	0.008	0.079	0.079	0.021	0.030	0.007	0.032	0.007	0.007

Specimen	Weld Location	d₁ (in)	d₂ (in)	d₃ (in)	d₄ (in)	d₂/d₄	d₅ (in)	T (in)	h₁ (in)	h₂ (in)	h (in)	t_r (in)	A_w (in²)
	2 & 4	0.033	0.024	0.023	0.004	0.070	0.033	0.017	0.018	0.003	0.019	0.005	0.004
	All	0.037	0.027	0.026	0.006	0.080	0.064	0.022	0.027	0.005	0.028	0.006	0.006

Appendix E Effective Length (L_e) Measurements

Table E.1 L_e Values

Specimen	L_e (in)		Specimen	L_e (in)		Specimen	L_e (in)
GM-81	5-1/8"		FIL-1	4-7/8"		SA-41	5"
GM-82	5-3/16"		FIL-2	4-3/4"		SA-42	5"
GM-83	5-1/4"		FIL-3	4-3/4"		SA-43	5-1/16"
GM-84	5-1/16"		FIL-4	4-15/16"		SA-44	4-7/8"
GM-85	5-1/4"		FIL-5	4-7/8"		SA-45	4-15/16"
GM-86	5"		FIL-6	4-3/4"		SA-46	5-1/8"
GM-87	5-5/16"		FIL-7	4-15/16"		SA-47	5"
GM-88	5-3/16"		FIL-8	4-7/8"		SA-48	4-15/16"
GM-89	5-1/16"		SA-21	4-3/4"		SA-61	4-15/16"
GM-810	5"		SA-22	5-3/16"		SA-62	5-3/16"
GM-811	5-1/8"		SA-23	4-15/16"		SA-63	5-3/16"
GM-812	5"		SA-24	5-1/8"		SA-64	5"
GM-813	5-7/16"		SA-25	5-1/16"		SA-65	5"
GM-814	5-1/8"		SA-26	5-1/8"		SA-66	4-15/16"
GM-815	5-1/16"		SA-27	5-1/16"		SA-67	4-15/16"
GM-816	5-1/8"		SA-28	5-1/8"		SA-68	5"

Table E.1 L_e Values (Continued)

Specimen	L_e (in)		Specimen	L_e (in)		Specimen	L_e (in)
SA-81	4-7/8"		OB-1	4-13/32"		UB-1	4-5/8"
SA-83	4-3/4"		OB-2	4-19/32"		UB-2	4-5/8"
SA-84	5"		OB-3	4-15/32"		UB-3	4-5/8"
SA-85	4-7/8"		OB-4	4-5/8"		UB-4	4-9/16"
SA-86	4-3/4"		OB-5	4-11/16"		UB-5	4-11/16"
SA-87	4-11/16"		OB-6	4-3/4"		UB-6	4-9/16"
SA-88	4-25/32"		OB-7	4-19/32"		UB-7	4-5/8"
SA-89	4-27/32"		OB-8	4-3/4"		UB-8	4-3/4"
SA-810	4-5/8"		OB-9	4-5/8"		UB-9	4-11/16"
SA-811	4-7/8"		OB-10	4-9/16"		UB-10	N/A
SA-812	4-31/32"		OB-11	4-1/2"		UB-11	4-7/8"
SA-813	4-11/16"		OB-12	4-5/8"		UB-12	4-11/16"
SA-814	4-7/8"		OB-13	4-9/16"		UB-13	4-7/16"
SA-815	4-11/16"		OB-14	4-5/8"		UB-14	4-19/32"
SA-816	4-27/32"		OB-15	4-17/32"		UB-15	4-5/8"
			OB-16	4-17/32"		UB-16	4-1/2"

Appendix F Locations of Tack Welds and Crack Initiation Points

Table F.1 Location of Tack Welds and Crack Initiation Points

Specimen	# of tack welds on the crack surface	# of tack welds at the center	# of tack welds off the center	# of crack initiation locations	# of cracks initiated at center	# of cracks initiated off the center from tack welds	# of cracks initiated off the center w/o tack welds	Note
GM-81	0	0	0	1	1	0	0	
GM-82	0	0	0	1	1	0	0	
GM-83	0	0	0	1	1	0	0	
GM-84								WR
GM-85	0	0	0	1	1	0	0	
GM-86	1	0	1	1	1	0	0	N
GM-87	0	0	0	1	1	0	0	
GM-88	0	0	0	1	0	1	0	
GM-810	1	0	1	1	1	0	0	N
GM-814	0	0	0	1	1	0	0	
GM-816	0	0	0	1	1	0	0	

Specimen	# of tack welds on the crack surface	# of tack welds at the center	# of tack welds off the center	# of crack initiation locations	# of cracks initiated at center	# of cracks initiated off the center from tack welds	# of cracks initiated off the center w/o tack welds	Note
SA-61	1	0	1	1	0	1	0	CTC
SA-62	1	0	1	1	1	0	0	N
SA-63	1	0	1	2	1	1	0	Y
SA-64	1	0	1	1	1	0	0	N
SA-65	1	0	1	2	1	1	0	Y
SA-66	1	1	0	1	1	0	0	TBD
SA-67	1	0	1	1	0	1	0	Y
SA-68	1	0	1	1	0	1	0	Y
SA-41	1	0	1	1	0	1	0	CTC
SA-42	1	1	0	1	1	0	0	TBD
SA-43	1	1	0	1	1	0	0	TBD
SA-44	1	0	1	2	1	1	0	Y
SA-45	1	1	0	1	1	0	0	TBD
SA-46	1	0	1	1	1	0	0	N

Specimen	# of tack welds on the crack surface	# of tack welds at the center	# of tack welds off the center	# of crack initiation locations	# of cracks initiated at center	# of cracks initiated off the center from tack welds	# of cracks initiated off the center w/o tack welds	Note
SA-47	1	0	1	1	0	1	0	Y
SA-48	1	0	1	2	0	1	1	Y
SA-21	1	0	1	1	0	1	0	CTC
SA-22	1	0	1	2	1	1	0	Y
SA-23	1	1	0	1	1	0	0	TBD
SA-24	1	0	1	1	0	1	0	Y
SA-25	1	0	1	1	1	0	0	N
SA-26	1	0	1	1	0	1	0	Y
SA-27	0	0	0	1	0	0	1	
SA-28	2	0	2	2	0	1	1	Y
FIL-1	2	0	2	2	1	1	0	Y
FIL-2	2	0	2	1	1	0	0	N
FIL-3	1	0	1	1	1	0	0	N

Specimen	# of tack welds on the crack surface	# of tack welds at the center	# of tack welds off the center	# of crack initiation locations	# of cracks initiated at center	# of cracks initiated off the center from tack welds	# of cracks initiated off the center w/o tack welds	Note
FIL-4	1	1	0	1	1	0	0	TBD
FIL-5	1	0	1	1	1	0	0	N
FIL-6	1	0	1	1	1	0	0	N
FIL-7	1	0	1	1	1	0	0	N
FIL-8	2	0	2	1	1	0	0	N

Notes:

Y -- crack initiated from tack weld

N -- crack did not initiate from tack weld

CTC -- close to center; crack initiated from tack weld but they are both very close to center (in the middle ¼)

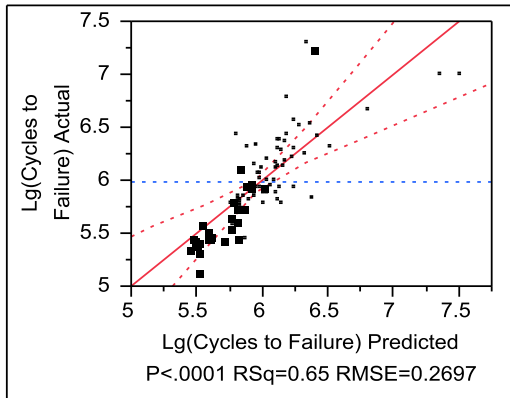
TBD -- to be decided; both crack and tack weld are at the center

Appendix G Model Fitting Report – All Possible Factors

Response Lg(Cycles to Failure)

Whole Model

Actual by Predicted Plot



Summary of Fit

RSquare	0.648499
RSquare Adj	0.565248
Root Mean Square Error	0.269732
Mean of Response	5.984361
Observations (or Sum Wgts)	95

Analysis of Variance

Source	DF	Sum of Squares	Mean Square	F Ratio
Model	18	10.201398	0.566744	7.7897
Error	76	5.529395	0.072755	Prob > F
C. Total	94	15.730794		<.0001*

Parameter Estimates

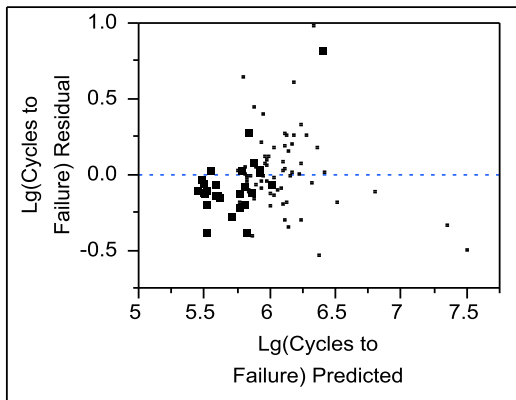
Term	Estimate	Std Error	t Ratio	Prob> t
Intercept	8.7116189	1.208894	7.21	<.0001*
Specimen Series[FIL]	-0.048266	0.118976	-0.41	0.6861
Specimen Series[GM-80]	0.1778059	0.121217	1.47	0.1465
Specimen Series[OB]	-0.090343	0.146611	-0.62	0.5396
Specimen Series[SA-20]	0.0305201	0.1246	0.24	0.8072
Specimen Series[SA-40]	-0.074673	0.107542	-0.69	0.4896
Specimen Series[SA-60]	-0.034251	0.102134	-0.34	0.7383
Specimen Series[SA-80]	0.0640179	0.198066	0.32	0.7474
Failure Mode[RUNOUT]	0.626088	0.131448	4.76	<.0001*
Failure Mode[WR]	-0.588611	0.119812	-4.91	<.0001*

Term	Estimate	Std Error	t Ratio	Prob> t
Failure Mode[WT @ DECK]	-0.033687	0.081587	-0.41	0.6808
Root Gap[Close]	-0.043123	0.073289	-0.59	0.5580
R-Ratio[0]	-0.20666	0.036598	-5.65	<.0001*
Weld Toe Size (d1)	2.0929949	1.29385	1.62	0.1099
Weld Penetration	-0.227691	0.691863	-0.33	0.7430
Weld Throat (t)	3.3445716	2.471598	1.35	0.1800
Weld Height (h)	-1.030001	1.18336	-0.87	0.3868
Weld Area (Aw)	0.1775615	3.757943	0.05	0.9624
Lg(SHS-0515 Extrapolation)	-2.541618	0.628414	-4.04	0.0001*

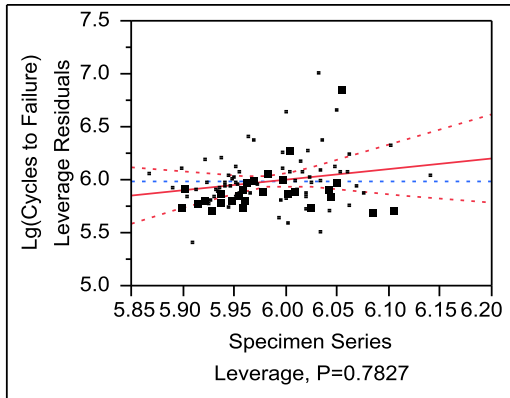
Effect Tests

Source	Nparm	DF	Sum of Squares	F Ratio	Prob > F
Specimen Series	7	7	0.2872910	0.5641	0.7827
Failure Mode	3	3	2.5228381	11.5586	<.0001*
Root Gap	1	1	0.0251885	0.3462	0.5580
R-Ratio	1	1	2.3198942	31.8863	<.0001*
Weld Toe Size (d1)	1	1	0.1903850	2.6168	0.1099
Weld Penetration	1	1	0.0078798	0.1083	0.7430
Weld Throat (t)	1	1	0.1332261	1.8312	0.1800
Weld Height (h)	1	1	0.0551195	0.7576	0.3868
Weld Area (Aw)	1	1	0.0001624	0.0022	0.9624
Lg(SHS-0515 Extrapolation)	1	1	1.1901269	16.3580	0.0001*

Residual by Predicted Plot



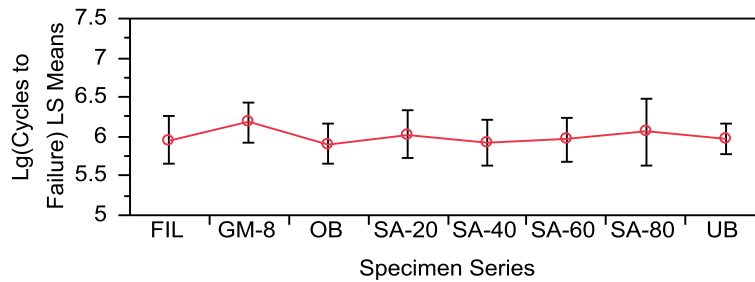
Specimen Series Leverage Plot



Least Squares Means Table

Level	Least Sq Mean	Std Error	Mean
FIL	5.9520332	0.15345434	5.78706
GM-80	6.1781048	0.13017238	6.24877
OB	5.9099557	0.12826725	5.99771
SA-20	6.0308190	0.15713228	5.70039
SA-40	5.9256259	0.14956588	5.70246
SA-60	5.9660481	0.13830853	5.73829
SA-80	6.0643168	0.21483135	6.16669
UB	5.9754876	0.09463522	6.04030

LS Means Plot



LSMeans Differences Tukey HSD

$\alpha=0.050$ $Q=3.11696$
 LSMean[i] By LSMean[j]

Mean[i]-Mean[j] Std Err Dif Lower CL Dif Upper CL Dif	FIL	GM-80	OB	SA-20	SA-40	SA-60	SA-80	UB
FIL	0	-0.2261	0.04208	-0.0788	0.02641	-0.014	-0.1123	-0.0235
	0	0.17923	0.20411	0.18221	0.16346	0.17039	0.25385	0.1484
	0	-0.7847	-0.5941	-0.6467	-0.4831	-0.5451	-0.9035	-0.486
	0	0.33258	0.67827	0.48916	0.5359	0.51707	0.67896	0.43909
GM-80	0.22607	0	0.26815	0.14729	0.25248	0.21206	0.11379	0.20262
	0.17923	0	0.21036	0.15124	0.17205	0.15096	0.27859	0.15573
	-0.3326	0	-0.3875	-0.3241	-0.2838	-0.2585	-0.7546	-0.2828
	0.78472	0	0.92384	0.6187	0.78875	0.68259	0.98213	0.68803
OB	-0.0421	-0.2681	0	-0.1209	-0.0157	-0.0561	-0.1544	-0.0655
	0.20411	0.21036	0	0.23021	0.21247	0.20918	0.2516	0.12962
	-0.6783	-0.9238	0	-0.8384	-0.6779	-0.7081	-0.9386	-0.4695
	0.59412	0.38755	0	0.59668	0.64659	0.59592	0.62988	0.33848
SA-20	0.07879	-0.1473	0.12086	0	0.10519	0.06477	-0.0335	0.05533
	0.18221	0.15124	0.23021	0	0.15119	0.14389	0.27331	0.18117
	-0.4892	-0.6187	-0.5967	0	-0.3661	-0.3837	-0.8854	-0.5094
	0.64674	0.32413	0.83841	0	0.57644	0.51329	0.81839	0.62004
SA-40	-0.0264	-0.2525	0.01567	-0.1052	0	-0.0404	-0.1387	-0.0499
	0.16346	0.17205	0.21247	0.15119	0	0.1417	0.2381	0.16548
	-0.5359	-0.7887	-0.6466	-0.5764	0	-0.4821	-0.8808	-0.5657
	0.48309	0.28379	0.67793	0.36605	0	0.40125	0.60347	0.46593
SA-60	0.01401	-0.2121	0.05609	-0.0648	0.04042	0	-0.0983	-0.0094
	0.17039	0.15096	0.20918	0.14389	0.1417	0	0.23723	0.16361
	-0.5171	-0.6826	-0.5959	-0.5133	-0.4013	0	-0.8377	-0.5194
	0.5451	0.25848	0.7081	0.38374	0.4821	0	0.64116	0.50052
SA-80	0.11228	-0.1138	0.15436	0.0335	0.13869	0.09827	0	0.08883
	0.25385	0.27859	0.2516	0.27331	0.2381	0.23723	0	0.23827
	-0.679	-0.9821	-0.6299	-0.8184	-0.6035	-0.6412	0	-0.6538
	0.90353	0.75456	0.9386	0.88539	0.88085	0.8377	0	0.83151
UB	0.02345	-0.2026	0.06553	-0.0553	0.04986	0.00944	-0.0888	0
	0.1484	0.15573	0.12962	0.18117	0.16548	0.16361	0.23827	0
	-0.4391	-0.688	-0.3385	-0.62	-0.4659	-0.5005	-0.8315	0
	0.486	0.2828	0.46955	0.50938	0.56566	0.5194	0.65385	0

Level	Least Sq Mean
GM-80 A	6.1781048
SA-80 A	6.0643168
SA-20 A	6.0308190
UB A	5.9754876
SA-60 A	5.9660481
FIL A	5.9520332
SA-40 A	5.9256259

Level	Least Sq Mean
OB	A 5.9099557

Levels not connected by same letter are significantly different.

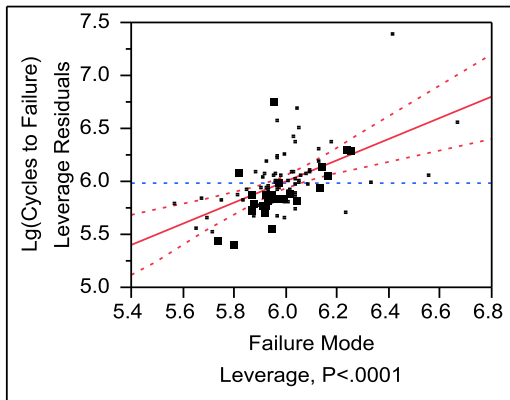
Power Details

Test
Specimen Series

Power							
α	σ	δ	Number	Power	AdjPower	LowerCL	UpperCL
0.0500	0.269732	0.054992	95	0.2285	0.0500	0.0500	0.9937

Least Significant Number				
α	σ	δ	Number(LSN)	
0.0500	0.269732	0.054992	343.1941	

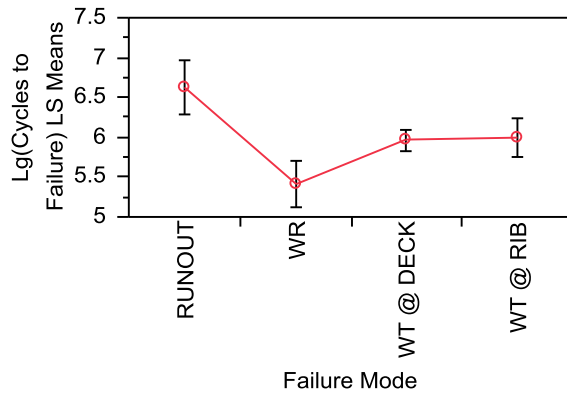
**Failure Mode
Leverage Plot**



Least Squares Means Table

Level	Least Sq Mean	Std Error	Mean
RUNOUT	6.6263869	0.16999077	6.99388
WR	5.4116878	0.14829728	6.04715
WT @ DECK	5.9666122	0.06499348	5.87738
WT @ RIB	5.9965086	0.12026369	6.11973

LS Means Plot



LSMeans Differences Tukey HSD

$\alpha=0.050$ $Q=2.6268$

LSMean[i] By LSMean[j]

Mean[i]-Mean[j] Std Err Dif Lower CL Dif Upper CL Dif	RUNOUT	WR	WT @ DECK	WT @ RIB
RUNOUT	0	1.2147	0.65977	0.62988
	0	0.20884	0.17917	0.20452
	0	0.66612	0.18913	0.09264
	0	1.76328	1.13042	1.16712
WR	-1.2147	0	-0.5549	-0.5848
	0.20884	0	0.17033	0.18228
	-1.7633	0	-1.0023	-1.0636
	-0.6661	0	-0.1075	-0.106
WT @ DECK	-0.6598	0.55492	0	-0.0299
	0.17917	0.17033	0	0.11808
	-1.1304	0.1075	0	-0.3401
	-0.1891	1.00235	0	0.28028
WT @ RIB	-0.6299	0.58482	0.0299	0
	0.20452	0.18228	0.11808	0
	-1.1671	0.10601	-0.2803	0
	-0.0926	1.06363	0.34007	0

Level		Least Sq Mean
RUNOUT	A	6.6263869
WT @ RIB	B	5.9965086
WT @ DECK	B	5.9666122
WR	C	5.4116878

Levels not connected by same letter are significantly different.

Power Details

Test
Failure Mode

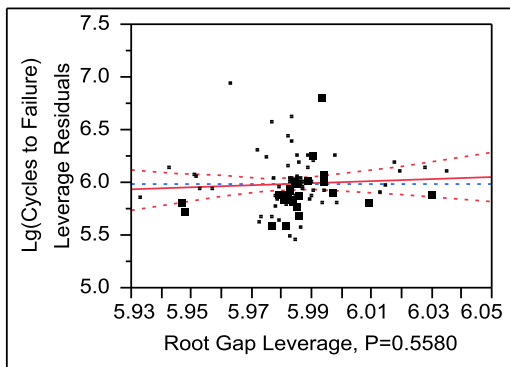
Power							
α	σ	δ	Number	Power	AdjPower	LowerCL	UpperCL
0.0500	0.269732	0.162961	95	0.9993	0.9979	0.6959	1.0000

Least Significant Number

α	σ	δ	Number(LSN)
0.0500	0.269732	0.162961	29.73076

Root Gap

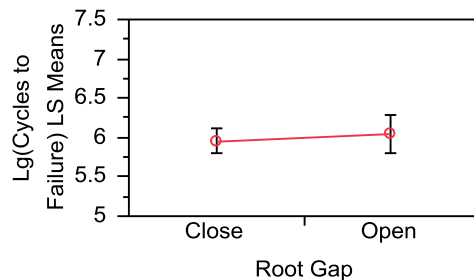
Leverage Plot



Least Squares Means Table

Level	Least Sq Mean	Std Error	Mean
Close	5.9571758	0.07953469	5.96860
Open	6.0434219	0.12243048	6.03100

LS Means Plot



LSMeans Differences Student's t

$\alpha=0.050$ $t=1.99167$
LSMean[i] By LSMean[j]

Mean[i]-Mean[j]	Close	Open
Std Err Dif		
Lower CL Dif		
Upper CL Dif		
Close	0	-0.0862
	0	0.14658
	0	-0.3782
	0	0.20569
Open	0.08625	0
	0.14658	0
	-0.2057	0
	0.37818	0

Level	Least Sq Mean
Open A	6.0434219
Close A	5.9571758

Levels not connected by same letter are significantly different.

Power Details

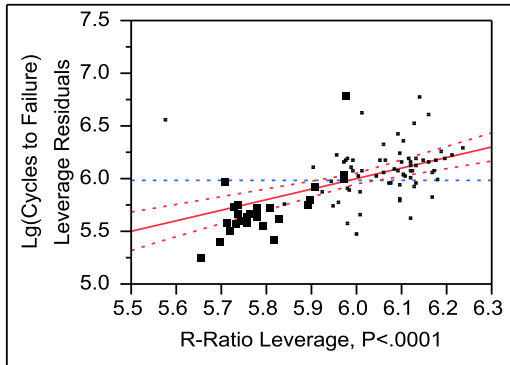
Test
Root Gap

Power								
α	σ	δ	Number	Power	AdjPower	LowerCL	UpperCL	
0.0500	0.269732	0.016283	95	0.0895	0.0500	0.0500	0.7215	

Least Significant Number			
α	σ	δ	Number(LSN)
0.0500	0.269732	0.016283	1056.562

Least Significant Value			
α	σ	Number	LSV
0.0500	0.269732	95	0.145968

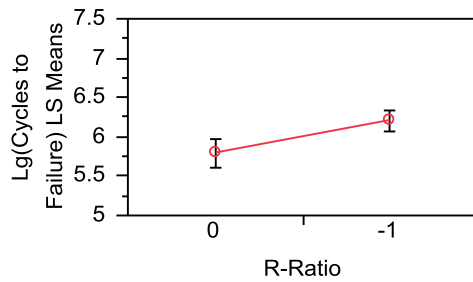
**R-Ratio
Leverage Plot**



Least Squares Means Table

Level	Least Sq Mean	Std Error	Mean
0	5.7936390	0.09316294	5.73669
-1	6.2069587	0.06761521	6.08786

LS Means Plot



LSMeans Differences Student's t

$\alpha=0.050$ $t=1.99167$

LSMean[i] By LSMean[j]

Mean[i]-Mean[j]	0	-1
Std Err Dif		
Lower CL Dif		
Upper CL Dif		
0	0	-0.4133
	0	0.0732
	0	-0.5591
	0	-0.2675
-1	0.41332	0
	0.0732	0
	0.26754	0
	0.5591	0

Level		Least Sq Mean
-1	A	6.2069587
0	B	5.7936390

Levels not connected by same letter are significantly different.

Power Details

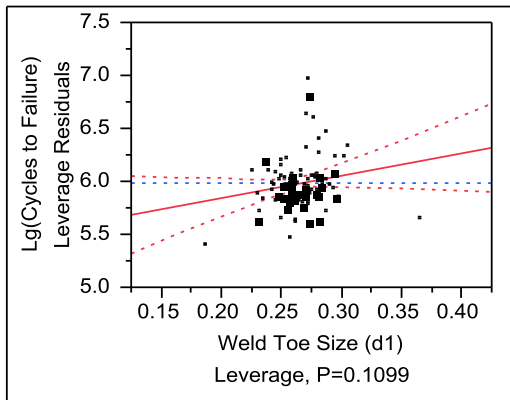
Test
R-Ratio

Power							
α	σ	δ	Number	Power	AdjPower	LowerCL	UpperCL
0.0500	0.269732	0.156269	95	0.9998	0.9997	0.9504	1.0000

Least Significant Number				
α	σ	δ	Number(LSN)	
0.0500	0.269732	0.156269	22.99376	

Least Significant Value				
α	σ	Number	LSV	
0.0500	0.269732	95	0.072891	

Weld Toe Size (d1) Leverage Plot



Power Details

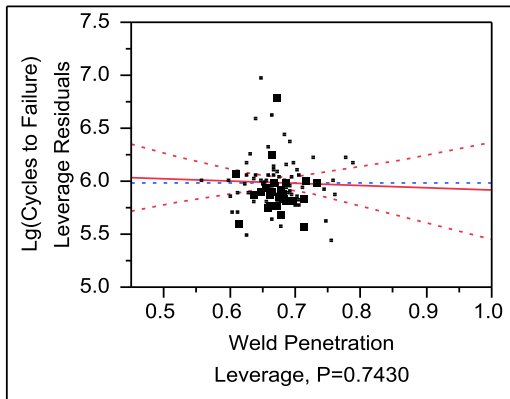
Test
Weld Toe Size (d1)

Power							
α	σ	δ	Number	Power	AdjPower	LowerCL	UpperCL
0.0500	0.269732	0.044767	95	0.3586	0.2330	0.0500	0.9456

Least Significant Number			
α	σ	δ	Number(LSN)
0.0500	0.269732	0.044767	142.2346

Least Significant Value			
α	σ	Number	LSV
0.0500	0.269732	95	2.576925

Weld Penetration Leverage Plot



Power Details

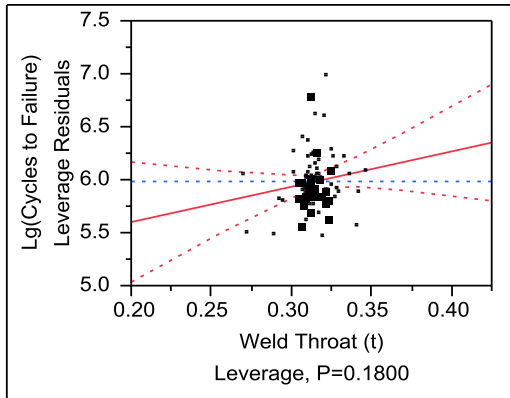
Test
Weld Penetration

Power							
α	σ	δ	Number	Power	AdjPower	LowerCL	UpperCL
0.0500	0.269732	0.009107	95	0.0622	0.0500	0.0500	0.6298

Least Significant Number			
α	σ	δ	Number(LSN)
0.0500	0.269732	0.009107	3371.972

Least Significant Value			
α	σ	Number	LSV
0.0500	0.269732	95	1.377966

**Weld Throat (t)
Leverage Plot**



Power Details

Test

Weld Throat (t)

Power

α	σ	δ	Number	Power	AdjPower	LowerCL	UpperCL
0.0500	0.269732	0.037448	95	0.2669	0.1410	0.0500	0.9103

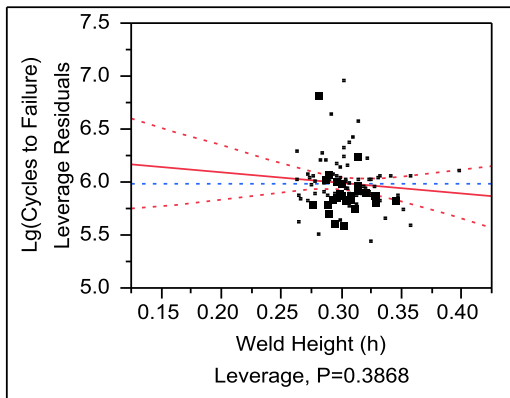
Least Significant Number

α	σ	δ	Number(LSN)
0.0500	0.269732	0.037448	201.9434

Least Significant Value

α	σ	Number	LSV
0.0500	0.269732	95	4.922615

**Weld Height (h)
Leverage Plot**



Power Details

Test
Weld Height (h)

Power							
α	σ	δ	Number	Power	AdjPower	LowerCL	UpperCL
0.0500	0.269732	0.024087	95	0.1380	0.0500	0.0500	0.8067

Least Significant Number

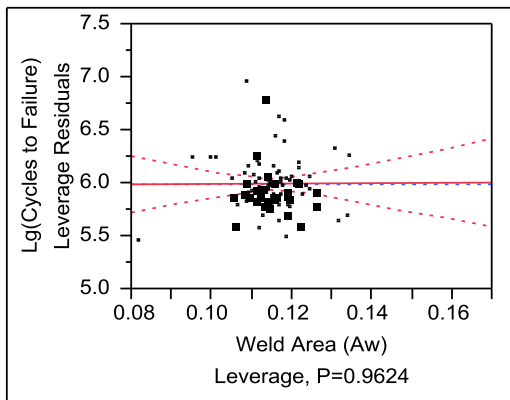
α	σ	δ	Number(LSN)
0.0500	0.269732	0.024087	484.2184

Least Significant Value

α	σ	Number	LSV
0.0500	0.269732	95	2.356866

Weld Area (Aw)

Leverage Plot



Power Details

Test
Weld Area (Aw)

Power							
α	σ	δ	Number	Power	AdjPower	LowerCL	UpperCL
0.0500	0.269732	0.001308	95	0.0502	0.0500	0.0500	0.5212

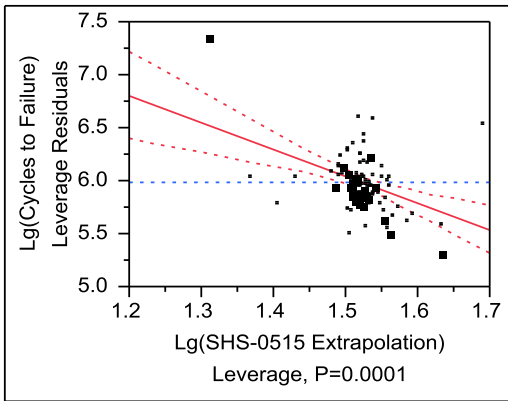
Least Significant Number

α	σ	δ	Number(LSN)
0.0500	0.269732	0.001308	163466.5

Least Significant Value

α	σ	Number	LSV
0.0500	0.269732	95	7.484591

**Lg(SHS-0515 Extrapolation)
Leverage Plot**



Power Details

Test
Lg(SHS-0515 Extrapolation)

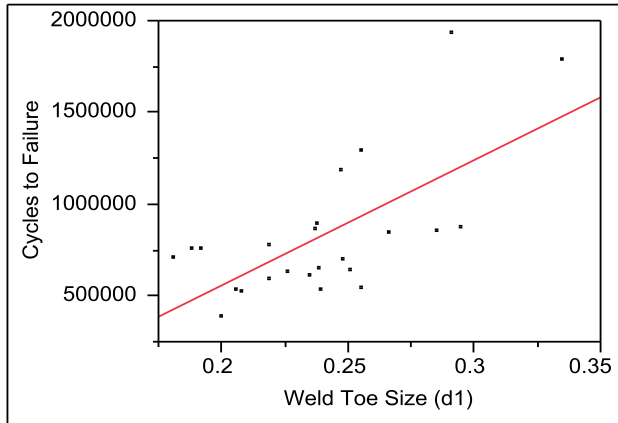
Power								
α	σ	δ	Number	Power	AdjPower	LowerCL	UpperCL	
0.0500	0.269732	0.111927	95	0.9790	0.9682	0.5267	1.0000	

Least Significant Number				
α	σ	δ	Number(LSN)	
0.0500	0.269732	0.111927	28.90652	

Least Significant Value				
α	σ	Number	LSV	
0.0500	0.269732	95	1.251595	

Appendix H Simple Linear Regression Report – R=-1 under 36.67 ksi

Bivariate Fit of Cycles to Failure by Weld Toe Size (d₁)



— Linear Fit

Linear Fit

$$\text{Cycles to Failure} = -819188.7 + 6862063.7 * \text{Weld Toe Size (d}_1\text{)}$$

Summary of Fit

RSquare	0.451067
RSquare Adj	0.426116
Root Mean Square Error	286194.3
Mean of Response	825433.5
Observations (or Sum Wgts)	24

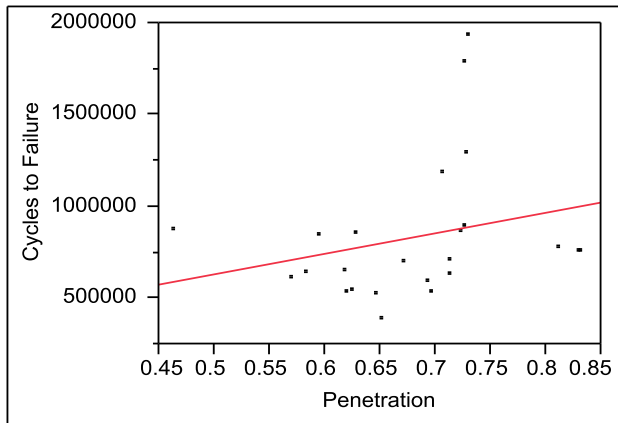
Analysis of Variance

Source	DF	Sum of Squares	Mean Square	F Ratio
Model	1	1.4807e+12	1.481e+12	18.0778
Error	22	1.802e+12	8.191e+10	Prob > F
C. Total	23	3.2827e+12		0.0003*

Parameter Estimates

Term	Estimate	Std Error	t Ratio	Prob> t
Intercept	-819188.7	391193.2	-2.09	0.0480*
Weld Toe Size (d ₁)	6862063.7	1613922	4.25	0.0003*

Bivariate Fit of Cycles to Failure by Penetration



— Linear Fit

Linear Fit

$$\text{Cycles to Failure} = 69284.905 + 1112966.7 * \text{Penetration}$$

Summary of Fit

RSquare	0.063423
RSquare Adj	0.020851
Root Mean Square Error	373829.1
Mean of Response	825433.5
Observations (or Sum Wgts)	24

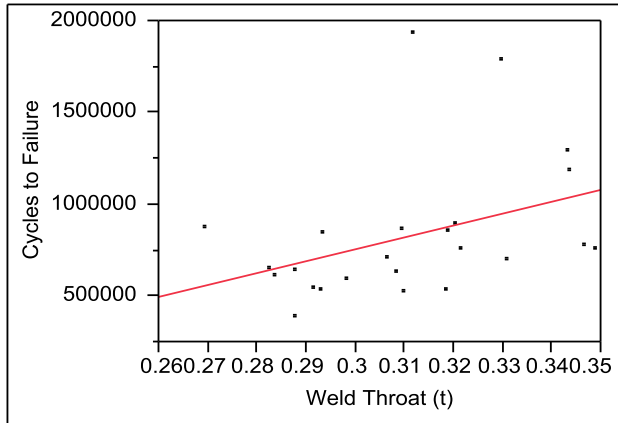
Analysis of Variance

Source	DF	Sum of Squares	Mean Square	F Ratio
Model	1	2.082e+11	2.082e+11	1.4898
Error	22	3.0745e+12	1.397e+11	Prob > F
C. Total	23	3.2827e+12		0.2352

Parameter Estimates

Term	Estimate	Std Error	t Ratio	Prob> t
Intercept	69284.905	624186.6	0.11	0.9126
Penetration	1112966.7	911842	1.22	0.2352

Bivariate Fit of Cycles to Failure by Weld Throat (t)



— Linear Fit

Linear Fit

$$\text{Cycles to Failure} = -1191561 + 6492515.5 * \text{Weld Throat (t)}$$

Summary of Fit

RSquare	0.147265
RSquare Adj	0.108504
Root Mean Square Error	356704.3
Mean of Response	825433.5
Observations (or Sum Wgts)	24

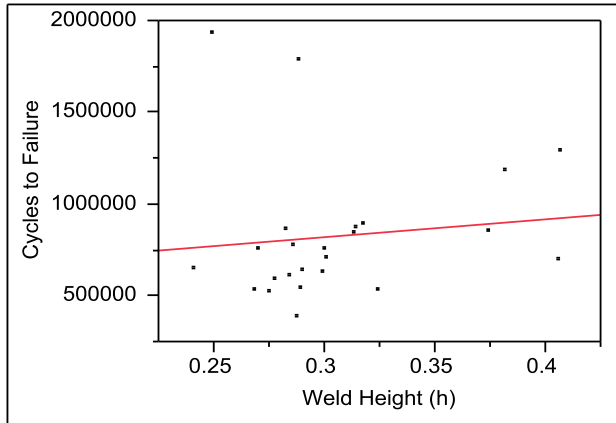
Analysis of Variance

Source	DF	Sum of Squares	Mean Square	F Ratio
Model	1	4.8342e+11	4.834e+11	3.7993
Error	22	2.7992e+12	1.272e+11	Prob > F
C. Total	23	3.2827e+12		0.0641

Parameter Estimates

Term	Estimate	Std Error	t Ratio	Prob> t
Intercept	-1191561	1037345	-1.15	0.2630
Weld Throat (t)	6492515.5	3330879	1.95	0.0641

Bivariate Fit of Cycles to Failure by Weld Height (h)



— Linear Fit

Linear Fit

$$\text{Cycles to Failure} = 527034.46 + 977616.4 * \text{Weld Height (h)}$$

Summary of Fit

RSquare	0.013335
RSquare Adj	-0.03151
Root Mean Square Error	383695.1
Mean of Response	825433.5
Observations (or Sum Wgts)	24

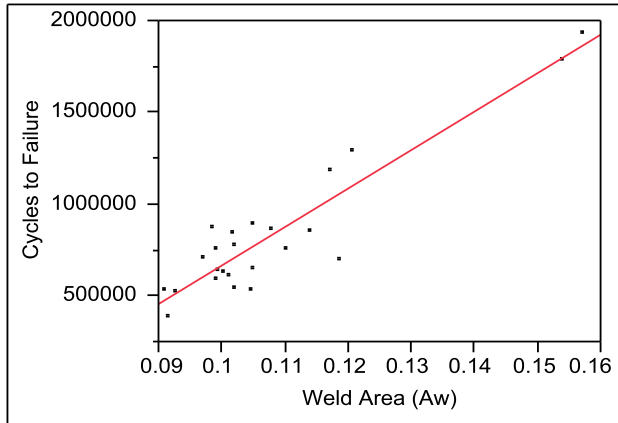
Analysis of Variance

Source	DF	Sum of Squares	Mean Square	F Ratio
Model	1	4.3773e+10	4.377e+10	0.2973
Error	22	3.2389e+12	1.472e+11	Prob > F
C. Total	23	3.2827e+12		0.5910

Parameter Estimates

Term	Estimate	Std Error	t Ratio	Prob> t
Intercept	527034.46	552820	0.95	0.3508
Weld Height (h)	977616.4	1792882	0.55	0.5910

Bivariate Fit of Cycles to Failure by Weld Area (A_w)



— Linear Fit

Linear Fit

$$\text{Cycles to Failure} = -1436370 + 20975808 * \text{Weld Area (A}_w\text{)}$$

Summary of Fit

RSquare	0.858473
RSquare Adj	0.85204
Root Mean Square Error	145318.4
Mean of Response	825433.5
Observations (or Sum Wgts)	24

Analysis of Variance

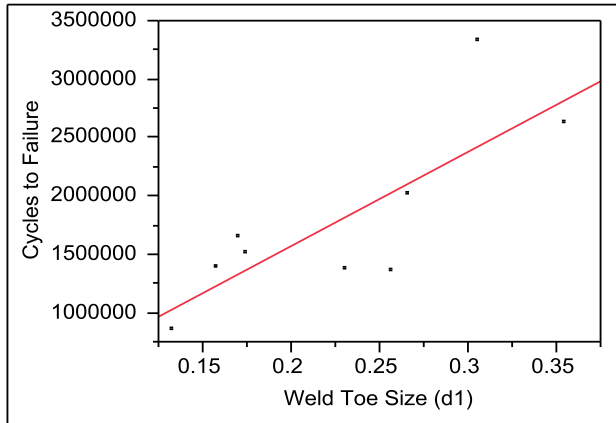
Source	DF	Sum of Squares	Mean Square	F Ratio
Model	1	2.8181e+12	2.818e+12	133.4476
Error	22	4.6458e+11	2.112e+10	Prob > F
C. Total	23	3.2827e+12		<.0001*

Parameter Estimates

Term	Estimate	Std Error	t Ratio	Prob> t
Intercept	-1436370	198028.3	-7.25	<.0001*
Weld Area (A _w)	20975808	1815781	11.55	<.0001*

Appendix I Simple Linear Regression Report – R=-1 under 33.33 ksi

Bivariate Fit of Cycles to Failure by Weld Toe Size (d₁)



— Linear Fit

Linear Fit

$$\text{Cycles to Failure} = -39743.38 + 8066060.4 * \text{Weld Toe Size (d}_1\text{)}$$

Summary of Fit

RSquare	0.630527
RSquare Adj	0.577745
Root Mean Square Error	492736.4
Mean of Response	1793627
Observations (or Sum Wgts)	9

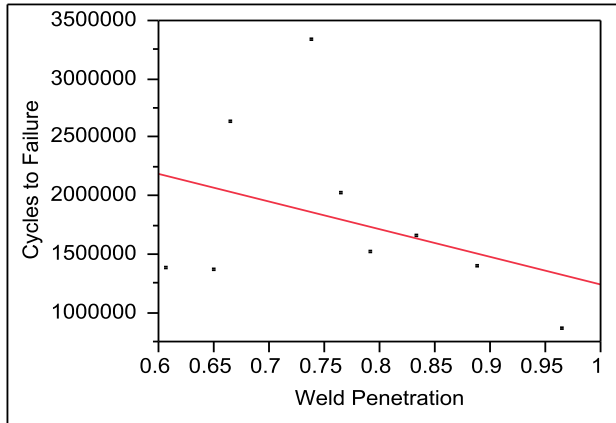
Analysis of Variance

Source	DF	Sum of Squares	Mean Square	F Ratio
Model	1	2.9003e+12	2.9e+12	11.9459
Error	7	1.6995e+12	2.428e+11	Prob > F
C. Total	8	4.5999e+12		0.0106*

Parameter Estimates

Term	Estimate	Std Error	t Ratio	Prob> t
Intercept	-39743.38	555291.5	-0.07	0.9449
Weld Toe Size (d ₁)	8066060.4	2333736	3.46	0.0106*

Bivariate Fit of Cycles to Failure by Weld Penetration



Linear Fit

Linear Fit

Cycles to Failure = 3623743.5 - 2386017.2*Weld Penetration

Summary of Fit

RSquare	0.135236
RSquare Adj	0.011698
Root Mean Square Error	753828.2
Mean of Response	1793627
Observations (or Sum Wgts)	9

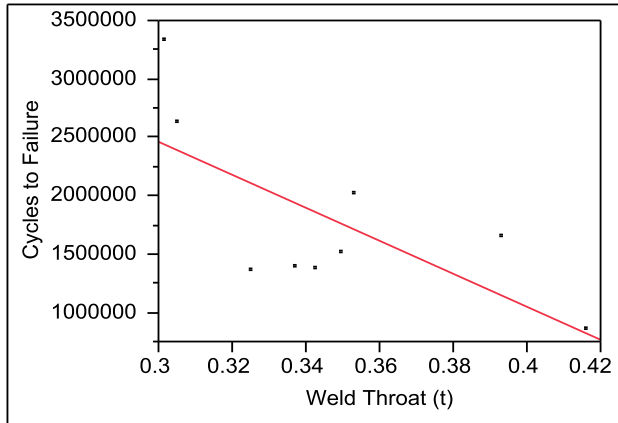
Analysis of Variance

Source	DF	Sum of Squares	Mean Square	F Ratio
Model	1	6.2207e+11	6.221e+11	1.0947
Error	7	3.9778e+12	5.683e+11	Prob > F
C. Total	8	4.5999e+12		0.3302

Parameter Estimates

Term	Estimate	Std Error	t Ratio	Prob> t
Intercept	3623743.5	1767130	2.05	0.0795
Weld Penetration	-2386017	2280489	-1.05	0.3302

Bivariate Fit of Cycles to Failure by Weld Throat (t)



Linear Fit

Linear Fit

$$\text{Cycles to Failure} = 6661117.1 - 14023531 * \text{Weld Throat (t)}$$

Summary of Fit

RSquare	0.485763
RSquare Adj	0.412301
Root Mean Square Error	581306.2
Mean of Response	1793627
Observations (or Sum Wgts)	9

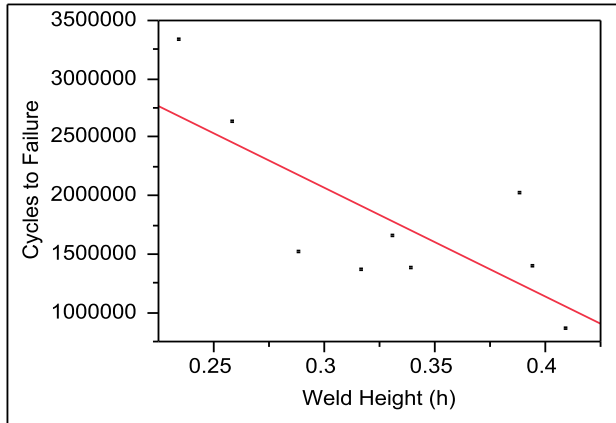
Analysis of Variance

Source	DF	Sum of Squares	Mean Square	F Ratio
Model	1	2.2344e+12	2.234e+12	6.6124
Error	7	2.3654e+12	3.379e+11	Prob > F
C. Total	8	4.5999e+12		0.0369*

Parameter Estimates

Term	Estimate	Std Error	t Ratio	Prob> t
Intercept	6661117.1	1902781	3.50	0.0100*
Weld Throat (t)	-14023531	5453527	-2.57	0.0369*

Bivariate Fit of Cycles to Failure by Weld Height (h)



Linear Fit

Linear Fit

$$\text{Cycles to Failure} = 4851938.6 - 9299861.9 * \text{Weld Height (h)}$$

Summary of Fit

RSquare	0.566106
RSquare Adj	0.504121
Root Mean Square Error	533968.2
Mean of Response	1793627
Observations (or Sum Wgts)	9

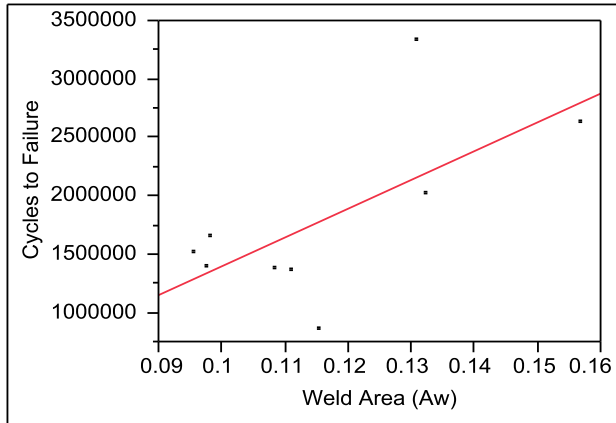
Analysis of Variance

Source	DF	Sum of Squares	Mean Square	F Ratio
Model	1	2.604e+12	2.604e+12	9.1330
Error	7	1.9959e+12	2.851e+11	Prob > F
C. Total	8	4.5999e+12		0.0193*

Parameter Estimates

Term	Estimate	Std Error	t Ratio	Prob> t
Intercept	4851938.6	1027522	4.72	0.0022*
Weld Height (h)	-9299862	3077306	-3.02	0.0193*

Bivariate Fit of Cycles to Failure by Weld Area (A_w)



— Linear Fit

Linear Fit

Cycles to Failure = $-1089134 + 24807434 * \text{Weld Area } (A_w)$

Summary of Fit

RSquare	0.442688
RSquare Adj	0.363072
Root Mean Square Error	605163.3
Mean of Response	1793627
Observations (or Sum Wgts)	9

Analysis of Variance

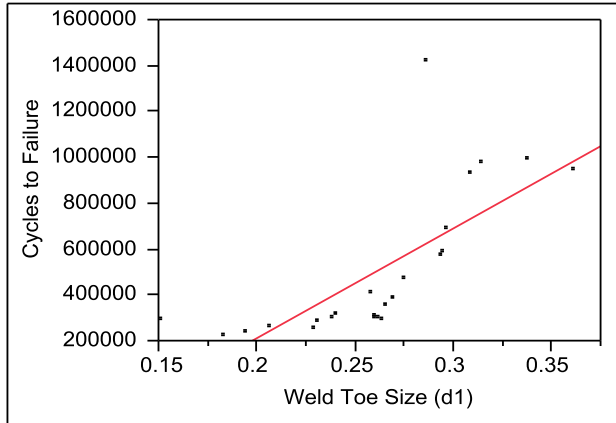
Source	DF	Sum of Squares	Mean Square	F Ratio
Model	1	2.0363e+12	2.036e+12	5.5603
Error	7	2.5636e+12	3.662e+11	Prob > F
C. Total	8	4.5999e+12		0.0505

Parameter Estimates

Term	Estimate	Std Error	t Ratio	Prob> t
Intercept	-1089134	1239061	-0.88	0.4086
Weld Area (A_w)	24807434	10520416	2.36	0.0505

Appendix J Simple Linear Regression Report – R=0 under 33.33 ksi

Bivariate Fit of Cycles to Failure by Weld Toe Size (d₁)



Linear Fit

Linear Fit

$$\text{Cycles to Failure} = -749653 + 4800849.3 \cdot \text{Weld Toe Size (d}_1\text{)}$$

Summary of Fit

RSquare	0.523656
RSquare Adj	0.502004
Root Mean Square Error	226231.1
Mean of Response	505018.9
Observations (or Sum Wgts)	24

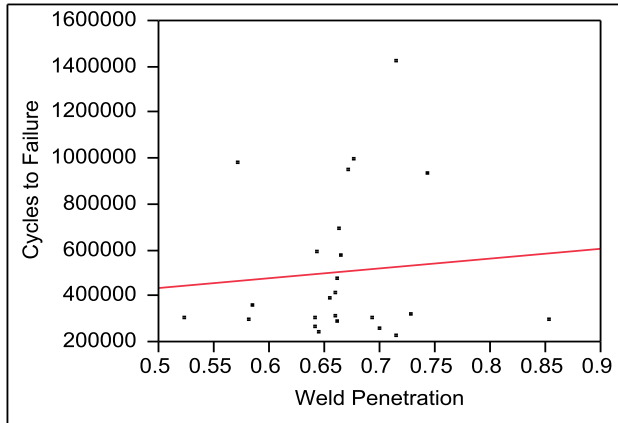
Analysis of Variance

Source	DF	Sum of Squares	Mean Square	F Ratio
Model	1	1.2378e+12	1.238e+12	24.1851
Error	22	1.126e+12	5.118e+10	Prob > F
C. Total	23	2.3638e+12		<.0001*

Parameter Estimates

Term	Estimate	Std Error	t Ratio	Prob> t
Intercept	-749653	259272.6	-2.89	0.0085*
Weld Toe Size (d ₁)	4800849.3	976212.1	4.92	<.0001*

Bivariate Fit of Cycles to Failure by Weld Penetration



Linear Fit

Linear Fit

Cycles to Failure = 231335.3 + 411643.15*Weld Penetration

Summary of Fit

RSquare	0.006951
RSquare Adj	-0.03819
Root Mean Square Error	326645.9
Mean of Response	505018.9
Observations (or Sum Wgts)	24

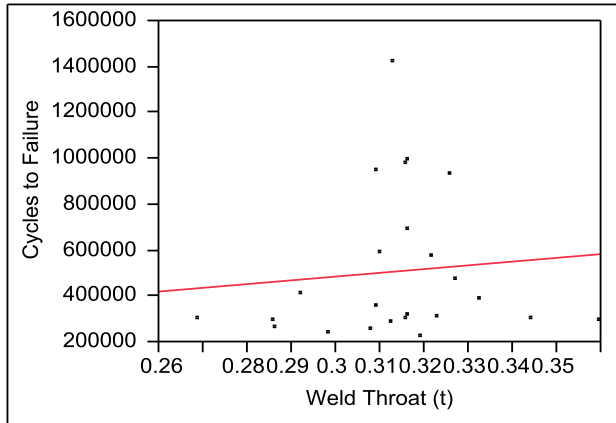
Analysis of Variance

Source	DF	Sum of Squares	Mean Square	F Ratio
Model	1	1.643e+10	1.643e+10	0.1540
Error	22	2.3473e+12	1.067e+11	Prob > F
C. Total	23	2.3638e+12		0.6985

Parameter Estimates

Term	Estimate	Std Error	t Ratio	Prob> t
Intercept	231335.3	700624.4	0.33	0.7444
Weld Penetration	411643.15	1049015	0.39	0.6985

Bivariate Fit of Cycles to Failure by Weld Throat (t)



Linear Fit

Linear Fit

Cycles to Failure = 13178.909 + 1568627.9*Weld Throat (t)

Summary of Fit

RSquare	0.008631
RSquare Adj	-0.03643
Root Mean Square Error	326369.5
Mean of Response	505018.9
Observations (or Sum Wgts)	24

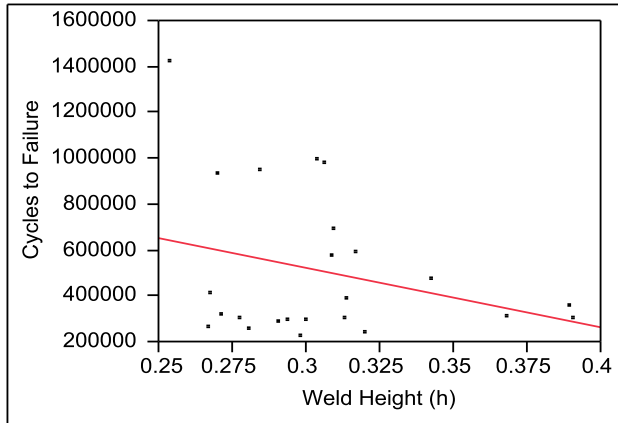
Analysis of Variance

Source	DF	Sum of Squares	Mean Square	F Ratio
Model	1	2.0402e+10	2.04e+10	0.1915
Error	22	2.3434e+12	1.065e+11	Prob > F
C. Total	23	2.3638e+12		0.6659

Parameter Estimates

Term	Estimate	Std Error	t Ratio	Prob> t
Intercept	13178.909	1125804	0.01	0.9908
Weld Throat (t)	1568627.9	3584241	0.44	0.6659

Bivariate Fit of Cycles to Failure by Weld Height (h)



Linear Fit

Linear Fit

$$\text{Cycles to Failure} = 1301339.5 - 2604713.6 * \text{Weld Height (h)}$$

Summary of Fit

RSquare	0.087336
RSquare Adj	0.045851
Root Mean Square Error	313146.4
Mean of Response	505018.9
Observations (or Sum Wgts)	24

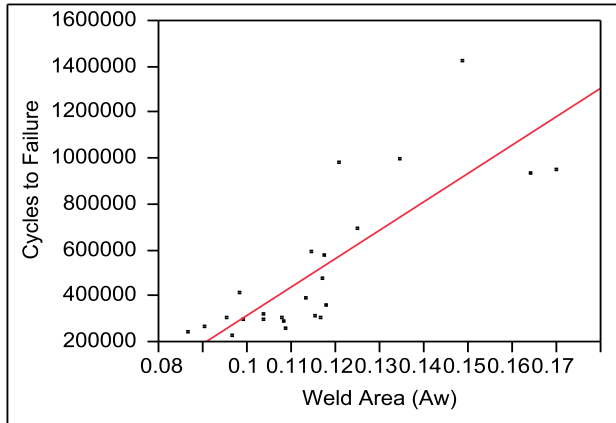
Analysis of Variance

Source	DF	Sum of Squares	Mean Square	F Ratio
Model	1	2.0644e+11	2.064e+11	2.1052
Error	22	2.1573e+12	9.806e+10	Prob > F
C. Total	23	2.3638e+12		0.1609

Parameter Estimates

Term	Estimate	Std Error	t Ratio	Prob> t
Intercept	1301339.5	552537.8	2.36	0.0278*
Weld Height (h)	-2604714	1795181	-1.45	0.1609

Bivariate Fit of Cycles to Failure by Weld Area (A_w)



Linear Fit

Linear Fit

$$\text{Cycles to Failure} = -924106.1 + 12361559 * \text{Weld Area } (A_w)$$

Summary of Fit

RSquare	0.657158
RSquare Adj	0.641574
Root Mean Square Error	191928.3
Mean of Response	505018.9
Observations (or Sum Wgts)	24

Analysis of Variance

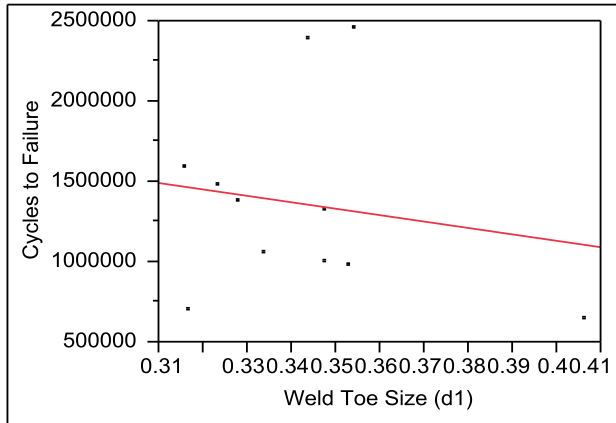
Source	DF	Sum of Squares	Mean Square	F Ratio
Model	1	1.5534e+12	1.553e+12	42.1695
Error	22	8.104e+11	3.684e+10	Prob > F
C. Total	23	2.3638e+12		<.0001*

Parameter Estimates

Term	Estimate	Std Error	t Ratio	Prob> t
Intercept	-924106.1	223535.1	-4.13	0.0004*
Weld Area (A_w)	12361559	1903593	6.49	<.0001*

Appendix K Simple Linear Regression Report – R=0 under 24.93 ksi, Specimens Failed at Weld Roots

Bivariate Fit of Cycles to Failure by Weld Toe Size (d₁)



— Linear Fit

Linear Fit

$$\text{Cycles to Failure} = 2743559.2 - 4032959.3 * \text{Weld Toe Size (d}_1\text{)}$$

Summary of Fit

RSquare	0.02864
RSquare Adj	-0.07929
Root Mean Square Error	625991
Mean of Response	1361904
Observations (or Sum Wgts)	11

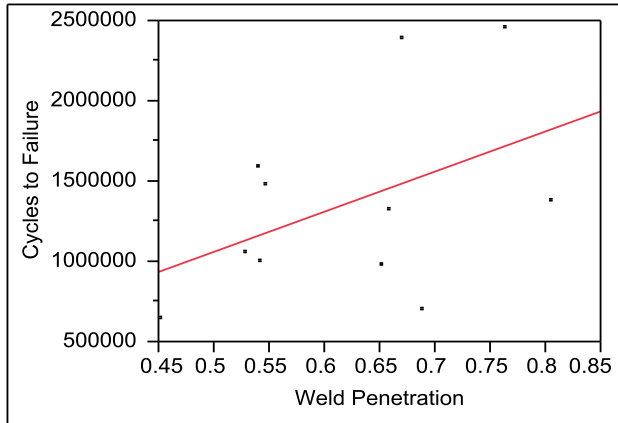
Analysis of Variance

Source	DF	Sum of Squares	Mean Square	F Ratio
Model	1	1.0399e+11	1.04e+11	0.2654
Error	9	3.5268e+12	3.919e+11	Prob > F
C. Total	10	3.6308e+12		0.6189

Parameter Estimates

Term	Estimate	Std Error	t Ratio	Prob> t
Intercept	2743559.2	2688775	1.02	0.3342
Weld Toe Size (d ₁)	-4032959	7828993	-0.52	0.6189

Bivariate Fit of Cycles to Failure by Weld Penetration



Linear Fit

Linear Fit

Cycles to Failure = -205884.4 + 2519846.2*Weld Penetration

Summary of Fit

RSquare	0.208138
RSquare Adj	0.120153
Root Mean Square Error	565200.9
Mean of Response	1361904
Observations (or Sum Wgts)	11

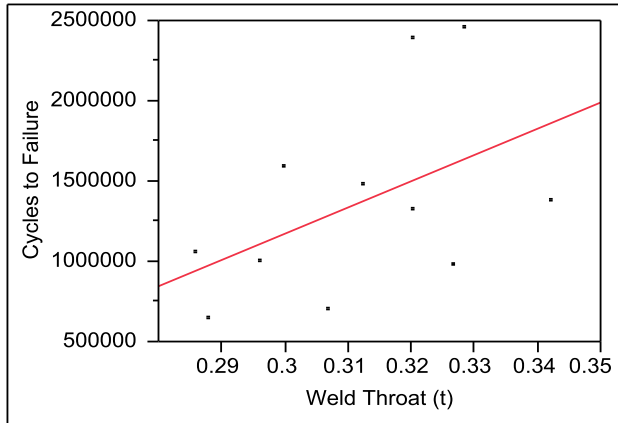
Analysis of Variance

Source	DF	Sum of Squares	Mean Square	F Ratio
Model	1	7.557e+11	7.557e+11	2.3656
Error	9	2.8751e+12	3.195e+11	Prob > F
C. Total	10	3.6308e+12		0.1584

Parameter Estimates

Term	Estimate	Std Error	t Ratio	Prob> t
Intercept	-205884.4	1033479	-0.20	0.8465
Weld Penetration	2519846.2	1638333	1.54	0.1584

Bivariate Fit of Cycles to Failure by Weld Throat (t)



Linear Fit

Linear Fit

$$\text{Cycles to Failure} = -3721984 + 16319952 * \text{Weld Throat (t)}$$

Summary of Fit

RSquare	0.236645
RSquare Adj	0.151828
Root Mean Square Error	554933.8
Mean of Response	1361904
Observations (or Sum Wgts)	11

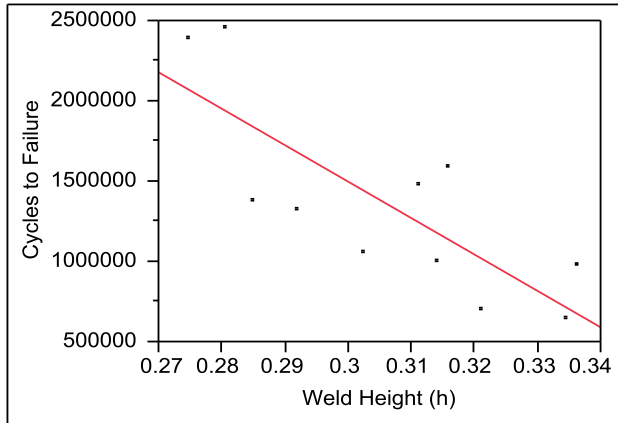
Analysis of Variance

Source	DF	Sum of Squares	Mean Square	F Ratio
Model	1	8.592e+11	8.592e+11	2.7901
Error	9	2.7716e+12	3.08e+11	Prob > F
C. Total	10	3.6308e+12		0.1292

Parameter Estimates

Term	Estimate	Std Error	t Ratio	Prob> t
Intercept	-3721984	3048206	-1.22	0.2531
Weld Throat (t)	16319952	9770393	1.67	0.1292

Bivariate Fit of Cycles to Failure by Weld Height (h)



Linear Fit

Linear Fit

$$\text{Cycles to Failure} = 8316577.1 - 22722289 * \text{Weld Height (h)}$$

Summary of Fit

RSquare	0.627773
RSquare Adj	0.586414
Root Mean Square Error	387509.1
Mean of Response	1361904
Observations (or Sum Wgts)	11

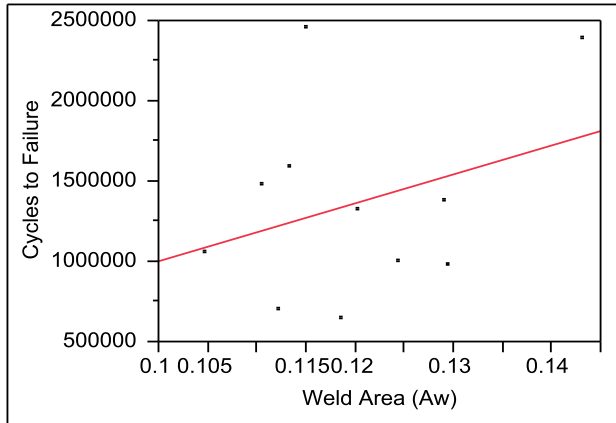
Analysis of Variance

Source	DF	Sum of Squares	Mean Square	F Ratio
Model	1	2.2793e+12	2.279e+12	15.1788
Error	9	1.3515e+12	1.502e+11	Prob > F
C. Total	10	3.6308e+12		0.0036*

Parameter Estimates

Term	Estimate	Std Error	t Ratio	Prob> t
Intercept	8316577.1	1788901	4.65	0.0012*
Weld Height (h)	-22722289	5832214	-3.90	0.0036*

Bivariate Fit of Cycles to Failure by Weld Area (A_w)



Linear Fit

Linear Fit

Cycles to Failure = $-818002.2 + 18161758 \cdot \text{Weld Area } (A_w)$

Summary of Fit

RSquare	0.106694
RSquare Adj	0.007438
Root Mean Square Error	600313.5
Mean of Response	1361904
Observations (or Sum Wgts)	11

Analysis of Variance

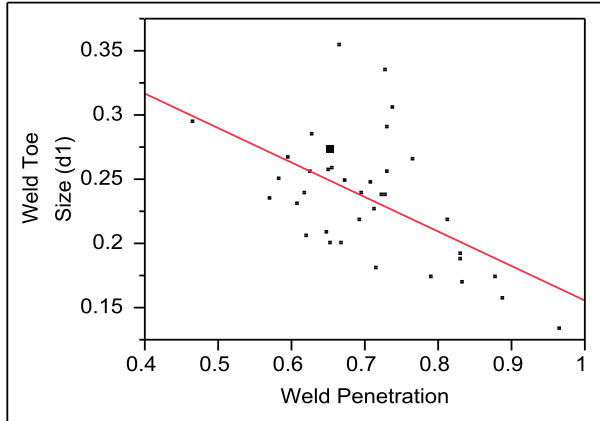
Source	DF	Sum of Squares	Mean Square	F Ratio
Model	1	3.8738e+11	3.874e+11	1.0749
Error	9	3.2434e+12	3.604e+11	Prob > F
C. Total	10	3.6308e+12		0.3269

Parameter Estimates

Term	Estimate	Std Error	t Ratio	Prob> t
Intercept	-818002.2	2110329	-0.39	0.7073
Weld Area (A_w)	18161758	17517294	1.04	0.3269

Appendix L Correlation between Factors – R=-1, Failed at WT@DECK

Bivariate Fit of Weld Toe Size (d₁) by Weld Penetration



— Linear Fit

Linear Fit

$$\text{Weld Toe Size (d}_1\text{)} = 0.4240169 - 0.2678957 * \text{Weld Penetration}$$

Summary of Fit

RSquare	0.309965
RSquare Adj	0.29025
Root Mean Square Error	0.040783
Mean of Response	0.235334
Observations (or Sum Wgts)	37

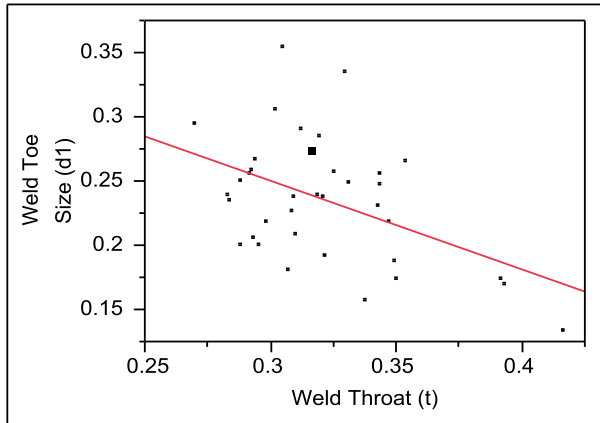
Analysis of Variance

Source	DF	Sum of Squares	Mean Square	F Ratio
Model	1	0.02615012	0.026150	15.7221
Error	35	0.05821468	0.001663	Prob > F
C. Total	36	0.08436480		0.0003*

Parameter Estimates

Term	Estimate	Std Error	t Ratio	Prob> t
Intercept	0.4240169	0.048056	8.82	<.0001*
Weld Penetration	-0.267896	0.067563	-3.97	0.0003*

Bivariate Fit of Weld Toe Size (d1) by Weld Throat (t)



— Linear Fit

Linear Fit

Weld Toe Size (d_1) = 0.457307 - 0.6915607*Weld Throat (t)

Summary of Fit

RSquare	0.215565
RSquare Adj	0.193152
Root Mean Square Error	0.043484
Mean of Response	0.235334
Observations (or Sum Wgts)	37

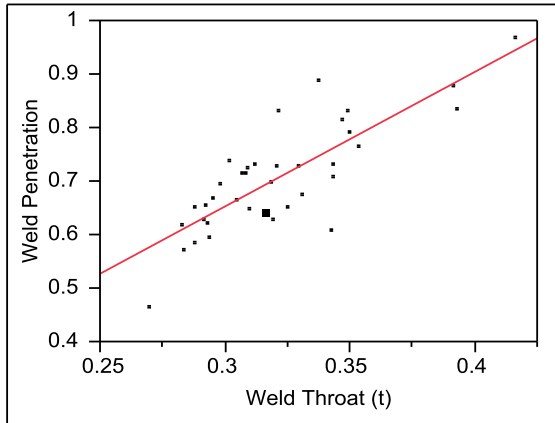
Analysis of Variance

Source	DF	Sum of Squares	Mean Square	F Ratio
Model	1	0.01818606	0.018186	9.6181
Error	35	0.06617874	0.001891	Prob > F
C. Total	36	0.08436480		0.0038*

Parameter Estimates

Term	Estimate	Std Error	t Ratio	Prob> t
Intercept	0.457307	0.07193	6.36	<.0001*
Weld Throat (t)	-0.691561	0.22299	-3.10	0.0038*

Bivariate Fit of Weld Penetration by Weld Throat (t)



— Linear Fit

Linear Fit

$$\text{Weld Penetration} = -0.101674 + 2.5110728 * \text{Weld Throat (t)}$$

Summary of Fit

RSquare	0.658043
RSquare Adj	0.648273
Root Mean Square Error	0.059665
Mean of Response	0.704316
Observations (or Sum Wgts)	37

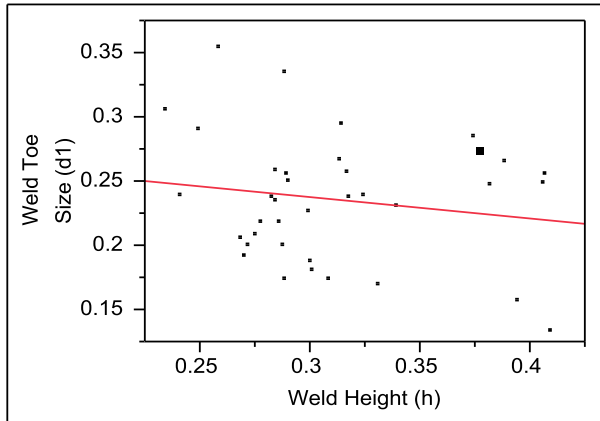
Analysis of Variance

Source	DF	Sum of Squares	Mean Square	F Ratio
Model	1	0.23977097	0.239771	67.3521
Error	35	0.12459865	0.003560	Prob > F
C. Total	36	0.36436961		<.0001*

Parameter Estimates

Term	Estimate	Std Error	t Ratio	Prob> t
Intercept	-0.101674	0.098698	-1.03	0.3100
Weld Throat (t)	2.5110728	0.305973	8.21	<.0001*

Bivariate Fit of Weld Toe Size (d₁) by Weld Height (h)



— Linear Fit

Linear Fit

Weld Toe Size (d₁) = 0.2867172 - 0.1649254*Weld Height (h)

Summary of Fit

RSquare	0.027815
RSquare Adj	0.000038
Root Mean Square Error	0.048408
Mean of Response	0.235334
Observations (or Sum Wgts)	37

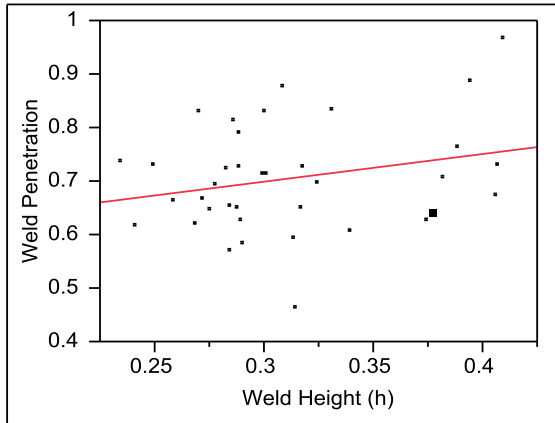
Analysis of Variance

Source	DF	Sum of Squares	Mean Square	F Ratio
Model	1	0.00234659	0.002347	1.0014
Error	35	0.08201821	0.002343	Prob > F
C. Total	36	0.08436480		0.3238

Parameter Estimates

Term	Estimate	Std Error	t Ratio	Prob> t
Intercept	0.2867172	0.051961	5.52	<.0001*
Weld Height (h)	-0.164925	0.164813	-1.00	0.3238

Bivariate Fit of Weld Penetration by Weld Height (h)



— Linear Fit

Linear Fit

$$\text{Weld Penetration} = 0.5453818 + 0.5101303 * \text{Weld Height (h)}$$

Summary of Fit

RSquare	0.061614
RSquare Adj	0.034803
Root Mean Square Error	0.098839
Mean of Response	0.704316
Observations (or Sum Wgts)	37

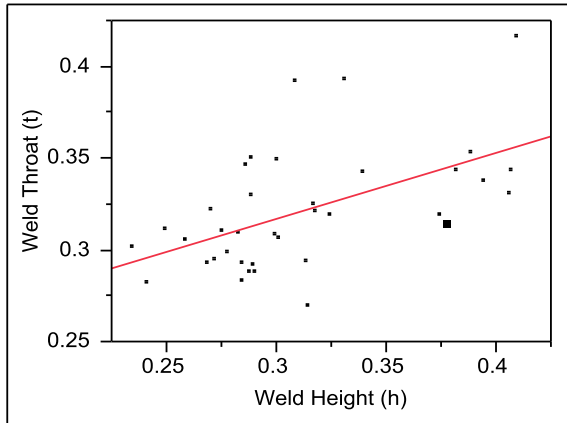
Analysis of Variance

Source	DF	Sum of Squares	Mean Square	F Ratio
Model	1	0.02245038	0.022450	2.2981
Error	35	0.34191923	0.009769	Prob > F
C. Total	36	0.36436961		0.1385

Parameter Estimates

Term	Estimate	Std Error	t Ratio	Prob> t
Intercept	0.5453818	0.106093	5.14	<.0001*
Weld Height (h)	0.5101303	0.336509	1.52	0.1385

Bivariate Fit of Weld Throat (t) by Weld Height (h)



— Linear Fit

Linear Fit

$$\text{Weld Throat (t)} = 0.2100055 + 0.3561769 * \text{Weld Height (h)}$$

Summary of Fit

RSquare	0.287816
RSquare Adj	0.267468
Root Mean Square Error	0.027816
Mean of Response	0.320974
Observations (or Sum Wgts)	37

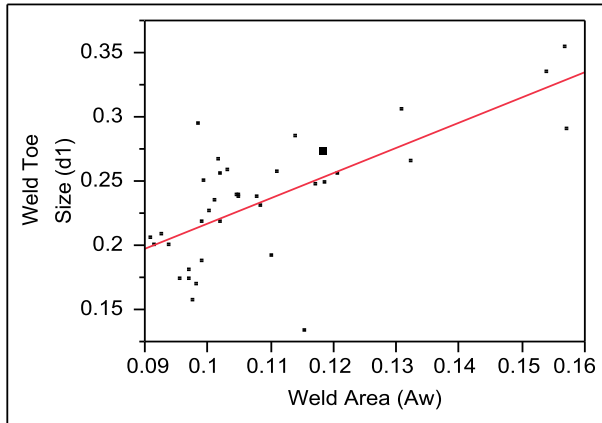
Analysis of Variance

Source	DF	Sum of Squares	Mean Square	F Ratio
Model	1	0.01094443	0.010944	14.1446
Error	35	0.02708134	0.000774	Prob > F
C. Total	36	0.03802577		0.0006*

Parameter Estimates

Term	Estimate	Std Error	t Ratio	Prob> t
Intercept	0.2100055	0.029858	7.03	<.0001*
Weld Height (h)	0.3561769	0.094704	3.76	0.0006*

Bivariate Fit of Weld Toe Size (d_1) by Weld Area (A_w)



— Linear Fit

Linear Fit

Weld Toe Size (d_1) = 0.0210381 + 1.9597471*Weld Area (A_w)

Summary of Fit

RSquare	0.48748
RSquare Adj	0.472837
Root Mean Square Error	0.035148
Mean of Response	0.235334
Observations (or Sum Wgts)	37

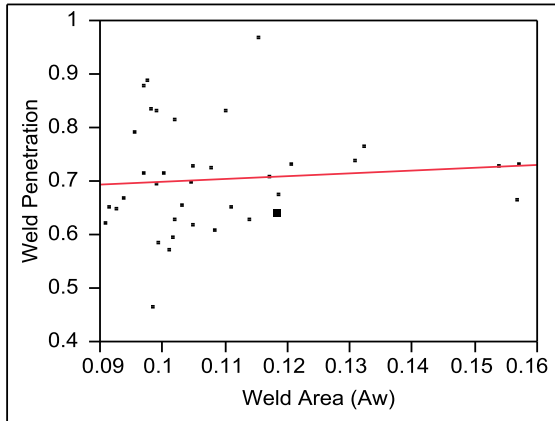
Analysis of Variance

Source	DF	Sum of Squares	Mean Square	F Ratio
Model	1	0.04112617	0.041126	33.2900
Error	35	0.04323863	0.001235	Prob > F
C. Total	36	0.08436480		<.0001*

Parameter Estimates

Term	Estimate	Std Error	t Ratio	Prob> t
Intercept	0.0210381	0.037588	0.56	0.5792
Weld Area (A_w)	1.9597471	0.339659	5.77	<.0001*

Bivariate Fit of Weld Penetration by Weld Area (A_w)



— Linear Fit

Linear Fit

$$\text{Weld Penetration} = 0.6509173 + 0.4883309 * \text{Weld Area } (A_w)$$

Summary of Fit

RSquare	0.007008
RSquare Adj	-0.02136
Root Mean Square Error	0.101674
Mean of Response	0.704316
Observations (or Sum Wgts)	37

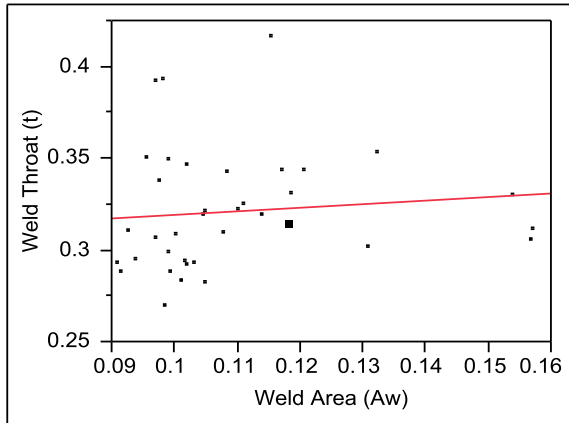
Analysis of Variance

Source	DF	Sum of Squares	Mean Square	F Ratio
Model	1	0.00255356	0.002554	0.2470
Error	35	0.36181605	0.010338	Prob > F
C. Total	36	0.36436961		0.6223

Parameter Estimates

Term	Estimate	Std Error	t Ratio	Prob> t
Intercept	0.6509173	0.108732	5.99	<.0001*
Weld Area (A_w)	0.4883309	0.982541	0.50	0.6223

Bivariate Fit of Weld Throat (t) by Weld Area (A_w)



— Linear Fit

Linear Fit

$$\text{Weld Throat (t)} = 0.3003584 + 0.1885341 * \text{Weld Area (A}_w\text{)}$$

Summary of Fit

RSquare	0.01001
RSquare Adj	-0.01828
Root Mean Square Error	0.032796
Mean of Response	0.320974
Observations (or Sum Wgts)	37

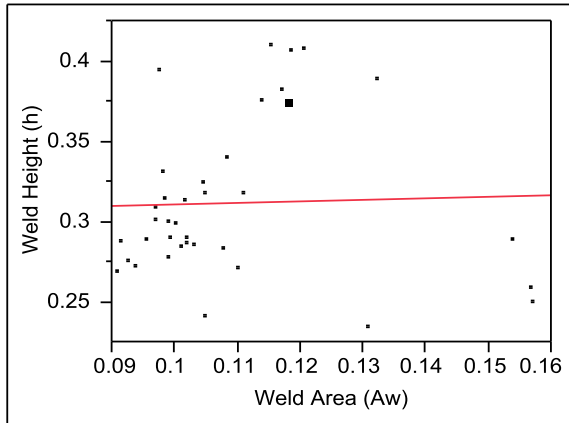
Analysis of Variance

Source	DF	Sum of Squares	Mean Square	F Ratio
Model	1	0.00038063	0.000381	0.3539
Error	35	0.03764514	0.001076	Prob > F
C. Total	36	0.03802577		0.5558

Parameter Estimates

Term	Estimate	Std Error	t Ratio	Prob> t
Intercept	0.3003584	0.035073	8.56	<.0001*
Weld Area (A _w)	0.1885341	0.316929	0.59	0.5558

Bivariate Fit of Weld Height (h) By Weld Area (A_w)



— Linear Fit

Linear Fit

$$\text{Weld Height (h)} = 0.3010419 + 0.096147 * \text{Weld Area (A}_w\text{)}$$

Summary of Fit

RSquare	0.001147
RSquare Adj	-0.02739
Root Mean Square Error	0.049619
Mean of Response	0.311555
Observations (or Sum Wgts)	37

Analysis of Variance

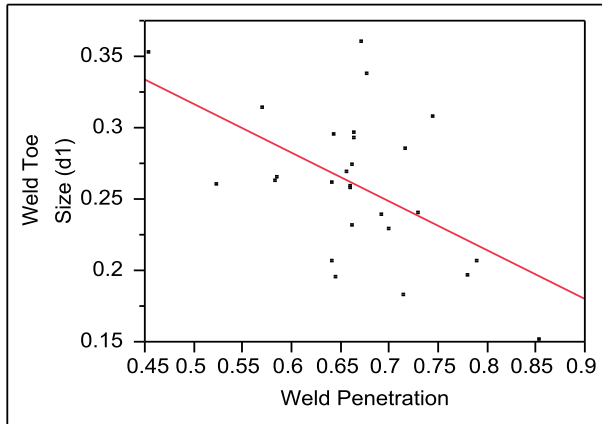
Source	DF	Sum of Squares	Mean Square	F Ratio
Model	1	0.00009899	0.000099	0.0402
Error	35	0.08617136	0.002462	Prob > F
C. Total	36	0.08627035		0.8422

Parameter Estimates

Term	Estimate	Std Error	t Ratio	Prob> t
Intercept	0.3010419	0.053063	5.67	<.0001*
Weld Area (A _w)	0.096147	0.4795	0.20	0.8422

Appendix M Correlation between Factors – R=0, Failed at WT@DECK

Bivariate Fit of Weld Toe Size (d₁) by Weld Penetration



— Linear Fit

Linear Fit

$$\text{Weld Toe Size (d}_1\text{)} = 0.4871367 - 0.3406662 * \text{Weld Penetration}$$

Summary of Fit

RSquare	0.285675
RSquare Adj	0.257102
Root Mean Square Error	0.044417
Mean of Response	0.260281
Observations (or Sum Wgts)	27

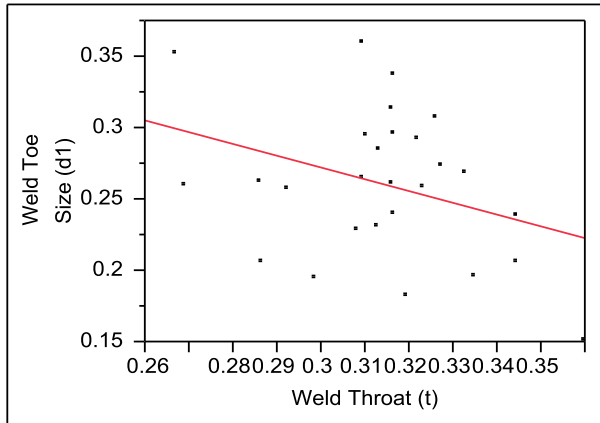
Analysis of Variance

Source	DF	Sum of Squares	Mean Square	F Ratio
Model	1	0.01972531	0.019725	9.9981
Error	25	0.04932266	0.001973	Prob > F
C. Total	26	0.06904797		0.0041*

Parameter Estimates

Term	Estimate	Std Error	t Ratio	Prob> t
Intercept	0.4871367	0.072252	6.74	<.0001*
Weld Penetration	-0.340666	0.107738	-3.16	0.0041*

Bivariate Fit of Weld Toe Size (d₁) by Weld Throat (t)



— Linear Fit

Linear Fit

$$\text{Weld Toe Size (d}_1\text{)} = 0.5187096 - 0.8237288 * \text{Weld Throat (t)}$$

Summary of Fit

RSquare	0.116608
RSquare Adj	0.081272
Root Mean Square Error	0.049395
Mean of Response	0.260281
Observations (or Sum Wgts)	27

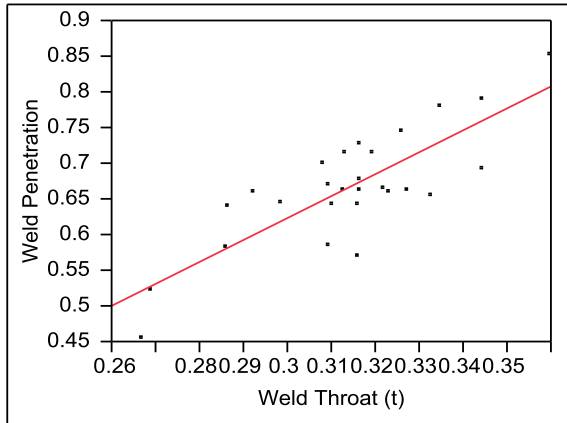
Analysis of Variance

Source	DF	Sum of Squares	Mean Square	F Ratio
Model	1	0.00805153	0.008052	3.3000
Error	25	0.06099643	0.002440	Prob > F
C. Total	26	0.06904797		0.0813

Parameter Estimates

Term	Estimate	Std Error	t Ratio	Prob> t
Intercept	0.5187096	0.142577	3.64	0.0012*
Weld Throat (t)	-0.823729	0.453448	-1.82	0.0813

Bivariate Fit of Weld Penetration by Weld Throat (t)



Linear Fit

Linear Fit

Weld Penetration = -0.296432 + 3.0674458*Weld Throat (t)

Summary of Fit

RSquare	0.656898
RSquare Adj	0.643174
Root Mean Square Error	0.048297
Mean of Response	0.665916
Observations (or Sum Wgts)	27

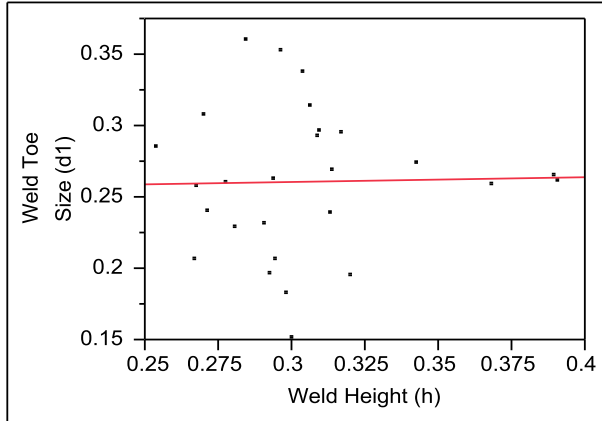
Analysis of Variance

Source	DF	Sum of Squares	Mean Square	F Ratio
Model	1	0.11165132	0.111651	47.8647
Error	25	0.05831607	0.002333	Prob > F
C. Total	26	0.16996739		<.0001*

Parameter Estimates

Term	Estimate	Std Error	t Ratio	Prob> t
Intercept	-0.296432	0.139409	-2.13	0.0435*
Weld Throat (t)	3.0674458	0.443373	6.92	<.0001*

Bivariate Fit of Weld Toe Size (d₁) by Weld Height (h)



— Linear Fit

Linear Fit

$$\text{Weld Toe Size (d}_1\text{)} = 0.248529 + 0.0385998 * \text{Weld Height (h)}$$

Summary of Fit

RSquare	0.000664
RSquare Adj	-0.03931
Root Mean Square Error	0.052537
Mean of Response	0.260281
Observations (or Sum Wgts)	27

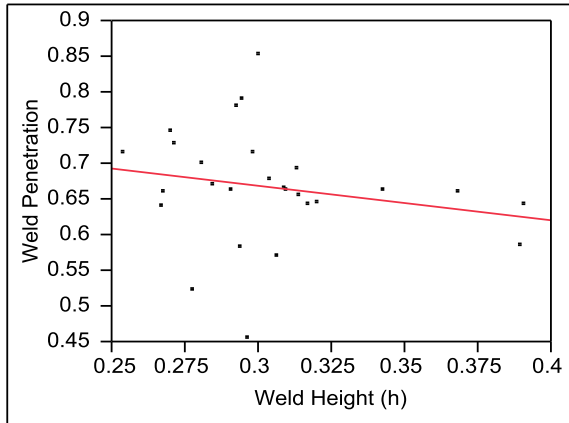
Analysis of Variance

Source	DF	Sum of Squares	Mean Square	F Ratio
Model	1	0.00004585	0.000046	0.0166
Error	25	0.06900212	0.002760	Prob > F
C. Total	26	0.06904797		0.8985

Parameter Estimates

Term	Estimate	Std Error	t Ratio	Prob> t
Intercept	0.248529	0.091743	2.71	0.0120*
Weld Height (h)	0.0385998	0.299484	0.13	0.8985

Bivariate Fit of Weld Penetration by Weld Height (h)



— Linear Fit

Linear Fit

Weld Penetration = 0.8082784 - 0.4675728*Weld Height (h)

Summary of Fit

RSquare	0.039583
RSquare Adj	0.001166
Root Mean Square Error	0.080806
Mean of Response	0.665916
Observations (or Sum Wgts)	27

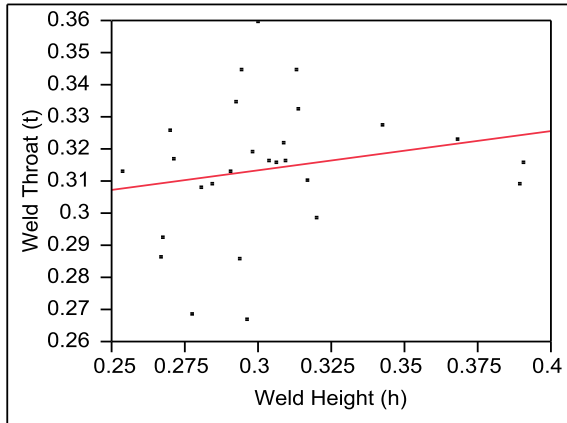
Analysis of Variance

Source	DF	Sum of Squares	Mean Square	F Ratio
Model	1	0.00672781	0.006728	1.0304
Error	25	0.16323957	0.006530	Prob > F
C. Total	26	0.16996739		0.3198

Parameter Estimates

Term	Estimate	Std Error	t Ratio	Prob> t
Intercept	0.8082784	0.141109	5.73	<.0001*
Weld Height (h)	-0.467573	0.460633	-1.02	0.3198

Bivariate Fit of Weld Throat (t) by Weld Height (h)



— Linear Fit

Linear Fit

Weld Throat (t) = 0.2758924 + 0.1242723*Weld Height (h)

Summary of Fit

RSquare	0.040051
RSquare Adj	0.001653
Root Mean Square Error	0.021346
Mean of Response	0.31373
Observations (or Sum Wgts)	27

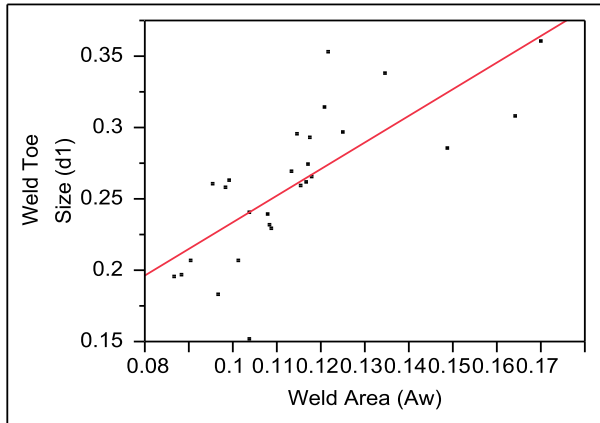
Analysis of Variance

Source	DF	Sum of Squares	Mean Square	F Ratio
Model	1	0.00047525	0.000475	1.0431
Error	25	0.01139090	0.000456	Prob > F
C. Total	26	0.01186616		0.3169

Parameter Estimates

Term	Estimate	Std Error	t Ratio	Prob> t
Intercept	0.2758924	0.037275	7.40	<.0001*
Weld Height (h)	0.1242723	0.121681	1.02	0.3169

Bivariate Fit of Weld Toe Size (d_t) by Weld Area (A_w)



— Linear Fit

Linear Fit

$$\text{Weld Toe Size } (d_t) = 0.0475974 + 1.8608132 * \text{Weld Area } (A_w)$$

Summary of Fit

RSquare	0.556369
RSquare Adj	0.538623
Root Mean Square Error	0.035004
Mean of Response	0.260281
Observations (or Sum Wgts)	27

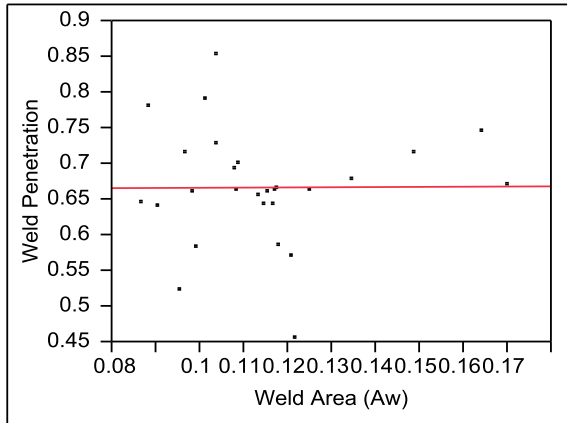
Analysis of Variance

Source	DF	Sum of Squares	Mean Square	F Ratio
Model	1	0.03841612	0.038416	31.3531
Error	25	0.03063185	0.001225	Prob > F
C. Total	26	0.06904797		<.0001*

Parameter Estimates

Term	Estimate	Std Error	t Ratio	Prob> t
Intercept	0.0475974	0.038576	1.23	0.2287
Weld Area (A_w)	1.8608132	0.332325	5.60	<.0001*

Bivariate Fit of Weld Penetration by Weld Area (A_w)



— Linear Fit

Linear Fit

$$\text{Weld Penetration} = 0.6610442 + 0.0426275 * \text{Weld Area } (A_w)$$

Summary of Fit

RSquare	0.000119
RSquare Adj	-0.03988
Root Mean Square Error	0.082449
Mean of Response	0.665916
Observations (or Sum Wgts)	27

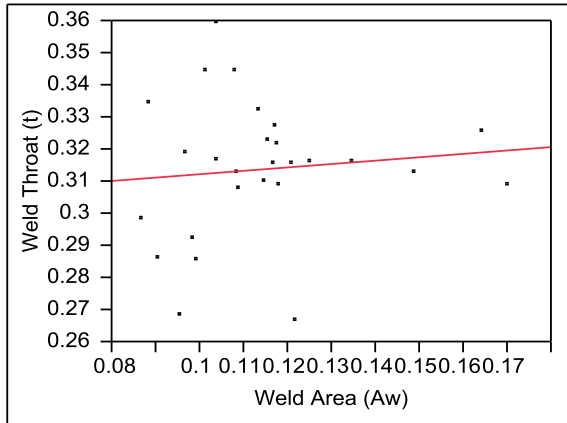
Analysis of Variance

Source	DF	Sum of Squares	Mean Square	F Ratio
Model	1	0.00002016	0.000020	0.0030
Error	25	0.16994723	0.006798	Prob > F
C. Total	26	0.16996739		0.9570

Parameter Estimates

Term	Estimate	Std Error	t Ratio	Prob> t
Intercept	0.6610442	0.090864	7.28	<.0001*
Weld Area (A_w)	0.0426275	0.782768	0.05	0.9570

Bivariate Fit of Weld Throat (t) by Weld Area (A_w)



Linear Fit

Linear Fit

$$\text{Weld Throat (t)} = 0.302183 + 0.1010239 * \text{Weld Area (A}_w\text{)}$$

Summary of Fit

RSquare	0.009542
RSquare Adj	-0.03008
Root Mean Square Error	0.021682
Mean of Response	0.31373
Observations (or Sum Wgts)	27

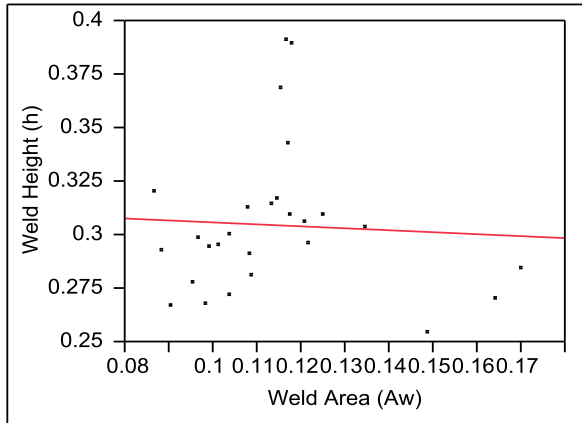
Analysis of Variance

Source	DF	Sum of Squares	Mean Square	F Ratio
Model	1	0.00011323	0.000113	0.2409
Error	25	0.01175293	0.000470	Prob > F
C. Total	26	0.01186616		0.6279

Parameter Estimates

Term	Estimate	Std Error	t Ratio	Prob> t
Intercept	0.302183	0.023895	12.65	<.0001*
Weld Area (A _w)	0.1010239	0.205849	0.49	0.6279

Bivariate Fit of Weld Height (h) by Weld Area (A_w)



Linear Fit

Linear Fit

$$\text{Weld Height (h)} = 0.3152192 - 0.0940432 * \text{Weld Area (A}_w\text{)}$$

Summary of Fit

RSquare	0.003189
RSquare Adj	-0.03668
Root Mean Square Error	0.035029
Mean of Response	0.30447
Observations (or Sum Wgts)	27

Analysis of Variance

Source	DF	Sum of Squares	Mean Square	F Ratio
Model	1	0.00009812	0.000098	0.0800
Error	25	0.03067529	0.001227	Prob > F
C. Total	26	0.03077341		0.7797

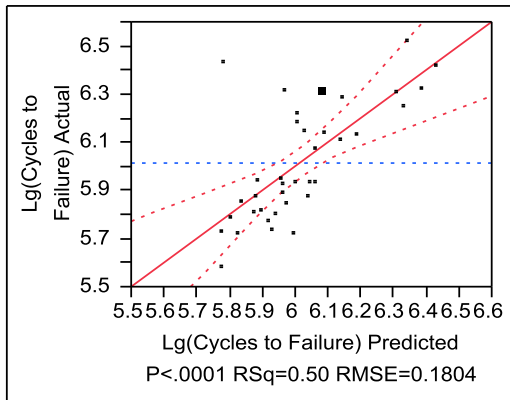
Parameter Estimates

Term	Estimate	Std Error	t Ratio	Prob> t
Intercept	0.3152192	0.038604	8.17	<.0001*
Weld Area (A _w)	-0.094043	0.33256	-0.28	0.7797

Appendix N Model Fitting Report – Weld Dimensions for R=-1, WT@DECK

**Model 1 — Response: Lg(Cycles to Failure)
Factors: d₁, Weld Penetration, Lg(Stress Range)**

**Whole Model
Actual by Predicted Plot**



Summary of Fit

RSquare	0.498672
RSquare Adj	0.453097
Root Mean Square Error	0.180399
Mean of Response	6.016217
Observations (or Sum Wgts)	37

Analysis of Variance

Source	DF	Sum of Squares	Mean Square	F Ratio
Model	3	1.0682591	0.356086	10.9417
Error	33	1.0739478	0.032544	Prob > F
C. Total	36	2.1422069		<.0001*

Parameter Estimates

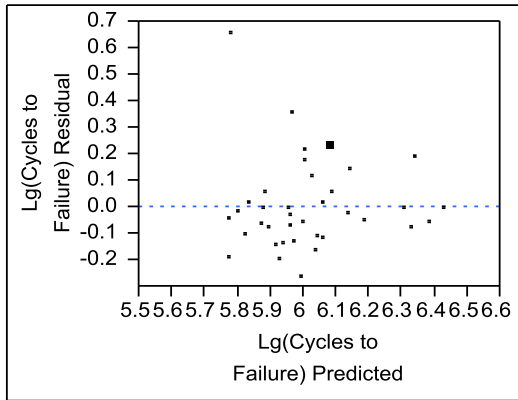
Term	Estimate	Std Error	t Ratio	Prob> t
Intercept	9.3558018	1.724952	5.42	<.0001*
Weld Toe Size (d ₁)	2.6877228	0.774157	3.47	0.0015*
Weld Penetration	1.0325622	0.387775	2.66	0.0119*
Lg(SHS-0515 Extrapolation)	-3.002061	0.979353	-3.07	0.0043*

Effect Tests

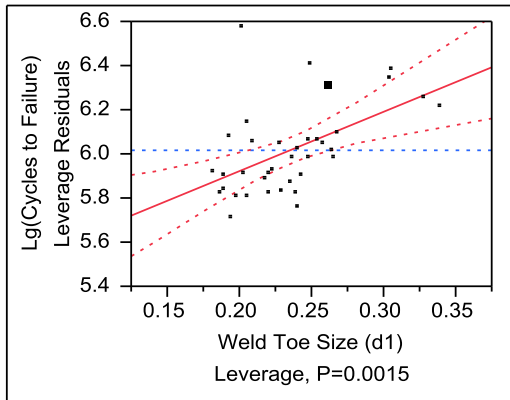
Source	Nparm	DF	Sum of Squares	F Ratio	Prob > F
Weld Toe Size (d ₁)	1	1	0.39226513	12.0534	0.0015*

Source	Nparm	DF	Sum of Squares	F Ratio	Prob > F
Weld Penetration	1	1	0.23075056	7.0904	0.0119*
Lg(SHS-0515 Extrapolation)	1	1	0.30579450	9.3964	0.0043*

Residual by Predicted Plot



Weld Toe Size (d1) Leverage Plot



Power Details

Test
Weld Toe Size (d_1)

Power							
α	σ	δ	Number	Power	AdjPower	LowerCL	UpperCL
0.0500	0.180399	0.102965	37	0.9206	0.8766	0.2866	0.9996

Least Significant Number

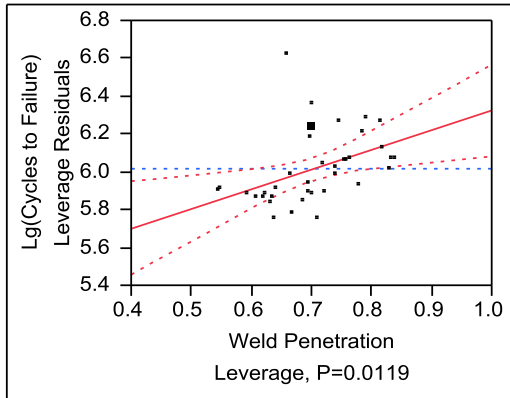
α	σ	δ	Number(LSN)
0.0500	0.180399	0.102965	14.90287

Least Significant Value

α	σ	Number	LSV
----------	----------	--------	-----

α	σ	Number	LSV
0.0500	0.180399	37	1.575035

Weld Penetration Leverage Plot



Power Details

Test
Weld Penetration

Power								
α	σ	δ	Number	Power	AdjPower	LowerCL	UpperCL	
0.0500	0.180399	0.078972	37	0.7339	0.6367	0.0936	0.9953	

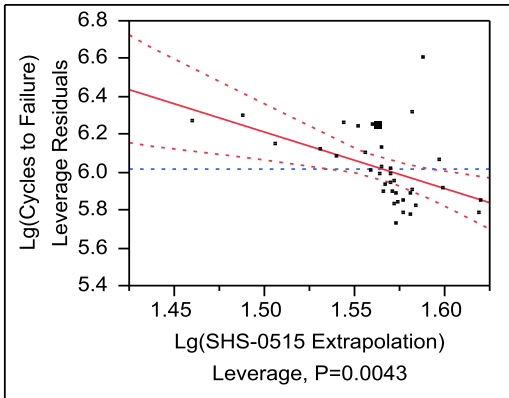
Least Significant Number

α	σ	δ	Number(LSN)
0.0500	0.180399	0.078972	22.87974

Least Significant Value

α	σ	Number	LSV
0.0500	0.180399	37	0.788934

**Lg(SHS-0515 Extrapolation)
Leverage Plot**



Power Details

Test

Lg(SHS-0515 Extrapolation)

Power

α	σ	δ	Number	Power	AdjPower	LowerCL	UpperCL
0.0500	0.180399	0.09091	37	0.8450	0.7750	0.1703	0.9986

Least Significant Number

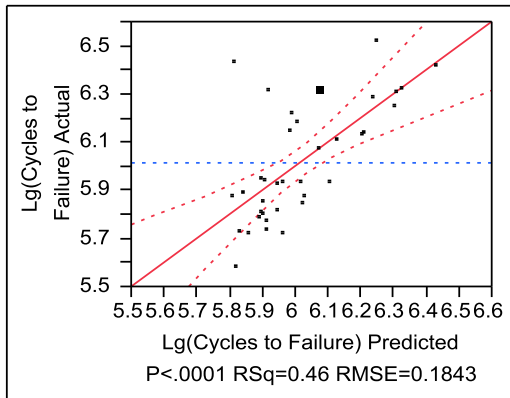
α	σ	δ	Number(LSN)
0.0500	0.180399	0.09091	18.0917

Least Significant Value

α	σ	Number	LSV
0.0500	0.180399	37	1.992509

**Model 2 — Response Lg(Cycles to Failure)
Factors: A_w, Lg(Stress Range)**

**Whole Model
Actual by Predicted Plot**



Summary of Fit

RSquare	0.460659
RSquare Adj	0.428933
Root Mean Square Error	0.184341
Mean of Response	6.016217
Observations (or Sum Wgts)	37

Analysis of Variance

Source	DF	Sum of Squares	Mean Square	F Ratio
Model	2	0.9868275	0.493414	14.5200
Error	34	1.1553794	0.033982	Prob > F
C. Total	36	2.1422069		<.0001*

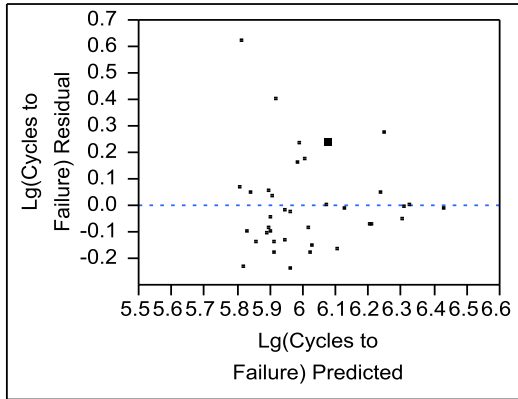
Parameter Estimates

Term	Estimate	Std Error	t Ratio	Prob> t
Intercept	10.404606	1.587992	6.55	<.0001*
Weld Area (A _w)	5.7886954	1.861287	3.11	0.0038*
Lg(SHS-0515 Extrapolation)	-3.20778	0.968921	-3.31	0.0022*

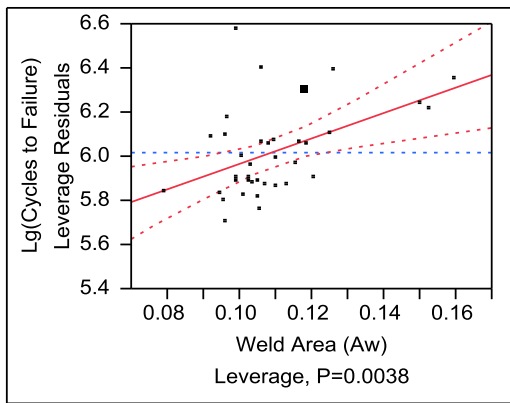
Effect Tests

Source	Nparm	DF	Sum of Squares	F Ratio	Prob > F
Weld Area (A _w)	1	1	0.32868535	9.6724	0.0038*
Lg(SHS-0515 Extrapolation)	1	1	0.37245867	10.9606	0.0022*

Residual by Predicted Plot



Weld Area (A_w) Leverage Plot



Power Details

Test

Weld Area (A_w)

Power

α	σ	δ	Number	Power	AdjPower	LowerCL	UpperCL
0.0500	0.184341	0.094252	37	0.8557	0.7897	0.1821	0.9988

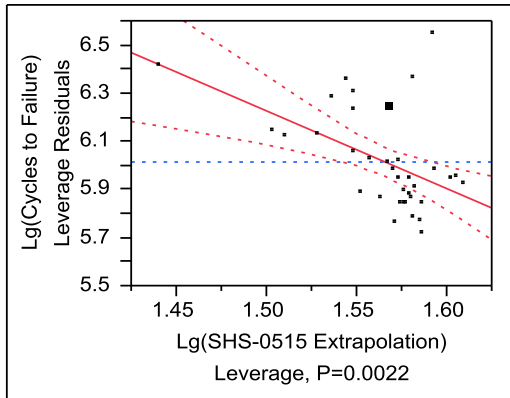
Least Significant Number

α	σ	δ	Number(LSN)
0.0500	0.184341	0.094252	17.48648

Least Significant Value

α	σ	Number	LSV
0.0500	0.184341	37	3.782591

**Lg(SHS-0515 Extrapolation)
Leverage Plot**



Power Details

Test

Lg(SHS-0515 Extrapolation)

Power

α	σ	δ	Number	Power	AdjPower	LowerCL	UpperCL
0.0500	0.184341	0.100332	37	0.8954	0.8425	0.2372	0.9994

Least Significant Number

α	σ	δ	Number(LSN)
0.0500	0.184341	0.100332	15.8043

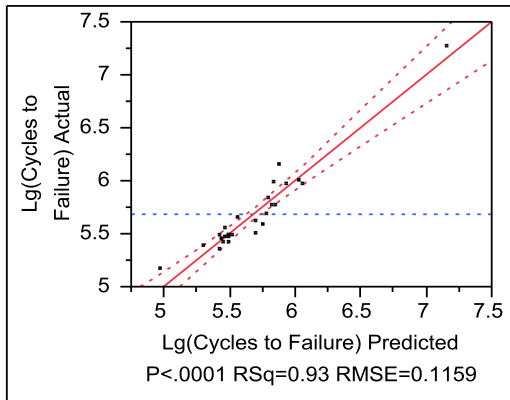
Least Significant Value

α	σ	Number	LSV
0.0500	0.184341	37	1.969085

Appendix O Model Fitting Report – Weld Dimensions for R=0, WT@DECK

**Model 1 — Response: Lg(Cycles to Failure)
Factors: d₁, Weld Penetration, h, Lg(Stress Range)**

**Whole Model
Actual by Predicted Plot**



Summary of Fit

RSquare	0.927798
RSquare Adj	0.91467
Root Mean Square Error	0.115948
Mean of Response	5.678756
Observations (or Sum Wgts)	27

Analysis of Variance

Source	DF	Sum of Squares	Mean Square	F Ratio
Model	4	3.8005784	0.950145	70.6751
Error	22	0.2957645	0.013444	Prob > F
C. Total	26	4.0963429		<.0001*

Parameter Estimates

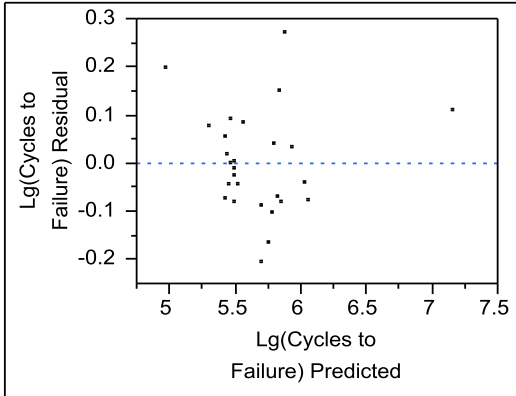
Term	Estimate	Std Error	t Ratio	Prob> t
Intercept	15.283477	0.939295	16.27	<.0001*
Weld Toe Size (d ₁)	2.3348004	0.541206	4.31	0.0003*
Weld Penetration	0.8611178	0.355939	2.42	0.0243*
Weld Height (h)	-2.489394	0.686998	-3.62	0.0015*
Lg(SHS-0515 Extrapolation)	-6.560151	0.461478	-14.22	<.0001*

Effect Tests

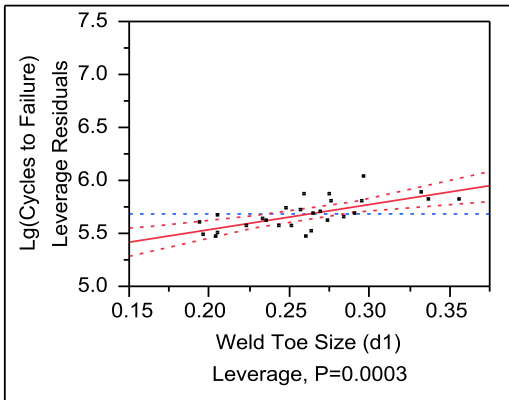
Source	Nparm	DF	Sum of Squares	F Ratio	Prob > F
--------	-------	----	----------------	---------	----------

Source	Nparm	DF	Sum of Squares	F Ratio	Prob > F
Weld Toe Size (d ₁)	1	1	0.2502061	18.6112	0.0003*
Weld Penetration	1	1	0.0786858	5.8529	0.0243*
Weld Height (h)	1	1	0.1765226	13.1304	0.0015*
Lg(SHS-0515 Extrapolation)	1	1	2.7167459	202.0811	<.0001*

Residual by Predicted Plot



Weld Toe Size (d₁) Leverage Plot



Power Details

Test
Weld Toe Size (d₁)

Power		δ	Number	Power	AdjPower	LowerCL	UpperCL
α	σ						
0.0500	0.115948	0.096265	27	0.9846	0.9679	0.5722	1.0000

Least Significant Number

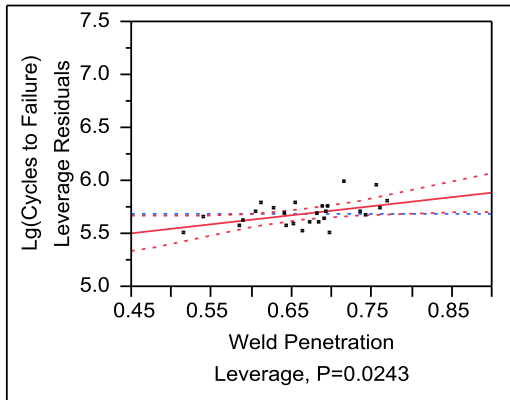
α	σ	δ	Number(LSN)
----------	----------	----------	-------------

α	σ	δ	Number(LSN)
0.0500	0.115948	0.096265	9.81339

Least Significant Value

α	σ	Number	LSV
0.0500	0.115948	27	1.122392

**Weld Penetration
Leverage Plot**



Power Details

Test
Weld Penetration

Power

α	σ	δ	Number	Power	AdjPower	LowerCL	UpperCL
0.0500	0.115948	0.053984	27	0.6379	0.5111	0.0626	0.9901

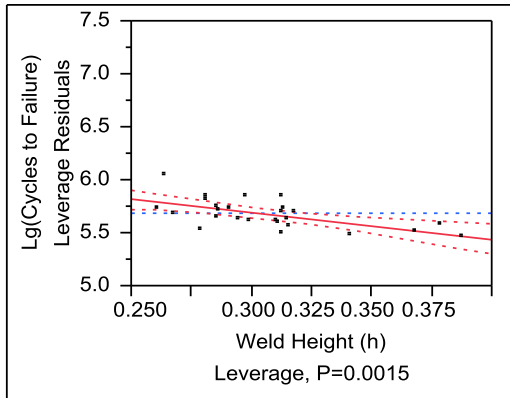
Least Significant Number

α	σ	δ	Number(LSN)
0.0500	0.115948	0.053984	20.7774

Least Significant Value

α	σ	Number	LSV
0.0500	0.115948	27	0.738173

Weld Height (h) Leverage Plot



Power Details

Test

Weld Height (h)

Power

α	σ	δ	Number	Power	AdjPower	LowerCL	UpperCL
0.0500	0.115948	0.080857	27	0.9334	0.8849	0.3167	0.9997

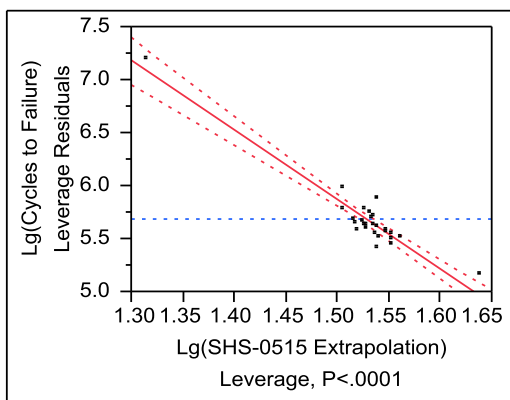
Least Significant Number

α	σ	δ	Number(LSN)
0.0500	0.115948	0.080857	11.70519

Least Significant Value

α	σ	Number	LSV
0.0500	0.115948	27	1.424746

Lg(SHS-0515 Extrapolation) Leverage Plot



Power Details

Test

Lg(SHS-0515 Extrapolation)

Power								
α	σ	δ	Number	Power	AdjPower	LowerCL	UpperCL	
0.0500	0.115948	0.317207	27	1.0000	1.0000	1.0000	1.0000	

Least Significant Number

α	σ	δ	Number(LSN)
0.0500	0.115948	0.317207	6.367677

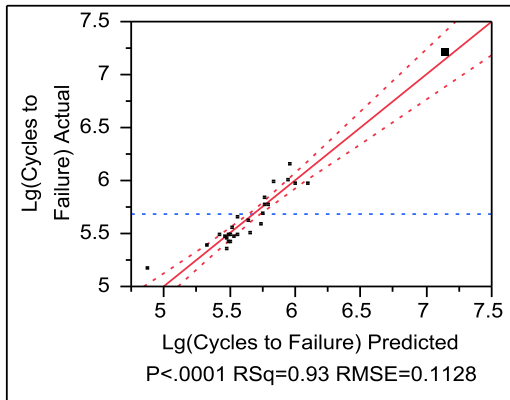
Least Significant Value

α	σ	Number	LSV
0.0500	0.115948	27	0.957047

Model 2 — Response Lg(Cycles to Failure)
Factors: h, A_w, Lg(Stress Range)

Whole Model

Actual by Predicted Plot



Summary of Fit

RSquare	0.928507
RSquare Adj	0.919181
Root Mean Square Error	0.112841
Mean of Response	5.678756
Observations (or Sum Wgts)	27

Analysis of Variance

Source	DF	Sum of Squares	Mean Square	F Ratio
Model	3	3.8034812	1.26783	99.5693
Error	23	0.2928617	0.01273	Prob > F
C. Total	26	4.0963429		<.0001*

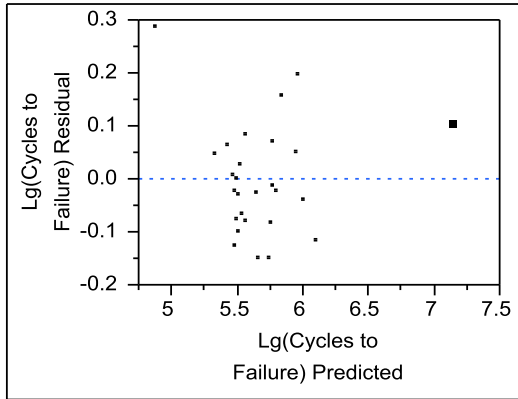
Parameter Estimates

Term	Estimate	Std Error	t Ratio	Prob> t
Intercept	16.22325	0.744378	21.79	<.0001*
Weld Height (h)	-2.663443	0.64831	-4.11	0.0004*
Weld Area (A _w)	4.8491831	1.087528	4.46	0.0002*
Lg(SHS-0515 Extrapolation)	-6.730165	0.433752	-15.52	<.0001*

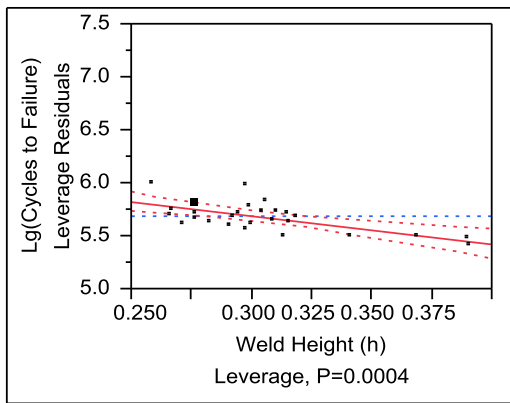
Effect Tests

Source	Nparm	DF	Sum of Squares	F Ratio	Prob > F
Weld Height (h)	1	1	0.2149094	16.8780	0.0004*
Weld Area (A _w)	1	1	0.2531576	19.8818	0.0002*
Lg(SHS-0515 Extrapolation)	1	1	3.0655099	240.7509	<.0001*

Residual by Predicted Plot



Weld Height (h) Leverage Plot



Power Details

Test

Weld Height (h)

Power

α	σ	δ	Number	Power	AdjPower	LowerCL	UpperCL
0.0500	0.112841	0.089217	27	0.9757	0.9529	0.4977	1.0000

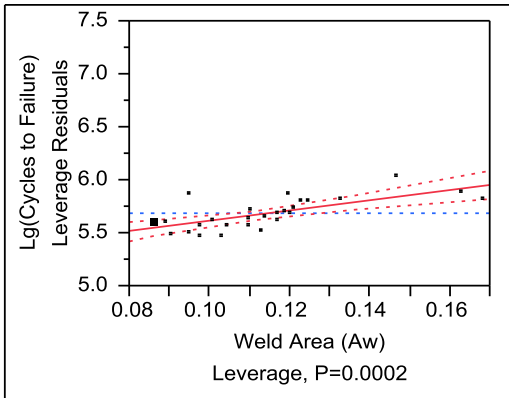
Least Significant Number

α	σ	δ	Number(LSN)
0.0500	0.112841	0.089217	9.767655

Least Significant Value

α	σ	Number	LSV
0.0500	0.112841	27	1.341132

**Weld Area (A_w)
Leverage Plot**



Power Details

Test

Weld Area (A_w)

Power

α	σ	δ	Number	Power	AdjPower	LowerCL	UpperCL
0.0500	0.112841	0.096831	27	0.9894	0.9774	0.6292	1.0000

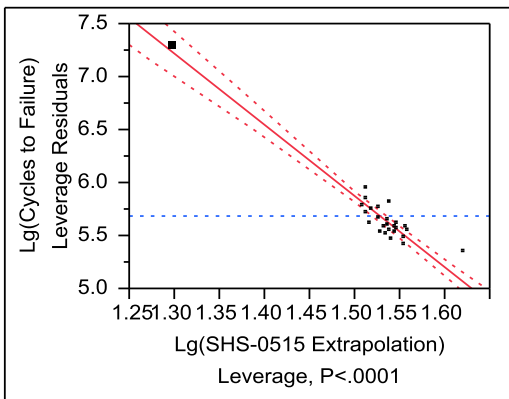
Least Significant Number

α	σ	δ	Number(LSN)
0.0500	0.112841	0.096831	8.987361

Least Significant Value

α	σ	Number	LSV
0.0500	0.112841	27	2.249723

**Lg(SHS-0515 Extrapolation)
Leverage Plot**



Power Details

Test

Lg(SHS-0515 Extrapolation)

Power								
α	σ	δ	Number	Power	AdjPower	LowerCL	UpperCL	
0.0500	0.112841	0.336953	27	1.0000	1.0000	1.0000	1.0000	

Least Significant Number

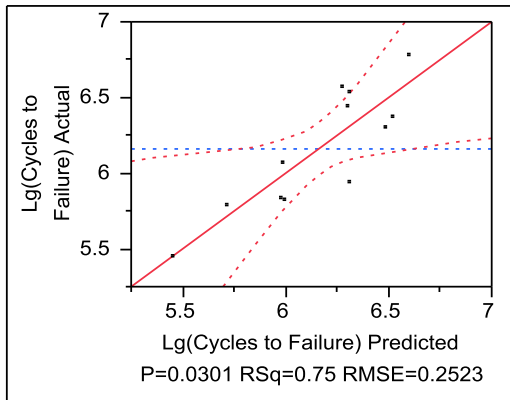
α	σ	δ	Number(LSN)
0.0500	0.112841	0.336953	5.365975

Least Significant Value

α	σ	Number	LSV
0.0500	0.112841	27	0.897285

Appendix P Model Fitting Report – Weld Dimensions for R=-1, WT@RIB

Model Response: Lg(Cycles to Failure)
Factors: d_1 , h, A_w , Lg(Stress Range)
Whole Model
Actual by Predicted Plot



Summary of Fit

RSquare	0.74518
RSquare Adj	0.599568
Root Mean Square Error	0.252267
Mean of Response	6.158763
Observations (or Sum Wgts)	12

Analysis of Variance

Source	DF	Sum of Squares	Mean Square	F Ratio
Model	4	1.3027049	0.325676	5.1176
Error	7	0.4454709	0.063639	Prob > F
C. Total	11	1.7481758		0.0301*

Parameter Estimates

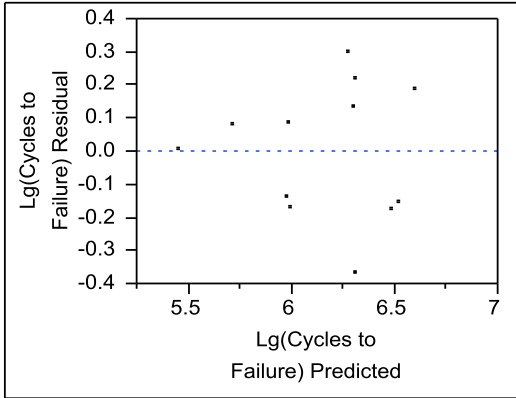
Term	Estimate	Std Error	t Ratio	Prob> t
Intercept	30.735989	6.460282	4.76	0.0021*
Weld Toe Size (d_1)	-2.633567	1.664437	-1.58	0.1576
Weld Height (h)	2.9013626	1.411404	2.06	0.0789
Weld Area (A_w)	5.3334463	4.388831	1.22	0.2637
Lg(SHS-0515 Extrapolation)	-16.10002	3.993553	-4.03	0.0050*

Effect Tests

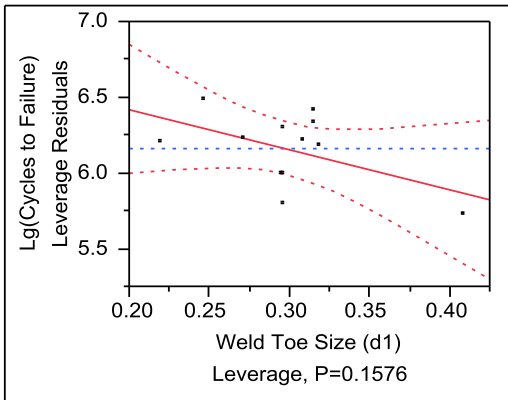
Source	Nparm	DF	Sum of Squares	F Ratio	Prob > F
--------	-------	----	----------------	---------	----------

Source	Nparm	DF	Sum of Squares	F Ratio	Prob > F
Weld Toe Size (d_1)	1	1	0.1593220	2.5035	0.1576
Weld Height (h)	1	1	0.2689198	4.2257	0.0789
Weld Area (A_w)	1	1	0.0939809	1.4768	0.2637
Lg(SHS-0515 Extrapolation)	1	1	1.0343211	16.2530	0.0050*

Residual by Predicted Plot



Weld Toe Size (d_1) Leverage Plot



Power Details

Test
Weld Toe Size (d_1)

Power		δ	Number	Power	AdjPower	LowerCL	UpperCL
α	σ						
0.0500	0.252267	0.115225	12	0.2780	0.1205	0.0500	0.9204

Least Significant Number

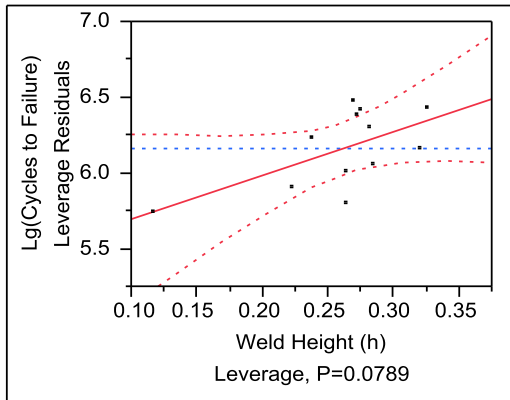
α	σ	δ	Number(LSN)
----------	----------	----------	-------------

α	σ	δ	Number(LSN)
0.0500	0.252267	0.115225	21.44484

Least Significant Value

α	σ	Number	LSV
0.0500	0.252267	12	3.935767

**Weld Height (h)
Leverage Plot**



Power Details

Test
Weld Height (h)

Power

α	σ	δ	Number	Power	AdjPower	LowerCL	UpperCL
0.0500	0.252267	0.1497	12	0.4265	0.2338	0.0500	0.9642

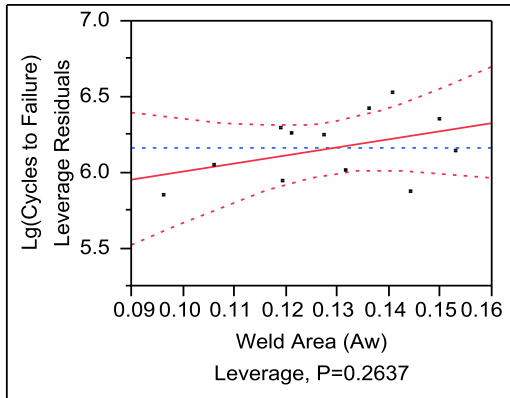
Least Significant Number

α	σ	δ	Number(LSN)
0.0500	0.252267	0.1497	14.36131

Least Significant Value

α	σ	Number	LSV
0.0500	0.252267	12	3.33744

Weld Area (A_w) Leverage Plot



Power Details

Test

Weld Area (A_w)

Power

α	σ	δ	Number	Power	AdjPower	LowerCL	UpperCL
0.0500	0.252267	0.088497	12	0.1839	0.0548	0.0500	0.8647

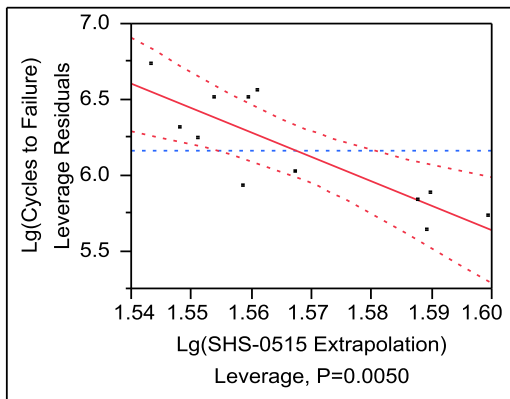
Least Significant Number

α	σ	δ	Number(LSN)
0.0500	0.252267	0.088497	33.98801

Least Significant Value

α	σ	Number	LSV
0.0500	0.252267	12	10.37794

Lg(SHS-0515 Extrapolation) Leverage Plot



Power Details

Test

Lg(SHS-0515 Extrapolation)

Power							
α	σ	δ	Number	Power	AdjPower	LowerCL	UpperCL
0.0500	0.252267	0.293587	12	0.9304	0.7970	0.3027	0.9997

Least Significant Number

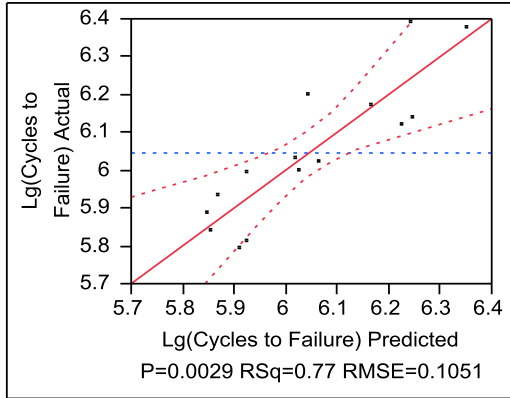
α	σ	δ	Number(LSN)
0.0500	0.252267	0.293587	7.870787

Least Significant Value

α	σ	Number	LSV
0.0500	0.252267	12	9.443252

Appendix Q Model Fitting Report – Weld Dimensions for R=-1, WR

Model Response: Lg(Cycles to Failure)
Factors: Weld Penetration, t, h, Lg(Stress Range)
Whole Model
Actual by Predicted Plot



Summary of Fit

RSquare	0.773414
RSquare Adj	0.68278
Root Mean Square Error	0.10513
Mean of Response	6.047148
Observations (or Sum Wgts)	15

Analysis of Variance

Source	DF	Sum of Squares	Mean Square	F Ratio
Model	4	0.37724997	0.094312	8.5333
Error	10	0.11052240	0.011052	Prob > F
C. Total	14	0.48777237		0.0029*

Parameter Estimates

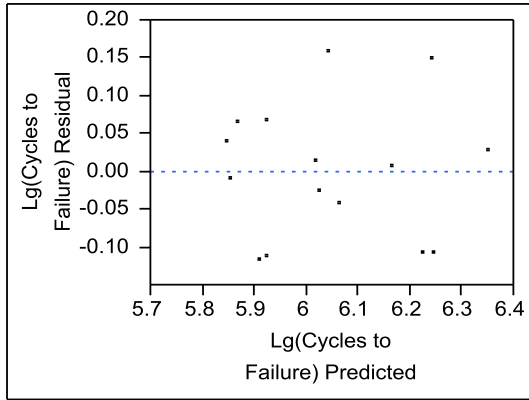
Term	Estimate	Std Error	t Ratio	Prob> t
Intercept	11.397681	2.109297	5.40	0.0003*
Weld Penetration	-1.327296	0.651102	-2.04	0.0688
Weld Throat (t)	7.2048062	3.672674	1.96	0.0782
Weld Height (h)	-8.131542	1.940014	-4.19	0.0019*
Lg(SHS-0515 Extrapolation)	-3.028905	1.75513	-1.73	0.1151

Effect Tests

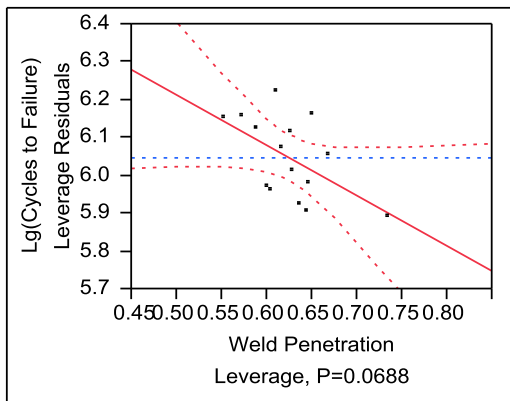
Source	Nparm	DF	Sum of Squares	F Ratio	Prob > F
Weld Penetration	1	1	0.04592915	4.1556	0.0688

Source	Nparm	DF	Sum of Squares	F Ratio	Prob > F
Weld Throat (t)	1	1	0.04253340	3.8484	0.0782
Weld Height (h)	1	1	0.19417180	17.5685	0.0019*
Lg(SHS-0515 Extrapolation)	1	1	0.03291567	2.9782	0.1151

Residual by Predicted Plot



Weld Penetration Leverage Plot



Power Details

Test
Weld Penetration

Power

α	σ	δ	Number	Power	AdjPower	LowerCL	UpperCL
0.0500	0.10513	0.055335	15	0.4533	0.2814	0.0500	0.9693

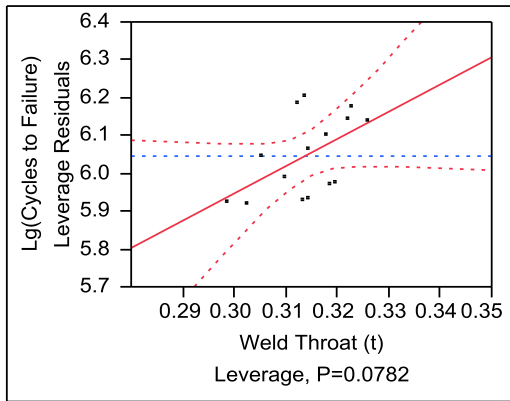
Least Significant Number

α	σ	δ	Number(LSN)
0.0500	0.10513	0.055335	17.10216

Least Significant Value

α	σ	Number	LSV
0.0500	0.10513	15	1.450745

**Weld Throat (t)
Leverage Plot**



Power Details

Test
Weld Throat (t)

Power

α	σ	δ	Number	Power	AdjPower	LowerCL	UpperCL
0.0500	0.10513	0.05325	15	0.4261	0.2569	0.0500	0.9642

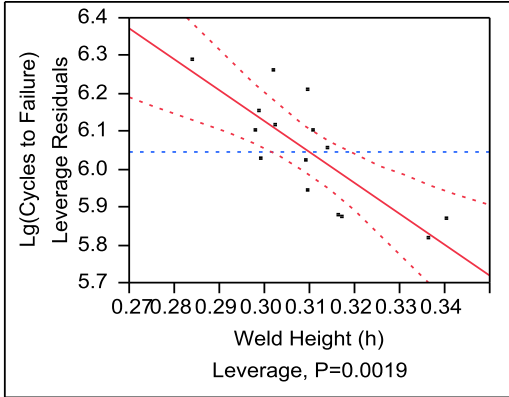
Least Significant Number

α	σ	δ	Number(LSN)
0.0500	0.10513	0.05325	18.14853

Least Significant Value

α	σ	Number	LSV
0.0500	0.10513	15	8.183228

**Weld Height (h)
Leverage Plot**



Power Details

Test

Weld Height (h)

Power

α	σ	δ	Number	Power	AdjPower	LowerCL	UpperCL
0.0500	0.10513	0.113775	15	0.9643	0.9015	0.4267	0.9999

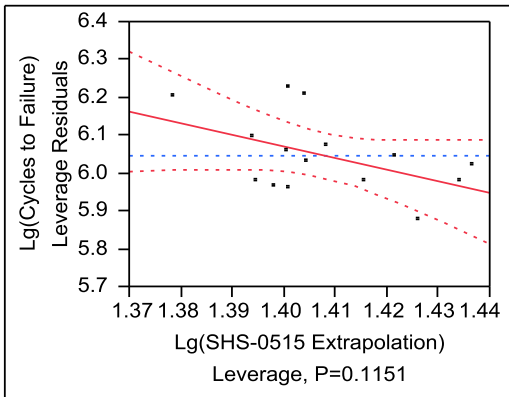
Least Significant Number

α	σ	δ	Number(LSN)
0.0500	0.10513	0.113775	8.162414

Least Significant Value

α	σ	Number	LSV
0.0500	0.10513	15	4.322622

**Lg(SHS-0515 Extrapolation)
Leverage Plot**



Power Details

Test

Lg(SHS-0515 Extrapolation)

Power								
α	σ	δ	Number	Power	AdjPower	LowerCL	UpperCL	
0.0500	0.10513	0.046844	15	0.3453	0.1868	0.0500	0.9444	

Least Significant Number

α	σ	δ	Number(LSN)
0.0500	0.10513	0.046844	22.34943

Least Significant Value

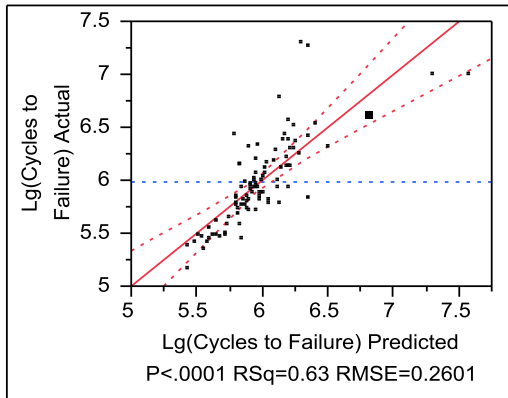
α	σ	Number	LSV
0.0500	0.10513	15	3.910674

Appendix R Model Fitting Report – All Significant Factors

Response: Lg(Cycles to Failure)

Whole Model

Actual by Predicted Plot



Summary of Fit

RSquare	0.630118
RSquare Adj	0.595711
Root Mean Square Error	0.26011
Mean of Response	5.984361
Observations (or Sum Wgts)	95

Analysis of Variance

Source	DF	Sum of Squares	Mean Square	F Ratio
Model	8	9.912260	1.23903	18.3133
Error	86	5.818534	0.06766	Prob > F
C. Total	94	15.730794		<.0001*

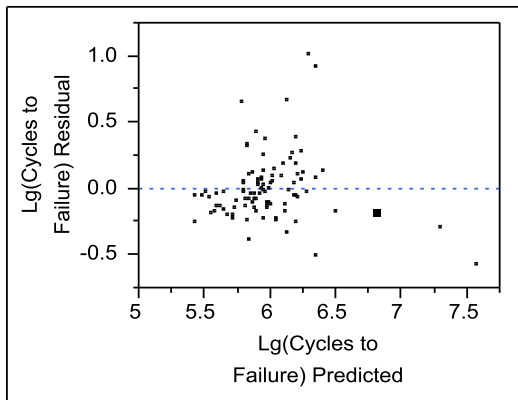
Parameter Estimates

Term	Estimate	Std Error	t Ratio	Prob> t
Intercept	8.5305546	1.078236	7.91	<.0001*
Failure Mode[RUNOUT]	0.6574197	0.119615	5.50	<.0001*
Failure Mode[WR]	-0.615869	0.090226	-6.83	<.0001*
Failure Mode[WT @ DECK]	-0.082254	0.068263	-1.20	0.2315
R-Ratio[0]	-0.200639	0.033224	-6.04	<.0001*
Weld Toe Size (d ₁)	1.9093636	0.636815	3.00	0.0035*
Weld Throat (t)	4.4303538	1.252693	3.54	0.0007*
Weld Height (h)	-1.475829	0.713366	-2.07	0.0416*
Lg(SHS - 0515 Extrapolation)	-2.599405	0.588326	-4.42	<.0001*

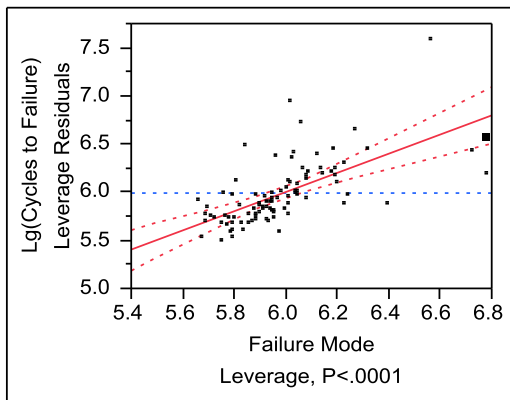
Effect Tests

Source	Nparm	DF	Sum of Squares	F Ratio	Prob > F
Failure Mode	3	3	4.4471989	21.9104	<.0001*
R-Ratio	1	1	2.4674820	36.4703	<.0001*
Weld Toe Size (d _i)	1	1	0.6082273	8.9898	0.0035*
Weld Throat (t)	1	1	0.8462571	12.5080	0.0007*
Weld Height (h)	1	1	0.2895762	4.2800	0.0416*
Lg(SHS - 0515 Extrapolation)	1	1	1.3207686	19.5214	<.0001*

Residual by Predicted Plot



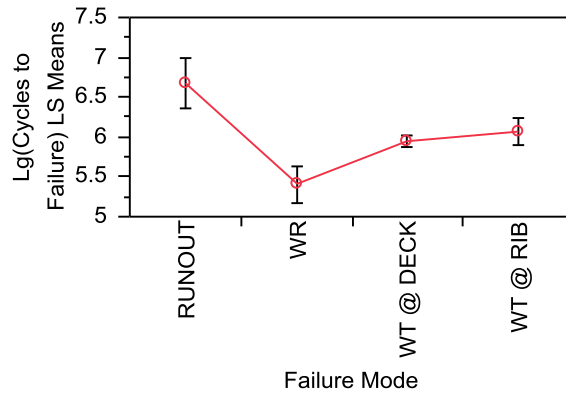
Failure Mode Leverage Plot



Least Squares Means Table

Level	Least Sq Mean	Std Error	Mean
RUNOUT	6.6779527	0.15451691	6.99388
WR	5.4046639	0.11625964	6.04715
WT @ DECK	5.9382787	0.03790074	5.87738
WT @ RIB	6.0612366	0.08701830	6.11973

LS Means Plot



LSMeans Differences Tukey HSD

$\alpha=0.050$ $Q=2.61998$

LSMean[i] By LSMean[j]

Mean[i]-Mean[j] Std Err Dif Lower CL Dif Upper CL Dif	RUNOUT	WR	WT @ DECK	WT @ RIB
RUNOUT	0 0 0 0	1.27329 0.17348 0.81876 1.72781	0.73967 0.16175 0.31589 1.16346	0.61672 0.18799 0.12419 1.10924
WR	-1.2733 0.17348 -1.7278 -0.8188	0 0 0 0	-0.5336 0.13344 -0.8832 -0.184	-0.6566 0.13795 -1.018 -0.2952
WT @ DECK	-0.7397 0.16175 -1.1635 -0.3159	0.53361 0.13344 0.18401 0.88322	0 0 0 0	-0.123 0.09507 -0.372 0.12612
WT @ RIB	-0.6167 0.18799 -1.1092 -0.1242	0.65657 0.13795 0.29516 1.01799	0.12296 0.09507 -0.1261 0.37204	0 0 0 0

Level		Least Sq Mean
RUNOUT	A	6.6779527
WT @ RIB	B	6.0612366
WT @ DECK	B	5.9382787
WR	C	5.4046639

Levels not connected by same letter are significantly different.

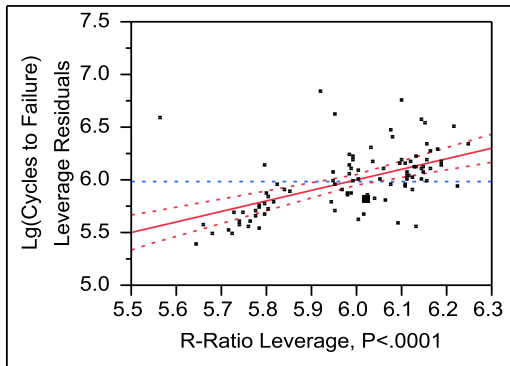
Power Details

Test
Failure Mode

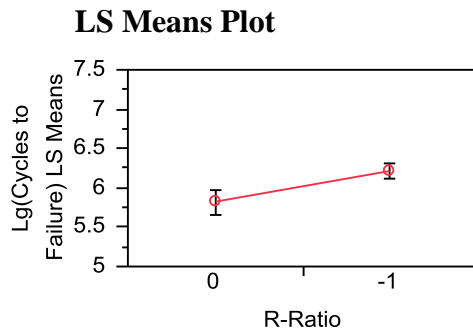
Power						
α	σ	δ	Number	Power	AdjPower	LowerCL UpperCL
0.0500	0.26011	0.216362	95	1.0000	1.0000	0.9954 1.0000

Least Significant Number				
α	σ	δ	Number(LSN)	
0.0500	0.26011	0.216362	17.3195	

R-Ratio Leverage Plot



Least Squares Means Table			
Level	Least Sq Mean	Std Error	Mean
0	5.8198938	0.07691318	5.73669
-1	6.2211721	0.04804312	6.08786



LSMeans Differences Student's t
 $\alpha=0.050$ $t=1.98793$
 LSMeans[i] By LSMeans[j]

Mean[i]-Mean[j]	0	-1
Std Err Dif		
Lower CL Dif		
Upper CL Dif		
0	0	-0.4013

	0	0.06645
	0	-0.5334
	0	-0.2692
-1	0.40128	0
	0.06645	0
	0.26919	0
	0.53337	0

Level		Least Sq Mean
-1	A	6.2211721
0	B	5.8198938

Levels not connected by same letter are significantly different.

Power Details

Test

R-Ratio

Power								
α	σ	δ	Number	Power	AdjPower	LowerCL	UpperCL	
0.0500	0.26011	0.161163	95	1.0000	0.9999	0.9796	1.0000	

Least Significant Number

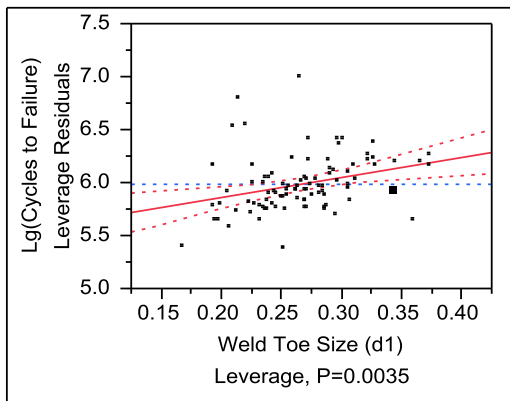
α	σ	δ	Number(LSN)
0.0500	0.26011	0.161163	15.27266

Least Significant Value

α	σ	Number	LSV
0.0500	0.26011	95	0.066046

Weld Toe Size (d_1)

Leverage Plot



Power Details

Test

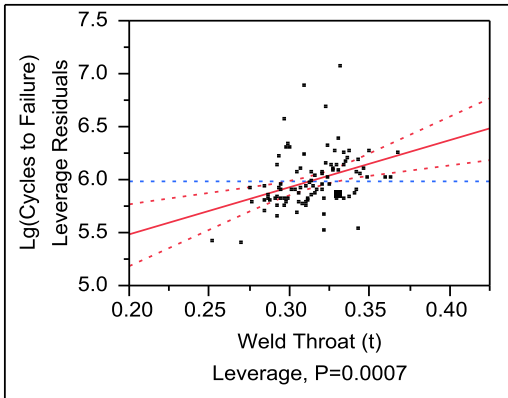
Weld Toe Size (d₁)

Power							
α	σ	δ	Number	Power	AdjPower	LowerCL	UpperCL
0.0500	0.26011	0.080015	95	0.8425	0.7876	0.1699	0.9985

Least Significant Number				
α	σ	δ	Number(LSN)	
0.0500	0.26011	0.080015	43.58826	

Least Significant Value				
α	σ	Number	LSV	
0.0500	0.26011	95	1.265946	

**Weld Throat (t)
Leverage Plot**



Power Details

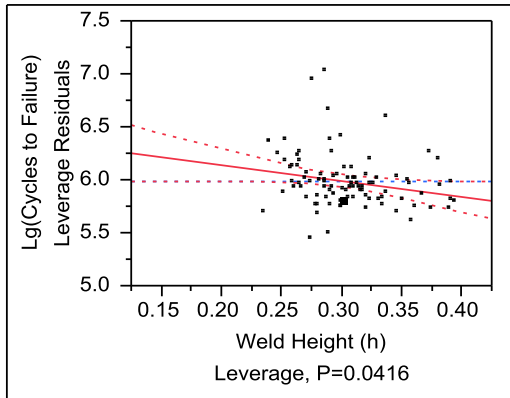
Test
Weld Throat (t)

Power							
α	σ	δ	Number	Power	AdjPower	LowerCL	UpperCL
0.0500	0.26011	0.094382	95	0.9378	0.9117	0.3344	0.9998

Least Significant Number				
α	σ	δ	Number(LSN)	
0.0500	0.26011	0.094382	32.43522	

Least Significant Value				
α	σ	Number	LSV	
0.0500	0.26011	95	2.490272	

**Weld Height (h)
Leverage Plot**



Power Details

Test

Weld Height (h)

Power

α	σ	δ	Number	Power	AdjPower	LowerCL	UpperCL
0.0500	0.26011	0.05521	95	0.5342	0.4222	0.0507	0.9799

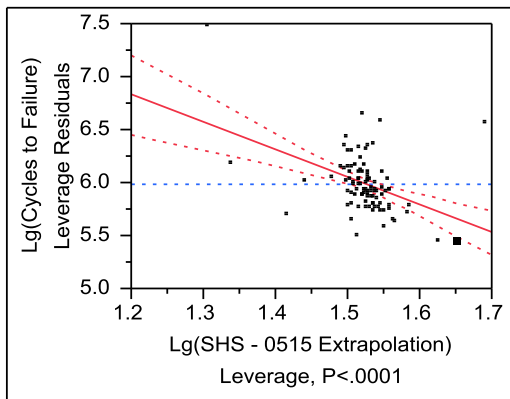
Least Significant Number

α	σ	δ	Number(LSN)
0.0500	0.26011	0.05521	87.93386

Least Significant Value

α	σ	Number	LSV
0.0500	0.26011	95	1.418124

**Lg(SHS - 0515 Extrapolation)
Leverage Plot**



Power Details

Test

Lg(SHS - 0515 Extrapolation)

Power								
α	σ	δ	Number	Power	AdjPower	LowerCL	UpperCL	
0.0500	0.26011	0.11791	95	0.9920	0.9875	0.6712	1.0000	

Least Significant Number

α	σ	δ	Number(LSN)
0.0500	0.26011	0.11791	22.53209

Least Significant Value

α	σ	Number	LSV
0.0500	0.26011	95	1.169554